JUSTUS-LIEBIG-
UNIVERSITÄT
GIESSEN

Analysis of Hepatitis C Virus *cis*-elements involved in the Initiation of Negative-Strand RNA Synthesis

Dissertation

to acquire the degree
doctor rerum naturalium
(Dr. rer. nat.)

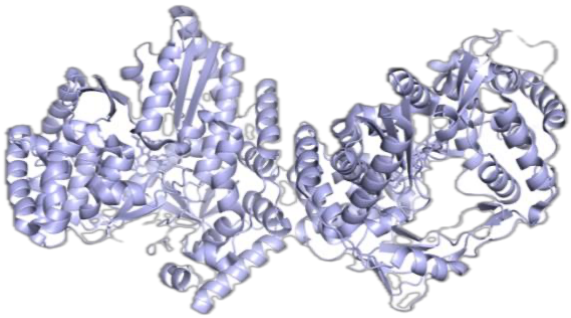

presented by

Attiya Qadoos Malik

M.Sc. Biochemistry

Institute of Biochemistry
Faculty of Medicine (FB 11)
Justus Liebig University

Giessen, March 2026

This dissertation was carried out between September 2020 and June 2025 in the research group of Prof. Dr. Michael Niepmann at the Institute of Biochemistry, Faculty of Medicine, Justus Liebig University Giessen. The doctoral research was funded by the German Research Foundation (Deutsche Forschungsgemeinschaft, DFG) within the framework of the Sonderforschungsgebiet SFB 1021 (*RNA viruses: RNA metabolism, host response and pathogenesis*).

1st Reviewer

Prof. Dr. Elena Evguenieva-Hackenberg
Institute of Microbiology and Molecular Biology
Faculty of Biology and Chemistry (FB 08)
Justus Liebig University Giessen

2nd Reviewer

Prof. Dr. Michael Niepmann
Institute of Biochemistry
Faculty of Medicine (FB 11)
Justus Liebig University Giessen

I. Table of Contents

II. List of Figures

III. List of Supplementary Figures

IV. List of Tables

V. Abbreviations

ΔIIIb	Delta IIIb (stem loop)
3D	Three Dimensional
40S	small ribosomal subunit
5EU	5-Ethynyl Uridine
AA	Amino Acid
Ago2	Argonaut 2
Amp	Ampicillin
AnP	Antarctic Phosphatase
Apo	Apolipoprotein
ATG14L	Autophagy Related Protein 14 Like Protein
$CaCl_2$	Calcium Chloride
CCC	Cytosine (3x) Nucleotide
CD81	Cluster of Differentiation 81
cDNA	complementary DNA
CERT	Ceramide Transfer Protein
CLDN1	Claudin 1
cLDs	cytosolic Lipid Droplets
Con 1	Consensus 1
cPLA2	cytosolic Phospholipase A2
CRE	*cis*-replicating element
CRE	*Cis*-Replication Element
CsCl	Caesium Chloride
Ct	Cycle Threshold
Cyp A	Cyclophilin A
DAAs	direct acting antivirals
DGAT1	Diacylglycerol O-acetyltransferase 1
DMEM	Dulbecco's modified eagle medium
DMSO	Dimethyl Sulfoxide
DMVs	Double Membrane Vesicles
DNA	Deoxyribonucleic Acid
dsRNA	double stranded RNA
DTT	Dithiothreitol
E1/E2	Envelope Proteins 1/2
EDTA	Ethylenediaminetetraacetic acid
eIF3	eukaryotic Initiation Factor 3
EMCV	Encephalomyocarditis Virus
ER	Endoplasmic Reticulum
ES7	Expansion Segment 7
EtOH	Ethanol
FAPP2	Four-Phosphate Adaptor Protein 2
FBS	Fetal Bovine Serum
FLuc	*Firefly* Luciferase
G418	Neomycin
GAPDH	Glyceraldehyde-3-phosphate dehydrogenase
GDD	Gly, Asp, Asp
GGG	Guanine (3x) Nucleotide
GND	Polymerase Deficient Construct (D318→N318)
GT1b	Trisialoganglioside 1b
GTP	Guanosine Triphosphate
HCV	Hepatitis C Virus
HDL	High Density Lipoproteins
HepG2	Hepatoblastoma-derived Cell line

HF	High Fidelity
HiBiT	High BiT (Protein Tag)
hnRNP	heterogenous nuclear Ribonucleoprotein
hp	hairpin
hpt	hours post transfection
HSPGs	Heparin Sulphate Proteoglycans
Huh-7/7.5	Human Hepatoma Cell line 7/7.5
IDT	Integrated DNA Technologies
IFN-α	Interferon-α
IGF2BP1	Insulin-like growth factor 2 mRNA-binding Protein 1
IMP1	IGF2 mRNA-binding Protein 1
IMP1	Insulin-like growth factor 2 mRNA-binding Protein
IRES	Internal Ribosomal Entry Site
ITAFs	Trans-Acting Factors
JFH-1	Japanese Fulminant Hepatitis-1
KCl	Potassium Chloride
K_D	Dissociation Constant
kDa	kilo Dalton
La	Lupus-associated autoantigen
LB	Lysogeny Broth
LDLR	Low-Density-Lipoprotein Receptor
LDs	Lipid Droplets
LRI	Long Range Interaction
LSm1-7	Heteroheptameric (seven member) ring protein complex
MAPK	Mitogen-activated Protein Kinase
MAVS	Mitochondrial Antiviral Signal Protein
Mg^{2+}	Magnesium Ion
$MgCl_2$	Magnesium Chloride
$MgSO_4$	Magnesium Sulfate
miR-122	micro RNA-122
MMVs	Multi-Membrane Vesicles
mRNA	messenger RNA
mutIIId/e	mutation in IIId and in IIIe stem loop
NaCl	Sodium Chloride
NANBH	non A, non B Hepatitis
NEB	New England Biolabs
neo	Neomycin-resistance gene
NGND	Polymerase Deficient Construct (D318→N318; D220→N220)
noRT	Without Reverse Transcriptase
NPC1	Niemann-Pick disease, type C1
NS2	Non Structural Protein 2
NS5A	Non Structural Protein 5A
NS5B	Non Structural Protein 5B
NSAP1	NS1-Associated Protein-1
NTP	Nucleoside 5´-triphosphates
OD	Optical Density
ORF	Open Reading Frame
OSBP	Oxysterol-Binding Protein
PBS	Phosphate-Buffered Saline
PCBP2	Poly(rC)-binding Protein 2
PCI	Phenol/Chloroform/Isoamyl alcohol
PenStrep	Penicillin-Streptomycin
PI4KIIIα	Lipid Kinase
PI4P	Phosphatidylinositol 4-phosphate
PIC	Preinitiation Complex

PREB	Prolactin Regulatory Element-Binding
PV	Poliovirus
RACK1	Receptor for Activated Protein C
RdRp	RNA-dependent RNA polymerase
RIG-I	Retinoic acid-Inducible Gene-I adaptor
RLuc	*Renilla* Luciferase
RLUs	Relative Light Units
RNA	Ribonucleic acid
RO	Replication Organelles
rpm	rounds per minute
RT	Reverse Transcriptase/Transcription
RT-qPCR	Reverse Transcription and quantitative PCR
S.O.C.	Super Optimal Broth
SD	Standard Deviation
SDS	Sodium Dodecyl Sulphate
SL	Stem Loop
SPP	Signal Peptide-peptidase
SRB1	Scavenger Receptor class B member 1
SREBP	Sterol Regulatory Element-binding-protein
Surf4	Surfeit Locus Protein 4
SVR	Sustained Virologic Response
TBE	Tris-borate EDTA
TBS	Tris-Buffered Saline
TES	N-[Tris(hydroxymethyl)methyl]-2-aminoethanesulfonic acid
tRNA	transfer RNA
U/C	Uridine/Cytosine
UTR	Untranslated Region
UV	Ultraviolet
VLDL	Very Low-Density lipoproteins
VR	Variable Region
WHO	World Health Organization
WT	Wild Type
XNR1	Exoribonucleases 1

VI. Zusammenfassung

Das Hepatitis-C-Virus (HCV) infiziert weltweit etwa 3 % der Bevölkerung. Aufgrund des häufig asymptomatischen Verlaufs über lange Zeiträume wird die Infektion oft erst spät diagnostiziert und kann zu schweren Lebererkrankungen wie Leberzirrhose, hepatozellulärem Karzinom oder chronischem Leberversagen führen. Das Genom von HCV liegt als positivsträngige RNA vor und wird über die Synthese eines komplementären negativsträngigen RNA-Intermediats repliziert. Obwohl zahlreiche Aspekte der HCV-Replikation gut charakterisiert sind, ist über die cis-wirkenden RNA-Elemente des positivsträngigen Genoms, die an der Initiation der negativsträngigen RNA-Synthese beteiligt sind, bislang nur wenig bekannt. Die Analyse der negativsträngigen RNA-Synthese ist mit erheblichen methodischen Herausforderungen verbunden, insbesondere aufgrund von Hintergrundsignalen, die eine präzise Detektion erschweren. Diese resultieren aus Fehlpriming während der in-vitro-Transkription, aus unspezifischem Priming während der reversen Transkription infolge der ausgeprägten Haarnadelstruktur am 3′-Ende des HCV-Genoms, sowie aus kontaminierender Rest-Plasmid-DNA und RNA aus den transfizierten Positiv-Strang-Replikons, die als falsche Matrize bei der cDNA-Synthese dienen kann. Darüber hinaus ist eine Messung der negativsträngigen RNA-Synthese erforderlich, die von anderen viralen Prozessen wie Translation und positivsträngiger RNA-Replikation entkoppelt ist. Zur Überwindung dieser Limitationen wurde ein subgenomisches HCV-Replikonsystem der vierten Generation in Kombination mit einem hochoptimierten, strang-spezifischen RNA-Nachweisverfahren etabliert. Dieses System ermöglicht die hochpräzise Detektion neu synthetisierter negativsträngiger RNA bei vernachlässigbarem Hintergrund. Kontaminierende Template-DNA aus der in-vitro-Transkription wurde durch zwei aufeinanderfolgende DNase-Verdau-Schritte und anschließende RNA-Aufreinigung mittels Monarch-Säulen nahezu vollständig entfernt. Darüber hinaus wurde die Qualität der aus TRIzol isolierten Gesamt-RNA durch zusätzliche DNase-Behandlungen, saure Phenol/Chloroform-Extraktion und säulenbasierte Aufreinigung weiter verbessert. Zur selektiven Detektion von nach der Transfektion der Replikons neu synthetisierter RNA wurde eine 5-Ethynyluridin-(5EU-)Markierung in Kombination mit Click-iT-Chemie eingesetzt. Die biotinylierte naszente RNA wurde mittels Streptavidin-Beads isoliert, streng gewaschen und anschließend durch RT-qPCR analysiert. Erhöhte Temperaturen während der reversen Transkription (65 °C) und der qPCR (62 °C) reduzierten unspezifische Amplifikationen zusätzlich. Auf diese Weise konnte der Hintergrund in Polymerase-defizienten Negativkontrollen auf etwa 0,02 – 0,035 % gesenkt werden, was einer etwa 975-fachen Verbesserung gegenüber früheren Methoden entspricht. Mit diesem System wurde die SLI-II-Region der HCV-5′-UTR als minimales, essenzielles cis-wirkendes Element für die Initiation der negativsträngigen RNA-Synthese identifiziert. Die SLI-III-Domäne, die die IRES-Region umfasst, trug etwa 34,5 % zur Gesamteffizienz der negativsträngigen RNA-Synthese bei, während translationsdefiziente Mutationen zu einer starken Reduktion führten. Diese Ergebnisse unterstreichen die zentrale Bedeutung einer intakten HCV-5′-UTR für die Genomreplikation und legen nahe, dass die Rekrutierung von eIF3 und der kleinen ribosomalen 40S-Untereinheit die negativsträngige RNA-Synthese positiv reguliert. Analog zum PCBP2-Protein könnten diese Faktoren die 5′- und 3′-Enden des viralen Genoms miteinander verbinden und so eine Genomzirkularisierung fördern. Eine kompetitive Bindung von NS5B-Dimeren oder -Oligomeren an die 5′-UTR könnte diese Brückenbildung auflösen und dadurch die Replikation über die Bindung von NS5B an das 3′-Ende ermöglichen. Solche Interaktionen könnten als Kontrollmechanismus fungieren, der entscheidet, ob das Genom translatiert und/oder repliziert wird. Der zuverlässige Nachweis der negativsträngigen RNA ist derzeit erst ab 24 hpt möglich, sodass weitere Optimierungen erforderlich sind, um frühe Initiationsereignisse zu untersuchen.

VII. Abstract

Hepatitis C Virus infects approximately 3 % of the global population. Because infection often remains asymptomatic for long periods, many cases progress unnoticed to severe liver diseases such as cirrhosis, hepatocellular carcinoma or chronic liver failure. HCV possesses a positive-strand RNA genome that replicates via negative-strand RNA intermediate. While many aspects of HCV replication are well studied, comparatively little is known about the *cis*-acting RNA elements on the positive-strand genome that are involved in the initiation of negative-strand RNA synthesis. Studying negative-strand RNA synthesis poses major technical challenges, particularly due to background signals that obscure accurate detection. The background signals arise from false priming (1) during *in vitro*-transcription and (2) during reverse transcription due to the strong hairpin structure at the 3´end of the RNA genome and (3) contaminating residual plasmid DNA and transfected RNA that serves as a false template during cDNA synthesis. Furthermore, it is essential to measure negative-strand RNA synthesis uncoupled from other viral processes such as translation and positive-strand RNA replication. To address these challenges, an HCV subgenomic (4th generation) replicon system was developed combined with a highly optimized strand-specific RNA detection assay. The system allows precise detection of newly synthesized negative-strand RNA with negligible background. Template DNA contamination from *in vitro*-transcribed RNA was (nearly) completely eliminated by two rounds of DNase digestion followed by RNA purification using Monarch kit columns. Total RNA extracted using TRIzol also underwent additional DNase treatments, acidic phenol/chloroform extraction and column-based purification to further enhance RNA quality. To selectively detect RNA new transcribed only after transfection of the replicon, 5EU-labelling was used in combination with Click iT chemistry. The 5EU-labelled nascent RNA was biotinylated, captured using streptavidin beads, and subjected to ten stringent washing steps before analysis by RT-qPCR. High temperature conditions during reverse transcription (65 °C) and qPCR (62 °C) further minimized nonspecific amplification. This approach reduced the background signals from polymerase deficient negative controls to only 0.02 - 0.035 %, representing an approximately 975-fold improvement over earlier methods in the Niepmann laboratory using 1st generation replicon system and conventional RNA purification procedures. Using this highly sensitive platform, the study identified the SLI-II region of the HCV 5´UTR as the minimal essential *cis*-acting element required for the initiation of negative-strand RNA synthesis. The SLI-III domain, which comprises the IRES region of the HCV 5´UTR, supported about 34.5 % of the overall efficiency of the negative-strand RNA synthesis. In contrast, mutations disrupting binding of eIF3 or the 40S subunit (ΔIIIb and mutIIId/e) caused a drastic reduction in negative-strand RNA levels, both in SLI-III as well as in complete 5´UTR construct. These findings underscore the essential role of an intact HCV 5´UTR in genome replication and suggest that recruitment of eIF3 and the small ribosomal 40S subunit positively regulate negative-strand RNA synthesis. Similar to the PCBP2 protein, these factors may bridge the 5´- and 3´-ends of the viral genome, promoting genome circularization. Competitive binding of NS5B dimer or oligomer to the 5´UTR may disrupt this interaction, enabling replication via NS5B binding to the 3´-end. Such interactions may function as a checkpoint determining whether the genome undergoes translation and/or replication. Detection of negative-strand RNA is currently reliable only from 24 hpt onward, and further optimization is required to analyse initiation events at earlier time points

Analysis of HCV *cis*-elements involved in the initiation of Negative-Strand RNA Synthesis

1. Introduction

1.1. HCV in general

Hepatitis is defined as an inflammation of liver tissues, which can result from a defective immune system, excessive alcohol consumption, diabetes mellitus and viral infections. Various viruses are known to cause hepatitis, including Hepatitis A, B, C, D, and E viruses, as well as cytomegalovirus**,** Epstein-Barr virus and the yellow fever virus. If the inflammation resolves within six months, the condition is classified as acute hepatitis; if it persists beyond six months, it is considered chronic hepatitis. Chronic hepatitis, if left untreated, can be life-threatening and may progress to hepatocellular carcinoma, liver cirrhosis, or chronic liver failure (John Hopkins Medicine. Hepatitis 2025).

Hepatitis C virus (HCV) replicates very slowly within the liver cells and often remains undetected until the onset of clinical symptoms. This delayed manifestation and diagnosis contributes to HCV's role as one of the major causes of chronic hepatitis. Usually, the virus is spread through blood transfusion or intravenous drug injection using contaminated needles or syringes. Common symptoms include jaundice, fever, abdominal pain and loss of appetite. Approximately 3% of the global population is infected with HCV. It is responsible for annually 860,000 deaths in WHO European Member states alone. Chronic HCV infection is widely prevalent across multiple regions including Mediterranean, Europe, Southeast Asia, Western Pacific, Africa and America (WHO, Global Hepatitis report, 2024).

1.2. HCV – From Discovery to Current Developments

HCV was initially isolated as NANBH (non A, non B hepatitis) infectious agent in patients who developed chronic hepatitis specifically after receiving blood transfusion. Blood from infected patients was inoculated to chimpanzee models, which subsequently developed hepatitis. The study led to the discovery of a new kind of virus which was named as HCV (Choo et al., 1989). Using advanced molecular cloning techniques, a small fragment of the HCV genome (HCV-1) was isolated in 1989 by a group of American scholars in Chiron Laboratories led by Michael Houghton. The contribution of another scientist, Harvey J. Alter, was the detailed study on blood transfusion events proving HCV as the infectious agent for chronic hepatitis in that context where Charlie M. Rice devoted his work to identify the viral cause of HCV related chronic hepatitis. In 2020, all three scholars were awarded with Nobel prize for their tremendous efforts in medicine (Laugi, 2020; Topi et al., 2024 and References therein).

Further achievement was the development of an HCV subgenomic replicon system using the Huh-7 hepatoma cell line by Volker Lohmann in the group of Ralf Bartenschlager in 1999, which paved the way for experimental studies on HCV replication and translation in cell culture systems (Lohmann et al., 1999). The first authentic full-length HCV genome, belonging to genotype 2a, was isolated by

T. Wakita's group in 2001 (Kato et al., 2001). The clone, named JFH-1 (Japanese Fulminant Hepatitis-1), was extracted from a Japanese patient with fulminant hepatitis. Remarkably, JFH-1 could produce viral particles in Huh-7, which were not only infectious for naïve cell cultures but also for chimpanzees. In 2002, establishment of a cell line highly permissive for HCV replication, Huh-7.5, by Charlie Rice's group was another contribution to advanced HCV research. Huh-7.5 is a derivative of Huh-7 cells, which was generated from Huh-7 cells with replicating subgenomic HCV replicons by prolonged interferon-α (IFN-α) treatment, and from which the subgenomic HCV replicons were removed successfully. By these selection processes, the cell line accumulated mutations that allowed more efficient HCV replication (Blight et al., 2002).

Earlier treatment strategies for chronic hepatitis C involved the use of antiviral ribavirin in combination with pegylated IFN-α. However, the therapy caused side effects in a non-negligible number of patients. Thanks to years of extensive research, direct acting antivirals (DAAs) belonging to the class of protease inhibitors, NS5A inhibitors and polymerase inhibitors are now successfully used in various genotype-specific combinations, offering highly effective treatment options for hepatitis C. One example is sofosbuvir (NS5B inhibitor) in combination with velpatasvir (NS5A inhibitor) which was the first pan genotypic DAA regimen showing about 90% sustained virological response (SVR). However, the development of a vaccine against HCV remains highly challenging due to the virus's genetic versatility, since HCV is subdivided into 8 genotypes and 93 confirmed subtypes. In addition, viral escape mutations lead to the failure of adaptive antiviral immunity in patients with chronic hepatitis C (Topi et al., 2024 and References therein). The World Health Organization (WHO) has set a goal to achieve 90 % global elimination of Hepatitis C virus by the year 2030 (WHO, Global Hepatitis report, 2024).

1.3. Structure and Classification of Hepatitis C Virus

HCV belongs to the Kingdom *Orthonavirae* of the Realm *Riboviria*. The main characteristic of the Kingdom is the viral genome made of ribonucleic acids, comprising of either a single positive-strand, a single negative-strand or a double strand RNA molecule. The genes encode an RNA-dependent RNA polymerase (RdRp), which takes over replication of viral genome inside the host cells. Further subdivided into families, the virus particles could be enveloped or nonenveloped. One example of enveloped positive-strand RNA viruses is Hepatitis C virus, which belongs to the family *Flaviviridae* and the genus *Hepacivirus*. Examples for nonenveloped positive-strand RNA viruses are e.g., Poliovirus and Mengovirus, which belong to the family *Picornaviridae* (Schoch et al., 2020).

Infectious HCV particles derived from the serum are 30 – 80 nm in diameter (Yuasa et al., 1991). The spherical viral particles are enveloped by lipid membranes with embedded viral surface glycoproteins, E1 and E2. The glycoproteins enable the virus to attach and enter the host cells. The 9.600 nucleotides long positive-strand RNA genome is encapsidated by core protein underneath the viral envelop (Moradpour and Penin, 2013).

1.4. Life cycle of HCV

HCV mainly attacks hepatocytes. The virus enters the cells with the help of surface proteins, releases its positive-strand RNA genome inside the cell cytoplasm, replicates with the help of its own RdRp polymerase, translates the virus-specific structural and non-structural proteins using host cell's machinery and releases as a full infectious particle after assembling structural and non-structural proteins (Lindenbach et al., 2013). The procedure can be subdivided into following steps.

1.4.1. Entry of Hepatitis C Virus

The viral particles interact with very low-density lipoproteins (VLDL) to form 'lipo-viral' particles (Lindenbach et al., 2013; Bley et al., 2020; Matthaei et al., 2024). The apolipoproteins Apo A-1, ApoB-48, ApoB-100, ApoC-1 and ApoE have been found associated to HCV particles derived from blood serum. The fusion with host VLDL particles helps the virus evade the host's immune response. In addition, the association with VLDL enhances their mobility by providing them appropriate buoyant density as well as target cell entry by providing cellular proteins that facilitate their entry into hepatocytes. Binding of lipo-viral particles to hepatocytes is accomplished by specific interaction of lipo-viral surface proteins with liver specific surface proteins, i.e., low-density-lipoprotein receptor (LDLR), heparin sulphate proteoglycans (HSPGs) and scavenger receptor class B member 1 (SRB1). The later one delipidates the lipo-viral particles and promotes the binding of surface protein E2 to CD81 receptors, which in turn activates the signal transduction through epidermal growth factor. CD81-bound HCV particles reach towards the claudin 1 (CLDN1) at the tight junction through lateral movement and are finally invaginated into hepatocytes by clathrin-mediated endocytosis. The low pH helps the fusion of the envelope protein with the endosomal membrane, and the positive-strand RNA genome is then released into the cytoplasm (Figure 1.1) (Lindenbach et al., 2013; Dubuisson et al., 2014).

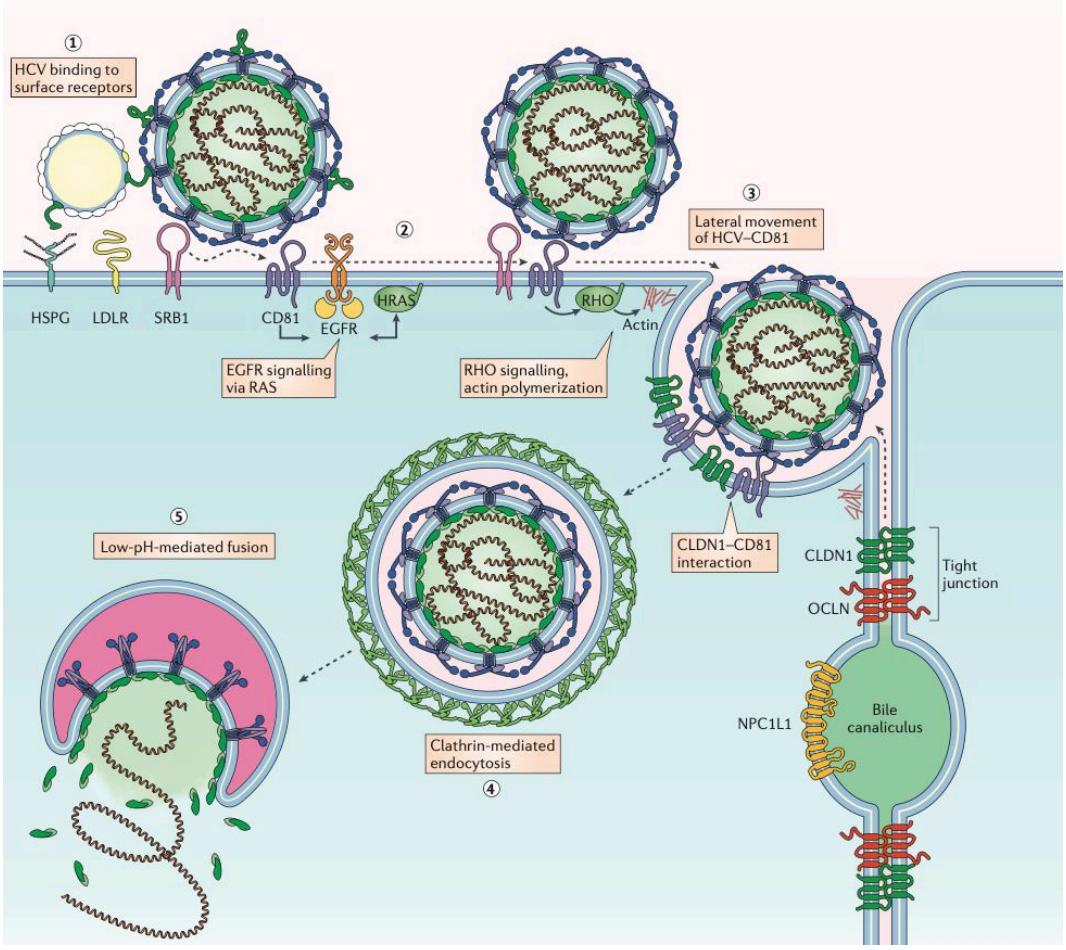

Figure 1.1. Entry of HCV into hepatocytes. The virus attaches to the surface as lipo-viral particle with the help of surface receptors, reaches to the tight junction through lateral movement and invaginates into the cells by clathrin-mediated endocytosis (Lindenbach et al., 2013).

1.4.2. Hepatitis C Virus Growth within Hepatocytes

The 9.6 kb long HCV positive-strand RNA-genome contains a single open reading frame (ORF) along with flanking 5′ and 3′ untranslated regions. The 5′UTR undergoes formation of specific 3D structures forming the Internal Ribosomal Entry Site (IRES), which facilitates the binding of cellular ribosomes as well as the eukaryotic initiation factor eIF3 and initiates the translation. A single polyprotein is translated which is processed by viral and host cell proteases into structural – core, E1 and E2 glycoproteins – and non-structural – P7 viroporin, NS2 protease, NS3/4A complex harbouring protease and NTPase RNA helicase activity, NS4B, NS5A and NS5B – proteins. NS5B is the RNA dependent RNA polymerase (RdRp) which is responsible for the replication of the viral genome. The initial step of replication of the positive strand RNA genome is the synthesis of a corresponding antigenome RNA strand, which is used as a template for the production of progeny positive-strands (Bartenschlager et al., 2010; Lohmann et al., 2013).

1.4.3. Assembly and Release of mature HCV Particles

Viral proteins, either structural or non-structural, play individual roles for assembly, maturation and release of nascent HCV particles inside the cells. After synthesis, the viral proteins remain partially embedded into ER membrane through their trans membrane domains. The core protein undergoes homodimerization and is transiently transferred to cytosolic lipid droplets (cLDs) with the help of MAPK-regulated cytosolic phospholipase A2 (cPLA2). The process is also supported by diacylglycerol O-acetyltransferase 1 (DGAT1). The viral envelop glycoproteins E1 and E2 make heterodimers protruding towards ER lumen. Inwards to ER lumen, a capsid is formed by bulging of ER membrane through the recruitment of glycoprotein-heterodimers E1/ E2, named as viral assembly site. The assembly of viral particles initiates with the interaction of non-structural protein NS5A with cLD-associated core proteins. In the meanwhile, interaction between p7-NS2 and NS3-4A promotes the recruitment of the core protein towards the virus assembly site. Positive-strand RNA is taken out of the cellular processes – replication or translation –, transferred to the assembly site and packaged inside the newly forming capsid. The nascent HCV particle is released inside the ER Lumen, which consists of envelope along with the surface proteins E1/E2, shielding a capsid made of core proteins harbouring positive-strand HCV-RNA genome. The virus undergoes further maturation processes while trafficking through Golgi apparatus until the final release. Through interaction with ApoE-associated VLDL or HDL, the viral particles acquire their characteristic low buoyant density. The viral protein p7 protects them from the low pH during the whole secretory pathway until their final release from the hepatocytes (Lindenbach et al., 2013 and references therein).

1.5. Structural and Functional Components of HCV RNA Genome and Antigenome

1.5.1. HCV RNA Genome

The Hepatitis C Virus genome consists of a single positive-strand RNA molecule encapsidated by core protein. The 9.600 nucleotides long positive-strand RNA genome encodes for ten viral structural and non-structural proteins (Moradpour and Penin, 2013). Highly conserved secondary and tertiary structure of the genome, specifically that of the 5′UTR and 3′UTR, makes both untranslated regions crucial for viral translation and replication (Niepmann et al., 2018; Fricke et al., 2015). Several stem loops and bulges, formed by the specific folding of 5′ and 3′ untranslated regions of the RNA genome, act as *cis*-elements playing vital role in both replication and translation. In fact, the spatial

and temporal arrangement of the *cis*-elements determines the upcoming task of the genome, whether facilitating ribosome binding at 5′-end for translation or recruiting viral specific RNA dependent RNA polymerase (RdRp) to the 3′-end for replication. Other factors like interactions of both genome ends, either with each other or with other *cis*-elements present in the RNA genome, are also very important for the genome's upcoming task (Scott et al., 2023; Gerresheim & Hess et al., 2020). A critical aspect in that context is the existence of other *cis*-elements formed on the RNA antigenome, which folds differently as compared to positive-strand RNA genome (Fricke et al., 2015). The antigenome-interaction with positive-strand RNA genome and the intramolecular interactions in negative-strand RNA (antigenome) may involve in replication/ translation or a switch between both processes.

The **5′UTR** region comprises four individual kinds of stem loop structures, which differ both in size and shape. At the very beginning of 5′-end there is a small stem loop I (SLI) followed by SLII. The region between SLI and SLII comprises two conserved binding sites for the liver specific micro RNA-122 (miR-122), which, upon binding in association with Argonaut 2 (Ago2) protein, enhances the overall translation rate of the virus (Conrad et al., 2013). The SLI-III domain attains a specific 3D form comprising the largest part of the viral IRES. The IRES recruits the small 40S ribosomal subunit at the smaller SLIII-loop IIId with a GGG sequence, whereas the translation initiation factor eIF3 is recruited at the apical site of SLIII – the smaller stem-loop IIIb. More downstream, the IRES SLIV extends to the protein coding region harbouring the AUG start codon site (Niepmann, 2013).

About 236 nucleotides long **3′UTR** region of HCV positive-strand RNA genome comprises three main parts: a variable region (VR), a poly (U/C) tract, and a highly conserved 3′-X-tail, the latter two being essential for the replication. The RNA secondary structure prediction suggests different conformations of the 3′-end region with formation of either three (SL1, 2 and 3) or two stem-loops (Niepmann et al., 2018). The extreme 3′-end forming SL1 contains a conserved terminal uridine (Fricke et al., 2015). Replication begins by binding of viral RdRp at this 3′-end of the positive-strand RNA genome.

There are several other stem-loop structures within the **coding region** of the RNA genome acting as *cis*-elements involved in translation and/ or replication. Downstream to the 5′UTR region, the first 177 nucleotides attain further stem-loop formation making part of SLIV, and complete SLV and SLVI. Upstream to the 3′UTR, the NS5B coding region contains a complete set of stem-loop structures (5BSL1, 2, 3.1, 3.2 and 3.3) named cis-replication element (CRE) (Fricke et al., 2015). Long-range as well as short-range **interactions** between these elements contribute to the regulation of viral translation and replication. One short-range interaction, for example, is found between the apical part of SLII and SLIV which alters the conformation of the IRES. The changed conformation makes the start codon AUG better accessible for the ribosomal 40S subunit and facilitates the translation of the RNA genome. Long-range interactions are found, for example, between SLIII-IIId (5′-end) and 5BSL3.2/ CRE. CRE is a versatile element which also builds interactions with the 3′-end (SL2). RNA-RNA interactions in such a coordinated manner play very important roles in the regulation of replication (Niepmann et al., 2018), translation and the switch between both processes (Gerresheim & Hess et al., 2020).

1.5.2. HCV RNA Antigenome

The very first antisense RNA synthesized from the positive-strand HCV RNA genome is very important for the proceeding RNA synthesis, as this single antisense molecule is responsible to generate progeny positive-strands in 10 – 100 fold excess (Lohmann, 2013). Structure determines the function, and in this case the antisense RNA molecule attains a totally different 3D structure

compared to sense RNA molecule. While the 5′-end of the positive-strand RNA genome folds into a complex IRES structure that mediates translation, the corresponding 3′-end of the negative-strand RNA adopts a completely different set of stem-loop structures instead of forming a mirror of the structures in the positive-strand, likely due to different G-U pairs in the respective strands. The same principle applies to the 3′-end of the positive-strand RNA genome, which completely differs from the 5′-end of the negative-strand RNA (antigenome) (Fricke et al., 2015). The distinct secondary structure folding patterns (Figure 1.2) (Dutkiewicz et al., 2008) observed in negative-strand RNA (antigenome) suggests, that it may harbour other *cis*-acting elements, potentially critical for the binding of the viral RdRp to 3′-end of the antigenome, thereby facilitating initiation of positive-strand RNA synthesis (Astier-Gin et al., 2005; Masante et al., 2008).

So far, numerous short-range and long-range RNA-RNA interaction possibilities have been elucidated among various *cis*-elements within the positive-strand RNA genome. These interactions play crucial roles in regulating viral translation and/or replication (Niepmann et al., 2018). The existence and the potential role of such kind of *cis*-elements on the negative-strand RNA genome are not yet well understood. Further research is required to determine whether RNA-RNA interactions occur between the elements of positive- and negative-strand RNAs, and whether such interactions may influence the efficiency or regulation of viral RNA replication.

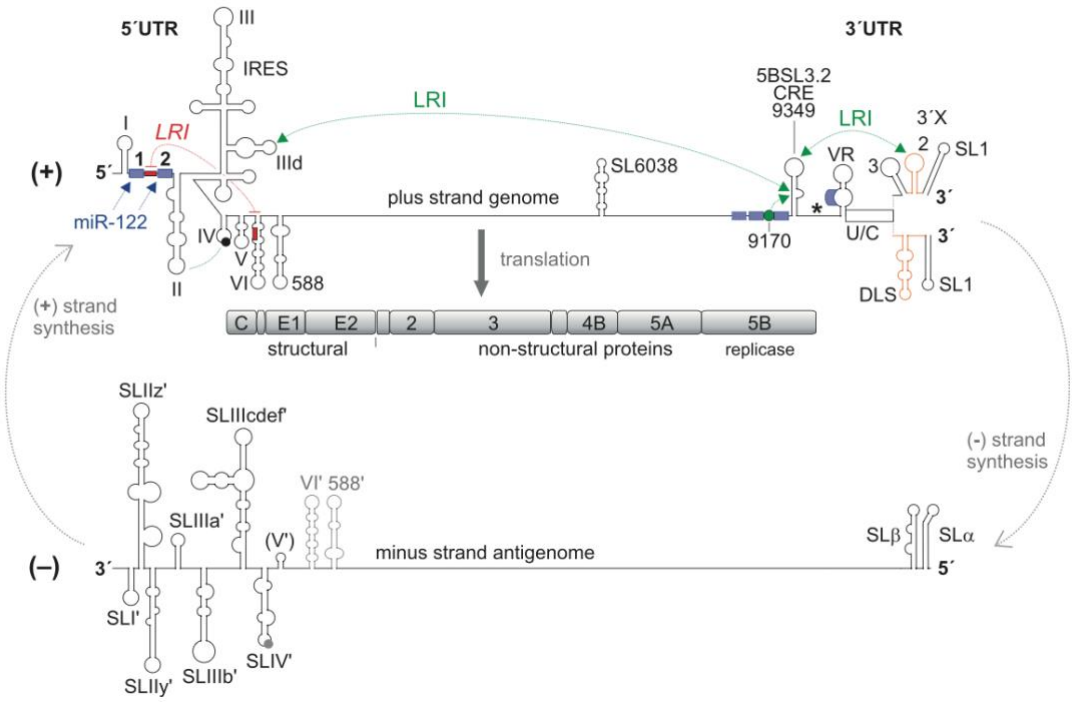

Figure 1.2. Schematic representation of the secondary structure of HCV positive-strand RNA genome and the complementary negative-strand RNA (antigenome). The 5′UTR of the positive-strand RNA genome comprises four stem-loop domains, SLI, SLII, SLIII and SLIV, while the black dot represents start-codon (AUG). The complementary 3′-region in negative strand forms different set of stem-loops. The 3′UTR of the positive-strand RNA genome comprises either two or three stem-loops, while the corresponding 5′-region in negative strand exhibits two stem-loops. Long-range interactions (LRI) within the positive-strand RNA genome are shown in red and green (Niepmann et al., 2018).

1.6. Translation of Hepatitis C Virus Genome

The 9.6 kb long HCV positive-strand RNA genome comprises one single ORF, where the presence of the IRES within the 5′UTR region eliminates the need for 5′-end capping for the initiation of translation. A short overview about the mechanism of IRES-mediated translation initiation in HCV is described in the following paragraph.

1.6.1. HCV Translation

IRES-mediated translation initiation differs from canonical eukaryotic translation initiation, which requires two key messenger RNA modifications: 5′-end capping by 7-methylguanylate and 3′ polyadenylation. In contrast, the IRES is capable of recruiting translation initiation components without any requirement of capping (Hellen et al., 2001). The HCV-IRES is located within the 5′UTR of the HCV positive strand RNA-genome and is arranged in a specific three-dimensional manner specialized for initiation of translation. The HCV-IRES spans from SLII of the 5′UTR up to SLIV, where the smaller sub domains (a - f) of the SLIII contain the binding sites for the ribosomal 40S subunit as well as the translation initiation factor eIF3. The IRES elements of Poliovirus (PV) and Encephalomyocarditis Virus (EMCV) were the first IRES elements discovered in the late 1980s (Pelletier et al., 1988; Jang et. al., 1988).

Although numerous aspects of the tightly regulated IRES-mediated translation-initiation in HCV have been elucidated, a concise overview is presented in the following lines. The whole mechanism can be summarized in three steps. The **first step** is the formation of a high affinity IRES binary complex with the ribosomal 40S subunit (Figure 1.3). A conserved ^{266}GGG^{268} sequence present at the SLIII sub-domain -IIId binds the ^{1116}CCC^{1118} of the expansion segment 7 (ES7) of the ribosomal 40S subunit with high affinity (K_D = 2 – 4 nM). This binding is the crucial anchor for the binary complex formation. Deletions or substitution of ^{266}GGG^{268} lead to decreased binary-complex affinity and IRES activity (Kieft et al., 2001; Malygin et al., 2013; Matsuda et al., 2014). The **second** step is the formation of the 48S PIC (preinitiation complex), in which the multi-subunit eIF3 complex and the Met-tRNA$_i^{Met}$-eIF2-GTP ternary complex are recruited to the 40S:IRES binary complex. In the **third step**, the initiation complex is completed as soon as the 60S subunit joins the 48S PIC. The procedure requires GTPase activation of eIF-2GTP by eIF5, GTP hydrolysis by eIF5B and dissociation of the factors. In the complex 80S-IRES-tRNA$_i$ the initiator tRNA is placed at the P-site, base paired with the start codon AUG present within the SLIV (Figure 1.3) (Johnson et al., 2017).

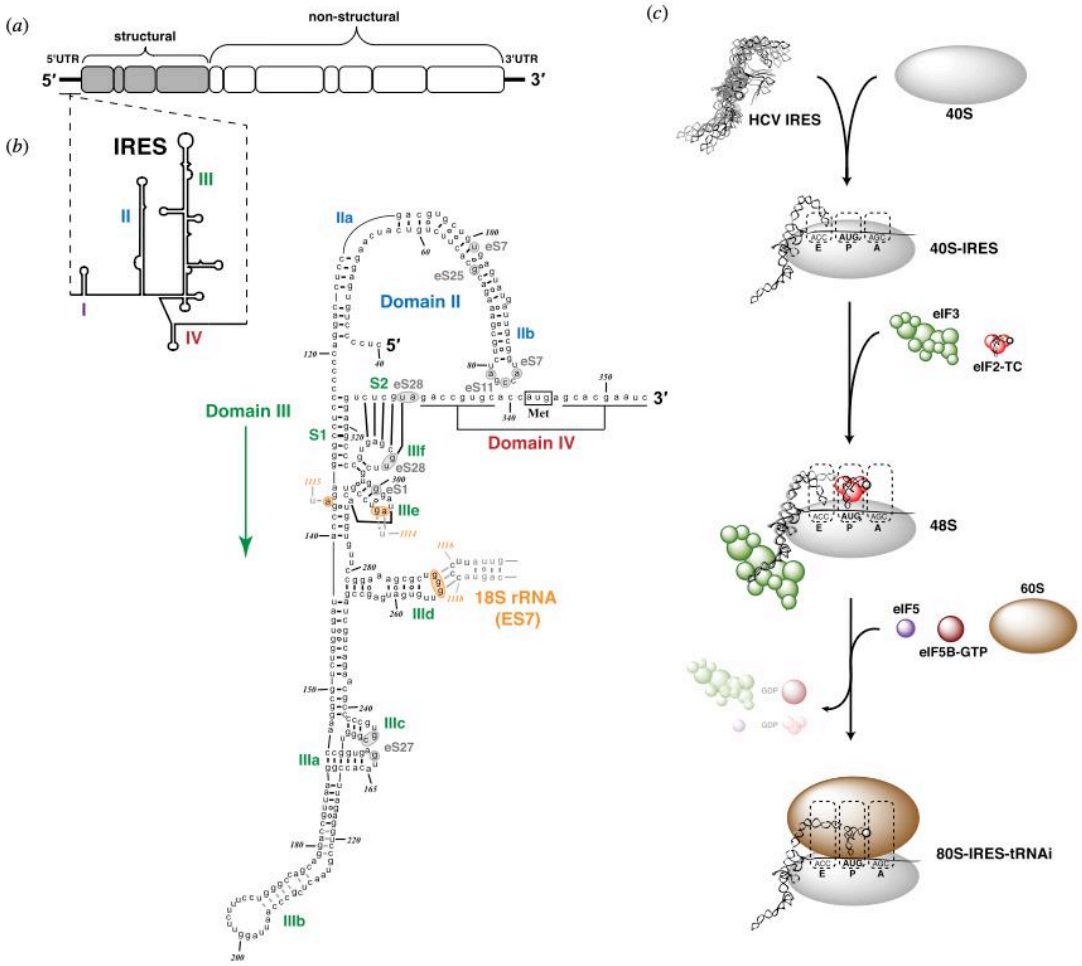

Figure 1.3. Mechanism of IRES-mediated translation in HCV. (a) Schematic representation of the HCV positive-strand RNA genome. (b) Secondary structure of SLI-IV in the 5′UTR. An intramolecular interaction is shown between SLII (blue labelling) and SLIV (red labelling). The 40S:IRES complex is formed by binding of SLIII domain IIId with Expansion segment 7 (ES7) of the ribosomal subunit through GGG base pairing. (c) IRES-mediated translation initiation. Formation of 48S PIC (preinitiation complex): eIF3 complex and the Met-$tRNA_i^{Met}$-eIF2-GTP ternary complex are recruited to 40S: IRES binary complex, the 60S subunit joins the 48S PIC forming the 80S-IRES-$tRNA_i$ complex (Johnson et al., 2017).

1.6.2. Regulation of Translation

Adaptability of the virus to unfavourable environmental conditions allows it to sustain translation via alternative pathways, even under stress conditions where eIF2 is inactivated through phosphorylation. Alternative factors include eIF3/eIF5B, eIF2A or eIF2D (Niepmann & Gerresheim, 2020 and References therein). Moreover, elevated intracellular Mg^{+2} concentration favours the binding of IRES with 40S subunit, thus manipulating the regulation of translation initiation (Kieft et al., 2001; Johnson et al., 2017 and references therein).

Translation in HCV is also regulated by cellular factors, namely IRES Trans-Acting Factors (ITAFs), which modulate HCV IRES activity. The factors often contain multiple RNA-recognition motif domains of other RNA binding domains which not only bind to 5′UTR/IRES but sometimes also to 3′UTR. The ability to bind both 5′ and 3′-ends, as well as the proteins such as 40S and eIF3, suggests a possible formation of an extensive network that connects all components of the translation initiation

machinery. Proteins binding directly to HCV RNA and positively affecting HCV translation include La, NSAP1, hnRNP L and D, IMP1, PCBP2 and LSm1-7 complex, whereas Gemin2 is supposed to affect the HCV translation negatively (Niepmann et al., 2020 and references therein).

1.6.3. HCV Proteins

The HCV positive-strand RNA genome encodes a single polyprotein, which is further processed co-translationally and post-translationally into viral structural and non-structural proteins (Figure 1.4).

Structural proteins include core and the glycoproteins, E1 and E2. Core protein (~ 21 kDa) is responsible for the nucleocapsid formation of HCV. From the emerging polyprotein, it is first cleaved by ER signal-peptidase into a (191 aa) immature form which is further processed by signal peptide-peptidase (SPP) into the mature 21 kDa (117 aa) core protein. Besides virion assembly and RNA chaperon activity, the core protein is also involved in interactions with several cellular factors (Moradpour and Penin, 2013 and references therein).

The highly glycosylated envelope proteins E1 (35 kDa) and E2 (70 kDa), cleaved by ER signal-peptidase, form heterodimers which are connected to each other through disulfide bonds (Vieyres et al., 2010). Each of the E1 and E2 proteins consists of a C-terminal transmembrane domain (~ 30 aa) and a larger N-terminal ectodomain (~ 160 aa and ~ 360 aa for E1 and E2, respectively) which are translocated into the ER lumen during synthesis. Both structural proteins, E1 and E2, play direct roles in viral assembly and virus-host interactions, particularly through their engagement with host cell receptors such as CD81 and scavenger receptor class B type 1 (Moradpour and Penin, 2013 and references therein).

Non-structural proteins include P7, NS2, NS3, NS4A, NS4B, NS5A and NS5B (RdRp). P7 (~ 7 kDa) belongs to the viroporin family, forming hexamers or heptamers with cation channel activity. The protein is cleaved by ER signal-peptidase. Though not relevant for viral replication *in vitro*, P7 plays a vital role for HCV infection *in vivo* as well as for assembly and release of infectious HCV particles *in vitro* (Steinmann and Pietschmann, 2010).

NS2 (~ 23 kDa) is a viral cysteine protease which mediates the site-specific cleavage of the precursor polyprotein at the NS2/NS3 junction. This proteolytic cleavage is essential to release functional NS3, enabling it to participate in downstream cleavage events and to promote viral replication.

The protein NS3 (~ 70 kDa) performs its enzymatic function as NTPase/RNA helicase as well as serine protease, in association with the neighbouring protein NS4A (~ 8 kDa) acting as a cofactor. NS4A is also involved in HCV RNA replication and virus particle assembly (Lindenbach et al., 2007; Murray et al., 2008). The NS3-4A complex mediates the cleavage of the precursor polyprotein at four junctions, namely NS3/4A (self-cleavage), NS4A/4B, NS4B/5A and NS5A/5B. Moreover, it is also involved in the cleavage and thus the resulting inactivation of mitochondrial host protein, the RIG-I adaptor MAVS. Besides replication, the NS3-4A complex plays essential role in persistence and pathogenesis of HCV. For that reason, it has been explored as a potential target for the development of direct acting antiviral drugs (Moradpour and Penin, 2013 and references therein).

NS4B (~ 27 kDa) has been reported to be directly involved in the induction of membranous web, the partially isolated membrane chambers for HCV replication (Moradpour and Penin, 2013 and references therein). By electron microscopy the NS4B protein has been shown to introduce significant disorder and discontinuities among synthetic membranes (Ouldali et al., 2021). This activity underscores its essential role in remodelling intracellular membranes to form the specific structure of the membranous web during viral replication. Being a master organizer of HCV

replication complexes, NS4B is also an attractive target for antiviral drug development (Rai & Deval, 2011).

NS5A (~ 58 kDa) is a phosphoprotein capable of RNA binding and is directly involved in the regulation of viral replication and assembly. The hypo-phosphorylated form (p56) is associated with replication, while the hyper-phosphorylated form (p58) is involved in assembly (Lohmann et al., 2013). During the viral assembly events, NS5A interacts with core protein at lipid droplets (LDs), with apolipoprotein E (ApoE) (Lindenbach et al., 2013) and with the cellular membrane sorting protein Annexin A2 (Backes et al., 2010).

NS5B (~ 68 kDa), as mentioned above, is the RNA dependent RNA polymerase (RdRp) and functions as the key catalytic component of the HCV replication machinery, synthesizing both positive- and negative-strand viral RNAs. The structure of NS5B (RdRp) resembles a right-hand model with three subdomains namely fingers, palm and thumb subdomains (Moradpour and Penin, 2013 and references therein). The active/catalytic site of the enzyme is situated in a groove formed by the interaction between fingers and thumb subdomains and is further provided by a ß-loop protruding from the thumb domain to avoid the binding of a duplex RNA (Long et al., 2021). The catalytic site contains a specific amino acid sequence GDD (Gly, Asp, Asp), which is considered as a hallmark for all RdRps. In RdRp, divalent metal ions such as Mg^{2+} or Mn^{2+} function as essential cofactors, which are coordinated between Asp 318 (the middle one from the hallmark GDD) and Asp 220 located in the palm domain of the enzyme. Deletion or substitution of one or both aspartate residues disrupts this coordination, impairing metal ion binding and consequently abolishing the polymerase activity of RdRp (Lohmann et al., 1997).

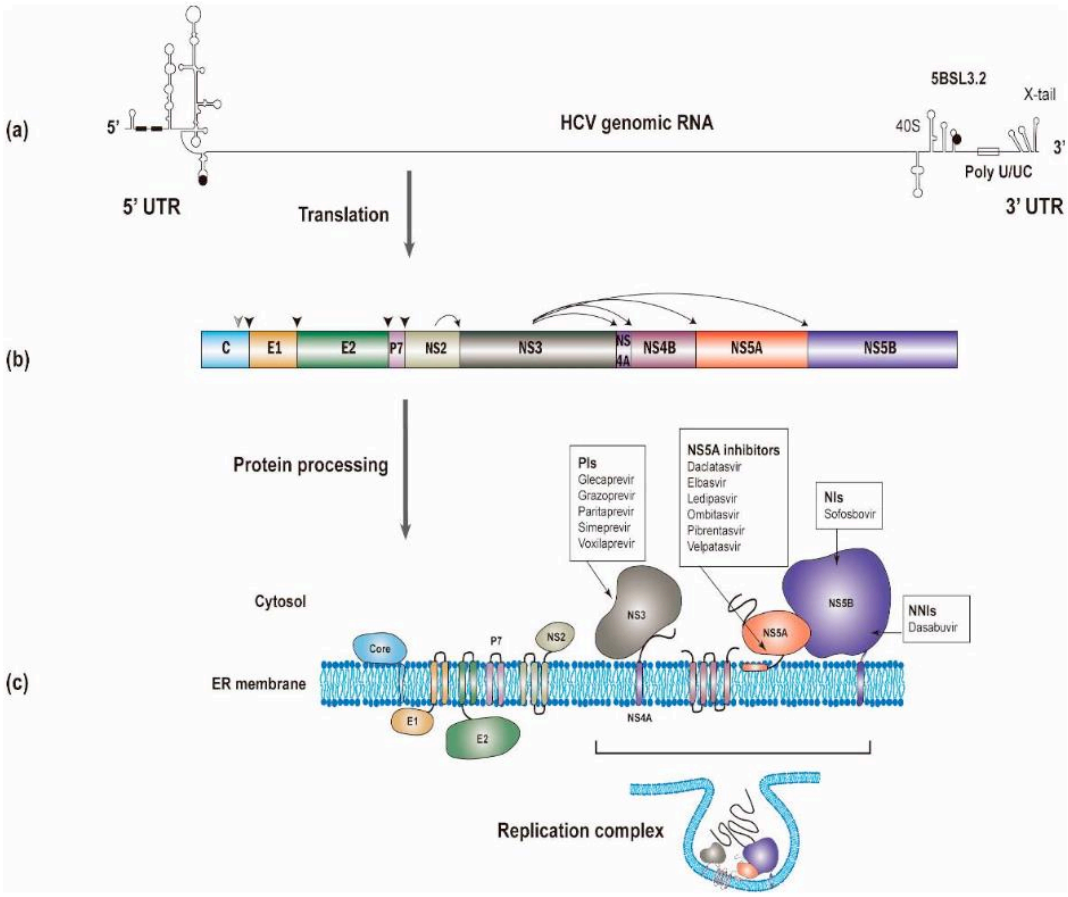

Figure 1.4. Translation of the HCV positive-strand RNA genome into a polyprotein, followed by processing and generation of individual HCV proteins. The positive-strand RNA genome with start and stop codons marked by black circles (a) translates into single polyprotein (b) which is processed co- and post-translationally into ten viral proteins which are associated directly or indirectly with the endoplasmic reticulum (c). Non-structural proteins –NS3, NS4A, NS4B, NS5A and NS5B – are involved in the replication organelle (RO) formation (Li et al., 2021).

1.7. Replication of Hepatitis C Virus

Unlike the situation with HCV translation, the Hepatitis C Virus uses its own replication machinery – the RNA dependent RNA polymerase (RdRp) – to replicate its genome within the hepatocytes. Most of the non-structural viral proteins, from NS3 to NS5B, along with the complete 5′ and 3′ UTR regions, are involved in the formation of viral replication complex. A crucial step in genome replication is the formation of viral replication organelles (RO) through compartmentalization of endoplasmic reticulum (ER) membranes, resulting in the structure known as membranous web. The vesicular membrane alterations are induced by viral protein NS4B within HCV-infected hepatocytes (Binder et al., 2013).

1.7.1. Formation of Replication Organelles (ROs)

The **ROs** (Figure 1.4) comprise mainly double membrane vesicles (DMVs) and multi-membrane vesicles (MMVs), which provide an isolated environment for the replication complex, preventing the replication intermediates from nucleases and proteases as well as from innate immune system detector proteins present in the surrounding cytosol. The formation of a membranous web is also a

characteristic feature of other positive-strand RNA viruses, such as coronavirus, picornavirus and norovirus (Wolff et al., 2020; Li et al., 2021). Under electron-microscopy, the DMVs (situated in the cytoplasm very near to LDs) are primarily observed as closed structures. However, a few appear to be connected to cytosol through small openings, likely allowing the influx of nucleotides and metabolites (Romero-Brey et al., 2012).

1.7.2. Viral and Cellular Factors Supporting RO-formation

Among all viral non-structural proteins only NS5A is specifically involved in DMV formation on its own (Egger et al., 2002; Romero-Brey et al., 2012/ 2015) which is enhanced when other NS proteins like NS3, NS4B and NS5B are also expressed (Li et al., 2021).

The viral NS proteins also recruit cellular factors to support the RO formation. For example, NS5A interacts with Cyclophilin A (Cyp A), receptor for activated protein C (RACK1) and ATG14L for the formation of ROs. In contrast, other cellular factors like Surf4 and PREB (prolactin regulatory element-binding) are recruited by NS4B during RO formation. Shaping of the ER membrane is associated with the modulation of the lipid environment to support the formation and maintenance of ROs. Lipid metabolism is regulated by SREBP (the sterol regulatory element-binding-protein) which is also involved in the expression of host cell genes required for lipid biosynthesis (Li et al., 2021). The viral proteins NS5A and NS4B activate the lipid kinase PI4KIIIα to produce appropriate amounts of phosphatidylinositol 4-phosphate (PI4P). PI4P supports transport of glycosphingolipids, cholesterol and ceramide for the formation of ROs through interaction with different lipid binding proteins like oxysterol-binding protein (OSBP), four-phosphate adaptor protein 2 (FAPP2), ceramide transfer protein (CERT) and NPC1 (Li et al., 2021). A certain level of PI4P is crucial for the RO-formation and, consequently, for HCV infection. When PI4P elevation is blocked by the interferon-stimulated gene C19orf66, HCV infection is inhibited (Li et al., 2021 and references therein). Moreover, factors related to macro-autophagy also play a very important role during RO-formation. The depletion of specific autophagy factors impairs HCV RNA replication and reduces the number of DMVs (Tabata et al., 2019).

1.7.3. HCV Replication Procedure

The minimal requirement for HCV replication is the presence of viral replicase, the RNA-dependent RNA polymerase NS5B, and HCV positive-strand RNA genome as a template within the ROs.

Replication begins with the synthesis of a complementary negative-sense RNA strand, which serves as a template for the production of further positive-strand HCV RNA molecules. The replication process can be divided into four steps: RNA binding, initiation, elongation and termination.

RNA binding to NS5B is a challenging step, as the 3′-end of the positive-strand HCV RNA genome, as mentioned above, contains a specific secondary structure composed of three or two stem-loop domains (Figure 1.2). The initiation-site, consisting of the terminal uridine (U), is concealed within the terminal base pair of the SL of the 3′ X-tail and thus is not readily accessible for binding to NS5B. The procedure requires cooperation of other non-structural proteins, such as the helicase activity of NS3, which facilitates the RNA binding and initiation. **Initiation** requires binding of GTP to an allosteric site of NS5B (ß-flap domain) resulting into conformational change of the replicase. GTP also facilitates the switch from initiation to **elongation**. NS5B elongates the entire RNA genome performing nascent RNA synthesis by 100 to 400 nucleotides per minute. The mechanism of termination remains to be elucidated (Li et al., 2021 and references therein). The newly synthesized negative-sense RNA contains a different kind of secondary structure, with a 3′-end easily accessible

for binding to NS5B, which makes it a better candidate as a template for further replication. Replication proceeds from the negative-strand, resulting in a ten- or hundred-fold higher abundance of the positive-strand RNA genome compared to the negative-strand RNA antigenome (Quinkert et al., 2005; Tabata et al., 2019; Li et al., 2021).

Along with NS5B (the viral RdRp), other non-structural proteins such as NS3, NS4A, NS4B and NS5A contribute to the replication process to various extents. Unwinding of nucleic acids (i.e., dsRNA intermediate) during replication is performed by the protein NS3 through its helicase domain. In association with NS3, the NS4A contributes to its helicase activity as well as to the HCV replication. Besides RO-formation, NS4B also undergoes oligomerization through self-interaction, which is important for the HCV replication (Gouttenoire et al., 2009). Moreover, only the combined action of NS3, NS5A and NS5B facilitates the initiation of replication from the specific HCV RNA template.

1.7.4. Regulation of Replication

Numerous regulatory viral and cellular factors affect directly or indirectly the HCV-replication. Very important among directly involved viral factors are, for example, the *cis*-elements residing within 3′UTR of the positive-strand RNA genome, as they facilitate the binding of NS5B for the initiation of overall replication. Being highly conserved, the sequence and the three-dimensional structure of 3′UTR of positive-strand HCV RNA genome is crucial for the replication. Another *cis*-acting element, i.e., CRE, present at SL3.2 position within the coding region of NS5B is directly involved in the initiation of replication (Niepmann et al., 2018). Binding of CRE to the apical portion of SL2 within the 3′UTR may give newly synthesized NS5B enough time for proper folding, and simultaneously positions it in close proximity to the 3′-end of the template RNA, facilitating efficient initiation of replication (Gerresheim & Hess et al., 2020).

The complete 5′UTR of the positive-strand RNA genome is necessary for the replication, and the same applies to the corresponding "opposite" 3′-end of the negative-strand which directly involves for the initiation of positive-strand RNA synthesis. However, the role of different *cis*-elements within both ends, i.e., 5′UTR of the positive strand and 3′-end of the negative-strand, remained to be further elucidated.

One of the cellular factors with a direct influence on HCV replication is the liver-specific microRNA-122 (miR-122). This approximately 22-nucleotide-long non-coding RNA is abundantly expressed in hepatocytes. In fact, it is the most highly expressed microRNA in hepatocytes. With approximately 660,000 copies per cell, it accounts for about 72 % of the total hepatocyte microRNA pool (Lagos-Quintana et al., 2002; Panigrahi et al., 2022). The positive-strand HCV RNA genome contains six target sites within 5′UTR, NS5B coding region and 3′UTR for miR-122 binding. Two of them are highly conserved, as described in the translation part, which are located between the SLI and SLII within the 5′UTR (Niepmann et al., 2018; Fricke et al., 2015). Binding of miR-122 to this region, in association with Ago2 protein, has revealed important roles during the HCV life cycle: (1) regulating translation and replication (2) acting as an RNA chaperone or ‘riboswitch’, (3) providing genome stability, (4) promoting viral translation, and (5) facilitating viral accumulation and virion assembly (Jopling et al., 2005; Niepmann et al., 2018; Rheault et al., 2023). A direct role of miR-122 in viral genomic RNA replication has been demonstrated in a study where miR-122 stimulated viral replication, leading to increased protein synthesis (Masaki et al., 2015; Panigrahi et al., 2022). In association with Ago2, miR-122 functions for the protection of viral genome from nucleolytic degradation by host 5′-3′ exoribonucleases 1 (XNR1) and XNR2 (Shimakami et al., 2012; Li et al.,

2013/2015). The NS5B-coding region and 3′UTR have shown varying results regarding their interaction with miR-122. According to one study, binding of miR-122 to NS5B-coding region directly correlates with genome replication (Gerresheim et al., 2017). However, a later study reported that miR-122 binding to NS5B region, IRES and 3′UTR contributes negligibly to viral protein expression, viral RNA accumulation and infectious particle production (Bernier and Sagan, 2019).

The highly conserved miR-122 binding sites between SLI and SLII of 5′UTR, known as S1 and S2, exhibit significantly different binding affinities (Nieder-Röhrmann et al., 2017). According to a study using an RNA probe representing the first 45 nucleotides (5′UTR) of the HCV genome (HCV45), the S1 site binds to miR-122 approximately 100 times more strongly than the S2 site. Poly (C) binding protein 2 (PCBP2) competes with miR-122 for binding to a 5′UTR region which overlaps S2. This competition is proposed to function as 'translation to replication switch': miR-122 binding promotes NS5B recruitment for replication, whereas PCBP2 binding facilitates genome circularization and promotes viral translation (Wang et al., 2011; Scott et al., 2023).

1.8. Replicon Systems used for the Study of HCV-Replication

The replicon systems enable the study of intracellular HCV replication, translation, life cycle and pathogenesis in cell culture models, reducing the time required and eliminating the need for animal models. The subgenomic replicon system comprises the full cassette of non-structural proteins (NS3-to-NS5B), along with the 5′ and 3′ UTR regions, representing the minimal requirements for replication and translation. In contrast, structural proteins required to virion assembly are missing from the subgenomic replicons. Using this principle, the first HCV subgenomic bicistronic replicon system, consensus 1 (Con 1), was generated from the consensus GT1b isolate by V. Lohmann in 1999. The bicistronic replicon system comprised of two gene clusters, (1) the first 16 codon of core protein fused in-frame to a selection marker, neomycin phosphotransferase gene (*neo*) downstream to 5′UTR, and (2) the NS3 to NS5B cassette along with the 3′UTR downstream to the IRES of the encephalomyocarditis virus (EMCV). The EMCV-IRES directs the translation of the NS3 to NS5B replication proteins. The bicistronic replicon system positioned downstream of the T7 promoter in a plasmid, is used as a template to synthesize RNA by conventional *in vitro*-transcription reaction. The *neo* gene, which confers resistance to G418, allows for the selection of "stable replicon cells" (Lohmann et al., 1999; Blight et al., 2000; Khan et al., 2020).

The basic classical bicistronic replicon-system described above has been widely used, with modifications tailored to specific study requirements. The basic system uses *neo* gene as a selection marker, which allows the generation of stable cell lines for replication studies. Due to its lengthiness and time-consuming nature, the use of *neo* gene was replaced by *firefly* luciferase (FLuc) or *Renilla* luciferase (RLuc) reporter genes. These allow transient transfection of the replicon system and enable detection of replication within hours, without the need for selection (Krieger et al., 2001; Lohmann et al., 2001; Khan et al., 2020). The inclusion of luciferase genes alongside the *neo* gene in the replicon system enables both selection and efficient detection of viral replication (Khan et al., 2020 and references therein).

Monocistronic replicons resemble the structure of viral genomes. The translation takes place directly under the influence of the HCV 5′UTR, as they lack the EMCV-IRES. In one example, the monocistronic model comprised the 5′UTR and first 12 codons of core sequence, followed by in-frame NS2 to NS5B sequence. Other examples involve the use of reporter genes under the control of the 5′UTR or selection markers such as hygromycin phosphotransferase, often combined with ubiquitin to enable specific cleavage (Khan et al., 2020 and references therein).

A practical modification of the bicistronic replicon system is the tricistronic model, which includes a third IRES – usually the poliovirus IRES – in-frame with a reporter gene such as the *firefly* luciferase gene. The 4th generation replicon system established and used during this work is one example of such a tricistronic replicon system. The system comprised three gene clusters: (1) HCV 5´UTR followed by downstream first 165 nucleotides of HCV core protein fused to C-terminal (3x) HiBiT-tag, (2) Poliovirus IRES (PV-IRES) with the *firefly* luciferase (FLuc) as downstream reporter gene, and (3) EMCV-IRES with the downstream NS3 to NS5B cassette followed by the complete HCV 3´UTR. However, the previously used 2nd generation and 1st generation replicon systems comprised only two gene clusters each (Supp. Figure 3.2.4). 3rd generation replicon system also comprised two gene clusters, which was modified to 4th generation replicon system after a series of optimization applications.

1.9. Limitations in Strand-Specific Detection

Studying the *cis*-elements on the HCV positive-strand RNA genome that are specifically involved in the initiation of RNA negative-strand synthesis during replication requires methods that allow direct and quantitative measurement of newly synthesized negative-strand RNA molecules. For the corresponding experiments, RNA corresponding to the replicon system is synthesized by *in vitro*-transcription, purified and transiently transfected to the host cells. The transfected HCV replicon RNA then undergoes the intracellular steps of an infection cycle within the host cells by starting replication of the viral RNA genome using its own replicase, the RNA-dependent RNA-polymerase, while viral translation is driven by host cell's translation machinery. After isolation of the HCV replicon RNA from the cells, reverse transcription followed by quantitative PCR (RT-qPCR) enables the detection and quantification of newly synthesized negative- and positive-strand RNA. The amount of viral proteins expressed from the progeny replicon RNAs within host cells serves an indirect measure of replication.

One parameter leading to false positive detection of replicon sequences during strand-specific RNA detection (RT-qPCR) is the detection of negative-strand sequences in the copurified double-stranded plasmid DNA used for the *in vitro*-transcription. Also, transfection of high amounts of replicon RNA can simply overload the sensitive negative-strand RNA detection assay. Moreover, the strong hairpin structure at the 3´-end of the positive-strand HCV RNA causes artificial self-priming and misleads the reverse transcriptase (RT) during the specific negative-strand RNA detection assay, thus producing non-relevant cDNA. These limitations of strand-specific detection can be observed from a previous result, where the non-replicating control of 1st generation replicon system also showed a high background signal for negative-strand RNA (Figure 1.5).

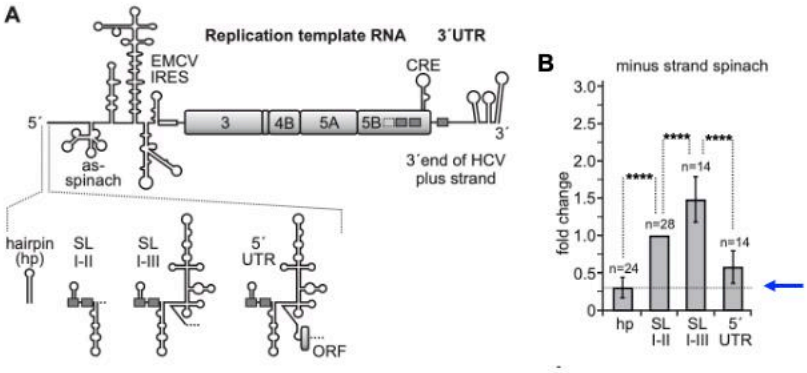

Figure 1.5. High background signals obtained from negative-strand RNA detection with previously used 1st generation replicon system. (A) Schematic representation of 1st generation replicon system along with different 5´UTR variants including hairpin structure hp, SLI-II, SLI-III and complete 5´UTR with initiation codon and a short ORF. (B) Negative-strand RNA abundance detected at 48 hpt. Signals of negative-strand RNA abundance in hairpin hp reaching nearly 1/4th of the level in SLI-II (blue arrow), indicating a high background (Shalamova, unpublished data).

A detailed overview about the effect of above-mentioned parameters on the specificity of the strand-specific measurement is given below.

1.9.1. Detection of Copurified Plasmid DNA

As described above, the RNA corresponding to the replicon system is *in vitro*-transcribed using a plasmid DNA as a template. The complete removal of the template DNA from the RNA to be transfected is crucial for the success of the method. The usual method applied for the removal of plasmid DNA is digestion with DNase followed by purification of the RNA. The enzyme DNase I, being a non-specific endonuclease, cleaves the phosphodiester bonds randomly digesting the template DNA into smaller fragments; however, these DNA fragments may hybridize to the *in vitro*-transcribed RNA. There is a high probability that the DNA-fragments hybridizing tightly to the RNA are copurified and enter the host cells along with the RNA during transfection. Due to their small size and negligible quantity, these fragments cannot be detected by gel-electrophoresis. However, they can contaminate the re-extracted total RNA (including the HCV replicon RNA) and distort the actual RT-qPCR signals by providing unwanted primers that generate false positive RT-qPCR signals in the negative-strand RNA detection assay.

1.9.2. Disturbance by high Amounts of Input RNA

The *in vitro*-transcribed positive-strand replicon RNA functions within the host cells when transfected in high amounts such as 2.5 – 4 µg for each well of a 6-well plate. However, only a small fraction of the transfected RNA actually establishes functional replication complexes and subsequently becomes protected by lipid membranes, whereas a large proportion of the transfected RNA is partially degraded but cannot be completely eliminated by the host cell immune response. Consequently, these small RNA fragments can overload the sensitive strand-specific RT-qPCR detection and act as unwanted primers in the RT-qPCR (Dobson et al., 2023).

1.9.3. Self-Priming by the strong 3´-end Hairpin Structure of the HCV RNA Genome

The 3´UTR of the positive-strand RNA genome can possibly attain two different secondary structures, one comprised of three stem loops, SL1, SL2 and SL3, and the other one undergoes a structure with two stem loop domains (Figure 1.2). In both cases, the extreme 3´-end folds into a stable hairpin structure making it less accessible to the viral replicase (RdRp), which may explain the limited number of negative-strands produced during replication. However, the same structural arrangement can have a different effect during reverse transcription, as the stable hairpin maybe mistakenly recognized as a template/primer site by the reverse transcriptase (RT) (Figure 1.6) (Schenborn et al., 1985; Triana-Alonso et al., 1995; Gholamalipour et al., 2018). Thus, the positive strands serve as a false template for RT, while the 3´-end of the refolded part of the hairpin acts as a primer ("Situation III" in Figure 1.6), leading to the synthesis of cDNA that falsely represents negative strands (since they are produced only by the detection method itself but not by the viral replicon system under investigation).

In addition, the strong hairpin structure at 3´-end of the positive-strand replicon RNA can likewise also mislead the T7 polymerase already during the *in vitro*-transcription reaction (i.e., even before the replicon RNA is transfected) (Figure 1.6). It is also hypothesized, that the T7 jumps from the 5´-end of the actual DNA template strand to the strongly folded 3´-end of the complementary DNA strand, instead of terminating at the 5´-end of the "regular" template DNA strand (Schenborn et al., 1985; Triana-Alonso et al., 1995; Nacheva et al., 2003; Gholamalipour et al., 2018). Thus, the T7 RNA polymerase runs back either on its template DNA ("Situation I" in Figure 1.6) or even on the just freshly made RNA product itself ("Situation II" in Figure 1.6), and by that the positive-strand RNA synthesized by *in vitro*-transcription is extended with the opposing sequence corresponding to negative-strand RNA sequences. These extensions that represent negative-strand RNA sequences, made by artificial copy-back priming as a side-effect of the method, also interfere with the actual RT-qPCR signals of the viral replicon system under investigation (Figure 1.6).

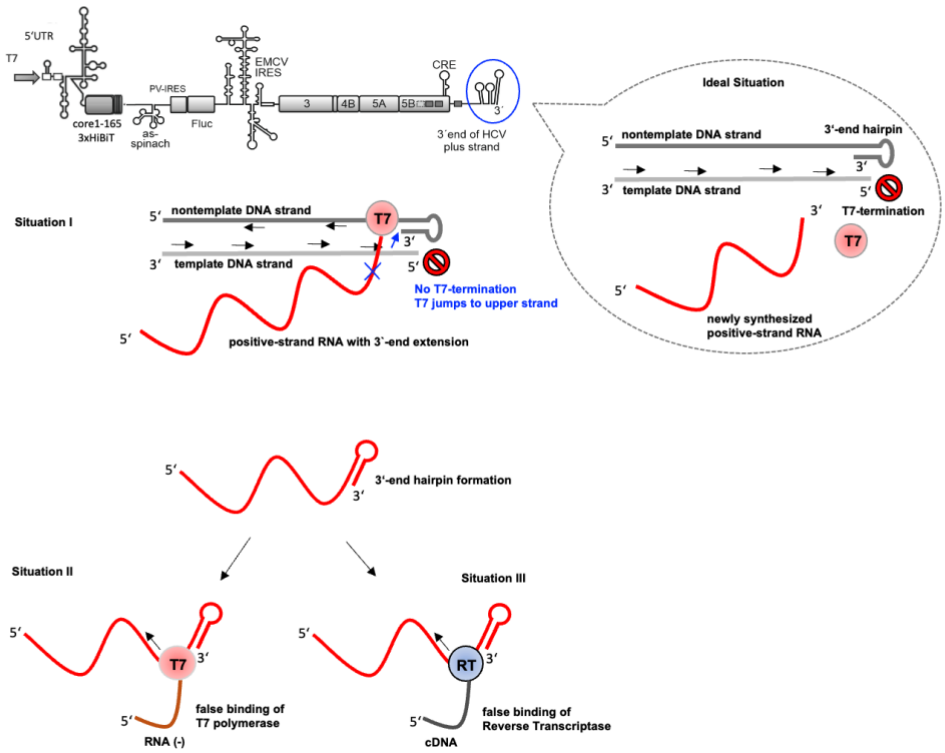

Figure 1.6. Illustration of the proposed copy-back transcription mechanism due to 3´-end priming in the complementary template DNA strand. During *in vitro*-transcription, the T7 polymerase (pink) normally terminates at the 5´-end of the template DNA (light grey). Ideally, the T7 polymerase should terminate at the 5´-end of the template DNA (Ideal Situation). Instead, 3´-end looping redirects it to the complementary DNA strand (dark grey), leading to continued RNA synthesis. The resulting RNA (red) corresponds to HCV subgenomic positive-strand RNA but carries extensions corresponding to the negative-strand RNA (antigenome) which correlate with actual RT-qPCR signals (Situation I). Moreover, binding of T7 polymerase to a false template (the positive-strand RNA transcript), due to the 3´-end hairpin can also lead to the synthesis of negative-strand RNA already during *in vitro*-transcription reaction (Situation II). Finally, also binding of reverse transcriptase during RT-qPCR to the false template (the positive-strand RNA with a 3´-end hairpin) can result in the synthesis of cDNA that falsely represents negative-strand RNA (Situation III).

1.10. Strategies to overcome Limitations in Strand-Specific Detection Assay

1.10.1. Previously Applied Strategies (not included in this study):

Several methods have been applied previously to improve the quality of replicon RNA; a few are briefly described below. *In vitro*-transcription reaction was performed using high temperature "Hi-T7" polymerase, which was supposed to function more specifically than conventional T7 polymerase by minimizing copy-back self-priming events (Dissertation Jonas Budnik). Another approach involved the use of Blocker- and Capture-oligos added during the *in vitro*-transcription reaction (Gholamalipour et al., 2018; Dissertation Jonas Budnik), which were intended to reduce the likelihood of false T7 binding by blocking the SL3 structure at the 3´-end. In another approach, biotinylated DNA was used as a template for *in vitro*-transcription, allowing to subsequently remove the plasmid template DNA from the *in vitro*-transcribed RNA using streptavidin magnetic beads (Dissertation Jonas Budnik). However, against all expectations, these strategies could not improve

(i.e. lower) the background signals during RT-qPCR reaction. To achieve more effective DNA removal, various purification strategies were applied including LiCl precipitation, gel filtration, DNase digestion using TURBO-DNase and phenol/chloroform extraction. A combination of gel purification and TURBO-DNase-digestion followed by phenol/chloroform extraction resulted in a relatively better suppression of background signals in RT-qPCR. However, this three-step purification approach proved impractical, as it significantly reduced the overall RNA yield below levels required for downstream use (Dissertation Jonas Budnik).

1.10.2. Strategies Applied in the present Study

Improvement strategies were applied for all stages of the strand-specific detection assay, which include synthesis of replicon RNA, transfection, total RNA extraction, reverse transcription and final quantitative PCR.

Strand-specific detection is only reliable when both the transfected RNA and the extracted total RNA are of a high purification quality. For the removal of template DNA after *in vitro*-transcription reaction, TURBO DNase digestion followed by column purification using Monarch Spin RNA Cleanup Kit (NEB) was performed twice. Other strategies proved unsuccessful, including CsCl gradient purification of the RNA, gel purification and gel filtration through column purification.

During isolation of RNA from the cells transfected with the *in vitro*-transcribed replicon RNAs, complete removal of genomic DNA is crucial for obtaining high-quality total RNA. To achieve this, after the standard TRIzol purification of the RNA from the transfected cells, additional DNase digestion was performed twice using two different enzymes, DNase I (NEB) and TURBO DNase (Thermo-Fischer-Scientific), with a subsequent step of phenol/chloroform extraction using acidic phenol (pH ~ 4.5) which selects for RNA over DNA during isolation, further followed by column purification of the RNA using the Monarch Spin RNA Cleanup Kit (NEB)) (please also see section 2.2.4.6).

The methods described above can help ensure higher-quality total RNA by effectively eliminating nearly all DNA contamination. However, also the presence of large amounts of input RNA poses an additional challenge by interfering with RT-qPCR signal accuracy. Here, the strategy of labelling nascent RNA in the cells with 5-ethynyl uridine (5EU) was applied. A click chemical reaction facilitates binding of biotin molecules to the 5EU-labelled RNA fraction within the total RNA. The biotinylated RNA can then be pulled down using streptavidin magnetic beads. This step highly selectively enriches only RNA which was newly synthesized within the cells after transfection, including newly synthesized HCV negative and positive strands, but at the same time avoids the transfected input RNA, the contaminating input DNA, as well as residual cellular DNA and RNA that may have escaped the other purification procedures.

To improve specificity of RT primers, a tag sequence (~ 30 nt) was added at the 5′-end of primers used for reverse transcription (Dobson et al., 2023). The qPCR primers were designed accordingly to complement the tag. Use of such artificial unique tag sequences largely improves RT and qPCR specificity.

The stable hairpin structure at the 3′-end of the transfected HCV positive strand replicon RNA posed another challenge, which was addressed by maintaining elevated temperatures throughout the RT-qPCR procedure. This included preheating the template RNA and primer at 70 °C, mixing the reverse transcription reaction components at 70 – 65 °C and conducting the reverse transcription itself at 65 °C. The high-temperature RT was followed by high-temperature quantitative PCR at 62 °C.

1.11. Aim of the Project

Hepatitis C Virus (HCV) infection can lead to liver cirrhosis and hepatocellular carcinoma, if not diagnosed in time and left untreated. Although direct acting antiviral drugs (DAAs) offer effective treatment options for HCV infection, the development of a vaccine is still ongoing. Therefore, a deeper understanding of all aspects of the viral life cycle is needed, including both viral and cellular factors that influence replication, translation and genome stabilization.

The replication of the HCV positive-strand RNA genome involves the synthesis of an intermediate negative-strand RNA antigenome, which appears to be a rather complex process. From one aspect, both replication and translation are regulated by the 9.6 nt long positive-strand RNA genome itself. It features a characteristic tertiary structure with various *cis*-acting elements, which induce subtle conformational changes whether facilitating ribosome-binding at the 5′-end for translation or recruiting polymerase (RdRp) to the 3′-end for replication. Several such regulatory *cis*-acting elements and the mechanisms related to their functions have been studied in detail over the past decade, however, those involved specifically in the initiation of negative-strand RNA-synthesis remain to be elucidated. Identifying those *cis*-elements is the primary objective of this study.

The first major challenge of this project is to fully decouple the replication process from translation. The next challenge is to isolate the initiation of replication from the overall replication process. Initiation refers to the synthesis of negative-strand RNA using the positive-strand RNA genome as a template, whereas overall replication refers mainly to the production of the progeny positive-strand RNA using the negative-strand as a template. The positive and negative strands adopt completely different secondary structures. Studying the role of specific *cis*-elements within a single genome using mutations presents another challenge, as a mutation in the 5′UTR of the positive-strand RNA genome can alter the structure and function of the corresponding 3′UTR in the negative-strand. Precisely attributing a specific role to an individual *cis*-acting element remains a significant challenge.

In addition to the challenges described above, the study also involves a number of technical difficulties. The study of individual *cis*-elements in initiation of replication requires the use of a replicon system, where three main obstacles are encountered during strand-specific detection that strongly contribute to the background signals: false priming (1) during *in vitro*-transcription and (2) during reverse transcription due to the strong hairpin structure at the 3′-end of the RNA genome and (3) contaminating residual plasmid DNA that serves as a false template during cDNA synthesis. A replicon system, in combination with an optimized strand-specific RNA detection assay, is required to overcome all above-mentioned obstacles and to enable a more detailed study of the *cis*-elements involved in initiating the synthesis of HCV RNA antigenome molecules during replication.

2. Materials and Methods

All the materials and methods used during this work are described below.

2.1. Materials

2.1.1. Cell lines

The main experiments were performed using Huh-7.5 cells from AG Niepmann laboratory, originally provided from Charlie M. Rice laboratory, Rockefeller University, USA. Huh-7.5 cells, derived from Huh-7 cells, are highly permissive for the HCV replication due to the mutational inactivation of interferon responsive genes, likely including the innate sensor RIG-I (Blight et al., 2002; Sumpter et al., 2005). Huh-7 is a hepatocyte-derived carcinoma cell line established in Sato Laboratory, Okayama, Japan. The cell line HepG2 was used for a comparison of replication capability during optimization series of experiments. It has been derived in 1975 from the liver tissues of an Argentinian male with well-differentiated hepatocellular carcinoma (Nakabayashi et al., 1982). All cell lines used during this work are shown in the table 2A.

Table 2A: Cell lines with their sources used for experimental as well as optimization purposes during the work

Name	Source
Huh-7.5 (passage no. 22)	AG Niepmann
Huh-7	
Huh-7.5 (passage no. 48)	Kindly provided by Prof. Dr. Charles M. Rice, via Prof. V. Lohmann, Molecular Virology, Universitäts Klinikum Heidelberg
HepG2	

2.1.2. Plasmids

The 4th generation replicon system comprises a set of eight plasmids, including one wild-type (WT) and one polymerase deficient construct (NGND) for each condition. The replicon system includes 5′UTR (variants) placed under either a T7 or a SP6 promoter, followed by *firefly* luciferase sequence under poliovirus IRES. The NGND constructs carry mutations within the active site of the NS5B RNA-dependent RNA polymerase, in which the aspartic acid residues D220 and D318 are substituted with asparagine residues (N220 and N318). This substitution inhibits polymerase function by preventing the binding of Mg^{2+} ions, which are essential cofactors. The negative control 'hp' contains a hairpin-like structure as a substitute of 5′UTR region, primarily providing stability to *in vitro*-transcribed RNA. The constructs SLI-II and SLI-III represent partial 5′UTR sequences, including stem loop I to II and I to III, respectively. SLI-III ΔIIIb represents the deletion of IIIb (eIF3 binding) region within stem loop II, while mutIIId/e refers to the mutation in stem loop regions IIId (GGG → CCC) and IIIe (GAUA → GAAA). The 5′UTR constructs consist of complete 5′UTR region along with core (AA 1 - 165) fused in-frame with the HiBiT tag. All plasmids designed or used during this work are listed in Table 2B to 2F below. Maps of representative plasmids are shown in supplementary figures 2.1 – 2.9. Maps of representative members of these plasmid families can be found in the appendix, and the "logical" organization of the replicon system expression cassette of the plasmids is shown in Fig. 3.2.1.

Table 2B: Plasmids representing 4th generation replicon system with their sizes and source designed during the work

Name	Size (bp)	Source
T7_hp_Fluc (WT/ NGND)	12.187	This work
T7_SLI-II_Fluc (WT/ NGND)	12.203	
T7_SLI-III_Fluc (WT/ NGND)	12.415	
T7_SLI-III_ΔIIIb_Fluc (WT/ NGND)	12.369	
T7_SLI-III_mutIIId/ IIIe_Fluc (WT/ NGND)	12.415	
T7_5′UTR_core_Hibit_Fluc (WT/ NGND)	13.113	
T7_5′UTR_ΔIIIb_Fluc (WT/ NGND)	13.067	
T7_5′UTR_mutIIId/ IIIe_Fluc (WT/ NGND)	13.113	
SP6_hp_Fluc (WT/ NGND)	12.187	
SP6_SLI-II_Fluc (WT/ NGND)	12.203	
SP6_SLI-III_Fluc (WT/ NGND)	12.415	
SP6_SLI-III_ΔIIIb_Fluc (WT/ NGND)	12.369	
SP6_SLI-III_mutIIId/IIIe_Fluc (WT/ NGND)	12.415	
SP6_5′UTR_core_Hibit_Fluc (WT/ NGND)	13.113	

Table 2C: Plasmids representing 3rd generation replicon system with their sizes and source designed during the work

Name	Size (bp)	Source
3rd_gen_HCV_core_EMCV-pUC18_10820 (WT/ NGND)	10.820	This work
3rd_gen-ins-2nd_gen_BB-SbfI_BbvCI (core-HiBiT) (WT/ GND)	10.860	
3rd_gen-ins-2nd_gen_BB-SbfI_BbvCI (core-HiBiT) (NGND)	10.860	
2nd_gen-ins-3rd_gen_BB-SbfI_BbvCI (WT/ GND)	10.193	

Table 2D: Plasmids representing 2nd generation replicon system with their sizes and source used during the work

Name	Size (bp)	Source
pUC18_P.s._WT_SLI-III_10182 (WT/ GND)	10.233	AG Niepmann

Table 2E: Donor plasmids used for the cloning of the 4th generation replicon system with their sizes and sources

Name	Size (bp)	Source
pUC18_P.s._WT_SLI-III_10182 (WT/ GND)	10.233	AG Niepmann
3rd_gen_HCV-core_EMCV-wo-NS3-5B-pUC18	5230	BioCat
3rd_gen_hp_cap_iSpinach in pUC18	3760	
3rd_gen_hp_T7-long in pUC18	3019	
3rd-gen-SLI-II.dna in pUC18	2795	
3rd-gen-SLI-III.dna in pUC18	3007	
3A-deltaIIIb-3rd-genSLI-III.dna in pUC18	2961	
3B-IIIdCCC-IIIeGAAA-3rd-genSLI-III.dna in pUC18	3007	
4A-deltaIIIb-3rd-gen-5UTR.dna in pUC18	3659	
4B-IIIdCCC-IIIeGAAA-3rd-gen-5UTR.dna in pUC18	3705	

Table 2F: Plasmids used as positive control during this work with their sizes and source

Name	Size (bp)	Source
pFK_i341 PiLucNS3-3′_dg_JFH-WT	12817	AG Lohmann
pFK_i341 PiLucNS3-3′_dg_JFH-dGDD	12808	

2.1.3. Oligonucleotides

2.1.3.1. DNA Primers

All oligonucleotides used in this study were purchased from either Bio-Rad or IDT. Lyophilized primers were dissolved in DNase/RNase-free deionized H_2O to prepare 0.1 mM stock solution. These were further diluted to 10 µM and 20 µM working solutions, depending on the application, including conventional PCR, RT-qPCR and sample preparation for sequencing. All primers, along with their IDs, sequences and sizes are listed in tables 2G to 2I below.

Table 2G: DNA primers used for RTqPCR with their sequences, sizes and purpose of use. Lower case letters represent non-viral tag sequences (Dobson et al., 2023) either added to 5´-end of RT primer or used as full qPCR primer. Exceptional case in Spinach_minus_RT_snap, where additional 5´-end sequences form loop with 3´-end.

Primer ID	Sequence (5´ – 3´)	Size (nt)	Purpose
D_TAG_RT_minus_2	gcaggagctaagcgctggTcaggagctaagGTAGCGACCCTTT GCAGGCAGCGGAACC	58	minus strand RT
D_TAG (as forward)	gcaggagctaagcgctggTcaggagctaag	30	minus strand qPCR
Amp_2_minus_R	ACGTGGCACTGGGGTTGTGCCG	22	
D_TAG_RT_plus_1	gcaggagctaagcgctggTcaggagctaagAAGACCCCTAGGA ATGCTCGTCAAGAAGACAGGGCC	66	plus strand RT
Amp_1_plus_F	CGAAGCCGCTTGGAATAAGGCCGGTGTG	28	plus strand qPCR
D_TAG (as reverse)	gcaggagctaagcgctggTcaggagctaag	30	
GAPDH 2_for	GTCTCCTCTGACTTCAACAGCG	22	qPCR
GAPDH 2_rev	ACCACCCTGTTGCTGTAGCCAA	22	RT and qPCR
RT_test_minus	AGTAGAGTGTGGCTACGGAGCCCACACTCTACT	33	minus strand RT
Spinach_minus_RT_snap	ctgaatgaaatgCCGTCCTTCACCATTTCATTCAG	35	minus strand RT
EMCV_plus_RT	CCCCTTGTTGAATACGCTTG	20	plus strand RT
EMCV_plus_qPCR_for	AGACCCCTAGGAATGCTCGT	20	plus and minus strand qPCR
EMCV_plus_qPCR_rev	CCGTCCTTCACCATTTCATT	20	
GAPDH 1_for	GAGTCAACGGATTTGGTCGT	20	qPCR
GAPDH 1_rev	GATCTCGCTCCTGGAAGATG	20	RT and qPCR
Beta V Tubulin_for	CTGGACCGCATCTCTGTGTACT	22	qPCR
Beta V Tubulin_rev	GCCAAAAGGACCTGAGCGAACA	22	RT and qPCR
Beta Actin (ACTB)_for	CACCATTGGCAATGAGCGGTTC	22	qPCR
Beta Actin (ACTB)_rev	AGGTCTTTGCGGATGTCCACGT	22	RT and qPCR

Table 2H: DNA primers used for cloning with their sequences, sizes and purpose of use. Lower case letters indicate to non-matching sequences incorporated to introduce (point) mutations in resulting amplicon

Primer ID	Sequence (5´ – 3´)	Size (nt)	Purpose
mut_D220N_for	CCCCATGGGTTTTTCGTATaacACCCGATGCTT CGACTCA	40	GND -> NGND
mut_D220N_rev	TGAGTCGAAGCATCGGGTgttATACGAAAAAC CCAT	37	
PCR_NS5B_for	GGAGCAGCATGCTCGCTGTTGCGATACCATAA CAAGGTG	39	
PCR_NS5B_rev	AGGAGGGAATTCGACGGTGAACCAACTGGATA AGTCCAG	39	
PV-IRES-FLuc-for	ggaggaatgtctagACCGTGGACCTCGAAAACAGACG	37	*Firefly* luciferase insertion to 4th generation replicon system
PV-IRES-FLuc-rev	GCTGGGCCAGCCTACCAAGTCC	22	
FLuc-XbaI-for	CCCGGCGCCATTCTATCCctTAGAGGATGGAACCG	35	
FLuc-XbaI-rev	CGGTTCCATCCTCTAagGGATAGAATGGCGCCGGG	35	
FLuc-EcoRI-for	ACAAAACAATTGCACTGATAATGAAcagCTCTG GATCTACTGGGTTACCTAAGGGTG	57	
FLuc-EcoRI-rev	ACACCCTTAGGTAACCCAGTAGATCCAGAGctgTT CATTATCAGTGCAATTGTTTTGTC	59	
FLuc-EMCV-for	TCCTCATAAAGGCCAAGAAGGGCGGAA	27	
FLuc-EMCV-rev	GCGCGGCCGCTTACAATTTGG	21	
LacZ_for	GCCAGTGCCAAGCTTGCATG	20	5´UTR fragments insertion to 4th gen. replicon system
SLIII_AflII_rev	CCAGAACTTAAGTACGAGACCTCCCGGGGCAC	32	
M13_ext_rev	GTCATAGCTGTTTCCTG	17	

Table 2I: DNA primers used for sample preparation for sequencing, with their sequences, sizes and purpose of use.

Primer ID	Sequence (5´ – 3´)	Size (nt)	Purpose
For_EMCV	GGCCGAAGCCGCTTGGAATAAG	22	Sequencing
Rev_NS3	GTCTCGGGGAGAGCAATGCT	20	
For_NS5B	TGACCAGGTACTCTGCCCCTC	21	
Rev_3UTR	AAAGGAACAGTTAGCTATGGA	21	
For_minusFishSite	GAGACCATTACGTATACCAGGTGTCC	26	

2.1.3.2. RNA Oligonucleotides

RNA oligonucleotides were used to prepare partial duplexes of liver specific microRNA-122 (miR-122) through a hybridization reaction. The sequences of both RNA oligos, along with their IDs, sizes and intended purposes are given in Table 2J below.

Table 2J: RNA primers used for the generating of liver specific micro-RNA (miR-122)

Primer ID	Sequence (5´ – 3´)	Size (nt)	Purpose
miR-122 mat	UGGAGUGUGACAAUGGUGUUUG	22	Generation micro-RNA duplex
miR-122*	AACGCCAUUAUCACACUAAAUA	22	

2.1.4. Chemical Reagents

2.1.4.1. Bacterial Cell Culture Reagents

Name	**Source**
Ampicillin (50 mg/ml)	Roth
Glucose	
Glycerol	
KCl	
LB Agar	
LB Medium	
$MgCl_2$	
MgSO4	
NaCl	
S.O.C. Medium	NEB
Sodium acetate	Roth
Tryptone	
Yeast Extract	

2.1.4.2. Human Cell Culture Reagents

Name	**Source**
DMSO (Dimethyl Sufoxide)	Thermo-Fischer-Scientific
Dulbeco's Modified Eagle Medium	Gibco
Dulbeco's Modified Eagle Medium (without phenol red)	
Fetal Bovine Serum (HI) Brazil	
Fetal Bovine Serum (HI) US	
Fetal Bovine Serum (non-HI) New Zealand	
Lipofectamine 2000	Thermo-Fischer-Scientific
MessengerMax transfection reagent	
Non-essential Amino acids	Gibco
Opti-MEM	
PBS (10x)	Roth
PenStrep	Gibco
TRIzol	Thermo-Fischer-Scientific

2.1.4.3. Reagents for Work with DNA and RNA

Name	Source
Antarctic Phosphatase reaction buffer (10x)	New England Biolabs
Chloroform	Roth
Cut Smart buffer (10x)	New England Biolabs
Dithiothreitol (DTT)	Roth
DNase I reaction buffer (10x)	New England Biolabs
dNTPs (100 mM)	Roth
Ethanol	
Isopropanol	
Phenol Chloroform Isoamyl Alcohol pH 4	Thermo-Fischer-Scientific
Phenol Chloroform Isoamyl Alcohol pH 6.5	
Phusion GC buffer (10x)	New England Biolabs
Phusion HF buffer (10x)	
RNA Polymerase buffer (10x)	
rNTPs (100 mM)	Roth
Sybr Gold Nucleic Acid Gel Stain	Thermo-Fischer-Scientific
TURBO DNase buffer (10x)	New England Biolabs

2.1.4.4. Ingredients of Homemade Buffers

Name	Source
Agarose	Roth
Boric acid	
Bromophenol Blue	
CsCl	
EDTA	
Ethidium Bromide	
Formaldehyde	
Formamide	
Glycin	
Guanidinium thiocyanate	
Hydrochloric acid	
Sodium acetate	
Sodium hydroxide	
Tris	
Urea	
Xylene cyanole	

2.1.4.5. Homemade Buffers

Ethidium bromide solution: 80 µl ethidium bromide was mixed with 400 ml of 1x TBE buffer.

TBE (10x): To prepare one liter TBE (10x), 108 g of Tris (89 mM) and 55 g of boric acid (89 mM) were dissolved in sterile ddH_2O. 40 ml of 0.5 M EDTA (2 mM) was added, filled up to 1 L and autoclaved.

2.1.5. Enzymes

Name	source
Antarctic Phosphatase	New England Biolabs
DNase I (RNase-free)	
LunaScript RT Master Mix Kit (Primer-free)	
Luna Universal qPCR Master Mix	
Maxima Reverse Transcriptase	Thermo-Fischer-Scientific
Murine RNase Inhibitor	New England Biolabs
Phusion High-Fidelity DNA polymerase	
Proteinase K	
Restriction enzymes	
• AflII	New England Biolabs
• AscI	
• BbvCI	
• BsiWI	
• BsrGI	
• EcoRI-HF	
• FseI	
• HindIII-HF	
• KpnI-HF	
• MluI-HF	
• MspI	
• NotI	
• SbfI	
• SpeI-HF	
• XbaI	
SP6 RNA Polymerase	
T4 DNA Ligase	
T7 RNA polymerase	
Taq DNA Polymerase	
TURBO DNase (2U/µl)	Thermo-Fischer-Scientific

2.1.6. Nucleic acid Ladders and Dyes

Name	Source
1 kb DNA Ladder	New England Biolabs
1 kb plus DNA ladder	
FA dye for RNA detection	Homemade
Gel loading purple dye (6x)	New England Biolabs
GlycoBlue Coprecipitant (15mg/ml)	Invitrogen
HyperLadder 1kb	Bioline
SYBR gold nucleic acid gel stain	Invitrogen

2.1.7. Kits

Name	Source
Click iT Nascent-RNA-Capture Kit	Invitrogen
GeneJET Gel extraction kit	Thermofischer
GeneJET PCR Purification kit	
GeneJET Plasmid Miniprep kit	
LunaScript RT SuperMix kit (Primer-free)	New England Biolabs
Monarch® Spin RNA Cleanup Kit	
Nano-Glo® HiBiT Lytic Detection System	Promega
NucleoBond Xtra Midi Plus EF (Maxiprep Kit)	Macherey-Nagel
NucleoBond Xtra Midi Plus EF (Midiprep Kit)	
Qubit DNA/RNA detection kit	Thermofischer
Steady-Glo® Luciferase Assay System	Promega

2.1.8. Softwares used for Data Processing

Name	Source
Cfx maestro Software for Real-time PCR	https://www.bio-rad.com/de-de/product/cfx-maestro-software-for-cfx-real-time-pcr-instruments
Coral Draw	https://www.coraldraw.com
Graph Pad Prism	https://www.graphpad.com
Image lab Software	https://www.bio-rad.com/de-de/product/image-lab-software
NEBioCalculator	https://nebiocalculator.neb.com
Pymol	https://www.pymol.org
RNA fold Web server	http://rna.tbi.univie.ac.at/cgi-bin/RNAWebSuite/RNAfold.cgi
Snapgene	https://www.snapgene.com
VARNA	https://varna.lisn.upsaclay.fr

2.1.9. Instruments

Name	Source
Accublock digital dry bath	Labnet International
AccuSpin Micro 17 Centrifuge	Fischer Scientific
Analytical Balance	Sartorius Laboratory
Avanti JXN -26 Centrifuge	Beckmann Coulter
Biophotometer	Eppendorf
Centrifuge 5417 R	Eppendorf
Centrifuge 5427 R	Eppendorf
Centrifuge Sigma 2-16 KL	Sigma
Certomat Shaking Incubator	Braun
CFX connect Real-time PCR Detection System	Bio-Rad
CO_2 Incubator	Binder
Duomax 1030 Rocking Platform Shaker	Heidolph Instruments
Electrophoresis Chamber Horizontal	von Keutz
Gel Doc 2000 Imaging System	Bio-Rad
Heated Magnetic Stirrer	Stuart
JA-10 Fixed Angle Aluminium Rotor	Beckman Coulter
LaminAir HA 2448 BS, Laminar Flow Hood	Heraeus
Lumat LB 9501, single tube Luminometer	Berthold
Microbiological incubator	Thermo Scientific
Microscope Leica DM IL	Leica
MiniStar Silverline Microcentrifuge	VWR
Optima LE-80K Ultracentrifuge	Beckmann
PCR Workstation	VWR
PlateFuge Microplate Microcentrifuge	Benchmark Scientific
Powerpack Basic	Bio-Rad
Qubit® 2.0 Fluorometer	Invitrogen
Thermal cycler T100	Bio-Rad
Thermodrucker P91	Mitsubishi
Thermomixer Shaker, Mixing Block MB102	Bioer
TProfessional Basic Thermocycler	Biometra
Ultraviolet light portable 230V 50Hz	Nuair USA
Vortex Genie 2™	Bender & Hobein AG
Water bath WB-12	Phoenix

2.2. Methods

2.2.1. Work with Human Cells

Most of the experiments were performed using the Huh-7.5 cell-line. Additional cell-lines, such as Huh-7 and HepG2, were used for optimizing various parameters during transfection with both 3rd generation and 4th generation replicon systems. All cell culture work was performed under a microbiological safety cabinet that was sterilized in advance with UV-light for at least 30 minutes. All utensils were disinfected with 70 % ethanol prior to use.

2.2.1.1. Preparation of Growth Medium

Dulbecco's modified eagle medium (DMEM) supplemented with high glucose was thoroughly mixed with 10 % heat-inactivated fetal bovine serum (FBS), 1 % Penicillin-Streptomycin (PenStrep) and 1 % non-essential amino acids. The complete medium was warmed up at 37 °C prior to use and stored at 4 °C otherwise.

2.2.1.2. Passage of the Cells

The cells were passaged at about 90 – 100 % confluency. The culture medium was removed, and the cells were washed with 1x PBS. An appropriate volume of trypsin (0.25 %) was added directly to the cells and incubated for 5 minutes at 37 °C. Specifically, 4 ml of trypsin was used for 150 mm plate and 1.5 ml for 100 mm plates. The trypsinization was stopped by adding complete DMEM – 6 ml for 150 mm plate and 3.5 ml for 100 mm plates – and mixing the resulting cell suspension thoroughly by pipetting up and down. 1/10 volume of the cell suspension was used to seed fresh plates containing pre-warmed complete medium.

2.2.1.3. Freezing and Thawing of the Cells

Cells can be stored long-term in small cryovials in a liquid nitrogen (N_2) tank. They can be easily thawed when required. The freezing medium contains a cryoprotectant, such as DMSO, which must be thoroughly removed during the thawing process to prevent cytotoxic effects.

Freezing: Cells were harvested at 100 % confluency from 150 mm plates. They were first washed with 1x PBS and then treated with 4 ml of 0.25 % trypsin. After incubation at 37 °C for 5 minutes, 6 ml complete DMEM was added, and the cells were gently mixed by pipetting up and down. The cell suspension was centrifuged at 1000 x*g* for 5 minutes at 4 °C to pellet the cells. The resulting cell pellet was resuspended in 6 ml of freezing medium (complete DMEM supplemented with 10 % DMSO) and transferred into 1 ml cryovials in 500 µl aliquots. Cryovials were initially stored at -40 °C in a cryo-container filled with ethanol, allowing a controlled cooling rate of approximately -1 °C per minute. The cryovials were finally transferred to N_2 tank for long-term storage.

Thawing: Cryovials were removed from the liquid N_2 tank and immediately transferred to 37 °C water bath for 30 – 60 seconds. As soon as the cells were thawed, the contents of each vial were promptly transferred to a sterile 15 ml falcon tube containing 10 ml of complete DMEM. The cell suspension was mixed thoroughly and centrifuged at 1000 x*g* for 5 minutes at 4 °C to pellet the cells. The supernatant was discarded, and the cell pellet was resuspended in 10 ml of fresh complete

DMEM. To ensure complete removal of DMSO, the centrifugation step was repeated. Finally, the washed cell pellet was resuspended in 10 ml of fresh DMEM, transferred to 100 mm culture plate and incubated at 37 °C in a humidified incubator supplemented with 5 % CO_2.

2.2.1.4. Cell Seeding

Cells were seeded 1- 2 days prior to transfection. They were harvested at 100% confluency and the number of cells per µl was determined using a Neubauer counting chamber. For 6-well plates, 0.3 x 10^6 cells were seeded per well in 2 ml of complete DMEM and mixed well by pipetting up and down. For 12-well plates, 0.16 x 10^6 cells were seeded per well in 1 ml of complete DMEM. The plates were incubated at 37 °C in a humidified incubator supplemented with 5 % CO_2 until the cells reached 90 % confluency.

2.2.2. Work with Bacterial Cells

2.2.2.1. Preparation of Growth Medium

Two different growth media were used for the bacterial cell growth: LB medium and S.O.C. medium.

LB medium: 20 g of powdered LB medium was dissolved in total 1L of sterile water, mixed thoroughly and autoclaved immediately. To maintain sterility, the bottle lids were covered with aluminum foil prior to autoclaving. Prepared media were stored at 4 °C and used exclusively under sterile conditions.

S.O.C. medium: In addition to the standard LB medium components, S.O.C. medium is supplemented with glucose to facilitate the rapid recovery of *E. coli* cells after heat shock. The components include Tryptone (2%), Yeast (0.5%), Glucose (20mM), KCl (2.5 mM), $MgCl_2$ (10 mM), $MgSO_4$ (10 mM) and NaCl (10 mM). All ingredient, except glucose, are dissolved in 1L of sterile deionized water, mixed thoroughly and autoclaved immediately. Glucose is added freshly under sterile conditions prior to use. The medium can be stored at 4 °C for several months.

2.2.2.2. Preparation of Chemically Competent Cells

Bacterial cells are made competent to facilitate the uptake of foreign DNA by subjecting them to stress conditions, such as heat shock. Treatment with concentrated salts increases the permeability of the cell membrane. During heat shock, the pores of the cell membranes enable the DNA to enter the cells through endocytosis.

During this study, two strains of *E. coli* competent cells were used: *DH5α* and TOP10. Competency was induced by treating the cells with concentrated $MgCl_2$ while keeping them at 4 °C throughout the process. The cells were subsequently stored in $CaCl_2$ and glycerol solution. An initial 5ml LB medium culture was inoculated with a single, well-isolated colony from an LB agar plate and grown overnight at 37 °C with agitation at 160 rpm. This subculture was then used to inoculate another 100 ml of fresh LB medium, which was grown at 37 °C with agitation at 160 rpm for 2 to 4 hours, until the optical density OD_{600} reached approximately 0.6 – 0.7. From this point onward, the cells were strictly kept cold (4 °C) for all subsequent chemical treatments. The cells were pelleted by centrifugation at 4,000 rpm for 10 minutes at 4 °C and the supernatant was discarded. The pellets

were then resuspended in 80 ml of ice cold $MgCl_2$ (0.1 M) and incubated on ice for 30 minutes. Following this, the cells were pelleted again under the same centrifugation conditions, and the supernatant was discarded. For storage, the cells were resuspended in 8 ml of chilled 0.1 M $CaCl_2$ solution containing 15 % glycerol solution. The chemically competent cells were immediately aliquoted in 1.5 ml tubes on ice, shock-frozen in liquid nitrogen and stored at -80 °C for long-term use. Cells prepared using this method remain competent for several months.

2.2.2.3. Transformation

The uptake of foreign DNA by bacterial competent cells is referred to as transformation. Under optimal growth conditions, bacterial cells divide approximately every 20 minutes, resulting in the simultaneous amplification of the transformed plasmid DNA.

In this study, *E. coil* strains *DHα5* or TOP10 were cultured at a relatively lower temperature (32 °C), which slowed the growth process and facilitated the accurate synthesis of large plasmid DNA (~12 kb), minimizing the risk of replication errors and the selection of smaller, defective plasmids.

E. coli competent cells were thawed on ice. A total of 100 µl of competent cells was added to 100 - 500 ng of plasmid DNA in a 1.5 ml cold sterile microcentrifuge tube. The tube was gently flicked 3 - 4 time to ensure proper mixing of the DNA with the competent cells. The mixture was incubated on ice for 30 minutes. Following incubation, the cells were heat shocked at 42 °C for exactly 45 seconds and immediately transferred back to ice. After 2 minutes' incubation on ice, 900 µl of S.O.C. medium was added to the tube. The cells were then incubated at 32 °C for 2 hours with agitation at 300 rpm to allow recovery and expression of the selection marker. Finally, the transformed cells were plated on sterile LB agar plates containing Ampicillin, using two different concentrations: 1x and 10x. Plates were incubated overnight at 32 °C.

2.2.2.4. Growth of the Bacterial Cells

Depending on the required yield of plasmid-DNA, *E. coli* cells were grown for either miniprep, midiprep or maxiprep procedures. Transformed *E. coli* colonies appeared on the LB agar plates supplemented with ampicillin after 18 – 24 hours of incubation at 32 °C. Moderately sized, well-isolated single colonies – preferably from the center of the LB/Agar/Amp plate – were selected for inoculating subcultures. For that purpose, a single colony was picked using a sterile pipette tip and was inoculated into 5 ml of sterile LB medium with 100 µg/ml of Ampicillin. The culture was incubated for at least 18 hours at 32 °C. From this subculture, 1 ml was used to inoculate 400 ml of LB medium supplemented with 100 µg/ml Ampicillin. This main culture was incubated over night at 32 °C until the cells reached maximum growth (OD_{600} ~ 2.5 – 3.5). At this stage, plasmid DNA was extracted using either a midiprep or maxiprep protocol, depending on the cell mass and the type of plasmid (low copy or a high copy number).

Minipreps were generally performed during cloning steps, where only small amounts of plasmid DNA were needed for sequencing. Approximately 4 - 5 ml of the bacterial subculture was sufficient for miniprep procedures.

2.2.3. Work with DNA

2.2.3.1. Cloning

Cloning enables the investigation of the specific function of a particular gene, a regulatory element within the gene, or even the role of a single nucleotide in a non-coding region of the genome. The HCV RNA genome contains specific secondary and tertiary structures including loops, stem loops and hairpins of various sizes. To study the functional contribution of such *cis*-elements located within the 5´UTR region of the genome, various cloning strategies were employed to introduce mutations. These methods include restriction enzyme-based cloning, site-directed mutagenesis, conventional PCR and assembly PCR cloning.

2.2.3.1.1. Restriction Enzyme-based Cloning

A custom-designed fragment of insert DNA was ordered from BioCat and cloned into pUC18 vector flanked by two restriction enzyme recognition sites, usually SbfI at the 5´ and AflII at the 3´-end. The insert was excised from the delivery plasmid using a double digestion with both enzymes. For the restriction reaction, 10 – 20 µg of donor plasmid was digested in a total volume of 100 µl, containing 10 µl (200 units) of each restriction enzyme, 10 µl of CutSmart buffer (NEB) and the appropriate volume of deionized H_2O. The mixture was incubated at 37 °C for 1 – 2 hrs. Following digestion, the enzymes were heat-inactivated at 65 °C for 20 minutes.

Meanwhile, the recipient vector was digested with the same restriction enzymes under identical conditions. To avoid the self-ligation of the sticky ends, a dephosphorylation reaction was performed immediately after heat-inactivation of the restriction enzymes. Antarctic Phosphatase (AnP)(NEB) was used to catalyze the dephosphorylation of 5´- and 3´-ends of DNA or RNA phosphomonoesters. To the 100 µl restriction reaction, 12 µl of AnP buffer, 4 µl of AnP enzyme and 4 µl of deionized water were added. The mixture was gently mixed and incubated at 37 °C for 30 minutes. The enzyme was then inactivated by heating at 80 °C for 2 minutes. Both the digested insert and recipient plasmid fragments were subsequently gel-purified and ligated as described in 2.2.3.3.

2.2.3.1.2. PCR Site-directed Mutagenesis

The method enables deletion, substitution or insertion of a few or even a single nucleotide within the gene of interest. The desired mutation is introduced by incorporating one to three mismatched nucleotides into both forward and reverse primers at the mutation site. In addition, a second primer pair is designed to amplify the flanking region surrounding the mutation site. These primers also include recognition sequences for restriction endonucleases at each end. The mutation site and its surrounding region are amplified in two separate PCR reactions, each using either the forward or reverse mutation-specific primer in combination with one of the outer flanking primers. The resulting two amplicons contain the desired mutation at opposite ends. In a subsequent assembly PCR, these two fragments are fused into a single larger fragment using only the outer primer pair. The ends of this final fragment are then trimmed using restriction enzymes and ligated into the original plasmid as described in 2.2.3.1.1.

Using the above-described techniques, the following mutations were introduced into the 4^{th} generation replicon system.

- **GND to NGND**

The HCV RNA polymerase NS5B requires Mg^{2+} as a cofactor, which binds between two Aspartic acid residues (D318 and D220) located within the enzyme's active site. Substitution of both Aspartic acid residues with Asparagine molecules (D318 → N318 and D220 → N220) was anticipated to completely inactivate the polymerase (Lohmann et al., 1997). This double mutant, referred to as NGND, was used as a negative control for the study of replication of the HCV genome. To generate the NGND mutant, a second point mutation (D220 → N220) was introduced into an already mutated GND construct (D318 → N318). This was achieved using site-directed mutagenesis with specifically designed primers: mut_D220N_for and mut_D220N_rev. Two independent PCR reactions were performed to amplify a 1576 bp fragment (from nucleotide 7712 to 9287) of the NS5B region. The resulting PCR products, each carrying the desired mutation at one end, were purified by gel extraction and used as template in a second PCR reaction using outer primers PCR_NS5B_for and PCR_NS5B_rev, to assemble the full-length mutated fragment (Fig. 2.2.1).

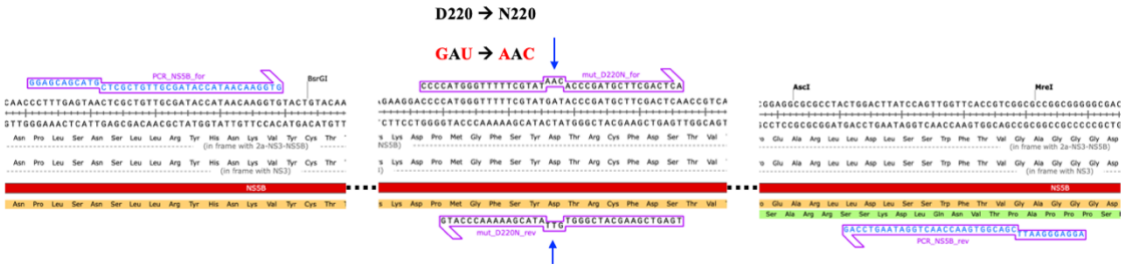

Figure 2.2.1. Site-directed mutagenesis and assembly PCR used to introduce the D220N substitution within the active site of NS5B. The figure shows snapshots from the SnapGene software, with NS5B sequence shown in red and the primers shown in purple. Primers 'mut_D220N_for' and 'mut_D220N_rev' were used for the mutation (indicated by blue arrows) in two separate PCR reactions. The outer two primers were then used in an assembly PCR to combine the two fragments.

The PCR product (~1600 bp) was again purified by gel extraction using GeneJET gel extraction kit (Thermos-Fischer-Scientific) and subsequently digested with the restriction enzymes BsrGI and AscI (NEB). The resulting 1509 bp fragment was ligated into the plasmid '3rd_gen-ins-2nd_gen_BB-SbfI_BbvCI (core-HiBiT) (GND)'. The resulting construct was designated '3rd_gen-ins-2nd_gen_BB-SbfI_BbvCI (core-HiBiT) (NGND)'. Successful cloning and incorporation of the intended mutation were confirmed by Sanger Sequencing using single-tube economy run service (Microsynth).

- **Insertion of *Firefly* Luciferase**

A 3161 bp construct comprising the *firefly* luciferase gene, an upstream PV-IRES and a portion of the downstream NS3 sequence was generated from the plasmid 'pFK_i341 PiLucNS3-3´_dg_JFH-WT' (provided by AG Lohmann) through a combination of PCR amplifications and site-directed mutagenesis. In the first round of PCR, four smaller fragments were amplified using four distinct primer pairs. In the second step, neighboring fragments were assembled into two longer PCR products. These two fragments were finally joined together to generate one 3161 bp construct. The ends of the assembled fragments were trimmed using appropriate restriction enzymes and ligated

into the '3rd_gen-ins-2nd_gen_BB-SbfI_BbvCI' plasmid backbone, resulting into the final construct named 'SP6_5´UTR_core_Hibit_Fluc'.

First round of PCR: In this step, four separate PCR products were synthesized using the plasmid 'pFK_i341 PiLucNS3-3´_dg_JFH-WT' (AG Lohmann) as a template. PCR was performed using Phusion hot start flex DNA polymerase (NEB). The primers used in these reactions are listed in Table 2K. The primer 'PV-IRES-Fluc-for' included a 15 nucleotides' overhang designed to introduce an XbaI-restriction site (TCTAGA) at the 5´-terminus. An already existing XbaI-site at the beginning of *firefly* luciferase gene was disrupted by a synonymous substitution of the two nucleotides (underlined) TCTAGA to CTTAGA. This was accomplished using the primers 'Fluc-XbaI-rev' and 'Fluc-XbaI-for' for the synthesis of PCR products 1 and 2, respectively. These mutations removed the restriction site without altering the encoded protein sequence. Similarly, the EcoRI-site located within the middle of luciferase-gene was also mutated using primers 'Fluc-EcoRI-rev' and 'Fluc-EcoRI-for' during the synthesis of PCR products 2 and 3, respectively. These mutations ensured that both the XbaI and EcoRI sites remained unique within the final construct 4th generation replicon system.

Table 2K: Primers used for the first round of PCR for the generation of the *firefly* luciferase insertion fragment.

	Size (bp)	Primer Forward	Primer Revese	Template
PCR product 1	741	PV-IRES-Fluc-for	Fluc-XbaI-rev	pFK_i341 PiLucNS3-3´_ dg_JFH-WT'
PCR product 2	594	Fluc-XbaI-for	Fluc-EcoRI-rev	
PCR product 3	1098	Fluc-EcoRI-for	Fluc-EMCV-rev	
PCR product 4	887	Fluc-EMCV-for	PV-IRES-Fluc-rev	

The desired PCR products were purified by gel extraction using GeneJET Gel Extraction kit (Thermo-Fischer-Scientific) following the manufacturer's guidelines. The yield of the PCR products after the purification was approximately 2 – 3 µg each.

Second round of PCR: In this step, two larger DNA fragments were synthesized using the four PCR products from the first round as templates. All reagents and PCR conditions were identical to those used in the first round, with the exception of the template DNA. PCR product 1 and 2 (~ 250 ng each) were used as templates for the synthesis of PCR product 5, while PCR product 3 and 4 (~ 250 ng each) were used as templates for the synthesis of PCR product 6. The primers used for both independent reactions are listed in the Table 2L below.

Table 2L: Primers used for the second round of PCR for the generation of the *firefly* luciferase insertion fragment.

	Size (bp)	Primer Forward	Primer Revese	Template
PCR product 5	1300	PV-IRES-Fluc-for	Fluc-EcoRI-rev	PCR product 1 and 2
PCR product 6	1934	Fluc-EcoRI-for	PV-IRES-Fluc-rev	PCR product 3 and 4

The PCR products were visualized on a 0.8 % agarose gel stained with SYBR Gold (Thermo-Fischer-Scientific). Bands corresponding to the desired product were excised and the DNA fragments were purified using GeneJET Gel Extraction Kit (Thermo-Fischer-Scientific), following the manufacturer's guidelines. The yield of each purified PCR product was approximately 2 – 3 µg.

Final round of PCR: In this step, PCR products 5 and 6 were assembled into a single full-length fragment using the primers shown in the Table 2M below. All reagents and PCR conditions remained same as described for former rounds.

Table 2M: Primers used for the final round of PCR for the generation of the *firefly* luciferase insertion fragment.

	Size (bp)	Primer Forward	Primer Revese	Template
PCR product 7	3176	PV-IRES-Fluc-for	PV-IRES-Fluc-rev	PCR product 5 and 6

The final PCR product (Product 7) was purified using the GeneJET Gel Extraction Kit, following the same procedure as in the previous rounds. This fragment was then trimmed by double restriction using XbaI and BbvCI enzymes (NEB) and inserted into the plasmid backbone '3rd_gen-ins-2nd_gen_BB-SbfI_BbvCI (core-HiBiT)', resulting in the construct 'SP6_5´UTR_core_Hibit_Fluc'. The entire procedure is illustrated in figure 2.2.2 below.

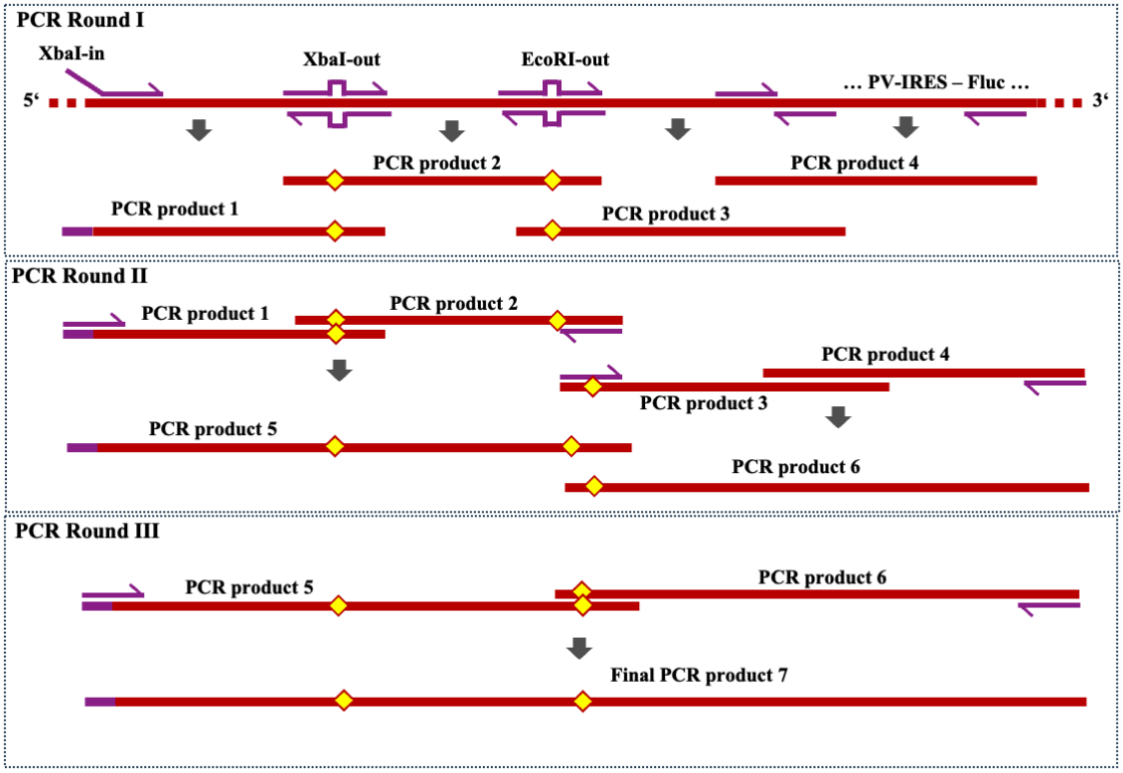

Figure 2.2.2. Schematic representation of site-directed mutagenesis and assembly PCR used to generate a mutated version of the *firefly* luciferase gene along with PV-IRES across three PCR rounds. An XbaI-restriction site was introduced at the 5´-end of the resulting PCR product. Two point-mutations were introduced using specific primers to disrupt the other XbaI and EcoRI restriction sites. The final 3161 bp construct, containing two point-mutations (indicated by yellow diamonds) and one newly inserted XbaI restriction-site, was generated after three rounds of PCR.

- **Substitution of SP6 by T7 promoter sequence**

The initial 4th generation constructs contained an SP6 promoter, which was later replaced by T7 promoter, as the SP6 RNA polymerase did not produce sufficient yield during *in vitro*-transcription. The entire 5´UTR fragment containing the T7 promoter was amplified from the delivery plasmid (BioCat) and inserted to 4th generation replicon system by restriction cloning as described in section

2.2.3.1.1. For PCR amplification, ‘LacZ_for’ was used as the forward primer and ‘SLIII_AflII_rev’ or ‘M13_ext_rev’ was used as the reverse primer.

2.2.3.2. Restriction

The plasmid DNA was linearized prior to use as a template for *in vitro*-transcription. For the restriction reaction, 10 µl of EcoRI-HF (NEB) was added to 10 – 20 µg of the plasmid DNA, along with 10x CutSmart buffer, in a final volume of 100 µl. The reaction was incubated at 37 °C for 2 – 4 hours, followed by enzyme inactivation by incubation at 65 °C for 20 minutes. For cloning purposes, several different enzymes from the same manufacturer were used, either for single or double restriction. The amount of restriction enzyme was adjusted according to the amount of DNA (1 µl of enzyme per 1 µg of DNA). The corresponding enzyme inactivation conditions – temperature and time– were taken directly from the NEB enzyme list on the website.

2.2.3.3. Polymerase Chain Reaction (PCR)

PCR was performed using DNA Phusion hot start flex polymerase (NEB). About 250 ng of the template DNA was mixed with 0.5 µM each of forward and reverse primers, 0.2 mM dNTPs, 2mM $MgCl_2$, 3 % DMSO, 1U (0.5 µl) of Phusion polymerase and 5x HF buffer. PCR steps included denaturation at 98 °C for 30 s, annealing at 59 °C for 30 s and extension at 72 °C for 45 s. The cycle was repeated 30 – 40 times. Initial denaturation was performed for 90 s at 98 °C and final extension at 72 °C for 10 min.

2.2.3.4. DNA Extraction by Gel-Purification

DNA fragments were isolated by gel extraction using the GeneJET Gel Extraction Kit (Thermo-Fischer-Scientific). For that purpose, the DNA fragments were first visualized on an agarose gel (0.8 % w/v agarose/ 1:10,000 SYBR gold) under UV light. The corresponding bands were excised from the gel with the help of a sterile scalpel and transferred to pre-weighed sterile 2 ml tubes. Binding buffer was added according to the weight of the gel slices (1:1; 1µl per 1mg gel), and the gel was heated to 60 °C for 30 minutes until completely dissolved. The tubes were inverted several times to ensure the complete melting of the gel. 100 % isopropanol was added in 1:1 ratio (1µl per 1mg gel slice) and mixed gently by inverting the tubes. 800 µl of the solubilized gel solution was loaded onto the GeneJET purification column. The column was centrifuged for 1 min at 12,000 x *g* and the flow-through was discarded. 700 µl wash buffer was applied to the column, centrifuged for 1 min at 12,000 x *g* and the flow-through was discarded. The wash step was repeated once. Finally, the DNA fragment was eluted in 20 -25 µl of elution buffer and the concentration was checked using a Qubit Fluorometer.

2.2.3.5. Ligation

A DNA fragment in question, either synthesized by PCR or excised from a (donor) plasmid by restriction reaction, was inserted into a new target (recipient) backbone vector by ligation. The amount of insert DNA, relative to the size and quantity of the backbone vector, was calculated using NEBioCalculator. In general, a 7:1 insert-to-vector ratio was applied throughout this work. The

calculated amount of insert-DNA was mixed with 1 – 2 µg of vector-DNA. 2 µl of T4 DNA ligase (NEB), along with the corresponding buffer, was added to the solution for a final reaction volume of 20 µl. The number of self-ligated vectors or contaminating recipient plasmids was estimated using two negative controls: a vector control (same ligation reaction without insert) and an insert control (same ligation reaction without vector). Thereby, the "vector" control checks for possible insufficient dephosphorylation of the vector, while the insert control checks for contaminating source vector in the "insert" fragment preparation. The mixture was incubated at 16 °C overnight. On the next day, the entire mixture was transformed into 100 µl of *E. coli* competent cells according to the section 2.2.2.3. The cells were plated on LB/agar/Amp plate. The reaction was considered successful when the number of potential clones significantly exceeded (at least three times more) the number of clones appearing on either of the negative control plates. Three well-isolated, moderately sized single clones were picked for further growth and subsequent plasmid preparation.

2.2.3.6. Plasmid Preparation by Mini/Midi/Maxiprep

Small amounts of the plasmid DNA (4 – 5 µg) can be isolated from 4 – 5 ml of bacterial culture using the GeneJET Plasmid Miniprep kit (Thermo-Fischer-Scientific). Bacterial cells were harvested at 9,000 x *g* in a microcentrifuge for 3 minutes, and the supernatant was discarded. The cells were resuspended in 250 µl of resuspension solution. Then, 250 µl of lysis solution was added to the cells, mixed gently by inverting the tubes 15 – 20 times, and incubated at room temperature for 5 minutes. After that, 350 µl of neutralization solution was added and mixed thoroughly by inverting the tubes 8 – 10 times. The mixture was centrifuged for 5 minutes at 12,000 x *g* at room temperature. All further centrifugation steps were performed at 12,000 x *g*. The supernatant was transferred to GeneJET spin columns and centrifuged for one minute. The flow-through was discarded. Plasmid DNA bound to the column filter was washed twice. For that purpose, 500 µl of Wash solution was added to the column and centrifuged for one minute. The flow-through was discarded, and the washing step was repeated. Finally, the plasmid DNA was eluted in 20 – 25 µl of prewarmed (70 °C) elution buffer and collected in 1.5 ml sterile tubes.

For the isolation of large amounts of plasmid DNA (~ 10^3 - 10^4 µg) Midi/Maxiprep were performed using the Endotoxin-free Plasmid DNA Purification Kit (Macherey-Nagel). The procedure requires 200/600 ml of overnight-grown bacterial culture at approximately OD_{600} ~ 2. The cells were pelleted at 5,000 x *g* for 10 minutes at 4 °C, and the supernatant was discarded. The cells were resuspended in 8/12 ml of resuspension buffer RES-EF supplemented with RNase A. To lyse the cells, 8/12 ml of lysis buffer LYS-EF was added to the cell-suspension and mixed by inverting the tubes several times. After 5 minutes of incubation at room temperature, 8/12 ml of neutralization buffer NEU-EF was added and mixed by inverting the tubes until the dark blue lysate tuned completely colorless. White-colored protein and chromosomal DNA precipitates in the lysate were pelleted by centrifugation at 5,000 x *g* for 10 minutes at 4 °C. The clear lysate was loaded onto pre-equilibrated Nucleobond Xtra Midi EF/Maxi EF columns. Loading and washing of the columns was done by gravity flow of the solution. The column was washed three times using buffers FIL-EF, ENDO-EF and WASH-EF sequentially, according to the manufacturer's guidelines and finally eluted in 5/15 ml of prewarmed (50 °C) elution buffer ELU-EF. To the eluted plasmid DNA, 3.5/10.5 ml of room-temperature isopropanol was added and mixed thoroughly by gentle vortexing. The DNA was pelleted at 15,000 x *g* for 30 minutes at 4 °C. The pellet was washed twice with 70 % EtOH and resuspended in 1 – 1.5 ml of deionized H_2O.

2.2.3.7. Sequencing

Successful cloning was checked by Sanger sequencing, performed by Microsynth using the Single Tube Economy Run. 1 – 1.2 µg of plasmid DNA was mixed with 4 µM primer in a total volume of 15 µl and sent for sequencing. The results could be downloaded from the official website after a few hours. The received sequence was aligned to the original sequence using the software SnapGene.

2.2.3.8. Purification of DNA (PCI)

During this method, plasmid DNA is extracted using Phenol:Chloroform:Isoamyl Alcohol 25:24:1 (PCI), pH ~ 6.0 (Thermo-Fischer-Scientific) and precipitated in ethanol (≥ 99.5 %, Roth). Plasmid DNA was diluted to 200 µl in deionized H_2O, and PCI was added in a 1:1 ratio. The solution was mixed thoroughly by gentle vortexing or inverting the tubes several times. The mixture was centrifuged at 14,000 x *g* for 5 minutes, which separated the aqueous phase from the PCI phase. The aqueous upper phase containing DNA was transferred to a fresh sterile tube. Then, 200 µl of chloroform (Roth) was added, and the solution was mixed gently by inversion. The solution was centrifuged again, and the aqueous upper phase was collected and transferred to a fresh sterile tube. The chloroform step was repeated to remove any traces of residual phenol, and the aqueous phase was collected in a fresh sterile tube.

To this aqueous phase, 1/10 volume of 3 M sterile sodium acetate was added. For precipitation, 2.5 volume of chilled ethanol (≥ 99.5 %, Roth) were added, and the mixture was stored at -20 °C overnight. Plasmid DNA was pelleted by centrifugation at 14,000 x *g* for 30 minutes at 4 °C. The supernatant was carefully removed without disturbing the pellet. To wash the pellet, 70 % ethanol was added carefully, and centrifugation was repeated for 5 minutes at 4 °C. The supernatant was carefully removed. The wash step was repeated, and the ethanol was thoroughly removed. The pellet was air-dried for 7 – 10 minutes and dissolved finally in 20 – 50 µl of deionized water.

2.2.3.9. Integrity Check by Gel-Electrophoresis

Integrity of DNA was checked by gel electrophoresis. For that purpose, a 0.8 % agarose gel was prepared in 1xTBE. 400 – 500 ng of DNA was mixed with Purple DNA Gel Loading Dye 6x (NEB) and loaded onto the gel. As a marker, 3 µl of DNA ladder, either 1 kb or 1 kb plus (NEB), was applied. The gel was run at 90 – 100 V for 45 minutes and then soaked in ethidium bromide solution for 30 minutes. Finally, the gel was visualized using the Gel Doc 2000 Imaging System (Bio-Rad).

2.2.3.10. Concentration Determination by Qubit 2.0 Fluorometer

The amount of nucleic acid, either DNA or RNA, was measured using the Qubit 2.0 Fluorometer, which allows accurate quantitation through highly sensitive fluorescence-based assays. To check the concentration, 1 µl of the sample was mixed thoroughly by vortexing with 198 µl of the appropriate buffer and 1 µl of dye in 0.5 ml transparent tubes. After two minutes of incubation at room temperature, the tube was inserted into the Qubit Fluorometer, and the concentration was measured in ng/µl. The system allows both broad-range and high-sensitivity measurement of double- and single-stranded nucleic acids.

2.2.4. Work with RNA

In general, all RNA work was performed strictly under RNase-free conditions if not stated otherwise. All reactions were prepared under a sterile chemical hood with laminar flow. The whole apparatus and surfaces were wiped with either 1 % SDS solution or RNaseZap (Thermo-Fischer-Scientific) prior to setting up the reactions.

2.2.4.1. *In vitro*-Transcription

The method allows synthesis of specific RNA from a template DNA with a promoter sequence at 5´-end. The 11.955 nt RNA corresponding to the 4th generation replicon system was always freshly synthesized before transfection into Huh-7.5 cells. The *in vitro*-transcription reaction was performed in sterile 0.2 ml PCR tubes in a total reaction volume of 50 µl. The reagents included 4 mM cold rNTPs, 5 mM additional $MgCl_2$, 10 mM DTT, 0.5 µl Murine RNase Inhibitor and 2 µl of T7 polymerase along with the corresponding buffer. All reagents were mixed thoroughly with 1 µg of template DNA and incubated at 37 °C for 4 hrs. The *in vitro*-transcription reaction mixture turned slightly turbid due to the newly synthesized RNA. 3 µl of this solution were checked for integrity by gel electrophoresis. The template DNA was digested using 2 µl of TURBO DNase (NEB), which was added directly to the *in vitro*-transcription reaction immediately after the completion and incubated for further 30 min at 37 °C. RNA was purified using Monarch RNA cleanup kit (NEB) according to the manufacturer's guidelines and eluted in deionized RNase-free water. Another round of digestion was subsequently performed using 2 µl of TURBO DNase (NEB) with the appropriate buffer and Murine RNase Inhibitor (0.5µl) in a total volume of 50 µl. The reaction was incubated at 37 °C for 30 minutes, followed by purification using the Monarch RNA cleanup kit (NEB). Integrity of RNA was finally checked by gel electrophoresis.

2.2.4.2. Purification of RNA by Acidic Phenol Chloroform Extraction

Synthesis of RNA by *in vitro*-transcription requires specific amounts of template DNA, which must be removed before transfecting the RNA into human cells. Separation of RNA from contaminating DNA is possible using acidic phenol (Phenol/Chloroform/Isoamyl Alcohol [IAA] 125:24:1 pH ~ 4.5, Thermo-Fischer-Scientific) for extraction. The technique is based on the solubility of nucleic acids in the aqueous phase at specific pH levels. Both DNA and RNA are soluble in the aqueous phase when the pH is around 6 -7. At lower pH, the DNA transfers to the organic phase, while RNA remains largely in the aqueous phase, largely due to the additional hydroxyl group at the 2´-position of the ribose.

All other steps for the RNA purification are the same as those described for DNA purification by phenol-chloroform extraction. The method enables the elimination of template DNA (fragments) from *in vitro*-transcribed RNA samples after DNase digestion. Moreover, genomic DNA contamination in total RNA extracted from human cells can also be largely removed using this technique.

2.2.4.3. CsCl Purification of RNA

During this method, 5.7 M CsCl solution (dissolved in EDTA) is used as a density gradient for the separation of proteins, DNA and RNA from the cell lysate through ultracentrifugation. The cell lysate

is layered on top of the CsCl cushion in a microcentrifuge tube. Through ultracentrifugation, RNA is pelleted at the bottom of the tube due to its high density. In the course of this work, the method was initially applied to purify RNA after *in vitro*-transcription from the contaminating template DNA, but unfortunately, the quality of the RNA could not be retained until the end of the procedure. Nevertheless, a brief description of the procedure applied is given below.

In a sterile ultracentrifuge tube, 8.75 ml of RNA dissolved in denaturing solution (4 M guanidine thiocyanate/25 mM Sodium citrate) was layered on top of 3.7 ml of 5.7 M CsCl to create a step gradient. The solution was centrifuged for 18 – 20 hours at 29,000 rpm in an SW 40 rotor at 18 °C. The supernatant was carefully removed, and the RNA pellet was slowly dissolved in TES solution (10 mM Tris-Cl pH 7.4, 5 mM EDTA, 1 % SDS) at room temperature. RNA was transferred to fresh sterile tubes, and the integrity was checked by gel electrophoresis.

The method was repeated with other densities of CsCl solution as well as other RNA denaturing solutions. The 5.7 M CsCl solution was concentrated to increase the density from 1.52 to 1.78 g/dm^3 and the procedure was repeated as described above. For another trial, 7 M urea was applied as the denaturing solution in combination with the high density CsCl solution. After each trial, the integrity of the RNA was checked by gel-electrophoresis, and the concentration was measured by Qubit Fluorometer. Finally, all these attempts proved unsuccessful to obtain high quality purified RNA without contaminating DNA.

2.2.4.4. Gel Filtration Purification of RNA

The method involves differential partitioning of nucleic acid molecules based on their size. In a sterile column, Sephadex G-100 beads (Merck) are captured as a stationary phase using glass wool plug at the bottom. A denaturing solution prepared either with guanidine (4 M guanidine thiocyanate/25mM Sodium citrate) or urea (7 M) is used as the mobile phase. 3 g of Sephadex G-100 beads-slurry, mixed with 140 ml of denaturing solution, was gradually transferred to the column in small portions until the whole mixture was added. The beads were retained in the column by the glass wool plug, while the denaturing solution flowed through. Additional denaturing solution was added to keep the upper surface of the beads wet. 50 µl of RNA dissolved in TES solution was mixed with 100 µl of denaturing solution and an appropriate amount of gel loading dye. The RNA mixture was added to the column as soon as the denaturing solution flowing into the column reached the top of the bead surface. The RNA mixture could be observed flowing through the column due to the color of the gel loading dye. As soon as it reached the bottom of the column, the flow-through was collected in 30 – 40 small fractions (5-7 drops each) in 0.5 ml sterile tubes. All fractions were loaded on 0.8 % agarose gel, and the samples corresponding to correct size of RNA were pooled together for subsequent assays.

2.2.4.5. Transfection of RNA by Lipofection

RNA was transfected into Huh-7.5 cells at ~ 90% confluency in 6-well or 12-well plates. The lipofection reagent, MessengerMaxx (Thermo-Fischer-Scientific), was used at a 3:1 ratio (3 µl for 1 µg of RNA). RNA and Lipofectamine (MessengerMaxx) were first mixed separately with Opti-MEM and then combined to make one transfection solution. For each well, 3.5 µg (6-well) or 1.9 µg (12-well) RNA (*in vitro*-transcribed) was thoroughly mixed with 100 µl of Opti-MEM by gentle vertexing. In another vial, the appropriate amount of MessengerMaxx was mixed with 100 µl of Opti-

MEM and mixed by vortexing. Both solutions were combined after 5 minutes of incubation at room temperature and incubated for a further 15 minutes. Meanwhile, the Huh-7.5 were washed with 1xPBS, and 800 µl (6-well) or 300 µl (12-well) Opti-MEM was gently added to the cells. At this point, 0.1 mM of 5-Ethynyl Uridine (5EU) was pre-mixed with the Opti-MEM if a nascent RNA capture assay was planned. The transfection solution was added dropwise to the cells, and the plates were gently rocked back and forth to ensure complete mixing of all reagents. The cells were finally incubated at 37 °C. The medium was replaced by complete medium after 4 hours.

2.2.4.6. Total RNA Extraction using TRIzol

For the purpose of strand-specific detection, total RNA was extracted from Huh-7.5 cells at certain time points (4, 24, 48 and 72 hpt). The medium was removed from the cells. 1 ml of TRIzol was added directly to the cells and incubated for 5 minutes at room temperature. The lysed cells were mixed thoroughly in TRIzol by pipetting up and down several times and transferred to 1.5 ml sterile tubes. Then, 200 µl chloroform was added to the cell lysate and mixed properly by inverting the tubes for at least 20 times. The solution was incubated for a further 3 minutes at room temperature and then centrifuged at 14,000 rpm for 15 minutes at 4 °C. The upper aqueous phase contained RNA as well as traces of residual genomic DNA. Approximately 400 – 500 µl of the upper phase was decanted and transferred to fresh 1.5 ml sterile tubes, carefully avoiding the interphase. Extending the standard RNA purification procedure using TRIzol, another 200 µl volume of chloroform was added and mixed thoroughly by inverting the tubes 10 – 20 times to remove residual traces of phenol. The solution was centrifuged at 14,000 rpm for 5 minutes at 4 °C. The upper aqueous phase was transferred to fresh 1.5 ml sterile tubes. An equal volume of ice-cold isopropanol, along with 1 – 1.5 µl of GlycoBlue, was added, mixed well and incubated at -20 °C overnight.

RNA was pelleted by centrifugation at 14,000 rpm for 30 minutes at 4 °C. The pellet was washed twice with 70 % ethanol and air-dried (under a sterile hood) for 10 minutes. The pellet was gently dissolved in 20 – 30 µl of deionized water.

At this stage, commonly used standard RNA purification procedures end. However, such RNA preparations still contain traces of genomic DNA or (transfected) plasmid DNA as contamination, which was now removed by repeated steps of DNase digestion followed by acidic phenol/chloroform purification (section 2.2.4.2). To eliminate contaminating DNA, 2 µl DNase I (NEB) was added to RNA along with 10x DNase I buffer, 0.5 µl murine RNase Inhibitor and deionized water up to 100 µl in sterile 1.5 ml tubes. The tubes were incubated at 37 °C for 30 minutes. At the end of the reaction, the mixture was diluted to 200 µl, and RNA was extracted using acidic PCI treatment. To ensure complete elimination of contaminating DNA, DNase digestion was repeated, this time using 2 µl of TURBO DNase (Thermo-Fischer-Scientific) along with the appropriate buffer and 0.5 µl of murine RNase Inhibitor in a final volume of 50 µl. Finally, RNA was additionally purified using Monarch kit (NEB) columns according to the manufacturer's instructions. The purified RNA (nearly free of contaminating DNA) was eluted in 20 – 25 µl of deionized water. The amount of RNA was determined using Qubit reader, and the integrity was checked by gel electrophoresis.

2.2.4.7. Reverse Transcription and quantitative PCR

RTqCR was applied for the strand-specific quantification of RNA synthesized inside the Huh-7.5 cells, triggered by 4th generation replicon system. For positive-strand as well as GAPDH mRNA

detection, 1 µg of RNA was heated to 70 °C in DNase-/ RNase-free PCR tubes for 5 minutes. In the meanwhile, 10 µM RT primer 'D_TAG_RT_plus_1' was also preheated at 70 °C. After 5 minutes, 1 µl of primer was added to the tubes, keeping them constantly at 70 °C on a heating incubator. The temperature was then decreased to 65 °C without removing the tubes from the incubator. During the temperature drop, 2 µl of LunaScript Reverse Transcriptase (primer-free) was added to the tubes to reach a total volume of 10 µl and mixed by pipetting up and down. For positive-strand detection, RT reaction was performed at 65 °C for 20 minutes followed by inactivation of the reverse transcriptase at 95 °C for 1 minute. RT for GAPDH was performed at 55 °C for 20 minutes, followed by inactivation at 95 °C for 1 minute and an infinite hold at 4 °C.

For the quantitative PCR reaction, 2 µl of 1:10 or 1:100 cDNA dilution was mixed with 10 µl of Luna Universal qPCR Master Mix, 0.1 µM forward and 0.2 µM reverse primer in a final reaction volume of 20 µl. The reaction mix was transferred to 96-well plates and sealed immediately to prevent any contaminations. The qPCR program for positive-strand detection was as follows: initial denaturation at 94 °C for 60 s; denaturation at 94 °C for 30s; annealing at 62 °C for 30 s and final melting curve analysis at 85 °C. For GAPDH detection: initial denaturation at 94 °C for 60 s; denaturation at 94 °C for 30s; annealing 55 °C for 30s and final melting curve analysis at 85 °C.

RTqPCR for negative-strand detection was performed as described in the following nascent RNA capture assay (2.2.4.8).

2.2.4.8. Nascent RNA Capture Assay

The nascent RNA capture assay allows the screening of newly synthesized RNA from the whole content of the total RNA present inside Huh-7.5 cells. In conventional transfection and RNA extraction protocols, the cell contains both the newly synthesized RNA produced after transfection and pre-existing RNA species that were already present before transfection. However, since the transfected RNA itself remains functional inside the cells even after 120 hpt (supplementary figure 3.2.3) and increases the RT-qPCR signals drastically – even in negative controls – during the strand-specific detection, this leads to false positive results in conventional transient expression experiments.

To overcome this problem, the nascent RNA is labelled using modified uridine molecules (5EU) which are directly added to the cell culture medium at the time of transfection. In this way, only the RNA newly synthesized after transfection is labelled with 5EU, while the bulk of pre-existing RNA in the cell remains unlabelled, as well as all DNA in the cell. Total RNA is extracted following the usual TRIzol extraction and purification procedure. In the total RNA preparation, an azide-modified biotin molecule is then covalently bound to the incorporated 5EU through a copper-catalyzed click reaction. The labelled RNA can then be efficiently captured using streptavidin magnetic beads and immediately used for strand-specific detection via RT-qPCR, while all non-5EU-labelled RNAs and DNA are removed during the washing steps. All necessary reagents for the assay were provided in the "Click iT Nascent RNA Capture kit (Thermo-Fischer-Scientific)".

Nascent RNA labeling with 5EU: As described previously (Transfection by lipofection, 2.2.4.5), 0.1 mM of 5EU was added to the Opti-MEM at the time of lipofection. After 4 hours, the Opti-MEM was replaced with complete medium supplemented with 0.2 mM 5EU. The 5EU concentration was refreshed every 24 hours.

5EU-Total RNA extraction: Total 5EU-RNA extraction was performed as described above (2.2.4.6) at specific time points (4, 24, 48 and 72 hpt). After the complete series of DNase digestion and purification steps, the total 5EU-RNA was eluted in 20 µl of deionized water. The concentration was determined using a Qubit Fluorometer, and the integrity was checked by gel electrophoresis. The yield was usually sufficient to proceed the subsequent biotinylation procedure. RNA was stored at -20 °C until further use.

Biotinylation: Purified total EU-RNA (8 - 10 µg) was mixed with 0.5 mM Biotin-azide (carboxamide-6-azidohexanyl biotin), 2 mM $CuSO_4$ and 25 µl Click-iT EU buffer (Component B) to prepare a final 50 µl reaction cocktail. To this cocktail, 1.25 µl of Click-iT reaction buffer additive 1 (Component E) was added and mixed immediately by pipetting up and down. This marked the initiating point of the click reaction between 5EU and biotin-azide. After 3 minutes, 1.5 µl Click-iT reaction buffer additive 2 (Component F) was added, which caused the solution to turn dark brown. The click reaction was incubated at room temperature with agitation at 300 rpm for 30 minutes.

The procedure was followed by extraction. To the click reaction, 700 µl chilled ethanol (100 %) and 75 µl of 5 M ammonium acetate was added to precipitate all RNA (including the biotinylated 5EU-RNA). The reaction tubes were incubated at -40 °C overnight. The RNA was pelleted by centrifugation at 14,000 rpm for 20 minutes at 4 °C. The supernatant was removed, and the pellet was washed twice with 70 % ethanol. The RNA was air-dried for 10 minutes and finally dissolved in 20 µl of deionized water. The concentration was determined by Qubit Fluorometer. Biotinylation did not significantly affect the total RNA yield; approximately 90 % of the starting material was recovered, as stated by the manufacturer. The RNA was stored at -20 °C.

Binding of Streptavidin Magnetic Beads: Before binding, streptavidin magnetic beads were washed three times using Click-iT Reaction Wash Buffer 2 (Component J) in 48 µl aliquots per vial. The beads were immobilized on a magnetic rack, the supernatant was removed, and the beads were resuspended in ten times the volume (480 µl) of Component J. The beads were immobilized again on the magnetic rack for 1 minute, and the supernatant was discarded. The washing step was repeated three times. Finally, the beads were resuspended in the same volume of Component J as the initial volume of the beads taken from the vial.

In the meanwhile, the RNA binding reaction was prepared. 31 µl of Click-iT RNA Binding Buffer (Component G) was added to 1 µg of the RNA preparation including the biotinylated 5EU-RNA, along with 0.5 µl of murine RNase inhibitor (NEB) and deionized water added to bring the final volume to 62 µl. The reaction tubes were heated up to 70 °C for 5 minutes. Next, 12 µl of streptavidin magnetic beads, previously washed and resuspended in Component J, were immediately added to the RNA binding reaction and mixed thoroughly by pipetting up and down. To facilitate the binding of biotinylated 5EU-RNA to the beads, the reaction tubes were agitated at 300 rpm at room temperature for 30 minutes.

Washing of the Beads: The streptavidin magnetic beads were then washed ten times to remove contaminating non-biotinylated RNA nucleotides, leaving only those molecules bound specifically to the beads that were synthesized during the time period of 5EU-labelling, i.e., after transfection of the HCV replicon system RNA (including HCV replicon system negative and positive strands as well as all cellular RNA synthesized during the above labelling time window). This step is crucial to obtain unambiguous results of strand-specific detection methods. The streptavidin magnetic beads were immobilized on a magnetic rack for 1 minute, the supernatant was discarded, and the beads were resuspended in 120 µl of Click-iT Reaction Wash Buffer 1 (Component I). The beads were immobilized again for 1 minute, and the supernatant was replaced by fresh 120 µl of Component I.

The wash step was repeated 5 times using Component I. Each time the beads were thoroughly resuspended in the fresh buffer by pipetting up and down for several times to ensure that any contaminating nucleotide hybridized nonspecifically to the target RNA were rinsed off. The washing procedure was then repeated an additional five times using 120 µl of Click-iT Reaction Wash Buffer 2 (Component J). Finally, the beads were resuspended in 12 µl of Component J and immediately used for the reverse transcription reaction.

Reverse Transcription: For minus-strand detection, 12 µl of RNA bound streptavidin beads, resuspended in sterile click-iT reaction Wash Buffer 2 (Component J), were diluted to a final volume of 15 µl in 0.2 ml DNase-/RNase-free PCR tubes and heated up to 70 °C for 5 minutes. In the meanwhile, 10 µM of the RT primer 'D_TAG_RT_minus_2' was also preheated at 70 °C. After 5 minutes, 1 µl of preheated primer was added to the bead suspension while maintaining the temperature at 70 °C using a heating incubator. Subsequently, the temperature was reduced to 65 °C, without removing the tubes from the incubator. During the temperature drop, 4 µl of LunaScript Reverse Transcriptase Master Mix (primer-free) (NEB) was added to the reaction and mixed by pipetting up and down. The reverse transcription reaction was performed at 65 °C for 30 minutes with gentle agitation at 300 rpm. Following the reaction, the PCR tubes were transferred to a thermal cycler for enzyme inactivation at 95 °C for 1 minute, followed by a hold at 4 °C. The beads were then centrifuged briefly, and 10 µl of resulting cDNA was carefully transferred to fresh, sterile 0.2 ml tubes for downstream applications.

Quantitative PCR reaction: The cDNA synthesized in the previous step was immediately used for quantitative PCR (qPCR). The cDNA, diluted 1:10 with DNase-/RNase-free deionized water, was mixed thoroughly with 10 µl of Luna Universal qPCR Master Mix, 0.1 µM of forward and 0.2 µM of reverse primer in a final reaction volume of 20 µl. The reaction mix was transferred to 96-well plate and sealed instantly to prevent any contamination. The qPCR program is described as follows: initial denaturation at 94 °C for 60 s; denaturation at 94 °C for 30 s; annealing at 62 °C for 30 s (40 cycles) and final melting curve analysis at 85 °C.

2.2.4.9. Strand-Specific RNA Detection Assay

Starting from the replicon RNA synthesis through to the final RT-qPCR reaction, the entire procedure comprises a series of optimized methods that must be carefully applied to ensure highly accurate measurement of negative-strand RNA abundance. The process includes *in vitro*-transcription of replicon RNA followed by DNase digestion, as described in Section 2.2.4.1. Subsequent steps, including transfection (Section 2.2.4.5) and all other procedures described up to section 2.2.4.8, collectively constitute the optimized strand-specific RNA detection assay.

2.2.5. Work with Proteins

2.2.5.1. *Firefly* Luciferase Assay

The assay is based on the activity of *firefly* luciferase to catalyze the mono-oxygenation of beetle luciferin. In the presence of ATP and molecular O_2, the *firefly* luciferase converts luciferin into oxyluciferin, along with the emission of light, which can be measured by a luminometer. The amount of light emitted is proportional to the amount of protein expression in the cells.

In the 4th generation replicon construct, *firefly* luciferase (61 kDa) was inserted at the 3´-site of 5´UTR region under PV-IRES. For the *firefly* luciferase assay, the reagent (Steady-Glo Luciferase Assay System, Promega) was prepared by adding lysis buffer to the lyophilized substrate (luciferin) and mixed thoroughly following manufacturer's guidelines. The protein expression was measured as a control of translation at the time points 4, 24, 48 and 72 hpt. The cells in 6-well plates were washed with 1x PBS, and 120 µl *firefly* luciferase assay reagent was added dropwise directly onto the cells. The cells were incubated in the dark at room temperature for 10 minutes. After that, the cells were detached from the bottom using an appropriate cell scraper, and the whole lysate was transferred to a transparent tube for measurement by luminometer.

2.2.5.2. HiBiT Assay

Expression of viral proteins inside Huh-7.5 cells was measured by bioluminescence using the Nano-glo HiBiT Lytic Detection System. The system consists of a tag (HiBiT-tag) fused to the protein of interest. The HiBiT-tag binds with a high affinity to LgBit, a complementing polypeptide that reconstitutes a bright luminescent NanoBit enzyme. The bioluminescence emitted by the reaction is measured by a luminometer.

The viral protein core was fused to (3x) 11-aa-long HiBiT-tag at its C-terminus. Protein expression was measured at the time points 4, 24, 48 and 72 hpt. The HiBiT lytic buffer was prepared by adding 1:50 volume of HiBiT substrate and 1:100 volume of LgBiT protein at room temperature. The medium was removed, and the cells were washed with 1x PBS. The HiBiT lytic buffer mixture was added dropwise directly onto the cells (120 µl for 6-well and 60 µl for 12-well plates) and incubated in the dark at room temperature for 10 minutes. The cells were detached from the bottom using an appropriate scraper, and the whole lysate was transferred to transparent tubes for the bioluminescence measurement.

2.2.6. Data Processing

The relative light units (RLUs) obtained from the *firefly* luciferase and HiBiT assay measurements were first normalised to the corresponding mock values (mock-normalised RLUs = RLUs {sample}/ RLUs {mock}). To assess fold changes over time, the mock-normalised RLUs were further normalised either to the highest observed protein expression level – specifically, the mock-normalised RLUs of the SLI-III WT construct at 48 hpt – or to the mock-normalised RLUs of the 5´UTR WT construct at 72 hpt. Data are presented as the mean from at least three biological replicates, with a standard deviation (± SD), calculated using Microsoft Excel für Mac (Version 16.100.30). Statistical significance was calculated using a Two-way ANOVA (* $p < 0.05$; ** $p < 0.01$; *** $p < 0.001$; **** $p < 0.0001$), with p-values > 0.05 considered not significant (ns). All statistical analysis were performed using GraphPad Prism 10 for macOS (version 10.4.2).

The Ct values obtained from RT-qPCR curves (Cfx maestro Software for Real-time PCR) were first normalised to the corresponding GAPDH value (ΔCt = Ct {sample} – Ct {GAPDH}). From these GAPDH-normalised logarithmic ΔCt values, the linearized values (2^-ΔCt) were calculated. To assess fold changes over time, the linear values (2^-ΔCt) were further normalized to the highest observed gene expression value – specifically, the 2^-ΔCt of the 5´UTR WT construct at 72 hpt (fold change = 2^-ΔCt {sample}/ 2^-ΔCt {5´UTR WT at 72 hpt}). Data are represented as the mean from at least three biological replicates, with standard deviation (± SD), calculated using Microsoft Excel für Mac (Version 16.100.30). Statistical significance was assessed from the normalised ΔΔCt values (ΔΔCt = ΔCt {5´UTR WT at 72 hpt}- ΔCt {sample}) using a One-way or a Two-way ANOVA (* $p < 0.05$; ** $p < 0.01$; *** $p < 0.001$; **** $p < 0.0001$), with p-values > 0.05 considered not significant (ns). All statistical analysis were performed using GraphPad Prism 10 for macOS (version 10.4.2). Error bars in the resulting figures represent the standard deviation (± SD) from at least three independent experiments.

3. Results and Discussion

3.1. Effective DNA removal, 5EU-labelling of nascent RNA and high temperature RT-qPCR collectively contribute to the elimination of background signals during strand-specific RNA detection

Study of *cis*-acting elements on RNA genomes requires two fundamental components: a reliable replicon system and a set of optimized experimental procedures. Significant effort was first dedicated to establishing a replicon system designed with components that meet all functional requirements. The second major task involved customizing a reliable strand-specific detection assay capable of minimizing all background signals. Establishment of the replicon system will be discussed in the next section, first, I will focus on the strategies applied to improve strand-specific detection.

Quantitative measurement of negative-strand RNA must be performed with great precision, as the highly sensitive RT-qPCR technique is prone to background signals caused by various sources of contamination. The quality of replicon RNA is the first critical factor which forms the foundation for the success of the entire procedure. Therefore, in comparison to standard procedures, extreme care was applied to purify the replicon RNA after *in vitro*-transcription prior to the transfection of the RNA into cells. The replicon RNA was synthesized by *in vitro*-transcription using linearized plasmid DNA as a template. To completely eliminate the plasmid DNA, the *in vitro*-transcribed RNA was then subjected to two subsequent rounds of TURBO DNase treatment, followed by purification using Monarch kit columns (2.2.4.1). Successful removal of template DNA was confirmed by visualising the RNA on a 0.8 % agarose gel before and after DNase digestion (Fig. 3.1.1 A).

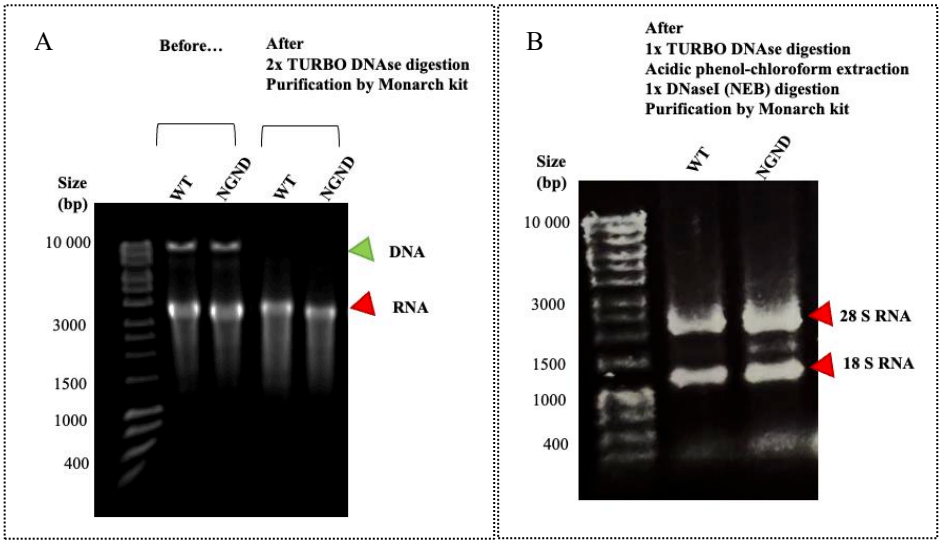

Figure 3.1.1. Representation of effective template DNA removal following (A) *in vitro*-transcription and (B) total RNA extraction. (A) Plasmid DNA was digested with TURBO DNase in two rounds, followed by purification using Monarch RNA purification columns (NEB). Approximately 500 ng of RNA was visualized on a 0.8 % agarose gel. **(B)** Total RNA was extracted using TRIzol and contaminating DNA was removed by two rounds of digestion using TURBO DNase (Thermo-Fischer-Scientific) and DNase I (NEB). Subsequent purification steps included acidic phenol-chloroform extraction, ethanol precipitation and final cleanup using Monarch RNA purification columns. Approximately 700 ng of RNA was visualized on a 0.8 % agarose gel.

Previously, TURBO DNase digestion was performed only once, however, experience has shown that performing two rounds of digestion followed by purification ensures more effective removal of residual DNA. Though purification of RNA can be performed by acidic phenol/chloroform (pH ~ 4.5) extraction (2.2.4.2), which may provide more efficient RNA isolation, the resulting RNA often loses its functionality. This is likely due to disruption of its secondary structure by the acidic environment, as suggested by repeated unsuccessful trials. Moreover, the purification using acidic phenol is adversely affected by the presence of any residual salt in the RNA solution (Supp. fig. 3.1.1). CsCl purification (2.2.4.3) proved to be highly detrimental to RNA. The method was successful in partially eliminating the residual DNA, but it caused significant RNA degradation (Supp. fig. 3.1.2). An additional drawback is the requirement of large quantities of RNA, most of which is degraded during prolonged ultracentrifugation at room temperature for approximately 18 – 20 hours. Purification of RNA by gel filtration (2.2.4.4.) also proved impractical due to very low RNA yield, which was insufficient for any transfection experiments.

Finally, highly purified RNA, virtually free of any residual DNA, should be transfected into appropriate Huh-7.5 cells permissive for HCV replication via lipofection. The procedure has been optimized by selecting the appropriate cell-type, using cell-culture medium supplemented with high quality heat-inactivated fetal bovine serum (FBS), determining the optimal amount of replicon RNA for transfection and choosing suitable transfection reagents. For the trial, three different cell types (Huh-7.5, Huh-7 and HepG2) were transfected with 0.8 – 1 µg of replicon RNA. Huh-7.5 cells at passage 22 were selected based on their ability to exhibit the highest protein expression at 24 hpt, compared to HepG2 and Huh-7 cells (Supp. fig. 3.1.3). The selected Huh-7.5 cells were cultured in DMEM supplemented with three different kinds of FBS and each condition was tested by transfecting an equal amount of replicon RNA. Heat-inactivated FBS sourced from the United States was selected, as cells grown in this medium showed the highest protein expression at 48 hpt (Supp. fig. 3.1.4). Next, the minimum amount of RNA required to observe an increase in protein expression at 48-72 hpt was tested, along with different transfection reagents (Supp. fig. 3.1.5) recommended by AG Lohmann. All selected conditions and reagents were validated using the positive control kindly provided by AG Lohmann (Supp. fig. 3.1.6), which confirmed the reliability of the applied conditions.

Only an appropriate amount of replicon RNA transfected into Huh-7.5 cells could induce translation and replication. Most of the input RNA declined over time, but surprisingly, a small fraction remained intact up to 120 hpt (Supp. fig. 3.1.7), which may correlate with the nascent RNA signals synthesized within the host cells after transfection. To discriminate the input RNA from nascent RNA, the cell culture medium was supplemented with appropriate amount of 5 Ethynyl Uridine (5EU), which enabled specific labelling of newly synthesized RNA only. Following the nascent RNA capture assay, the newly synthesized RNA was biotinylated and isolated using streptavidin magnetic beads (2.2.4.8.). The labelling with 5EU enormously contributed to the reduction of background signals during strand-specific detection (Fig. 3.1.2).

without 5EU-labelling

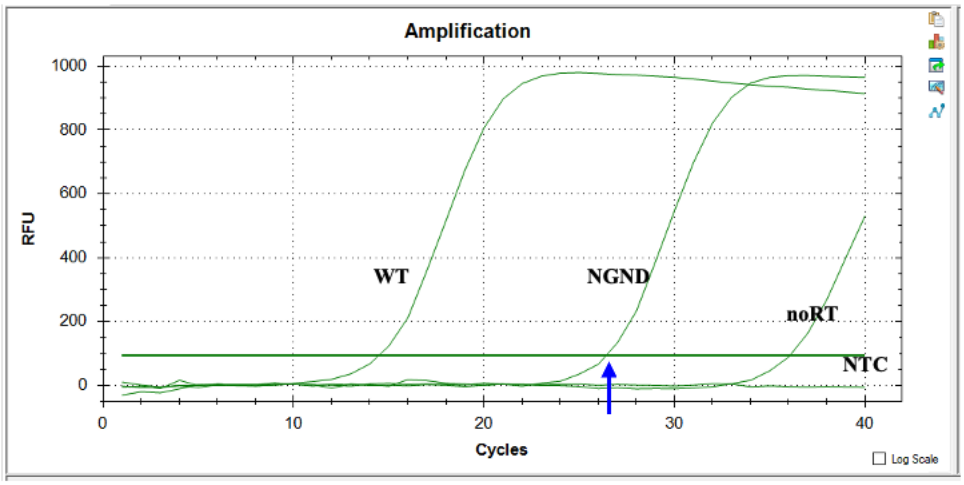

with 5EU-labelling

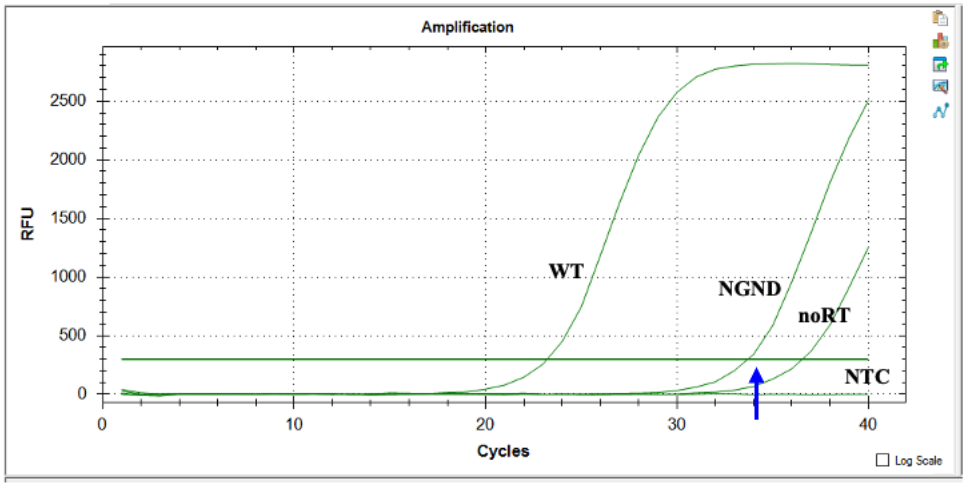

	without 5EU-labelling	with 5EU-labelling
5´UTR WT	14.49	23.19
5´UTR NGND	26.43	33.67
noRT	36.08	36.51

Figure 3.1.2. Comparison of Ct values obtained by RT-qPCR negative-strand RNA detection in 4th generation replicon system using 5´UTR wild-type and NGND (polymerase deficient) constructs. Huh-7.5 cells were transfected at ~ 90 % confluency with either 5EU co-transfection for nascent RNA labelling (lower graph) or without 5EU co-transfection (upper graph). Total RNA was extracted after 48 hpt, followed by two rounds of digestion using TURBO DNase (Thermo-Fischer-Scientific) and DNase I (NEB). Subsequent purification steps included acidic phenol-chloroform extraction, ethanol precipitation and final cleanup using Monarch RNA purification columns (2.2.4.6). 5EU-labelled nascent RNA was isolated using Click-iT Nascent RNA Capture kit. Negative-strand RNA was detected using specific tagged RT and qPCR primers and conducting the reaction at elevated temperatures (RT at 65 °C; qPCR at 62 °C). Ct values are shown below the graphs. High Ct values observed in the negative control of non-5EU-labelled samples indicate high background which was successfully reduced by nascent RNA capture using streptavidin magnetic beads.

In addition to the purification of replicon RNA, purifying total RNA extracted from the Huh-7.5 cells at various time points after transfection has been another challenging aspect. Conventional total RNA extraction using TRIzol was combined with further genomic DNA removal steps, followed by PCI

purification using acidic phenol/chloroform (pH ~ 4.5). At this stage, preserving the RNA secondary structure or functionality is no longer a priority, instead, achieving a high level of purification by removing all traces of contaminating genomic DNA (and even residual plasmid DNA from the previous *in vitro*-transcription) is essential. Incomplete removal of template DNA from the replicon RNA could result in its co-transfection into Huh-7.5 cells, where it may remain intact and contribute to high background signals. In addition to standard procedures, several additional steps were added after TRIzol purification of the RNA. To eliminate all DNA contaminants, DNase digestion was performed twice, followed by PCI purification using acidic phenol and cleanup with Monarch kit columns (2.2.4.6.) (Fig. 3.1.1 B).

The strong hairpin structure on the 3´-end of replicon RNA likely promotes self-priming, which could misguide both T7 polymerase during *in vitro*-transcription and reverse transcriptase during strand-specific detection. As a result, the replicon RNA may contain positive-strand RNA molecules with extensions corresponding to negative-strand RNA sequences (Fig. 1.6), leading to false positive signals in the procedure for the detection of negative-strand RNA. Labelling newly synthesized RNA with 5EU and isolating it from input replicon RNA provided a practical solution for this issue, since all negative strands premade by T7 RNA polymerase activity during *in vitro*-transcription are excluded from RNA recovery from the cells. Self-priming during reverse transcription was further minimized by conducting the reaction at elevated temperatures: preheating the purified total RNA to 70 – 65 °C and maintaining 65 °C throughout the reverse transcription reaction (2.2.4.7.).

Another factor that supported the overall optimization process was the use of tagged primers (Fig. 3.1.3). A non-viral tag sequence was added to the 5´-end of the reverse transcription primer, and the qPCR primers were designed accordingly. This arrangement enhanced the specificity of the reaction and significantly reduced the likelihood of nonspecific or irrelevant cDNA synthesis (Dobson et al., 2023).

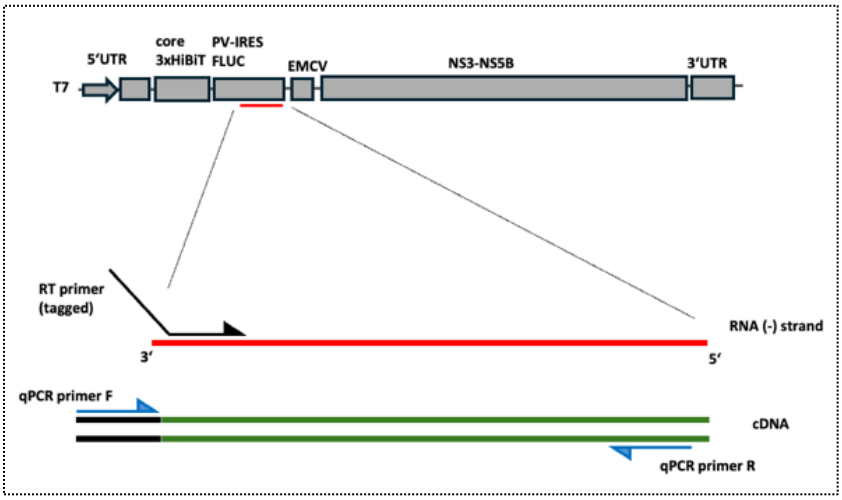

Primer ID	Sequence (5´ – 3´)
D_TAG_RT_minus_2	gcaggagctaagcgctggTcaggagctaagGTAGCGACCCTTT GCAGGCAGCGGAACC
D_TAG (as forward)	gcaggagctaagcgctggTcaggagctaag
Amp_2_minus_R	ACGTGGCACTGGGGTTGTGCCG

Figure 3.1.3. Schematic representation of primer binding to negative-strand RNA targeting the FLuc region. The tagged RT primer, D_TAG_RT_minus_2, contains a non-viral tag sequence (adopted from Dobson et al., 2023) shown in lower case letters. The forward qPCR primer, D_TAG, has the same non-viral tag sequence, while the reverse qPCR primer targets the FLuc sequence.

After applying all optimization procedures, a comparison was conducted to quantify the abundance of negative-strand RNA synthesized in Huh-7.5 cells at 48 hpt, with or without 5EU-labelling. In the absence of 5EU-labelling, negative-strand RNA was detected with a Ct value of approximately 14.49, whereas with 5EU-labelling it was detected with a significantly higher value of Ct 23.19. Notably, even the replication deficient construct (NGND) exhibited detectable negative-strand RNA in the absence of 5EU-labelling, with a Ct value of 26.43. Meanwhile, noRT controls yielded signals at Ct ~ 36 or above, indicating a high degree of purity in the extracted total RNA (Fig. 3.1.2).

The high negative-strand RNA abundance observed in samples without 5EU-labelling likely reflects the presence of input RNA remnants, particularly extended RNA species generated during *in vitro*-transcription, which remained intact throughout the workflow –from *in vitro*-transcription to reverse-transcription. Overall, these results demonstrate the reliability as well as the importance of the applied optimization procedures in effectively minimizing (nearly) all background signals in strand-specific RNA detection assay.

3.1.1. Discussion of strand-specific RNA detection

A comprehensive set of optimized experimental procedures was developed to study *cis*-acting elements involved in the initiation of negative-strand RNA synthesis in HCV. Previous investigations were hindered by a high background signal (L Shalamova, unpublished), primarily due to contaminants such as residual plasmid DNA, excessive input RNA and self-priming at the 3´-end of subgenomic positive-strand RNA. In this study, these interfering factors were substantially reduced through the implementation of a fully tailored protocol, referred to as the "strand-specific RNA detection assay" (2.2.4.9). Key steps of the strand-specific RNA detection assay include the efficient removal of plasmid-DNA following *in vitro*-transcription, achieved through two rounds of DNase treatment using TURBO-DNase (Thermo-Fischer-Scientific), followed by purification of replicon RNA with Monarch RNA purification columns (NEB) (Fig. 3.1.1). Nascent RNA was labelled with 5EU, biotinylated, and captured using streptavidin magnetic beads. Reverse transcription and quantitative PCR were then performed using tagged-primers and elevated temperatures to enhance strand-specificity. Implementation of this optimized workflow resulted in a significant reduction in background RT-qPCR signal (Fig. 3.1.2).

All optimization applications, specifically 5EU-labelling, successfully discriminated the nascent RNA synthesized in the host cells after transfection from the transfected input RNA. For negative-strand detection, the RT-qPCR signal for the 5EU-labelled negative control (NGND) was delayed by 7.24 cycles compared to the signal obtained without 5EU-labelling (Fig. 3.1.2). Similarly, the non-5EU-labelled positive-control was detected approximately 9 cycles earlier than the signals measured in 5EU-labelled total RNA. The Ct values of the noRT controls (~ 36) indicate that the total RNA was highly purified. The additional RNA detected in the non-5EU-labelled samples corresponds to the input RNA that was transfected into the Huh-7.5 cells and partially remained intact up to 48 hpt.

Although DNA contamination was thoroughly eliminated, there remains probability that trace amounts of DNA remnants could still be present in the purified total RNA. The advantage of using 5EU-labelling is that the copurification of not only any kind of RNA pre-existing in the cells but also of any DNA is highly unlikely, since the 5EU-labelling marks only RNA freshly synthesized during the time period of 5EU-labelling, i.e., between transfection of the replicon RNA to be investigated and cell lysis. Moreover, since the biotin-streptavidin binding is very tight, the biotinylated nascent RNA captured on streptavidin beads can undergo ten very stringent washes with two different buffers. In addition to other DNA removal methods, 5EU-labelling combined with ten washing steps provides an added layer of specificity for isolating newly synthesized RNA.

Self-priming of 3´-end of the positive-strand HCV RNA was another challenge addressed by using thermostable reverse transcriptase (NEB) and conducting both RT and qPCR reactions at high temperatures – 65 °C for reverse transcription and 62 °C for qPCR. Preheating the RNA and primer separately at 70 °C ensured complete denaturation. Subsequently mixing them while gradually decreasing the temperature from 70° to 65 °C promoted specific primer binding and reduced the likelihood of self- or false-priming. Performing reverse transcription at 65 °C further minimized the risk of RNA secondary structure formation and non-specific priming effects. Although no specific result was generated to demonstrate the specific effect of elevated temperature alone, it likely contributed to the overall improvement of the procedure. Similarly, the use of tagged RT primer may have further enhanced the specificity of the RT-qPCR reaction, as previously reported in the literature (Lim et al., 2013; Dobson et al., 2023).

3.1.2. Concluding Remarks

All the strategies mentioned above — specifically, the effective removal of contaminating DNA from both the replicon RNA and the extracted total RNA, the discriminating of input RNA from newly synthesized RNA through 5EU-labelling and the application of high temperature RT-qPCR — collectively contributed to a significant reduction in background signals during strand-specific detection. This optimized set of protocols can be applied to any other replicon-based system for strand-specific detection, and the improved removal of genomic DNA after harvesting RNA from cells may also generally contribute to more specific analysis of low abundantly expressed cellular RNAs, including long non-coding RNAs.

3.2. 4th generation replicon system established for strand-specific RNA detection provided suppression of nearly all background signals

The basic 4th generation replicon system is a tricistronic expression system that consists of the full HCV NS3-NS5B replication protein expression cassette derived from the Jc1/JFH1 strains, along with several other functional components. These include (from 5´ to 3´) the complete HCV 5´UTR, the HCV core region (1-165 aa) fused in-frame with a HiBiT tag (11 aa), followed by the *firefly* luciferase reporter gene under the control of the heterologous Poliovirus IRES. Downstream, another heterologous IRES (EMCV) is positioned upstream of the NS3-NS5B cassette, which is followed by a complete HCV 3´UTR (Fig. 3.2.1 A).

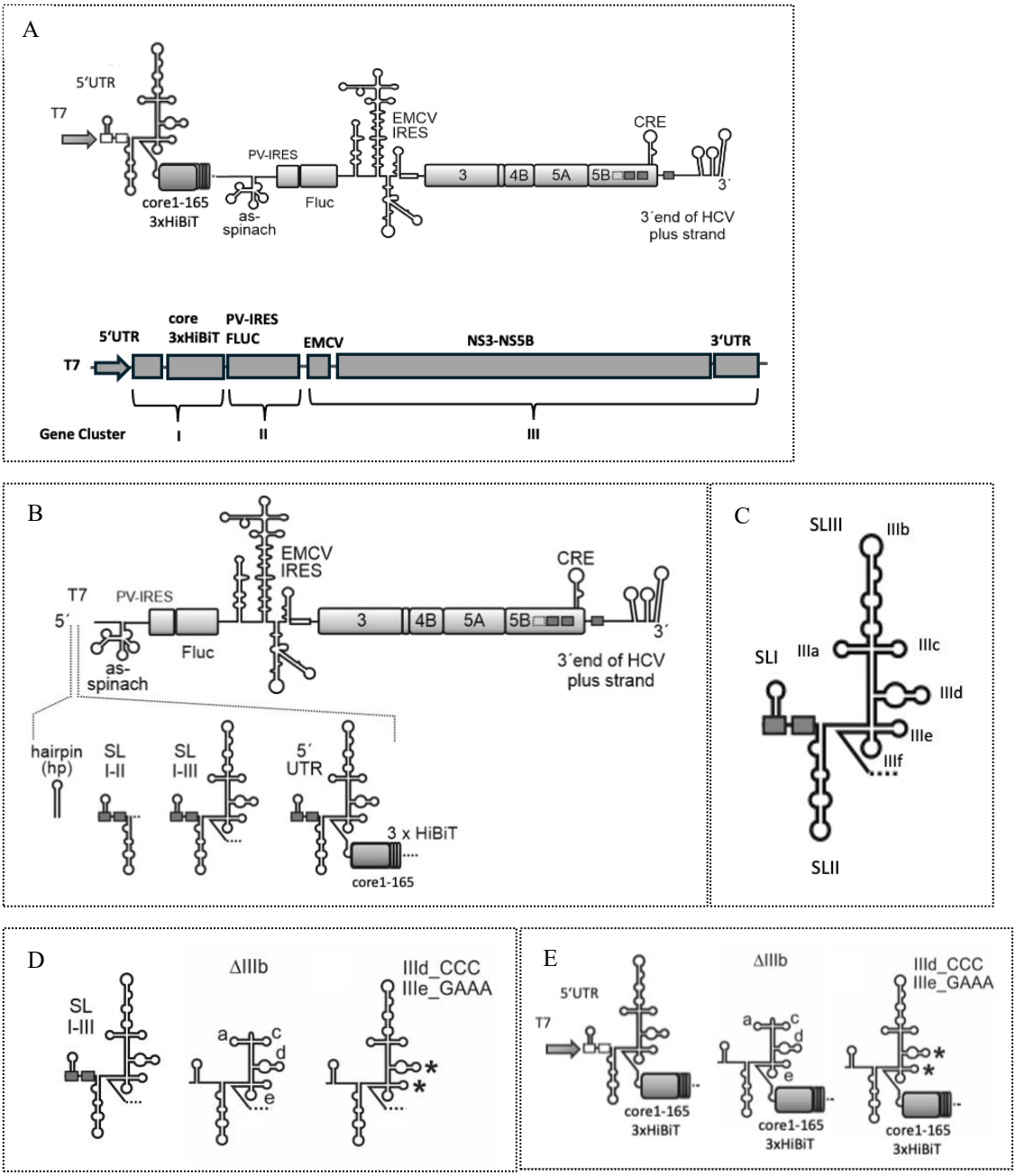

Figure 3.2.1. Schematic representation of tricistronic 4th generation replicon system and 5´UTR variants used for negative-strand RNA detection assays (A) Complete 5´UTR under T7 promoter with downstream core (1 -165 aa) in-frame with 3xHiBiT tag (Gen Cluster I), *firefly* luciferase in-frame with upstream PV IRES (Gene Cluster II) and viral NS3-NS5B cassette under EMCV-IRES with downstream 3´UTR (Gene Cluster III). **(B)** Schematic representation of hairpin and 5´UTR mutants – SLI-II, SLI-III and complete 5´UTR with HiBiT-tagged core-sequence – induced at 5´-end of basic 4th generation replicon system shown. **(C)** Representation of stem-loop subdomains IIIa, IIIb, IIIc, IIId, IIIe and IIIf in SLIII. **(D)** 5´UTR mutations in SLI-III construct, SLI-III ΔIIIb and SLI-III mutIIId/e. **(E)** 5´UTR mutations in 5´UTR construct, 5´UTR ΔIIIb and 5´UTR mutIIId/e.

Thus, the system is basically organized into three gene clusters (Fig. 3.2.1 A), all arranged within a DNA plasmid (T7_5´UTR_core_Hibit_Fluc) under the control of a T7 promoter:

Gene cluster I provides different extents of the authentic annotated HCV 5´UTR sequences which can act as *cis*-elements for the regulation of synthesis of the positive-strand or of the negative-strand.

In the basic version (hp), only a 5′ stem-loop provides basic protection of the RNA against degradation, whereas other versions provide increasing lengths of authentic HCV 5′UTR sequences, and in the full version the complete HCV 5′UTR is followed by the HCV core protein with a tagged triple HiBiT to provide also measurement options for the translation capacity of the HCV 5′UTR sequences (Fig. 3.2.1. B). In the intermediate SLI-III version, only the RNA structures that are sufficient for recruitment of eIF3 and the small ribosomal 40S subunit to the viral RNA are present, while the downstream *cis*-elements required for successful completion of a functional translation initiation event – the pseudoknot and SLIV including the authentic HCV AUG start codon – are missing.

Gene cluster II (Fig. 3.2.1 A and B) provides an expression cassette which can be used for independent quantification of *firefly* luciferase (FLuc) as an indirect measure for the abundance of positive strands produced by the replicon RNA within the cells. The heterologous Poliovirus IRES is used to avoid (1) recombination of the plasmid DNA during plasmid propagation and (2) minimize possible competition of the different IRES elements in the replicon for IRES-specific ITAFs, even though competition for basic translation components between the different IRES elements cannot be completely avoided.

Gene cluster III (Fig. 3.2.1 A and B) provides the HCV non-structural proteins NS3 to NS5B (from the Jc1 clone (Pietschmann et al., 2006)) which are required for intracellular replication of the replicon RNA, and the HCV 3′UTR provides the basic *cis*-signals required for the start of negative-strand synthesis.

By the use of the above independent gene clusters, the actual function under investigation, i.e., the possible role of HCV 5′UTR *cis*-elements in the regulation of negative- and positive-strand synthesis, is fully uncoupled from the need to express the replication protein cassette and the independent FLuc marker.

A self-cleaving HDV ribozyme is placed downstream of this entire RNA expression cassette, i.e., downstream of the HCV 3′UTR, in order to generate an exact 3′-end of the HCV 3′UTR at the end of the expression cassette (Supp. Fig. 2.1). Moreover, a T7 terminator is positioned even downstream of the HDV ribozyme to provide a strong terminating signal for the T7 polymerase, in order to avoid longer run-through transcripts on template plasmid DNAs that may have escaped complete restriction enzyme cleavage downstream of the entire replicon cassette.

Two versions of each of these constructs are used: one form with wild type NS5B polymerase (WT), and the other NS5B polymerase deficient mutant (NGND) (Supp. fig. 2.6) (where the upper strand always represents the sequence of HCV subgenomic positive-strand RNA). The polymerase deficient mutant (NGND) serves as a negative control in the replication assays. In the NGND mutant, two aspartic acid residues (D220 and D318) within the active pocket of NS5B have been substituted with asparagine residues (N220 and N318) (2.2.3.1.2), whereas in the underlying GND mutant there is only the D318N substitution (Lohmann et al., 1997). As to the nomenclature: in the Lohmann (1997) study, in the continuous 3 amino acid sequence "317-GDD-319" in the NS5B active centre the "D318" was changed to "N", and the mutant was named "GND". In the thesis presented here, additionally D220 (which is further upstream of the GDD sequence but also forms a discontinuous part of the active centre) was changed to "N", reflected by the nomenclature "N-GND" or in short "NGND". An overall improvement of the polymerase deficient negative control replicon system was anticipated due to the inactivating NGND double mutant, expecting even lower replication in the negative controls as well as even higher genetic stability. The successful establishment of the fully

functional 4th generation replicon system, however, involved overcoming several additional challenges, which are described in the following paragraph.

The 4th generation replicon system explained above is a modification of the originally planned 3rd generation replicon system. The characteristic features of 3rd gen replicon system include SP6 promoter, core (1-165 aa) fused to C-terminal 3xHiBiT tag and NS3 N-terminally fused to 3x Flag tag. The use of SP6 polymerase was intended due to its reported ability to produce transcripts with significantly reduced copyback (Schenborn et al., 1985) in comparison to T7 polymerase (Supp. Fig. 3.2.1). However, this characteristic of SP6 promoter and polymerase could not be confirmed in the present study. On the contrary, *in vitro*-transcription driven by SP6 promoter resulted in low RNA yield, which was mostly insufficient for transfection. Additionally, a smaller RNA byproduct of approximately 3000 nt – comparable in amount to the intended ~ 11,000 nt transcript – was consistently observed (Supp. Fig. 3.2.2). Nevertheless, Huh-7.5 cells were transfected by lipofection using 0.8 – 1 µg of purified 3rd generation replicon RNA. Gene expression driven by the 5´UTR was measured using the HiBiT assay at time points 24, 48, 72, 96 and 120 hours post-transfection (hpt). Although a relatively high expression of core protein at 48 hpt would have confirmed the functionality of 3rd generation replicon system, this was not the case. Instead, a steady decrease in the protein expression was observed from 24 hpt up to 120 hpt. Moreover, the polymerase deficient control (3G_GND) was also showing high levels of protein expression relative to (3G_WT) (Supp. Fig. 3.2.3). The actual reasons for the failure of replication of the 3rd generation replicon could not be tracked back and identified, but the above mentioned problems with RNA synthesis and the presence of possibly interfering RNA byproducts may have contributed to that failure. Therefore, the transfection experiments with 3rd generation replicon system were discontinued after a few trials.

The 4th generation replicon system was then evaluated alongside two additional constructs for comparative analysis. One of the mutants, hp (T7_hp_Fluc), features a complete substitution of the 5´UTR with a hairpin structure, also lacking the HiBiT-tagged core (Fig. 3.2.1 B). The hairpin is positioned at the extreme 5´-end to provide RNA stability. Due to the complete absence of HCV 5´UTR sequences, this mutant served as another kind of negative control in addition to the NGND polymerase mutation in the constructs, since it was expected to be incapable of replication at least at the stage of the initiation of positive-strand RNA synthesis from the negative-strand, i.e., it should not be capable of production of progeny positive-strands – an assumption that was confirmed by the inability of this construct to confer overall "roundabout" amplification, i.e., undergoing several subsequent rounds of negative and positive RNA strand synthesis which results in genome amplification (see below). The other mutant, SLI-III (T7_SLI-III_Fluc WT/NGND), contains only the first three stem-loop domains of the 5´UTR region and lacks the HiBiT-tagged core (Fig. 3.2.1 B). The SLI-III region of the 5´UTR includes the essential internal ribosome entry site elements (IRES) required for the binding of eIF3 and the small ribosomal 40S subunit. One question addressed by the SLI-III mutant in the 4th generation replicon system was, if its replication capacity is limited compared with the complete HCV 5´UTR.

As detailed above, the basic tricistronic 4th generation replicon system enables quantitative measurement of gene expression using two different assays: *firefly* luciferase (FLuc) and HiBiT. FLuc is expressed under the control of the Poliovirus IRES in Gene Cluster II, while HiBiT is placed under the control of the HCV 5´UTR of the positive-strand genome, in-frame with the core region (1-165 aa) in Gene Cluster I (Fig. 3.2.1 A). Thereby, expression from the FLuc gene in Gene Cluster II was regarded an indirect measure for overall positive-strand abundance, initially assuming that expression from Gene Cluster II is largely independent of any features of the sequences in the flanking Gene Clusters I and III. However, HiBiT expression in Gene Cluster I was supposed to

reflect the specific ability of the HCV 5´UTR sequences under investigation to direct a functional translation initiation event, the above described other two mutants, hp and SLI-III, allow gene expression measurement solely via *firefly* luciferase assay (Fig. 3.2.1 B).

The replicon system was evaluated by measure of viral gene expression (translation) by FLuc assay, which serves as an indirect indicator of positive-strand abundance and by that of replication. In case of successful replication, a peak of gene expression was expected at about 48 - 72 hpt. Similarly, successful replication would also be indicated by a peak in a negative-strand RNA abundance within the same time frame. Strand-specific RNA detection was employed to confirm viral replication and to quantitatively assess specifically negative-strand RNA synthesized in host cells by the viral NS5B polymerase.

All three constructs — hp, SLI-III and 5´UTR — were transfected to Huh-7.5 cells (2.2.4.5). Due to cost reasons, 5EU-labelling was exclusively performed on samples that were subsequently used for the negative-strand RNA detection. For quantitative PCR, a 1:10 dilution of the cDNA sample was used for negative-strand RNA detection, while a 1:100 dilution was used for positive-strand RNA detection (Supp. Fig. 3.2.6). Strand-specific detection (2.2.4.8) and FLuc assay (2.2.5.1) were performed in a time-course manner at 4, 24, 48 and 72 hpt. The corresponding results are presented in figures 3.2.2 A(i) and (ii), B(i) and B(ii) and C.

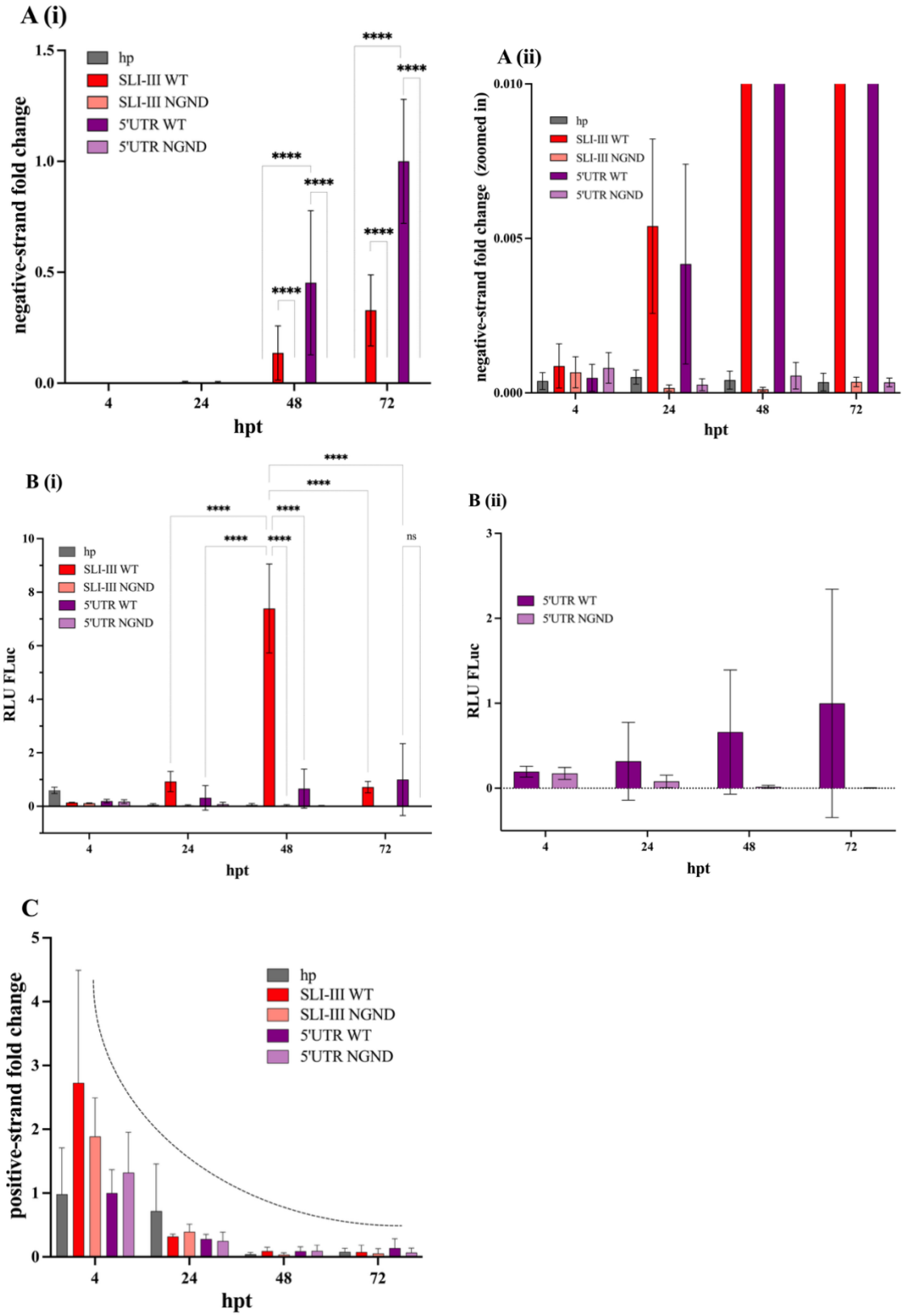

Figure 3.2.2. Evaluation of the functionality of the 4th generation replicon system by negative-strand RNA detection (A(i) and A(ii)), *firefly* luciferase assay (B(i) and B(ii)) and positive-strand RNA detection (C) using hp, SLI-III WT/NGND and complete 5´UTR WT/NGND. A total of 3.5 µg of replicon RNA was transfected into Huh-7.5 cells at ~ 90 % confluency. Total RNA was extracted after 4, 24, 48 and 72 hpt for strand-specific RNA detection. *Firefly* luciferase assay was performed in parallel. Positive- and negative-strand RNA was detected using specific tagged RT and qPCR primers

(Figure 3.1.3), with reactions conducted at elevated temperatures (RT at 65 °C; qPCR at 62 °C). **(A(i) and (ii))** Relative expression levels (2^-ΔCt values normalised to 5´UTR WT at 72 hpt) obtained from negative-strand RNA detection. Huh-7.5 cells were co-transfected with 5EU for nascent RNA labelling. The experiment was performed with n = 3 biological replicates. For the fold change measurement, the Ct values were first normalised to GAPDH (ΔCt) and linearized by applying 2^-ΔCt to each sample. The data were then normalised to the 5´UTR WT at 72 hpt. Statistical analysis was performed using logarithmic values normalised to the 5´UTR WT at 72 hpt (ΔΔCt). Two-way ANOVA was performed using GraphPad Prism. Error bars represent standard deviation (±SD) of mean. Asterisks mark p-values from Two-way ANOVA (*: $p < 0.05$; **: $p < 0.01$; ***: $p < 0.001$; ****: $p < 0.0001$). Both SLI-III and 5´UTR constructs showed statistically significant differences compared to their negative controls (NGND) and the hp at 48 and 72 hpt. A(ii) shows a zoomed-in view of A(i). **(B(i) and (ii))** *firefly* luciferase expression results. The experiment was performed with at least n = 4 biological replicates. Relative expression levels (RLUs) (normalised to mock and finally to the 5´UTR at 72 hpt) were analysed by two-way ANOVA using GraphPad Prism. Error bars represent standard deviation (±SD) of mean. Asterisks mark p-values from Two-way ANOVA (*: $p < 0.05$; **: $p < 0.01$; ***: $p < 0.001$; ****: $p < 0.0001$). The SLI-III construct (at 48 hpt) showed a statistically significant difference compared to the negative control (NGND) and complete 5´UTR at 4, 24, 48 and 72 hpt. B(ii) represents a zoomed-in view of B(i) showing only 5´UTR WT and NGND conditions. **(C)** Relative expression levels (2^-ΔCt values normalised to the 5´UTR WT at 4 hpt) obtained from positive-strand RNA detection. Ct values (normalised to GAPDH) were linearized (2^-ΔCt) and then normalised to the expression levels of the 5´UTR WT at 4 hpt. The experiment was performed with n = 3 biological replicates.

As expected, the abundance of negative-strand RNA gradually increased and was the highest at 72 hpt in both the 5´UTR and SLI-III constructs, providing the first confirmation of the functionality of the 4th generation replicon system (Fig. 3.2.2 A(i)). Importantly, no negative-strand RNA was detectable in replication-deficient constructs (NGNDs), further validating both the reliability and the success of removing contaminating DNA and RNA that previously gave rise to false positive signals. The negative control hp showed about 0.00035-fold background compared to 5´UTR WT at 72 hpt. Likewise, polymerase deficient constructs –SLI-III NGND and 5´UTR NGND – showed about 0.00035- and 0.00034-fold background, respectively, when compared with their counterpart WT at 72 hpt (Fig. 3.2.2 A(ii), right panel). This means that the negative control is approximately 3,000-fold lower than the positive WT value. Compared with the previous results of L. Shalamova (see Introduction, Fig. 1.5 B) which showed a background of 0.25 (i.e., 25 %) in the negative control, this is a dramatic reduction of the background to only 0.035 % (i.e., approximately 700-fold reduction of the background).

As anticipated, the hp construct (which lacks all HCV sequences in the 5´ region) also showed no detectable positive signal. This confirms that the annotated HCV 5´UTR sequences are required for replication, either on the physical level of the positive-strand RNA (genome) or on the level of the negative-strand RNA (antigenome), or both. These findings collectively support the robustness and specificity of the 4th generation replicon system (Fig. 3.2.2 A(i) and (ii)).

The abundance of the positive-strand RNA, as expected, showed a steady decrease over time (Fig. 3.2.2 C). As already described, the samples used for positive-strand RNA detection correspond to non-5EU-labelled RNA. The detected signals likely reflect not only nascent RNA synthesized within Huh-7.5 cells post transfection but also input RNA that remained intact and detectable up to 72 hpt. These results confirm that the system enabled the measurement of negative-strand RNA synthesis independently of positive-RNA synthesis, which consistently declined over time (Fig. 3.2.2 C).

The *firefly* luciferase assay provided an indirect measure for the abundance of positive-strand RNA in Huh-7.5 cells. As described above, the positive strand RNA quantified by RT-qPCR (Fig. 3.2.2 C) primarily reflected the high amount of input RNA (3.5 µg per 6-well) transfected into the cells, which

remained relatively high at early time points (4 and 24 hpt) and subsequently declined over time. In contrast, the *firefly* luciferase (expressed from Gene Cluster II) assay was designed to evaluate the level of protein expression within the cells following transfection with the replicon RNA. Considering this objective, the FLuc expression was expected to increase progressively over time in Huh-7.5 cells. All three constructs – hp, SLI-III and 5´UTR – showed different FLuc expression over time (Fig. 3.2.2 B(i)). In comparison to the other two constructs, the negative control construct (hp) did not show any detectable FLuc expression, except at the early time point (4 hpt). The strong hairpin structure likely conferred greater stability to the replicon input RNA than the complete or truncated 5´UTR at approximately 4 hpt. The FLuc signals subsequently disappeared as the replicon RNA degraded over time (Fig. 3.2.2 B(i)). The lack of FLuc expression of the hp construct confirms the reliability of this negative control during the evaluation of the 4th generation replicon system. When analysing only the full 5´UTR construct (Fig. 3.2.2 B(ii)), a steady increase in FLuc expression was observed, with little to no detectable signal in the corresponding polymerase deficient construct (NGND) at 48 and 72 hpt. These findings confirm that Gene Cluster II can be translated successfully from the replicon RNA within Huh-7.5 cells, thus further supporting the functionality of the 4th generation replicon system.

Surprisingly, the truncated version of 5´UTR, namely SLI-III, exhibited a highly significant increase in FLuc expression at 48 hpt, which was approximately 7.5-fold higher than that of the full 5´UTR construct at 72 hpt. However, this expression sharply declined by 72 hpt to a level slightly below than that of the full 5´UTR (Fig. 3.2.2 B(i)). Although the physical presence of HCV 5´UTR elements should not affect protein expression under Gene Cluster II (FLuc expression), the significantly higher FLuc expression observed in the SLI-III construct at 48 hpt compared to the 5´UTR construct suggests some kind of influence, which may or may not be related to the missing 5´-end elements in SLI-III construct. In general, for HCV translation, the downstream 5´UTR elements such as the pseudoknot structure SLIII-f, SLIV containing AUG start-codon and SLVI play very important roles in regulating HCV-translation (Kieft et al. 2001). It can only be speculated that the truncated IRES present in the SLI-III construct is able to capture, but not productively utilize, translation components such as eIF3 and the small ribosomal 40S subunit. These sequestered components may then be provided in *cis* from the incomplete HCV IRES in Gene Cluster I to the Poliovirus IRES in Gene Cluster II, thereby enhancing Poliovirus IRES-driven translation from Gene Cluster II (Jünemann et al. 2006). Further investigation is needed to understand the possible relation between HCV-5´UTR elements and the elevated FLuc expression observed in the SLI-III construct (Fig. 3.2.2 B(i)). The slightly higher *firefly* luciferase expression observed for hp at 4 hpt may be attributed to unrelated factors, most likely the increased ribosomal affinity for the PV-IRES, given that the HCV-IRES (5´UTR) is entirely absent in this construct (Fig. 3.2.2 B(i)).

A closer examination of the graph (Fig. 3.2.2 A(ii)) suggests that negative-strand RNA synthesis may begin as early as 24 hpt in the full 5´UTR construct. The construct containing a hairpin structure, the hp, exhibited no detectable negative-strand signals (Fig. 3.2.2 A(i)), confirming its utility as an additional negative control in the strand-specific assay. This confirmed also that the complete 5´UTR region is essential for efficient viral replication.

Collectively, these results confirm that the 4th generation replicon system is a reliable tool for studying *cis*-acting elements involved in negative-strand RNA synthesis. Importantly, the combination of this replicon construct with the optimized experimental protocols (as described in preceding section) provides a robust platform for such investigations.

3.2.1. Discussion of replicon system development

A 4th generation replicon system was established that, when combined with an optimized strand-specific-detection assay, enables significantly more accurate quantification of negative-strand RNA compared to all other previously used replicon systems including 1st generation, 2nd generation and 3rd generation replicon systems (Supp. Fig. 3.2.4). This new tricistronic model contains three gene clusters, in contrast to the two used in earlier replicon systems (Fig. 3.2.1 A). Its design enables quantitative measurement of protein expression using two reporter genes – *firefly* luciferase and 3xHiBiT – whereas the 2nd generation replicon system contained only one reporter element, the HiBiT (Supp. Fig. 3.2.4)), which was placed in the replication protein gene group corresponding to Gene Cluster III in the 4th generation replicon system. Moreover, the previously used polymerase deficient construct, GND, carried a single D318N mutation in the active site of NS5B. In contrast, the current model, NGND, included the additional D220N substitution, which disrupts Mg^{2+} binding more efficiently and ensures low background signals (Fig. 3.2.2 A(i) and (ii)). Other negative controls such as GNN model, harbouring both D318N and D319N mutations (Rheault et al., 2023) or ΔGDD model (kindly provided by Lohmann group) have also been reported. In this study, however, the NGND model demonstrated also very low background and may provide improved genetic stability due to the double mutation.

Other factors also contributed to the enhanced performance of the replicon system. One debatable aspect was the choice of promotor sequence on the replicon plasmid. Though SP6 polymerase has been reported to produce fewer RNA side-products in comparison with T7 polymerase (Schenborn et al., 1985), the opposite was observed in this study (Supp. Fig. 3.2.1 and 3.2.2). Surprisingly, equal amounts of a byproduct RNA were observed on the gel alongside the intended transcripts. This suggests that the reported low side-product profile of SP6 may be limited to shorter RNA transcripts, as described in the literature and may not extend to larger transcripts such as ~ 11,000 nt RNA and larger, as used in this study. Another possible explanation for the RNA byproducts is cryptic termination of the polymerase at the 3´-end of poliovirus IRES, located upstream of the *firefly* luciferase gene (Supp. Fig. 3.2.5). While the use of T7 polymerase also resulted in similar short RNA byproducts, it had a key advantage: the yield of the intended RNA was approximately ten times higher than that of the byproducts (Supp. Fig. 3.2.2).

Firefly luciferase was used as the primary reporter-gene in the 4th generation replicon system and used as an additional (even if indirect) measure for the quantification of replicon positive-strand RNA abundance, while HiBiT provided an additional reporter to monitor protein expression driven by the authentic 5´-terminal HCV 5´UTR sequences. Although both allow for quantitative measurement of protein expression, each has its own advantages and limitations. HiBiT, for example, consists of only 11 amino acids and can easily be incorporated in-frame with sequences of core or NS3. In contrast, *firefly* luciferase (~1,000 amino acids) is a much larger protein and is expressed under the control of poliovirus IRES. Due to its size (~ 60 kDa) and its very specific enzymatic detection assay, *firefly* luciferase is unlikely to produce background signals; for instance, mock controls typically show only 29 – 50 relative light units (RLUs), while positive controls yield in the range of 2.5×10^6 RLUs. HiBiT, however, exhibits higher background levels in mock controls – approximately 2,500 RLUs – despite showing relatively lower values in positive controls (2.5×10^5 RLUs). These relatively high baseline values may be caused by the fact that similar other (cellular) peptides may mimic HiBiT and cause the high background, making HiBiT less reliable than *firefly* luciferase for sensitive detection.

The 4th generation replicon system, evaluated using the optimized set of strand-specific assay as described above, showed a steady increase in negative-strand RNA abundance for the complete 5′UTR and SLI-III construct, reaching the peak at 72 hpt. Notably, no or negligible signals were detected in the corresponding negative controls, including NGNDs and hp (Fig. 3.2.2 A(i) and (ii)), which marks a significant success over previous replicon systems and their specificity of negative-strand RNA detection. These results confirm that the 4th generation replicon system, in combination with optimized set of protocols, represents the most functional and reliable tool for negative-strand RNA detection compared to all previously used replicon systems and assays. The system enables an accurate monitoring of negative-strand RNA synthesis, which may begin as early as 24 hpt (Fig. 3.2.2 A(ii)), while interpretation at this early time point remains challenging, as the biological significance is not yet fully apparent. Experimenting with additional 5′UTR variants may help identify *cis*-acting elements that improve the ability to study the initiation of negative-strand RNA synthesis.

The 5′UTR construct exhibited higher levels of negative-strand RNA abundance compared to SLI-III construct, confirming previous findings that the full-length 5′UTR is crucial for the efficient replication (Niepmann et al., 2018). As shown in the Fig. 3.2.2 A(i), the SLI-III domains accounted for about 33% of the total negative-strand RNA abundance at 72 hpt, confirming it as a low-level replicating variant (Fig. 3.2.2 A(i)). Surprisingly, *firefly* luciferase assay results showed approximately 7.5-fold higher level of protein expression in the SLI-III construct compared to the full 5′UTR, while the 5′UTR construct itself exhibited a steady increase in FLuc-expression over time, mirroring the trend observed in negative-strand RNA levels (Fig. 3.2.2 B(i) and (ii)). The significantly higher FLuc expression in the SLI-III construct may be attributed to other factors that require further investigation. The absence of the SLIV domain in the SLI-III construct may disrupt specific long-range interactions with 3′-end of the positive-strand RNA, which are potentially important for NS5B binding. The combination of reduced replication and enhanced FLuc expression suggests a disturbance in the regulatory balance between these two processes. The significantly enhanced FLuc expression observed in the SLI-III construct, which does not correlate with the corresponding negative-strand RNA levels, points to an interesting underlying mechanism and should not be interpreted as procedural leakiness. One possible explanation could be that the SLI-III construct lacks those *cis*-elements that are necessary to allow the HCV IRES to actually undergo a functional translation initiation event, which would include the release of eIF3 from the RNA and incorporation of the (initiation competent) 40S subunit into a complete translating (and thus initiation incompetent) 80S ribosome. Instead, accumulation of eIF3 and 40S subunits on the SLI-III sequences may allow transfer of these components to another translation initiation site (here the downstream Poliovirus IRES), where they are available for more efficient translation initiation (Fehr et al., 2012). Considered the other way around, a fully functional HCV translation initiation site in Gene Cluster I binds but then also functionally uses up eIF3 and the 40S, thereby reducing their availability for the downstream IRES.

The increasing trend in FLuc expression over time, observed with the full 5′UTR construct (Fig. 3.2.2 B (ii)), can serve as an additional indicator of replication, supporting the results of the highly sensitive negative-strand RNA detection assay, which showed significantly elevated values compared to the corresponding negative controls (Fig. 3.2.2 A(i)). Additional 5′UTR variants should be investigated to enable a more detailed and in-depth analysis of the *cis*-acting elements involved in the initiation of negative-strand RNA synthesis.

3.2.2. Concluding Remarks

The established 4th generation replicon system and the set of optimized experimental protocols, in particular including 5EU labelling and isolation only of newly synthesized RNA (described in the preceding section), together provide a robust platform for strand-specific RNA detection. Efficient viral replication requires an intact 5´UTR. A truncated version, such as the SLI-III mutant shows reduced levels of negative-strand RNA abundance compared to the full length 5´UTR, although the SLI-III mutant confers significantly higher levels of gene expression from Gene Cluster II. This may also suggest that the SLIV in 5´UTR and the core-coding region may be critical for maintaining specific long-range interactions that are potentially involved for the NS5B binding at the 3´-end of the positive-strand RNA genome, and/or provide sequences which are required on the level of the negative-strand antigenome. The established replicon system can be used to study additional 5´UTR variants to investigate which *cis*-elements within 5´UTR of a positive strand RNA genome are involved in initiating negative-strand RNA synthesis.

3.3. Efficient negative-strand RNA synthesis requires the complete 5´UTR of a positive-strand HCV RNA genome, while the minimal essential *cis*-acting requirement for RNA synthesis appears to be the SLI-II region

All *cis*-elements within the uniquely folded 5´UTR of a positive-strand RNA genome may play distinct roles in replication, translation or in regulating the switch between the two. The *cis*-acting elements facilitating specifically the initiation of synthesis of the negative-strand RNA may reside within the 3´UTR region of the positive strand itself as well as in its 5´UTR. This principle of end-to-end stimulation of a certain biochemical process (e.g., the initiation of translation in cellular and viral (m)RNAs, or, in this case, the initiation of negative-strand RNA synthesis) is reasonable, as the presence of one end of the RNA signals in *cis* to the other end that the RNA is intact rather than degraded, and therefore "worth" initiating efficient translation or replication. The most well-known example of such end-to-end stimulation in *cis* is the stimulation of translation initiation at the 5´-end of capped mRNAs by the poly(A) tail at the mRNA´s 3´-end. Viral RNA genomes, including HCV, also employ such end-to-end stimulation of translation initiation (Ito et al., 1999; Song et al., 2006 and references therein). In either case, each individual SL domain within the full 5´UTR must be thoroughly investigated to elucidate its potential function. To this end, the complete 5´UTR of 4th generation replicon positive-strand RNA was mutated to design four distinct variants: SLI-II, SLI-III, SLI-III ΔIIIb and SLI-III mutIIId/e (Fig. 3.2.1 B and D).

The SLI-II construct is a modified version of the SLI-III construct (which was described in the previous section), differing only by the absence of the complete stem-loop domain III. It only contains the first two stem loop domains of the 5´UTR, a region which also harbours two binding sites for the liver-specific miR-122.

Two other variants – SLI-III ΔIIIb and SLI-III mutIIId/e – represent mutated SLIII domains. As already described, the stem-loop domain III of the 5´UTR region is further subdivided into smaller stem-loop domains – IIIa, IIIb, IIIc, IIId, IIIe and IIIf – all of which together form a main three-dimensional part of the IRES structure that is crucially involved in the initiation of viral translation (Fig. 3.2.1 C) (Niepmann et al., 2018). The SLI-III ΔIIIb construct lacks the IIIb domain and therefore prevents binding of eIF3 in the apical region of the SLIII domain. The SLI-III mutIIId/e construct

contains mutations in both stem loops IIId and IIIe. SLIIId directly interacts with the 40S ribosomal subunit via a GGG sequence (Kieft et al., 2001) and alternatively interacts with the *cis*-replicating element (CRE) in 5BSL3.2 to promote replication (Fricke et al., 2015; Romero-López et al., 2017). Moreover, LRI predictions suggest that the RNA sequence GAUA, positioned at the apical region of subdomain IIIe, interacts with the apical loop of 5BSL3.1 (Fricke et. al., 2015) (Fig. 4.3). The precise functional role of this long-range interaction is still unclear. However, mutations in IIId, GGG → CCC, disable the IRES to bind 40S and promote translation (Kieft et al., 2001), and also mutation in IIIe, GAUA → GAAA, impairs 40S ribosome binding and translation (Kieft et al., 2001). These alterations can lead to a drastic decrease in both translation and replication efficiency (Johnson et al., 2017). The question underlying the design and use of these SLIIIb and SLIIId/e mutants in the study presented here is, if binding of eIF3 and/or the ribosomal 40S subunit to the 5′-end of the HCV positive-strand RNA influences the efficiency of negative-strand RNA synthesis initiation at the HCV RNA 3′-end. On one hand, it could be speculated if the ribosomal 40S subunit bound to the 5′-end also interacts with the 3′-end (Bai et al., 2013), in order to stimulate the initiation of negative-strand RNA synthesis, according to the above mentioned idea of an RNA integrity check. On the other hand, another reasonable consideration is that binding of components at the 5′-end or the 3′-end may mutually inhibit activity at the other end, according to the idea, that simultaneously loading the RNA with ribosomes and with the NS5B replicase would cause collisions of ribosomes and replicase. The extent to which these elements are involved in the initiation of negative-strand RNA synthesis is addressed in detail in this study.

Using the strand-specific RNA detection assay, the negative-strand RNA abundance was measured (as previously described) in all above mentioned constructs along with hp and 5′UTR. All six constructs — hp, SLI-II, SLI-III, SLI-III ΔIIIb, SLI-III mutIIId/e and 5′UTR — and two -NGND controls were transfected to Huh-7.5 cells (2.2.4.5). 5EU-labelling was exclusively performed on samples that were subsequently used for the negative-strand RNA detection. For quantitative PCR, a 1:10 dilution was used for negative-strand RNA detection, while a 1:100 dilution was used for positive-strand RNA detection. Strand-specific detection (2.2.4.8) and FLuc assay (2.2.5.1) were performed in a time-course manner at 4, 24, 48 and 72 hpt. The corresponding results are presented in figures (Fig. 3.3.1 A(i) and (ii), B(i) and (ii) and C).

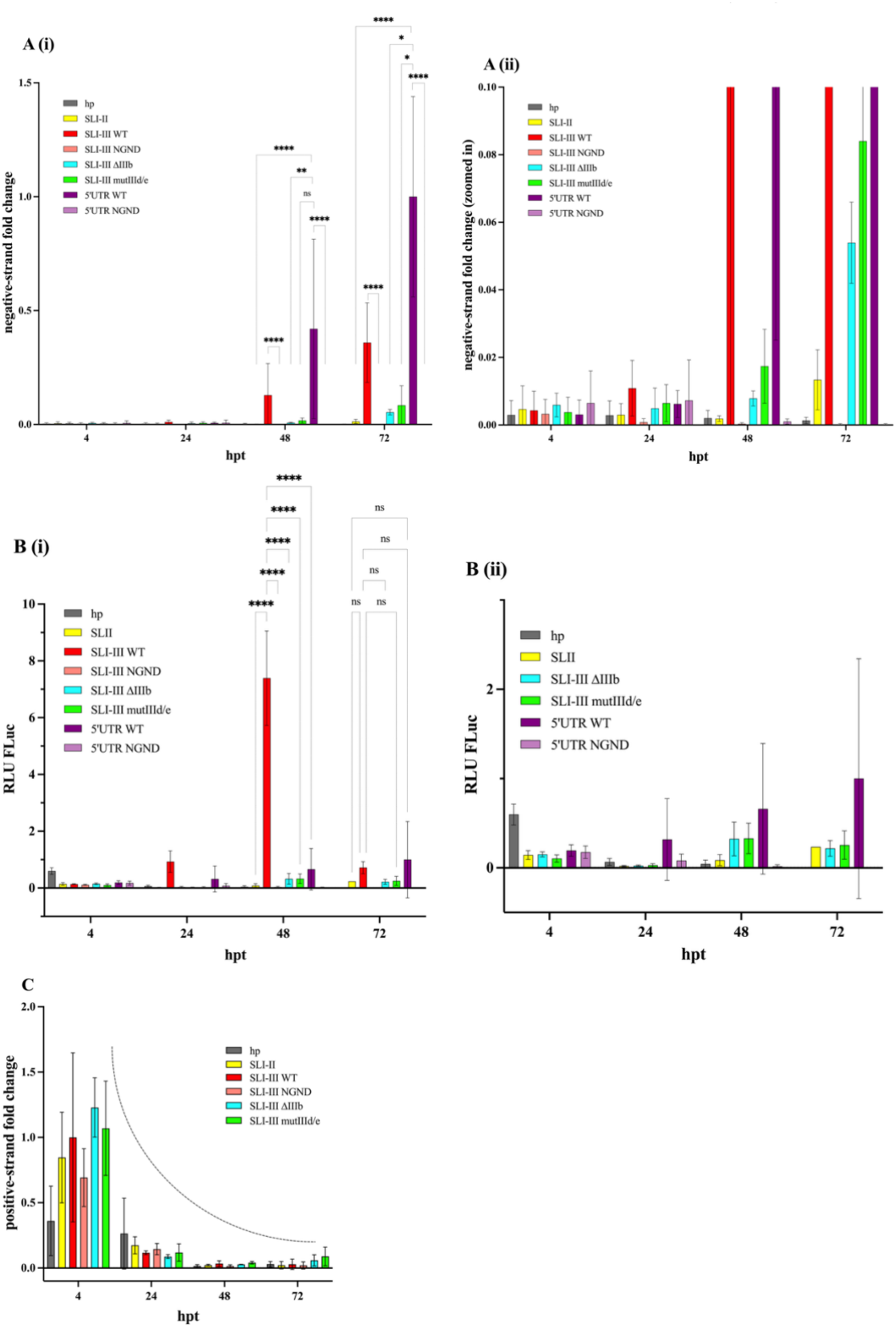

Figure 3.3.1. Contribution of distinct 5´UTR variants in negative-strand RNA synthesis using hp, SLI-II, SLI-III WT/NGND, SLI-III ΔIIIb, SLI-III mutIIId/e and complete 5´UTR WT/NGND constructs in 4th generation replicon system. Negative-strand RNA detection (A(i) and A(ii)), *firefly* luciferase assay (B(i) and B(ii)) and positive-strand RNA detection (C). A total of 3.5 µg of replicon RNA was transfected into Huh-7.5 cells at ~ 90 % confluency. Total RNA was extracted after 4, 24, 48 and 72 hpt for strand-specific RNA detection. *Firefly* luciferase assay was performed in

parallel. Positive- and negative-strand RNA was detected using specific tagged RT and qPCR primers (Figure 3.1.3), with reactions conducted at elevated temperatures (RT at 65 °C; qPCR at 62 °C). **(A(i) and (ii))** Relative expression levels (2^-ΔCt values normalised to 5´UTR WT at 72 hpt) obtained from negative-strand RNA detection. Huh-7.5 cells were co-transfected with 5EU for nascent RNA labelling. The experiment was performed with at least n = 4 biological replicates for hp, SLI-II, SLI-III WT/NGND, 5´UTR WT/NGND and with n =3 biological replicates for SLI-III ΔIIIb and mutIIId/e. For the fold change measurement, the Ct values were first normalised to GAPDH (ΔCt) and linearized by applying 2^-ΔCt to each sample. The data were then normalised to the 5´UTR WT at 72 hpt. Statistical analysis was performed using logarithmic values normalised to the 5´UTR WT at 72 hpt (ΔΔCt). Two-way ANOVA was performed using GraphPad Prism. Error bars represent standard deviation (±SD) of mean. Asterisks mark p-values from Two-way ANOVA (*: $p < 0.05$; **: $p < 0.01$; ***: $p < 0.001$; ****: $p < 0.0001$). Both SLI-III and 5´UTR constructs showed statistically significant differences compared to their negative controls (NGND) and the hp at 48 and 72 hpt. SLI-II showed 1.34 % of the total negative-strand RNA level in complete 5´UTR WT at 72 hpt. A(ii) shows a zoomed-in view of A(i). **(B(i) and (ii))** *firefly* luciferase expression results. The experiment was performed with at least n = 3 biological replicates, with exceptional case of SLI-II at 72 hpt (n = 1). Relative expression levels (RLUs) (normalised to mock and finally to the 5´UTR at 72 hpt) were analysed by two-way ANOVA using GraphPad Prism. Error bars represent standard deviation (±SD) of mean. Asterisks mark p-values from Two-way ANOVA (*: $p < 0.05$; **: $p < 0.01$; ***: $p < 0.001$; ****: $p < 0.0001$). The SLI-III WT construct (at 48 hpt) showed a statistically significant difference compared to the negative control (NGND) and complete 5´UTR WT at 4, 24, 48 and 72 hpt. B(ii) presents a zoomed-in view of B(i) excluding SLI-III WT and NGND. Error bars represent standard deviation (±SD) of mean. Asterisks mark p-values from Two-way ANOVA (*: $p < 0.05$; **: $p < 0.01$; ***: $p < 0.001$; ****: $p < 0.0001$) **(C)** Relative expression levels (2^-ΔCt values normalised to the SLI-III WT at 4 hpt) obtained from positive-strand RNA detection. Ct values (normalised to GAPDH) were linearized (2^-ΔCt) and then normalised to the expression levels of the SLI-III WT at 4 hpt. The experiment was performed with n = 4 biological replicates.

As noted in the previous section, negative-strand RNA detection results confirm the reliability of the procedure, as the negative controls – hp, SLI-III NGND and 5´UTR NGND – showed very low or negligible background signals at all time points, with particularly minimal background at 72 hpt (percentage relative to 5´UTR WT: hp = 0.14; SLI-III NGND = 0.02; 5´UTR NGND = 0.02), supported by high statistical significance (Fig. 3.3.1 A(i) and (ii)). The very short, truncated 5´UTR variant SLI-II, with a value of 1.34 %, showed only minimal negative-strand RNA abundance at 72 hpt, indicating its limited role in initiating replication. The weak signals detected at 4 and 24 hpt (Fig. 3.3.1 A(ii)) likely reflect the high sensitivity of the assay, capable of detecting trace amounts of contaminating input-RNA. SLI-III comprises the largest and the most functionally important portion of the 5´UTR; nevertheless, the abundance of negative-strand in this construct reached only about 36 % of the maximum level observed with the complete 5´UTR. The SLI-III mutants – SLI-III ΔIIIb, SLI-III mutIIId/e – are translation deficient constructs which impair the binding of eIF3 (SLIIIb) and the ribosomal 40S subunit (SLIIId/e), respectively (Kieft et al., 2001). In the negative-strand synthesis assay employed here, both SLI-III mutants – SLI-III ΔIIIb and mutIIId/e – showed low levels of negative-strand RNA abundance, approximately 5.4 % and 8.4 %, respectively, of the maximum level observed with the complete 5´UTR construct at 72 hpt (Fig. 3.3.1 A(i) and (ii)). In comparison with the parental SLI-III construct, these mutants reached about 15 – 23 % of the negative-strand RNA abundance observed at 72 hpt (Fig. 3.3.1 A(i) and (ii)), which is remarkable though statistically not significant.

Positive-strand RNA levels declined over time as expected including the truncated variants of the 5´UTR (Fig. 3.3.1 C). The result showed that the tested truncated 5´UTR variants – SLI-II, SLI-III ΔIIIb, SLI-III mutIIId/e – exhibited a similar decline in positive-strand RNA abundance over time, consistent with the other examined constructs (Fig. 3.2.2 C). In conclusion, differences in negative strand abundance shown in panel A and FLuc expression from transfected or progeny positive-

strands shown in panel B are not due to differential degradation of the transfected plus strands among all used constructs. The experiment was not repeated for 5´UTR and the corresponding NGND, as both had already been tested in triplicates in the previous experiment (Fig. 3.2.2 C).

Similar to negative-strand RNA results, the constructs SLI-II, SLI-III ΔIIIb, SLI-III mutIIId/e also exhibited unexpectedly low levels of *firefly* luciferase at 48 and 72 hpt (Fig. 3.3.1 B(i)). Due to the markedly higher peak for the SLI-III construct at 48 hpt, this data point was excluded from the graph to allow a clearer visualization of the signals from the other constructs (Fig. 3.3.1 B(ii)).

Overall, FLuc expression across all constructs generally mirrored their corresponding negative-strand RNA level, although the correlation was not statistically significant in comparison to the 5´UTR construct (Fig. 3.3.1 B(i) and (ii)). Notably, the negative controls – hp and both NGNDs – consistently showed negligible signals, particularly at 48 and 72 hpt, which supports the specificity of the system. The weak signals detected at 4 hpt are likely attributable to input RNA expression which disappeared by 24 hpt (Fig. 3.3.1 B(i) and (ii)). Moreover, the fact that reasonable amounts of FLuc expression were only found at later time points may be due to quick partial degradation of the transfected positive-strand RNA molecules, while only a very few intact replicon RNA molecules establish functional membranous replication complexes where they are protected from degradation. In this context, it is important to know that the RT-qPCR amplicon used for positive-strand detection is rather short. Thus, positive signals in the RT-qPCR for positive-strands do not necessarily mean that those positive-strands are intact over their entire length, but they may undergo partial degradation even from very early time points. A side effect of this degradation of transfected positive-strands may be that, particularly at early time points, there are increased amounts of short degradation products of these positive strands within the cells, which may hybridize to the negative strands. By then acting as unintended primers in the RT reaction, they may cause higher background signals in negative-strand RNA detection at early time points compared with the lower background observed at later times after transfection, when the input positive-strand RNAs are largely degraded. Based on their distinct expression patterns in both negative-strand RNA detection and FLuc expression assays, all constructs were analysed individually and described in the discussion section below.

3.3.1. Discussion of 5´UTR *cis*-elements involved in RNA replication

The negative-strand RNA abundance in the 5´UTR variants – SLI-II, SLI-III, SLI-III ΔIIIb and SLI-III mutIIId/e – showed distinct levels, reflecting their relative contribution to the total negative-strand RNA abundance observed by the complete 5´UTR construct (Fig. 3.3.1 A(i) and (ii)). The shortest variant, SLI-II, showed the lowest abundance, accounting for only 1.34 % of the value obtained with the 5´UTR WT at 72 hpt. SLI-III exhibited 36 % of the total negative-strand RNA abundance, which is slightly higher than in the previous series of experiments (Fig. 3.2.2 A(i)). This variation is likely due to the increasing number of biological replicates, which can introduce greater variability and lead to fluctuations in percentage contributions. Interestingly, the translation-deficient constructs SLI-III ΔIIIb and SLI-III mutIIId/e produced only 5.4 % and 8.4 % of the total negative-strand RNA abundance, respectively. This was remarkable since the mutations are, at least in the SLI-III mutIIId/e, very small and are not supposed to change the overall RNA secondary structure in the positive-strand. Moreover, both types of mutations (ΔIIIb and mutIIId/e) change the primary sequence of the positive-strand (as well as the sequence and structure of the antisense negative-strand) in very different ways. Therefore, it can be assumed that functional aspects of these mutants, i.e., binding of eIF3 and the small ribosomal 40S subunit, cause the decrease in negative-strand RNA synthesis efficiency.

Positive-strand RNA abundance (Fig. 3.2.2 C and Fig. 3.3.1 C) showed a constant decrease in the signals over time. As described in the previous section, this assay was performed to validate the specificity of the negative-strand RNA detection. While negative-strand RNA abundance directly reflects ongoing replication, the detected positive-strand RNA abundance primarily represents the large amounts of input RNA transfected to the Huh-7.5 cells. This high input – 5 x 10^{11} copies of replicon RNA transfected to 1.2 x 10^{6} Huh-7.5 cells – resulted in strong signals at early time points (Fig. 3.2.2 B(i) and (ii); Fig. 3.3.1 B(i) and (ii)). Over time, the input RNA was degraded by host's innate immune response, leading to a gradual decline in the signals. Although an increase in negative-strand RNA abundance should, in principle, be reflected in positive-strand levels as well, the overwhelming presence of input RNA makes it difficult to distinguish newly synthesized positive-strand RNA from the transfected replicon RNA. The strategy employed for negative-strand RNA analysis – nascent RNA 5EU-labelling – effectively addressed this issue. However, due to the high costs, this approach was exclusively applied for negative-strand RNA detection.

With the exception of SLI-III, all other constructs exhibited *firefly* luciferase signals that, to some extent, reflected the progression of negative-strand RNA levels over time, although the changes were not statistically significant (Fig. 3.3.1 B(i)(ii)). On one hand, the FLuc signals for the polymerase-inactive NGND control of the complete 5´UTR dramatically dropped compared to the 5´UTR WT (Fig. 3.3.1 B(ii)), particularly at 48 and 72 hpt, when input positive-strands had been largely degraded. (Despite the great difference between the FLuc levels of 5´UTR WT and its NGND, a statistical significance could not be achieved, which is mostly due to the high variability across biological replicates and the limited number of replicates.) On the other hand, the SLI-III construct consistently showed higher FLuc expression at 48 hpt across multiple experimental repeats, in comparison with all other constructs tested. An argument supporting the reliability of the assay is the steady increase in FLuc expression up to 72 hpt observed in 5´UTR construct (Fig. 3.2.2 B(i)(ii) and Fig. 3.3.1 B(i)(ii)), which closely mirrors the trend seen in negative-strand RNA abundance (Fig. 3.2.2 A(i) and Fig. 3.3.1 A(i)). In the full 5´UTR construct, negative-strand RNA abundance and FLuc expression increased in parallel, indicating that replication and FLuc expression (Gene Cluster II) proceeded concurrently. In contrast, the SLI-III construct showed limited negative-strand RNA synthesis (36 %) yet exhibited disproportionately high levels of FLuc expression (Gene Cluster II). Based on the results, two distinct patterns can be observed and analysed: **Pattern I** is characterized by concurrent replication (Fig. 3.2.2 A(i) and Fig. 3.3.1A(i)) and FLuc expression (Fig. 3.2.2 B(ii) and Fig. 3.3.1 B(ii)) as seen in the full 5´UTR construct (Fig. 3.3.2 A), **Pattern II**, by contrast, exhibits relatively lower levels of replication – though it follows a similar increasing trend over time ((Fig. 3.2.2 A(i) and Fig. 3.3.1 A(i)) – but shows a significant peak in FLuc expression (translation under Gene Cluster II) at 48 hpt (Fig. 3.2.2 B(i) and Fig. 3.3.1 B(i)), as observed in SLI-III construct (Fig. 3.3.2 B). Taking these two patterns into account, the remaining 5´UTR variants can be categorized accordingly.

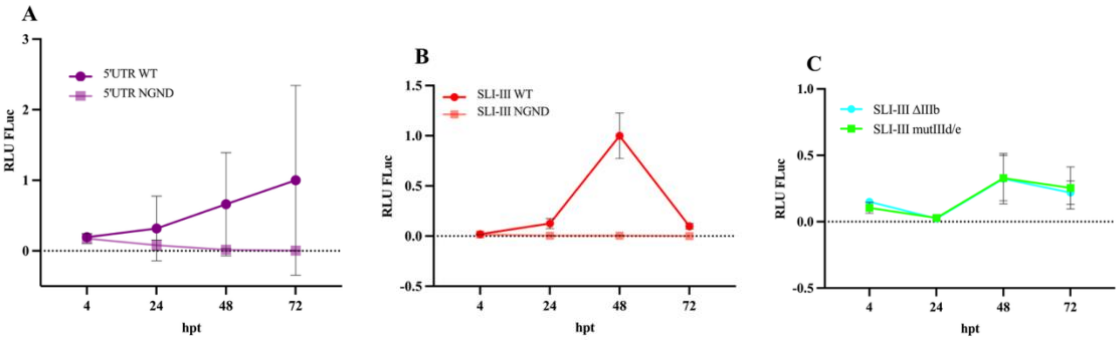

Figure 3.3.2. Patterns of FLuc expression and replication observed in distinct 5´UTR variants. (A) Pattern I: Concurrent FLuc expression and replication, indicated by a consistent, parallel increase both in *firefly* luciferase activity and negative-strand RNA levels up to 72 hpt, as observed in the 5´UTR WT and the SLI-II construct. **(B) Pattern II:** FLuc expression peaks at 48 hpt and declines drastically at 72 hpt, while negative-strand RNA levels (although much lower than those of the 5´UTR WT construct) exhibit a steady increase up to 72 hpt, as observed in the SLI-III WT construct. In contrast, FLuc activity in both mutants –SLI-III ΔIIIb and mutIIId/e – shown in **(C)** tends to resemble Pattern I more closely, although with a slight decline at 72 hpt. Error bars represent standard deviation (±SD) of the mean.

The shortest 5´UTR truncated variant, SLI-II, exhibits very limited negative-strand RNA as well as *firefly* luciferase signals, making it very challenging to categorize this construct. Only upon a closer, zoomed-in view (Fig. 3.3.1 A(ii)) can the trends in replication and translation (under Gene Cluster II) be clearly discerned. In the SLI-II construct a negligible level of negative-strand RNA – comparable to that observed in hp construct – was detected at 48 hpt, which increased significantly by 72 hpt. As previously noted, the signals at 4 and 24 hpt are likely due to contamination by partial positive-strand RNA degradation products (Fig. 3.2.2 A(ii) and Fig. 3.3.1A(ii)). Given the similar increasing trend observed in the *firefly* luciferase data, the SLI-II construct can be categorized under Pattern I (Fig. 3.3.2 A).

In contrast to the parental SLI-III construct, the SLI-III ΔIIIb and SLI-III mutIIId/e constructs showed a trend in FLuc (Fig. 3.3.1 B(ii)) that changes from pattern II to pattern I (Fig. 3.3.2 C), though exhibiting the same steady increase in the negative-strand abundance (Fig. 3.3.1 A(i) and (ii)). Both constructs showed a modest peak at 48 hpt, which only very slightly declined by 72 hpt (Fig. 3.3.1 B(i) and (ii)), a pattern that is very different from that of the parental SLI-III WT construct. This may support the idea that functional aspects, like binding of eIF3 and/or the small ribosomal 40S subunit rather than primary sequence or secondary structure aspects of the mutated sequences, are important for the regulation of negative-strand synthesis initiation. The similar pattern can also be imagined for 5´UTR mutants – 5´UTR ΔIIIb and mutIIId/e – following their FLuc trend at 48 and 72 hpt (see below Fig. 3.4.1).

Closer examination of the negative-strand RNA data highlights the limitation of the assay at earlier time points – specifically at 4 and 24 hpt. Since the project aims to identify the *cis*-elements involved in the initiation of the negative-strand synthesis, detecting negative-strand RNA at these early stages may not be feasible due to the higher background, in particular at these early time points after transfection of the positive-strand replicon RNA. The background in negative-strand detection appears to become much lower during longer incubation of the cells, and this decline in background correlates with the decrease in positive-strand abundance, giving the impression that the background may result from contamination (Fig. 3.2.2 A(ii) and Fig. 3.3.1 A(ii)). Hence, it can be assumed that partial degradation products of transfected replicon RNA molecules that fail to establish functional replication complexes may hybridize to longer sections of partially degraded RNA, thereby

generating primer-template combinations that result in false-positive signals in the negative-strand detection assay at earlier time points. The decrease in these false-positive background signals at later time points after transfection is likely due to the ongoing degradation of these RNAs in cells over time. To potentially address this problem, the use of increasing concentrations of chemicals that disrupt nucleic acid hybridization, such as urea or guanidinium, could be tested in future assays by incorporating them into the Click-iT nascent RNA purification wash buffers, in order to wash off non-biotinylated RNA fragments that have hybridized to biotinylated RNAs.

Moreover, it is also possible that negative-strand RNA becomes detectable only after its intracellular abundance surpasses a certain threshold. The initiation of replication is a complex process involving formation of replication organelles (ROs) and the recruitment of NS5B at the 3´-end of the positive-strand RNA genome (Li et al., 2021). NS5B may exhibit a significantly higher affinity for the negative-strand RNA template than for the positive-strand RNA template, as the synthesis of positive-strand genome is approximately 100 folds higher as compared to negative-strand RNA (Lohmann, 2013). Possibly, once a single negative-strand RNA (antigenome) is produced, the system's equilibrium may shift towards replication, leading to a robust synthesis of both positive- and negative-strand RNAs. Catching the precise moment when the first antigenome is generated maybe extremely challenging using the current approach. However, the involvement of various 5´UTR elements in negative-strand RNA synthesis – particularly in the context of their secondary structures – is discussed in more detail in the Final Discussion section.

3.3.2. Concluding Remarks

Negative-strand RNA detection using the 4th generation replicon system enabled the identification of the least essential 5´UTR variant – SLI-II – involved in negative-strand RNA synthesis. The *cis*-elements present in SLI-III were able to support 33 – 36 % of the level of negative-strand RNA synthesis observed with the complete 5´UTR at 72 hpt. Deletion of domain IIIb and mutations in IIId and IIIe led to a drastic reduction in replication, however, low levels of negative-strand RNA could be still detected. To investigate the effects of these mutations in more detail, the same mutations were also introduced into 5´UTR, which are described in the following section. Furthermore, it is crucial to examine the role of these 5´UTR elements in the context of their predicted secondary structures.

3.4. Mutations in the IRES-region of the HCV 5´UTR impair negative-strand RNA synthesis, a defect that miR-122 is unable to compensate for

In the previous section, the truncated 5´UTR variants, SLI-III ΔIIIb and SLI-III mutIIId/e, were evaluated for relative negative-strand RNA production and FLuc expression. In the SLI-III constructs, described in the previous section, two functional aspects can be affected by the mutation. First, the mutations alter the primary sequence of the 5´-end region. Second, they differentially affect factor binding: the WT construct binds eIF3 and 40S subunits, whereas the ΔIIIb mutant abolishes eIF3 binding and the mutIIId/e mutant abolishes 40S binding (Kieft et al., 2001). Moreover, the pseudoknot structure and the SLIV containing the authentic HCV AUG start codon are also absent in these SLI-III mutants, therefore, no functional translation initiation event can be activated. Therefore, the same mutations (ΔIIIb and mutIIId/e) were then introduced into the complete 5´UTR to generate two constructs: 5´UTR ΔIIIb and 5´UTR mutIIId/e. Both constructs, along with the complete 5´UTR construct and the corresponding negative control (NGND), were transfected into Huh-7.5 cells (2.2.4.5). These complete 5´UTR-constructs contain the core region fused to 3xHiBiT. Thus, the construct – besides allowing analysis of the role of these sequences in the regulation of

negative-strand synthesis – additionally permits assessment of the ability of the genuine HCV 5´UTR sequences to initiate translation (via HiBiT measurement), while FLuc expression from Gene Cluster II and provision of replication proteins by Gene Cluster III remain uncoupled from any functions at the very 5´-end of the replicon (Fig. 3.2.1 A).

Negative-strand detection (2.2.4.8) was performed only at 72 hpt, while the FLuc assay (2.2.5.1) was conducted at both 48 and 72 hpt. To enable a more comprehensive comparison of protein expression, the HiBiT assay was also performed in parallel at 24, 48 and 72 hpt, with and without co-transfection of the liver-specific micro-RNA (miR-122). The results are presented in the figures (Fig. 3.4.1 A and B; Fig. 3.4.2 A, B and C).

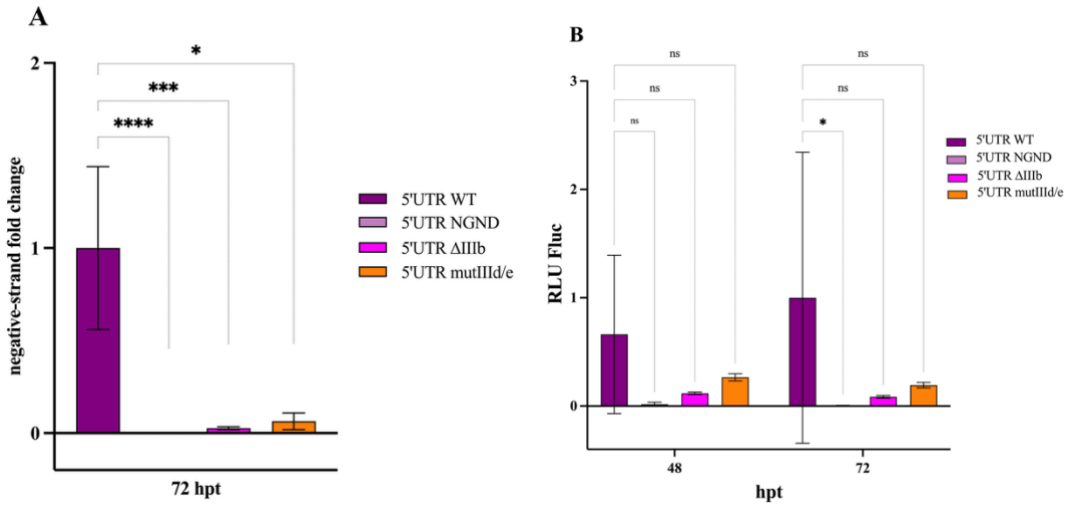

Figure 3.4.1. Contribution of 5´UTR mutants, 5´UTR ΔIIIb and mutIIId/e, in negative-strand RNA synthesis compared to complete 5´UTR constructs in 4th generation replicon system. A total of 3.5 µg of replicon RNA was transfected into Huh-7.5 cell at ~ 90 % confluency. Total RNA was extracted after 72 hpt for strand-specific RNA detection. *Firefly* luciferase assay was performed at 48 and 72 hpt. Negative-strand RNA was detected using specific tagged RT and qPCR primers (Figure 3.1.3), with reactions conducted at elevated temperatures (RT at 65 °C; qPCR at 62 °C). **(A)** Relative expression levels (2^-ΔCt values normalised to 5´UTR WT at 72 hpt) obtained from negative-strand RNA detection. Huh-7.5 cells were co-transfected with 5EU for nascent RNA labelling. The experiment was performed with n = 3 biological replicates. For the fold change measurement, the Ct values were first normalised to GAPDH (ΔCt) and linearized by applying 2^-ΔCt to each sample. The data were then normalised to the 5´UTR WT at 72 hpt. Statistical analysis was performed using logarithmic values normalised to the 5´UTR WT at 72 hpt (ΔΔCt). One-way ANOVA was performed using GraphPad Prism. Error bars represent standard deviation (±SD) of mean. Asterisks mark p-values from One-way ANOVA (*: $p < 0.05$; **: $p < 0.01$; ***: $p < 0.001$; ****: $p < 0.0001$). **(B)** *Firefly* luciferase expression results. The experiment was performed at 48 and 72 hpt, with n = 3 biological replicates. Relative expression levels (RLUs) (normalised to mock and finally to the 5´UTR at 72 hpt) were analysed by two-way ANOVA using GraphPad Prism. Error bars represent standard deviation (±SD) of mean. Asterisks mark p-values from Two-way ANOVA (*: $p < 0.05$; **: $p < 0.01$; ***: $p < 0.001$; ****: $p < 0.0001$).

The absence of the IIIb domain disrupts eIF3 binding, leading to translational blockade. Surprisingly, also the 5´UTR ΔIIIb construct showed only minimal to no negative-strand RNA levels (Fig. 3.4.1 A). A similar effect was expected for the 5´UTR mutIIId/e construct, as the mutations in IIId/e region disrupt binding of the ribosomal 40S subunit. The result shows a low level of negative-strand RNA, significantly lower than the level observed with the 5´UTR WT construct, yet still indicative of

limited negative-strand RNA abundance (Fig. 3.4.1 A). However, the negative-strand RNA abundance in the 5´UTR mutIIId/e mutant (6.35 %) was slightly higher than that in the 5´UTR ΔIIIb mutant (2.6 %) (Fig. 3.4.1 A).

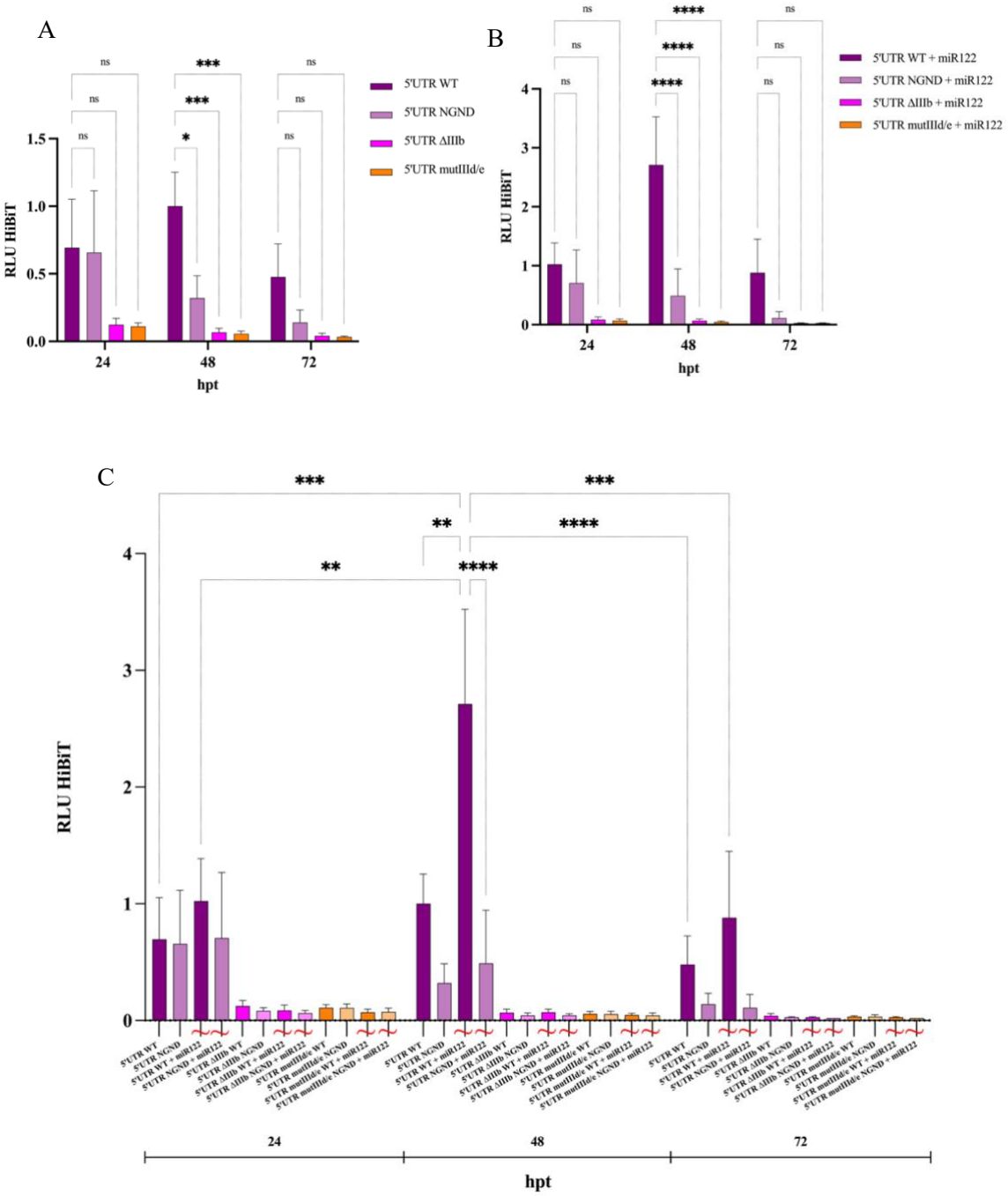

Figure 3.4.2. HiBiT expression in the 5´UTR ΔIIIb and 5´UTR mutIIId/e mutants, compared to the complete 5´UTR construct in the 4th generation replicon system, as an indirect measure of replication. A total of 3.5 µg of replicon RNA was transfected into Huh-7.5 cell at ~ 90 % confluency. HiBiT assays were performed at 24, 48 and 72 hpt, without **(A)** and with **(B)** miR-122 co-transfection, with all results combined for a comparison shown in panel **(C).** The experiment was performed with n = 3 biological replicates. Relative expression levels (RLUs) (normalised to mock and finally to the 5´UTR at 48 hpt) were analysed by Two-way ANOVA using GraphPad Prism. Error bars represent standard deviation (±SD) of mean. Asterisks mark p-values from Two-way ANOVA (*: $p < 0.05$; **: $p < 0.01$; ***: $p < 0.001$; ****: $p < 0.0001$).

Firefly luciferase assay results from Gene Cluster II as an indirect measure for replicon RNA abundance demonstrated a similar expression trend, the 5´UTR mutIIId/e construct reached ~ 19% of the expression level observed for the 5´UTR at 72 hpt, while the 5´UTR ΔIIIb construct exhibited a lower expression level of approximately 8.5 % (Fig. 3.4.1 B).

As stated above, the HCV IRES driven protein expression of Gene Cluster I was also assessed using the HiBiT detection assay. The protein expression was measured at 24, 48 and 72 hpt, with and without co-transfection of the liver specific miR-122 (Fig. 3.4.2 A, B and C). Very high signals appeared both for the 5´UTR WT and NGND at 24 hpt, while the mutated versions appeared on much lower level, though not statistically significant (Fig. 3.4.2 A). This indicates likely the input RNA, which the host cell's translation machinery started to translate immediately after the transfection. At 48 hpt the signals for both negative and positive constructs became clearer exhibiting significantly higher amounts of FLuc and HiBiT expression in 5´UTR WT (Fig. 3.4.2 A). In the meanwhile, the signals for mutated variants – 5´UTR ΔIIIb and 5´UTR mutIIId/e – declined showing negligible FLuc and HiBiT expression (Fig. 3.4.2 A). At 72 hpt an overall decrease of the signals can be observed, though not significant but consistently showing the effect observed at 48 hpt (Fig. 3.4.2 A).

The liver-specific miR-122 was co-transfected to assess whether its binding to positive-strand RNA could compensate the defect in 5´UTR mutated variants. The results showed that although co-transfection with miR-122 enhanced HiBiT expression (Gene Cluster I) by approximately 2.5 fold (Fig. 3.4.2 C), it did not compensate for any of both deficiencies present in ΔIIIb and mutIIId/e (Fig. 3.4.2 B). Among the six miR-122 binding sites distributed across the positive-strand HCV RNA genome, two – located between SLI and SLII – are highly conserved. Binding of miR-122 at this region, in association of Ago2, induces conformational changes in the IRES structure and promotes translation (Niepmann et al., 2018/ 2020). Our results are consistent with these previously established findings. The miR-122 binding, however, remained ineffective in the translation-deficient constructs. Translation activity of both constructs – 5´UTR ΔIIIb and 5´UTR mutIIId/e – remained unchanged (i.e., on a very low level) at 48 as well as 72 hpt (Fig. 3.4.2 B and C). Despite the high variability in protein expression (both in Gene Cluster I and II) at 72 hpt – as measured by HiBiT and *firefly* luciferase assay – it consistently peaked at 48 hpt (Fig. 3.4.1 B; Fig. 3.4.2 A), similar to FLuc expression observed for SLI-III mutants (Fig. 3.3.1 B(ii)). High variability in protein expression may be attributed to other cellular factors, as elaborated in the Final Discussion section.

3.4.1. Discussion of effects of IRES mutation

Negative-strand abundance was markedly reduced at 72 hpt in the 5´UTR ΔIIIb and mutIIId/e constructs, reaching approximately 2.6 % and 6.35 %, respectively, relative to complete 5´UTR WT (Fig. 3.4.1 A). At the same time point, both translation deficient constructs exhibited reduced protein expression from the neighbouring FLuc in Gene Cluster II, with FLuc levels at ~ 19% for the 5´UTR mutIIId/e construct and ~ 8.5% for 5´UTR ΔIIIb construct, relative to the FLuc expression observed in complete 5´UTR WT. Moreover, FLuc expression in both translation deficient constructs was higher at 48 hpt compared to that at 72 hpt (Fig. 3.4.1 B).

The significantly reduced negative-strand RNA levels indicate limited replication in the 5´UTR ΔIIIb and mutIIId/e variants. This replication defect is likely the consequence of their impaired translation efficiency (Johnson et al., 2017), which in turn hinders effective viral RNA synthesis. Based on both negative-strand RNA abundance and the observed trend in FLuc expression in Gene Cluster II, the 5´UTR mutIIId/e construct demonstrates partial functionality, performing slightly better than the 5´UTR ΔIIIb construct (Fig. 3.4.1 A and B). In HCV IRES-mediated translation initiation, the multi-subunit eIF3 complex is recruited to 40S:IRES binary complex by interacting with the apical loop

IIIb of the SLIII domain. In the absence of IIIb, eIF3 can still bind to the mutated IRES, albeit with low affinity (Kieft et al., 2001; Johnson et al., 2017). However, due to the lack of specific interaction between eIF3 and IIIb, the resulting complex is nonfunctional leading to reduced translational activity (Johnson et al., 2017). Translation initiation begins with the binding of 40S subunit to the IRES, forming 40S:IRES binary complex. This interaction in anchored by high affinity Watson-Crick base pairing (K_D = 2 – 4 nM) between the conserved ^{266}GGG^{268} sequence in IRES subdomain IIId and the ^{1116}CCC^{1118} of the expansion segment 7 (ES7) of ribosomal 40S subunit. Deletion or substitution of this conserved sequence in IIId leads to decreased binary-complex affinity and diminishes IRES activity (Johnson et al., 2017 and references therein).

The current replicon system (4th generation) shows a limited replication in translation deficient constructs of both the complete 5′UTR and the SLI-III series (Fig. 3.4.1 A; Fig. 3.3.1 A). The direct effects of both mutations – ΔIIIb and mutIIId/e – on translation could be measured only by HiBiT expression (Gene Cluster I reporter system), and the HiBiT measurements were only possible in the complete 5′UTR constructs. In the 5′UTR mutants, the lower HiBiT expression compared to the WT construct at 48 and 72 hpt confirmed the inability of both the ΔIIIb and mutIIId/e constructs to recruit the translation machinery (Fig. 3.4.2 A). The same limited translation in 5′UTR mutants compared to the corresponding WT could also be observed for the FLuc expression (Gene Cluster II) for an extended period after transfection (Fig. 3.4.1 B), which is likely a secondary effect of impaired RNA replication. In summary, expression from Gene Cluster II (FLuc) likely serves as indirect evidence for the activity of Gene Cluster I (5′UTR and its variants) in the current replicon system. Applying this reasoning to the SLI-III mutants, which lack Gene Cluster I reporter system and possess only the Gene Cluster II reporter system (FLuc), it can be assumed that these mutants which are unable/less capable to recruit the translation machinery to Gene Cluster I, exert a similar effect on Gene Cluster II as secondary effect on impaired RNA translation (Fig. 3.3.1 B(i) and (ii)).

Other important components of the SLI-III region include long-range interactions (LRIs) between individual stem loops and other genomic *cis*-acting elements. Specifically, the apical part of subdomain IIId forms a long-range interaction with the *cis*-replicating element (CRE) located within 5BSL3.2, which promotes replication. Likewise, subdomain IIIe is predicted to interact with the apical loop of 5BSL3.1 (Fricke et al., 2015), although the functional role of this interaction remains unclear. Since the ΔIIIb construct retains wild-type IIId and IIIe sequences, a relatively higher abundance of negative-strand RNA was expected compared to the mutant IIId/e construct. It was assumed that the preserved LRIs could have supported replication. However, this was not observed. Surprisingly, the mutIIId/e construct displayed slightly higher levels of negative-strand RNA than ΔIIIb construct. Considering the presence of intact LRIs in ΔIIIb, a better replication efficiency was anticipated, but this expectation was not met. Based on the results, it remains unclear, to what extent the limited translation and/or the absence of LRIs contribute to the reduced abundance of negative-strand RNA in both 5′UTR mutants. Thus, this leaves room for another interpretation of these results, i.e., that the binding of eIF3 and/or the ribosomal 40S subunit are important for mediating the positive effect of the HCV 5′UTR sequences to the RNA 3′-end where negative-strand initiation takes place. The effects of these mutations are discussed in greater detail (in Final Discussion) in the context of their predicted secondary structures – both in the 5′UTR of the positive-strand RNA and in the corresponding 3′UTR of the intermediate negative-strand RNA.

The reporter system used in Gene Cluster I of the 4th generation replicon system in the complete 5′UTR series was a triple (3x) sequence of the small HiBiT tag, fused to the C terminus of the core region downstream of the 5′UTR. The insertion of such a small tag is highly practical, as it is unlikely to interfere with the structure of the protein of interest. However, its small size can also lead to less

precise measurements; the tag may be misidentified due to the sequence similarities with other cellular proteins, or it may become inaccessible if buried within a tightly folded protein structure. However, in this context, the HiBiT measurement is the only option for monitoring translation driven by the HCV IRES.

The binding of liver-specific miR-122 to the conserved S1 and S2 regions located between SLI and SLII in the 5´UTR of the positive-strand HCV RNA enhanced HCV IRES-driven core-HiBiT translation in the 5´UTR WT construct. In contrast, HiBiT expression in both mutants – 5´UTR ΔIIIb and mutIIId/e –remained unchanged despite the presence of miR-122 (Fig. 3.4.2 B). miR-122 plays several essential roles in the HCV life cycle, including maintaining genome stability, acting as a riboswitch and contributing to virion assembly (Rheault et al., 2023). Using replicon RNA, it is possible to study two key roles of miR-122: genome stability and riboswitch function. Binding of miR-122, in association with Ago2, to the 5´UTR induces a conformational change in the IRES region, thereby facilitating ribosome binding and promoting translation (Henke et al., 2008; Schult et al., 2018; Niepmann et al., 2018/ 2020; Rheault et al., 2023). Depending on the context, miR-122 can assume different functional roles. As shown in the results (Fig. 3.4.2 A and B), in the absence of miR-122, HiBiT expression levels for the WT and NGND constructs at 24 hpt were nearly identical. Upon miR-122 co-transfection, however, a clear increase in HiBiT expression was observed in the WT construct, which became significantly higher at 48 hpt, suggesting enhanced replication, whereas a constant decrease was observed in NGND HiBiT level (Fig. 3.4.2 B). The role of miR-122 in promoting translation is evident from the ~ 2.5-fold increase in protein expression compared to HiBiT levels in the absence of miR-122 (Fig. 3.4.2 C). It was initially hypothesized that the presence of miR-122 might partially compensate for the translational deficiency in the ΔIIIb and mutIIId/e constructs; however, this assumption was disproven. The results from these specific mutations strongly support previously established findings that a defective IRES impairs both translation and replication (Ray et al., 2004). The results also indicate that the miR-122 binding alone cannot be the sole factor responsible for the genome linearization from a circularized state to facilitate translation, implying a more complex mechanism than previously proposed (Scott et al., 2023).

3.4.2. Concluding Remarks

The absence of IIIb domain in the SLIII of 5´UTR, which is known to disrupt eIF3 binding (Kieft et al., 2001), leads to limited HCV IRES driven translation in Gene Cluster I and a significant reduction in negative-strand RNA synthesis. Similarly, the mutation in subdomain IIId (GGG → CCC), which impairs the formation of the binary complex between the IRES and the 40S ribosomal subunit, results in decreased overall translation and negative-strand RNA synthesis. The impact of the IIIe mutation (GAUA → GAAA) could not be evaluated independently, as it was combined with the IIId mutation in the 5´UTR mutIIId/e construct. A significant increase in HiBiT expression in the 5´UTR WT construct following miR-122 co-transfection highlighted its specific role in promoting translation. However, miR-122 co-transfection did not compensate for the translational deficiencies in the mutated constructs (5´UTR ΔIIIb and mutIIId/e), further confirming, as discussed above, that binding of eIF3 and the 40S subunit contributes to negative-strand RNA synthesis mediated by the 3´-end of the positive strand.

4. Final Discussion

This study aims to elucidate the *cis*-acting elements within the 5´UTR of the positive-strand HCV RNA genome that are involved in initiating synthesis of the negative-strand RNA (the antigenome). The positive- and negative-strand RNAs adopt distinct secondary RNA structures, and any mutation introduced into a specific region of the positive-strand RNA inevitably also affects the complementary region in the negative-strand (Fricke et al., 2015). Consequently, it is inherently challenging to assign a definitive functional role to a particular sequence element on only one strand without influencing the structure or function of the other.

A 4th generation replicon system was established and employed in combination with an optimized set of strand-specific RNA detection protocols. This approach resulted in highly significant reduction of background signals (Fig. 3.2.2 A(i) and (ii)) compared with previous procedures. The background still fluctuates a little more in the beginning phases of replication at 4 hours post transfection (Fig. 3.2.2. A(ii)) when high amounts of transfected positive-strand RNA are still around (Fig. 3.2.2 C). This is likely due to the interference by degraded RNA oligonucleotides derived from the transfected positive strands with the negative-strand RNA detection assay, which may hybridize to newly synthesized negative strands and are inevitably co-purified, even under 5EU-labelling conditions. In contrast, at later stages of replication, the "hp" negative control background drops to about 0.035 % (Fig. 3.2.2 A(ii)) and to 0.13 % (Fig. 3.3.1 A(ii)), while the background of the NGND polymerase-deficient controls decreases to 0.035 % (Fig. 3.2.2 A(ii)) and to 0.02 % (Fig. 3.3.1 A(ii)) relative to the 5´UTR WT at 72 hpt. This background is roughly a factor of 300-fold lower for the hp construct and about 975-fold lower for the NGND negative controls compared with previous studies from the Niepmann laboratory using 1st generation replicons and conventional RNA purification procedures (L. Shalamova, dissertation).

The residual background signals, particularly at earlier times after transfection, commonly arise from residual input RNA and plasmid DNA contamination. While residual plasmid DNA, that is only partially degraded, can directly serve as a qPCR amplicon template independent of the reverse transcription reaction. Residual RNA as well as DNA can also be nucleolytically degraded into oligonucleotides of sizes that allow their unintended function as primers. These oligonucleotides may hybridize to the desired replicon RNAs and remain associated during RNA purification, since no further hydrogen-bond denaturing steps were included in the RNA purification procedures after the initial cell lysis in guanidinium. This limitation might be addressed in future studies by attempting to remove such hybridized small oligonucleotides from the EU-Biotin-labelled nascent RNAs with the inclusion of hydrogen-bond denaturing agents, like adding 8 M urea in the wash buffers (Kurzban et al., 1991; Tagwerker et al., 2006) during Click-iT purification. In addition, self-priming events occur during *in vitro*-transcription and reverse transcription. The latter artifacts are often attributed to 3´-end looping of the positive-strand replicon RNA. Several strategies contributed to the effective elimination of background signals, including effective removal of plasmid DNA, 5EU-labelling of nascent RNA and the use of high-temperature RT-qPCR. The strand-specific RNA detection assay, developed through this approach, is broadly applicable and can be readily adapted to other replicon-based systems employed in viral replication studies, as well as to the direct analysis of viral RNA genomes.

In general, comparison of newly synthesized negative strands with the transfected positive strands (Fig. 3.2.2 and Fig. 3.3.1) indicates that only a very small fraction of the transfected positive-strand

replicon RNA successfully establishes functional replication complexes. Moreover, it requires approximately 24 to 48 hours to establish detectable negative-strand RNA production.

It is also interesting to note that HiBiT expression driven by the 5′-terminal HCV IRES can take place from the transfected positive-strand replicon RNAs at relatively early time points (Fig. 3.4.2). In contrast, translation of the internal Poliovirus IRES-FLuc cistron begins no earlier than 24 hpt at very low levels and subsequently increases strongly (Fig. 3.2.2 B(i) and (ii); Fig. 3.3.1 B(i) and (ii)) in all constructs bearing HCV 5′UTR sequences, whereas the "hp" construct, which lacks any 5′-terminal HCV sequences, shows also moderate FLuc expression at 4 hpt (Fig. 3.3.1B). Thus, the presence of HCV sequences (minimal SLI-II) appears to suppress translation of the Poliovirus IRES-FLuc cistron in the internal Gene Cluster II, independent of the ability of the HCV sequences to bind eIF3 or the 40S subunit.

Several different 5′UTR variants were tested using this 4th generation replicon system to assess negative-strand RNA abundance at 4, 24, 48 and 72 hpt. The very basic control construct "hp" which lacks any HCV sequences at its 5′-end but contains only a hairpin to protect the 5′-end from degradation, shows no detectable activity, with levels nearly as low as the background observed in the polymerase-deficient NGND mutants (Fig. 3.2.2 A(ii); Fig. 3.3.1 A(ii)). This low activity is not attributable to possible faster degradation of its transfected positive-strand RNA compared with other RNAs (Fig. 3.2.2 C, Fig. 3.3.1 C). Thus, RNA synthesis in this construct is virtually not possible, even though the replication proteins and all RNA *cis*-elements involved in the initiation of negative-strand RNA synthesis are present at the very 3′-end of the negative strand or further upstream (e.g., the CRE). In turn, this means that HCV sequences at the 5′-end of the HCV positive-strand RNA genome are required for RNA strand synthesis, whether by virtue of their physical presence at the 5′-end of the positive strand or by the physical presence of their reverse complement RNA at the 3′-end of the negative strand.

Among all constructs containing HCV sequences, the complete 5′UTR WT construct exhibited the highest level of negative-strand RNA at 72 hpt. Accordingly, this construct was designated as the reference for the comparative analysis of negative-strand RNA abundance across all other 5′UTR variants and time points. The minimal essential *cis*-acting requirement for the initiation of negative-strand RNA synthesis was identified as the presence of SLI-II within 5′UTR. The SLI-II construct generated approximately 1.34 % of the total negative-strand RNA abundance observed in the 5′UTR WT construct at 72 hpt (Fig. 3.3.1 A(i) and (ii)). The SLI-III construct produced 33 % (Fig. 3.2.2 A(i)) and 36 % (Fig. 3.3.1 A(i)) of the total negative-strand RNA abundance in two independent experimental sets. These results indicate that the SLI-III region contributes approximately 34.5 % of the overall efficiency of negative-strand RNA synthesis.

Of the above constructs, first the SLI-II requires some deeper consideration. On one hand, Friebe and coworkers (Friebe and Bartenschlager, 2009) showed that, in the context of otherwise complete 5′UTR sequences, mutations (i.e., "loss of function") in the SLIIz′ region of the negative-strand 3′-end (which largely corresponds to SLII in the 5′-region of the positive-strand and the single-stranded region between SLI and SLII) largely abolish HCV replication. Thus, this SLI-II region (in the positive-strand RNA) or its reverse complement SLIIz′ region (in the negative-strand RNA) is essential for HCV RNA replication. On the other hand, in this work, the presence (so to speak "gain of function") of only these SLI-II sequences is not sufficient to allow more than about 1.34 % negative-strand RNA production efficiency (Fig. 3.3.1 A(ii)). This indicates that, in addition to SLI-II sequences (physically present either in the negative strand, the positive strand, or both), further downstream sequences are required for efficient negative-strand RNA production.

Mutations introduced into the subdomains IIIb, IIId and IIIe of the SLI-III region led to a marked reduction in negative-strand RNA synthesis (Fig. 3.3.1 A(i) and (ii)), paralleled by strong reduction of protein expression from the internal FLuc gene in Gene Cluster II (Fig. 3.3.1 B(i) and (ii)). Deletion of IIIb resulted in varying levels of negative-strand RNA synthesis, depending on the construct. The SLI-III ΔIIIb retained 5.4 % of the total negative-strand RNA abundance relative to the 5´UTR WT at 72 hpt (Fig. 3.3.1 A(i) and (ii)), whereas 5´UTR ΔIIIb exhibited only 2.6 % of that (Fig. 3.4.1 A). This latter value is only slightly higher than the level observed with the minimal SLI-II (1.34 %) construct under the same conditions (Fig. 3.3.1 A(ii)). The 5´UTR and SLI-III constructs carrying mutations in subdomains IIId and IIIe contributed to the total negative-strand RNA abundance within a similar range. The SLI-III mutIIId/e construct exhibited 8.4 % (Fig. 3.3.1 A(i) and (ii)), whereas the 5´UTR mutIIId/e construct showed 6.35 % activity relative to the 5´UTR at 72 hpt (Fig. 3.4.1 A). Overall, the mutated variants of 5´UTR consistently exhibited slightly lower levels of negative-strand RNA compared to their corresponding SLI-III mutants. These findings underscore the critical importance of the complete 5´UTR in facilitating effective negative-strand RNA synthesis. In addition, these results suggest that the *cis*-acting elements essential for stimulating the initiation of negative-strand RNA synthesis are likely located in the SLI-III region of the 5´UTR. In contrast, the downstream portion of the 5´UTR, encompassing SLIV and core-coding region, may play a more important role in regulating replication and translation processes. Previously, it has been shown that modifications within SLIIz´ and SLIIy´ of the negative-strand RNA (corresponding to the SLI-II region in positive-strand RNA) severely impair replication, where alterations in more upstream regions of the negative strand exert only mild effects (Friebe and Bartenschlager, 2009). However, modifying only the negative-strand RNA may also alter the corresponding positive-strand RNA during subsequent rounds of replication, thereby affecting both strands and preventing the assignment of a specific function to a defined site on either RNA strand.

Another study demonstrated that deletion of the SL-A1 stem-loop in 3´-end of negative-strand RNA (corresponding to the SLI region in the 5´UTR of the positive-strand RNA) reduced RNA synthesis by 39 %, indicating its necessity for efficient replication. In contrast, modifications or even complete deletion of the SL-B1 stem-loop did not impair RNA synthesis and in some cases enhanced it (Astier-Gin et al., 2005). Based on these findings (Astier-Gin et al., 2005; Friebe and Bartenschlager, 2009), the SLI-II sequence– which corresponds to SLI´, SLIIz´ and SLIIy´ regions on the negative-strand – should have been sufficient to support replication, however, the very low negative-strand RNA yield (1.34 % for SLI-II construct) observed in the work presented here (Fig. 3.3.1 A(i) and (ii)) contradict these earlier reports and instead underscores the importance of the complete 5´UTR for efficient replication.

To investigate potential *cis*-acting elements involved in HCV replication, a comparative analysis of secondary structure predictions for the 5´UTR elements in both the positive- and negative-strand RNA was performed (Fig. 4.1 and Fig. 4.2 A, B, C, D, E and F). Secondary structures were calculated for each 5´UTR element used in this work, independently of neighbouring elements. In these predictions, the hairpin (hp) construct exhibited a similar structure in both RNA strands (Fig. 4.2 A). This construct functioned effectively as a negative control in the negative-strand RNA detection assay, confirming that the absence of complete 5´UTR in the subgenomic positive-strand RNA prevented NS5B from starting RNA synthesis at the corresponding 3´-end of the positive strand. In the native HCV genome, both RNA termini are known to communicate through LRIs between *cis*-acting elements inducing conformational changes essential for replication or translation, depending on viral or cellular cues (Figure 1.2). As a non-viral sequence, the hp structure likely failed to engage in such interactions, resulting in a rigid conformation that did not support either process.

Consequently, the construct was unable to initiate replication as no negative-strand RNA production could be observed up to 72 hpt (Fig. 3.2.2 A(i)). Reflecting the reduced RNA abundance, the FLuc expression (under Gene Cluster II) also declined over time (Fig. 3.2.2 B(i) and Fig. 3.3.1 B(i)).

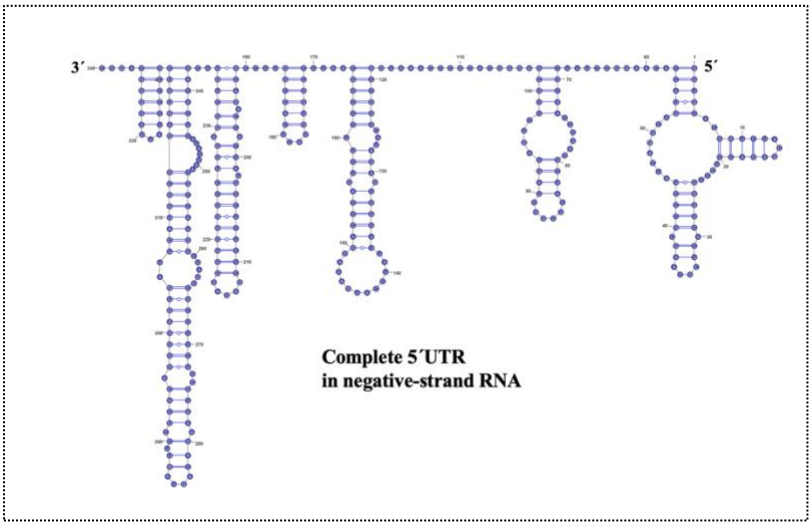

Figure 4.1. RNA secondary structure prediction of the complete 5´UTR in negative-strand RNA obtained using Vienna RNA fold web server and visualized with VARNA.

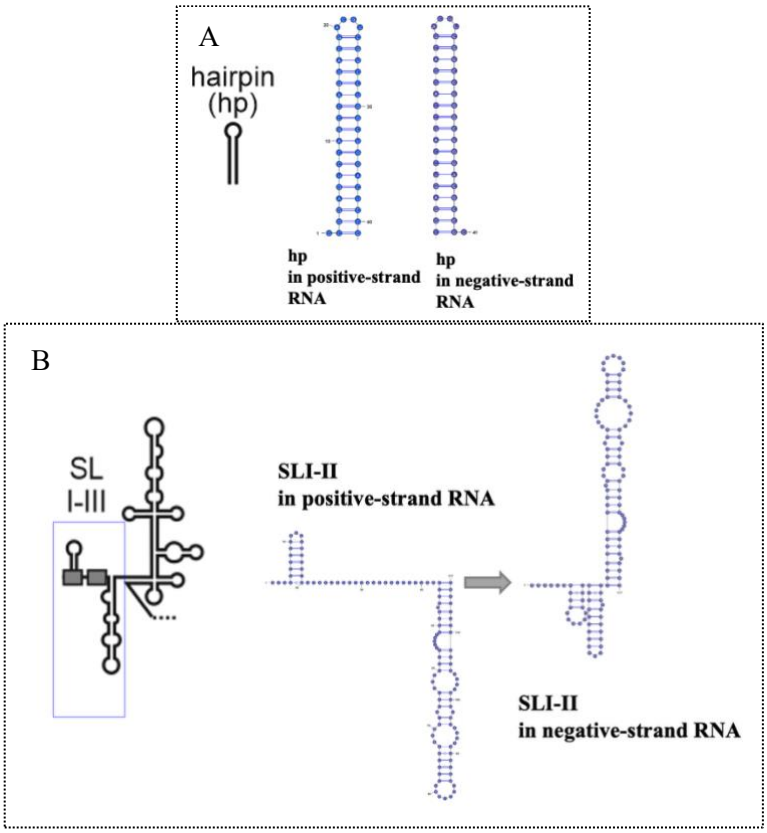

Figure 4.2. RNA secondary structure predictions of 5´UTR elements belonging to 4th generation replicon system and corresponding mutations obtained using Vienna RNA fold web server and visualized with VARNA. **(A)** hp structure; **(B)** SLI-II structure (continued..)

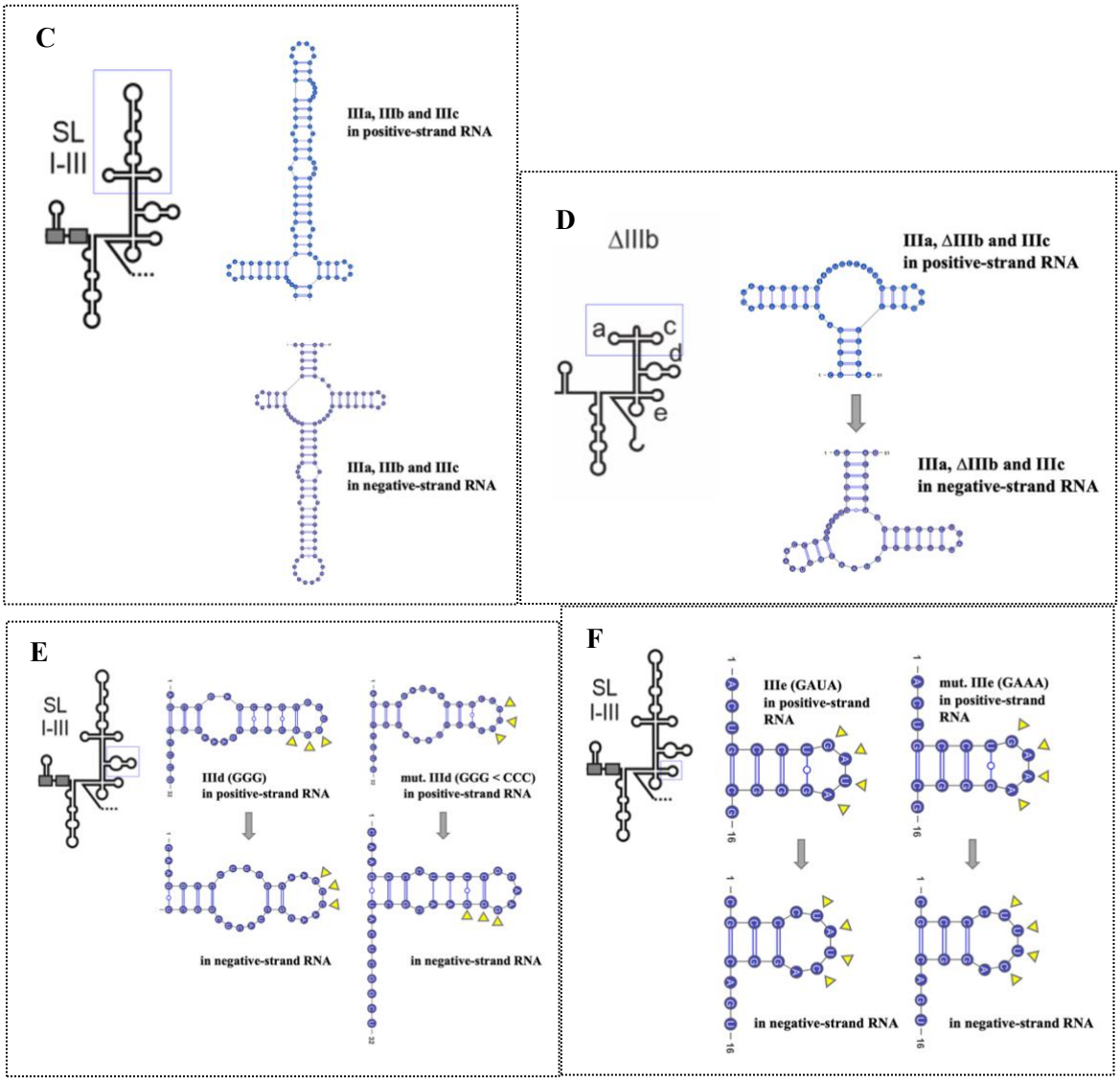

Figure 4.2. RNA secondary structure predictions of 5´UTR elements belonging to 4th generation replicon system and corresponding mutations obtained using Vienna RNA fold web server and visualized with VARNA. **(C)** Domains IIIa, IIIb and IIIc within SLIII. **(D)** Domains IIIa, ΔIIIb and IIIc within SLIII; **(E)** Domain IIId with the GGG → CCC mutation; **(F)** Domain IIIe with the GAUA → GAAA mutation. All structures are shown in both positive- and negative-strand RNA.

The SLIII region (HCV IRES) of the positive-strand RNA forms three stem loops – SL-IIIa´, SLIIIb´ and SLIIIcdef´ – in the 3´UTR of the negative-strand RNA (Friebe and Bartenschlager, 2009). Deletion of SLIIIb´ (178 – 220 nt) and mutation within SLIIIcdef´ produces only minor defects in replication (Friebe and Bartenschlager, 2009). A later study identified the region between nucleotides 177 and 222 from the 3´-end of the negative-strand RNA as essential for efficient initiation of RNA synthesis by recombinant NS5B (Mahias et al., 2010). Similarly, deletion of nucleotides 102 to 239 in the negative-strand 3´UTR reduced the RNA synthesis by 51 %, whereas another deletion (219 – 239) caused only 19 % reduction (Astier-Gin et al., 2005). Collectively, these studies suggest that the reverse complements of 5´UTR sequences downstream of SLI-II contribute to but are not strictly required for the replication. In the present study, taking the negative-strand RNA synthesis as an indicator for replication efficiency, the SLI-III construct achieved approximately 34.5 % of the

replication observed for the wild type (Fig. 3.2.2 A and Fig. 3.3.1 A). Although a positive-strand replicon RNA was transfected into Huh-7.5 cells, it is highly likely that the corresponding negative-strand RNA synthesized intracellularly adopts analogous structural adjustments. Deletion of SLIIIb and mutation in IIId/e resulted in a pronounced reduction in the negative-strand RNA synthesis, emphasizing the importance of these structural elements for replication, although these findings are not fully consistent with previous reports.

The 5´UTR region adopts a different secondary structure in the complementary negative-strand RNA, forming an alternative set of stem-loop structures (Fig. 4.1). The binding of the NS5B to the structured hairpin-like 3´-end of the positive-strand RNA genome is likely more challenging compared to its interaction with a relatively loose-structured 3´-end of the negative-strand RNA. This structural asymmetry may underlie the functional asymmetry observed during replication, wherein a low number of negative-strand RNAs serve exclusively as template for the synthesis of about 10- to 100-fold more progeny positive-strand RNA genomes (Lohmann et al., 2013).

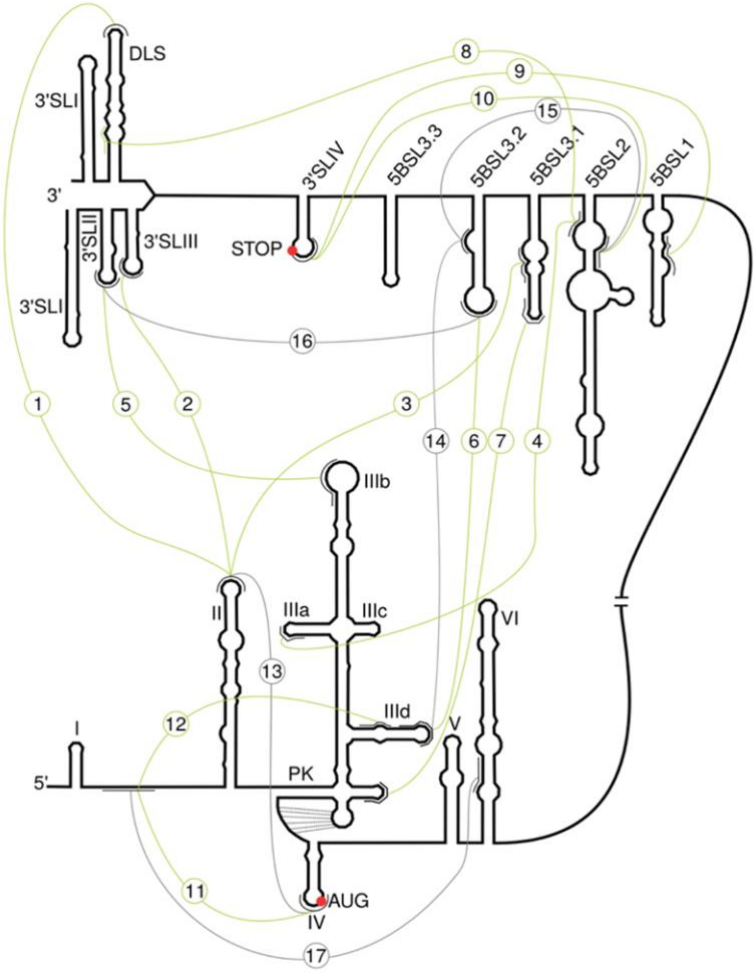

Figure 4.3. Overview of long-range interactions in the HCV 5´UTR, NS5B coding region – specifically the *cis*-replicating element CRE– as well as the 3´UTR variable region and X-tail. Known interactions from literature (No. 13 – 17) and further validated are shown in gray; newly calculated interactions (1 - 12) are shown in green (Fricke et al., 2015).

The observation that the SLI-II construct accounts for 1.34 % of the total RNA abundance – comparable to 2.6 % in the 5´UTR ΔIIIb construct – suggests that the SLI-II region alone may possess the structural features necessary to coordinate NS5B binding at the 3´ terminus of the positive-strand RNA. The bioinformatically predicted long-range interactions are illustrated in the figure 4.3 (Fricke et al., 2015). The region between SLI and II is predicted to engage in LRIs with SLVI in the core-coding region (no. 17) and with SLIV, which contains the AUG start codon (no. 11). However, the SLI-II construct used in this study is unable to engage in these LRIs, as it lacks the IRES and downstream elements, including SLIV and core-coding region (Fig. 3.2.1 B). The LRIs relevant to the SLI-II construct are interactions 1, 2 and 3 (Fig. 4.3), which are predicted to involve the apical portion of SLII and three possible loop structures at the 3´-end (Fricke et al., 2015). These interactions may be suggested to facilitate the circularization of the positive-strand RNA genome. Circularization of the positive-strand HCV RNA genome promotes viral translation, as it facilitates the ribosome re-entry (Scott et al., 2023). The limited negative-strand RNA abundance (1.34 %) observed in the SLI-II construct suggests the occurrence of some circularization event, which may have promoted translation of viral proteins, particularly those necessary for the replication, such as NS5B replicase.

According to the literature, the NS5 replicase of the flaviviruses specifically interacts with the stem-loop S (SLA) structure located at the 5´-end of the positive-strand RNA. This interaction inhibits translation, promotes genome circularization and facilitates the switch from translation to replication (Fajardo et al., 2020). Based on these findings and supported by binding affinity experiments, a mechanistic model has been proposed for HCV genome replication (Scott et al., 2023). NS5B is confirmed to exhibit high binding affinity for SLI-II region within the complete 5´UTR, particularly when this region is bound by miR-122 at its two conserved binding sites (S1 and S2). In this model NS5B is first recruited to the 5´UTR of the positive-strand HCV RNA genome, where miR-122 occupancy may help stabilize the structure. This recruitment is proposed to induce a conformational shift from a circular to a linear genome configuration, thereby separating the 5´- and 3´-ends. Subsequently, a second NS5B molecule binds to the 3´-end of the genome, where it initiates replication (Scott et al., 2023). A cooperative mode of action of the NS5B replicase, most likely mediated by dimerization, has also been proposed previously by Gerresheim and Hess (Gerresheim & Hess et al., 2020).

Based on experiments using a limited set of 5´UTR elements, the model of Scott et al. (2023) suggests that only SLI and the region (CUCCC) between SLI and SLII are sufficient for NS5B recruitment. Although a very limited replication activity was observed for SLI-II in this study (Fig. 3.3.1 A(ii) and B(ii)), given the high levels of miR-122 in Huh-7.5 cells and the capacity of SLI-II to support minimal replication activity via NS5B interaction, a similar mechanism can be proposed. The early stage of HCV infection is characterized by enhanced translation and limited replication (Rheault et al., 2023), where the cooperative binding of two miR-122/Ago complexes stimulates translation (Henke et al., 2008; Nieder-Röhrmann et al., 2017). A similar phase can be inferred in the replicon-based system for the period shortly after transfection of subgenomic replicon RNA into Huh-7.5 cells. Then, the human PCBP2 binds to the CUCCC sequence located within the S2 miR-122 binding site and promotes circularization of the HCV genome which promotes translation initiation (Wang et al., 2011; Scott et al., 2023). In addition, the longer CCCCCCCUCCC sequence between SLI and SLII (Fricke et al., 2015) may support PCBP2 binding to the 5´UTR, while the SLIIId/e/f region and the SLIV remain accessible for binding of the 40S subunit. By competing with miR-122 binding, PCBP2 thereby likely reduces translation efficiency. eIF3 and the small ribosomal 40S subunit (Bai et al., 2013) as well as IGF2BP1/IMP1 (Weinlich et al., 2009) and other cellular factors (reviewed in

Niepmann & Gerresheim, 2020) contribute to this PCBP2-mediated 5´UTR – 3´UTR interaction. This structural arrangement may allow viral translation to proceed for a defined period – potentially with ribosomes retained within the circularized RNA – thereby ensuring the production of sufficient levels of the viral NS5B polymerase and other proteins of the replication cassette. Cooperative binding of miR-122/Ago2 complexes at both S1 and S2 regions (Nieder-Röhrmann et al., 2017) induces linearization of the circularized positive-strand RNA genome; there may be a certain equilibrium between the conformation of the HCV RNA bound by a PCBP2 dimer and the conformation bound by a tandem miR-122/Ago complex. Once enough NS5B has been produced, the protein binds to miR-122 occupied 5´UTR with a high affinity. Another NS5B binds to 3´-end. The proposed mechanistic model may be functionally linked to the phenomenon of NS5B dimerization /oligomerization and cooperative RNA synthesis activity (Wang et al., 2002). It can be hypothesized that during the establishment phase, NS5B accumulates in the form of dimers. At the point of transition from translation to replication, one NS5B monomer from the dimer binds with high affinity to the miR-122:HCV_{45} complex at the 5´UTR of the circularized positive-strand RNA. This binding event may induce a conformational change in the 5´UTR that disrupts the bridge formation between the RNA ends, thereby releasing the 3´-end. The second NS5B monomer from the dimer, benefiting from spatial proximity within the dimer, is then able to rapidly engage the newly exposed 3´-end before it re-folds into stable secondary hairpin structure. Upon binding to 3´-end, the NS5B dimer may perhaps dissociate, with each monomer assuming a functional role, initiating the synthesis of negative-strand RNA. Binding of a NS5B dimer to the positive- and negative- strands may also be supported by an additional NS5B-binding site in the essential CRE 5BSL3.2 (Lee et al., 2004). The system then continues with regular replication, preferentially synthesizing positive-strand RNAs over negative-strands, until sufficient pool of positive-strand RNA accumulates, typically by 72 hpt. The proposed model is illustrated in the figure 4.4.

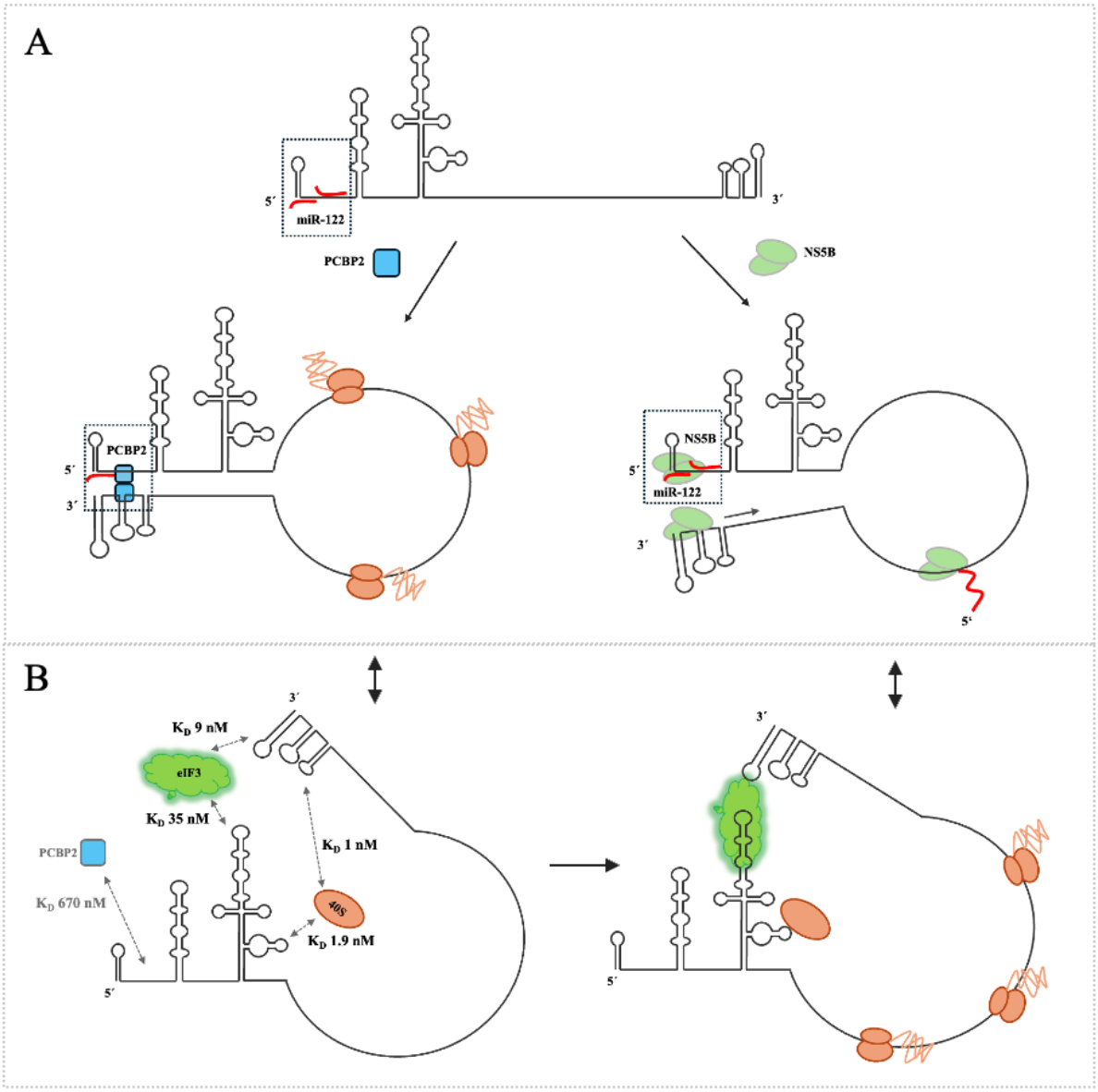

Figure 4.4. Proposed mechanism of bridge formation between 5′- and 3′-ends of HCV RNA genome, facilitated either by PCBP2 protein *in vitro* (Scott et al. 2023) or by eIF3 and 40S subunit *in vivo* (proposed on the basis of results obtained in this study), for HCV replication and translation. (A) miR-122 binding promotes genome linearization. During the establishment phase (left), translation is enhanced (left) as the human protein PCBP2 competitively binds to site S2 (a conserved miR-122 binding site). This interaction facilitates genome circularization by bridging 5′- and 3′-ends of the HCV genome. In the maintenance phase (right) both S1 and S2 are occupied by miR-122, which disrupts the bridge formation. One molecule of the NS5B dimer binds with a high affinity to the miR-122-occupied 5′UTR, while the second NS5B molecule interacts with the 3′-end, taking advantage of their spatial proximity to initiate synthesis of the negative-strand RNA (antigenome). Adapted from Scott et al., 2023. (B) The translation initiation factor eIF3 and the ribosomal 40S subunit bind to 5′- and 3′-ends of the HCV genome with higher affinities (see K_D values, left) compared to the PCBP2 protein. Competitive binding of these components to the HCV genome ends facilitates genome circularization (right), which in turn facilitates translation and synthesis of viral proteins necessary for replication such as the NS5B polymerase. As a result, negative-strand RNA abundance also increases.

This proposed model provides insight into underlying mechanisms by which the various *cis*-acting elements investigated in this study contribute to HCV replication. In the SLI-II region, LRIs 1, 2 and 3 (Fricke et al., 2015) (Fig. 4.3), together with the host protein PCBP2, are likely to facilitate genome circularization. Therefore, ribosomes may be retained within the circularized RNA structure of the SLI-II construct and by that may also support the translation of the NS3 – NS5B replication proteins (Gene Cluster III), in addition to supporting FLuc expression, which reached exceptionally for the SLI-III construct to 7.5-fold higher level at 48 hpt than that of the complete 5′UTR at 72 hpt (Fig. 3.3.1 B).

However, the SLI-II construct could reach only about 1.34 % negative-strand RNA activity compared with the full 5′UTR construct at 72 hpt (Fig. 3.3.1 A). In contrast, the SLI-III construct as well as the construct with the complete 5′UTR achieved much higher negative-strand RNA synthesis activity (Fig. 3.2.2 A; Fig. 3.3.1 A). Remarkably, the mutations disabling the recruitment of eIF3 or the 40S subunit to the IRES dramatically reduced the negative-strand synthesis activity of these mutant replicons. Thus, despite differences in their ability to confer functional translation from the genuine HCV IRES at the 5′-end of the genome, both constructs lack a common factor, that strongly stimulates negative-strand synthesis at the 3′-end. Moreover, the applied mutations (ΔIIIb and mutIIId/e) are located in different regions of the 5′UTR and, according to predictions, are not expected to substantially alter the overall RNA secondary structures of these regions in either positive- or the negative-strand RNA (Fig. 4.2 D, E and F). Despite slight variations (Fig. 4.2 D, E and F), the overall effect of both types of mutations in both types of constructs (SLI-III or 5′UTR) is severely detrimental to roughly similar extents for the production of negative strands (Fig. 3.3.1 A and Fig. 3.4.1). However, these mutations are placed in different regions of the HCV sequence. The IIId/e mutations involve only a few nucleotide exchanges that even do not change the secondary structures of the positive-strand as well as the negative-strand RNA (Fig. 4.2 E and F); the delta-IIIb mutation has similar (mirror) effects in positive and negative strands on RNA structure (Fig. 4.2 D). Thus, local *cis*-effects of these mutations on the RNA structure are rather unlikely to mediate such similar effects of these mutations on RNA synthesis. In contrast, the function of the affected RNA regions in binding eIF3 and the small ribosomal 40S subunit (which is disabled by the mentioned mutations) could perhaps better explain the similar extent of the detrimental effects of these mutations on negative-strand RNA synthesis. In conclusion, it might be assumed that eIF3 and the ribosomal 40S subunit are positively involved in the initiation of negative-strand RNA synthesis by their interactions with the HCV 5′UTR (Kieft et al., 2001) and with the 3′UTR (Bai et al., 2013). Taken together, it can be concluded that it is not essentially the exact nature of these mutations that is relevant for the function of these RNAs, but rather the function that is conferred by the affected sequence elements – namely, the recruitment of eIF3 and the small ribosomal 40S subunit.

Both eIF3 and the 40S subunit can interact with the HCV 5′UTR and with the HCV 3′UTR. In *in vitro* filter binding assays, purified eIF3 binds to the HCV 5′UTR RNA with a K_D of 35 nM (Kieft et al., 2001), and eIF3 binds to the HCV 3′UTR with even higher affinity of about 9 nM (Bai & Doudna, 2013) under very similar buffer conditions (in the presence of 300 mM potassium). The 40S subunit binds to the HCV 5′UTR with a K_D of about 1.9 nM (Kieft et al., 2001) and to the 3′UTR with a K_D of about 1 nM, both under the above mentioned similar buffer conditions. Thus, the 40S subunit as well as eIF3 bind to the HCV 3′UTR with even higher affinity than to the HCV IRES.

Circularization of the HCV RNA by binding of PCBP2 to both HCV genome ends has been also shown in *in vitro*-assays (Wang et al., 2011; Scott et al., 2023) with only low monovalent cation concentrations (50 or 0 mM potassium, respectively) and subsequent glutardialdehyde fixation for electron microscopy. Scott et al. (2023) reported a dissociation constant (K_D) of approximately 670

nM for the PCBP2-IRES interaction, measured at 100 mM NaCl in the absence of Mg^{2+}. However, all these assays have been performed under non-competitive conditions, that is, not in cells or cell extracts where thousands of different proteins compete for the described interactions.

From the above described studies, we can conclude that the affinity of eIF3 and the 40S ribosomal subunit for the HCV 5´UTR and 3´UTR may not be lower than that of PCBP2 for these RNAs and may, in fact, be higher. This interpretation is consistent with the finding that HCV replication efficiency is strongly reduced by the ΔIIIb and mutIIId/e mutations. Thus, the eIF3/40S-mediated bridge between HCV 5´UTR and 3´UTR appears to be at least as important as the PCBP2-mediated bridge and can be assumed to complement and strongly support the mode of negative-strand RNA synthesis initiation as proposed by Scott et al. (2023).

Although strand-specific RNA detection in this study yielded highly accurate and consistent measurements in most cases, the second indicator of replication, the FLuc reporter activity, proved less reliable, particularly at the critical time points 48 and 72 hpt, likely due to transfer of translation components in *cis* on the same RNA molecule from one "capture" site to another functional translation initiation site (Jünnemann et al., 2007). Despite showing a general trend, the differences in FLuc expression levels often remained statistically non-significant. The use of HiBiT as an alternative reporter gene did not result in substantial improvement, aside from a modest enhancement in signal clarity at 48 hpt upon co-transfecting miR-122.

Taken together, identifying a single *cis*-acting element responsible for initiating the synthesis of the very first negative-strand RNA molecule remains a significant challenge. The current approach still lacks the temporal resolution and the detection specificity necessary to pinpoint the exact moment of negative-strand RNA initiation or to isolate the individual *cis*-element responsible for this critical step in the HCV replication cycle.

5. Limitations of this Study

In this study, lipofection was used to transfect replicon RNA for strand-specific RNA detection. While this method enabled highly accurate quantification of negative-strand RNA, it did not permit a time-resolved analysis of the initial onset of *de novo* negative-strand RNA synthesis. The first negative-strand RNA molecules were expected to appear at approximately 12 hpt, followed by the onset of positive-strand RNA synthesis around 16 hpt.

A further limitation arose from assay costs, which restricted the detection of positive-strand RNA to conventional RT-qPCR rather than the more precise Click iT nascent RNA labelling method. As a result, the analysis of early replication events remained incomplete. In future studies, it would be interesting to see when exactly the newly synthesized negative strands and when exactly the newly synthesized positive strands can be detected.

Moreover, lipofection allowed statistically reliable negative-strand RNA quantification only from 24 hpt onward. This delay is likely attributable to the substantial amounts of input RNA that remain protected within liposomes in Huh-7.5 cells and are continuously delivered to the cytosol for extended periods of time, thereby interfering with the selective detection of nascent intracellular RNA. Although electroporation could potentially circumvent this issue, previous experience in the Niepmann Laboratory demonstrated considerable variability in RT-qPCR results due to inconsistent cell recovery following electroporation, necessitating large numbers of replicates to achieve robust statistical significance. Nevertheless, the use of electroporation combined with 5EU-labelling to detect both negative- and positive-strand RNA at earlier time points (4, 8, 12, 16, 24 and 48 hpt) may offer a more informative and comprehensive approach for future studies.

Another limitation may arise from the presence of large amounts of input RNA, namely the likely generation of false-positive results by degradation products of the input RNA acting as unwanted primers in the RT reaction. This hypothesis is supported by the fact that this background in negative-strand detection declines over time and makes assays "cleaner" after longer incubation times, since the input RNA, that is not engaged in functional replication complexes, is increasingly degraded in the cells. As mentioned above, this problem could perhaps be addressed by including additional washing steps in the Click-iT purification of the 5EU-labelled nascent RNAs using chemicals like urea that disturb nucleic acid-nucleic acid hybridization. Such treatment may be appropriate to strip off unwanted RNA oligonucleotides that originate from degradation of the vast amounts of transfected input RNA and act as unwanted primers in the downstream RT reaction. Solving this problem could perhaps support assays that allow to detect newly synthesized negative- and positive-strand RNAs more reliably at early time points, and by that allow to investigate the very early steps of RNA synthesis with the replicon system.

The background described above is also related to another limitation of the experimental system as used thus far. The initial intention behind developing this 4th generation replicon system was to completely uncouple the analysis of negative-strand synthesis initiation from all other molecular events taking place on the replicon RNA during the replication cycle. However, the background of the negative-strand detection assay described above partially compromised this uncoupled analysis of negative-strand synthesis, as the relatively high background at very early time points interfered with the corresponding measurements. Consequently, newly synthesized negative strands could be detected significantly above background only at 24 hpt or later, and it must be considered that by that time "roundabout" amplification of new negative and positive strands had already occurred. This

consideration applies, at least, to those constructs that contain sufficient HCV sequences at the 3´-end of the negative-strand RNA to allow the initiation of positive-strand synthesis by NS5B, i.e., all constructs containing SLI-II or more.

Improvement of the assay by removing hybridized oligonucleotides that act as unwanted primers could allow analysis of the detection of newly synthesized negative strands, as well as newly emerging positive strands, at very early time points such as 8, 12 and 16 hpt. In combination, electroporation might provide even better temporal resolution of the onset of negative- and positive-strand production. An ideal assay would detect the first 5EU-labelled negative strands shortly before the appearance of the first 5EU-labelled progeny positive strands. Only such an observation would then – admittedly in a somewhat circular argumentation – allow the conclusion that the detection of negative-strand synthesis is truly uncoupled from other replication-associated events.

6. Outlook

The strand-specific RNA detection assay should be further optimized by employing electroporation as an alternative transfection method, thereby enabling the detection of both negative- and positive-strand RNA at shorter intervals and earlier time points.

For a more detailed investigation of *cis*-elements, the 5′UTR mutation applied in this study could be introduced into 3′-end of the negative-strand RNA by using the complementary DNA sequence as the template for *in vitro*-transcription, followed by the generation of negative-strand-based replicon system. Performing the same strand-specific RNA detection assay with this system would allow direct confirmation of the activity of specific *cis*-elements in the negative-strand RNA. In addition, introducing mutations into the 3′UTR of the positive-strand HCV RNA replicon could further elucidate the role of LRIs between the two genome ends. Furthermore, the potential roles of the 3′UTR and the upstream NS5B miR-122 binding sites could be re-evaluated using this assay. If assay sensitivity permits, a replicon could also be developed in which the EMCV IRES driving translation of the HCV replication proteins is replaced by a hybridized G-capped oligonucleotide for ribosome recruitment. This would allow translation of the HCV replication proteins only in the very first round of replication. In contrast, replication proteins could not be expressed from progeny positive-strands that lack the hybridized G-capped oligonucleotide. Consequently, RNA synthesis would be restricted to the first round of negative-strand RNA synthesis, whereas "roundabout" amplification would be excluded even in cases where HCV sequences are present at the 3′-end of the negative strand that would otherwise permit initiation of progeny positive-strand synthesis.

The proposed mechanistic model (Fig. 4.4) requires further investigation. In particular, the binding affinity of NS5B to the miR-122 occupied 5′UTR and its variants used in this study should be experimentally validated. Methods such as isothermal titration calorimetry (ITC) may provide precise thermodynamic insights into this interaction.

Using the above described strategy, NS5B binding to 3′UTR and its mutated versions should be investigated in detail, to elucidate its specific structure facilitating NS5B binding.

Additionally, the genome circularization events in 5′UTR constructs used in this study should be captured using high resolution electron microscopy, which can help to reveal the *cis*-elements facilitating the linearization of the circularized positive-strand RNA genome. These maybe the ones responsible for the initiation of negative-strand synthesis.

7. References

Astier-Gin, T., Bellecave, P., Litvak, S., & Ventura, M. (2005). Template requirements and binding of hepatitis C virus NS5B polymerase during in vitro RNA synthesis from the 3‘-end of virus minus-strand RNA. *The FEBS Journal*, *272*(15), 3872–3886. https://doi.org/10.1111/j.1742-4658.2005.04804.x

Backes, P., Quinkert, D., Reiss, S., Binder, M., Zayas, M., Rescher, U., Gerke, V., Bartenschlager, R [Ralf], & Lohmann, V [Volker] (2010). Role of annexin A2 in the production of infectious hepatitis C virus particles. *Journal of Virology*, *84*(11), 5775–5789. https://doi.org/10.1128/JVI.02343-09

Bai, Y., Zhou, K., & Doudna, J. A. (2013). Hepatitis C virus 3‘UTR regulates viral translation through direct interactions with the host translation machinery. *Nucleic Acids Research*, *41*(16), 7861–7874. https://doi.org/10.1093/nar/gkt543

Bartenschlager, R [Ralf], Cosset, F.-L [Francois-Loic], & Lohmann, V [Volker] (2010). Hepatitis C virus replication cycle. *Journal of Hepatology*, *53*(3), 583–585. https://doi.org/10.1016/j.jhep.2010.04.015

Bernier, A., & Sagan, S. M. (2019). Beyond sites 1 and 2, miR-122 target sites in the HCV genome have negligible contributions to HCV RNA accumulation in cell culture. *The Journal of general virology*, *100*(2), 217–226. https://doi.org/10.1099/jgv.0.001217

Binder, M., Sulaimanov, N., Clausznitzer, D., Schulze, M., Hüber, C. M., Lenz, S. M., Schlöder, J. P., Trippler, M., Bartenschlager, R [Ralf], Lohmann, V [Volker], & Kaderali, L. (2013). Replication vesicles are load- and choke-points in the hepatitis C virus lifecycle. *PLoS Pathogens*, *9*(8), e1003561. https://doi.org/10.1371/journal.ppat.1003561

Bley, H., Schöbel, A., & Herker, E. (2020). Whole Lotta Lipids-from HCV RNA Replication to the Mature Viral Particle. *International Journal of Molecular Sciences*, *21*(8). https://doi.org/10.3390/ijms21082888

Blight, K. J., Kolykhalov, A. A., & Rice, C. M. (2000). Efficient initiation of HCV RNA replication in cell culture. *Science (New York, N.Y.)*, *290*(5498), 1972–1974. https://doi.org/10.1126/science.290.5498.1972

Blight, K. J., McKeating, J. A., & Rice, C. M. (2002). Highly permissive cell lines for subgenomic and genomic hepatitis C virus RNA replication. *Journal of Virology*, *76*(24), 13001–13014. https://doi.org/10.1128/jvi.76.24.13001-13014.2002

Choo, Q. L., Kuo, G., Weiner, A. J., Overby, L. R., Bradley, D. W., & Houghton, M. (1989). Isolation of a cDNA clone derived from a blood-borne non-A, non-B viral hepatitis genome. *Science (New York, N.Y.)*, *244*(4902), 359–362. https://doi.org/10.1126/science.2523562

Chomczynski, P., & Sacchi, N. (2006). The single-step method of RNA isolation by acid guanidinium thiocyanate-phenol-chloroform extraction: Twenty-something years on. *Nature Protocols*, *1*(2), 581–585. https://doi.org/10.1038/nprot.2006.83

Conrad, K. D., Giering, F., Erfurth, C., Neumann, A., Fehr, C., Meister, G., & **Niepmann**, M. (2013). Microrna-122 dependent binding of Ago2 protein to hepatitis C virus RNA is associated with enhanced RNA stability and translation stimulation. *PloS One*, *8*(2), e56272. https://doi.org/10.1371/journal.pone.0056272

Cui, F., Blach, S., Manzengo Mingiedi, C., Gonzalez, M. A., Sabry Alaama, A., Mozalevskis, A., Séguy, N., Rewari, B. B., Chan, P.-L., Le, L.-V., Doherty, M., Luhmann, N., Easterbrook, P., Dirac, M., Martel, C. de, Nayagam, S., Hallett, T. B., Vickerman, P., Razavi, H., . . . Low-Beer, D. (2023). Global reporting of progress towards elimination of hepatitis B and hepatitis C. *The Lancet. Gastroenterology & Hepatology*, *8*(4), 332–342. https://doi.org/10.1016/S2468-1253(22)00386-7

Dobson, S. J., Ward, J. C., Herod, M. R., Rowlands, D. J., & Stonehouse, N. J. (2023). A highly discriminatory RNA strand-specific assay to facilitate analysis of the role of cis-acting elements in foot-and-mouth disease virus replication. *The Journal of General Virology*, *104*(7). https://doi.org/10.1099/jgv.0.001871

Dubuisson, J., & Cosset, F.-L [François-Loïc] (2014). Virology and cell biology of the hepatitis C virus life cycle: An update. *Journal of Hepatology*, *61*(1 Suppl), S3-S13. https://doi.org/10.1016/j.jhep.2014.06.031

Dutkiewicz, M., Swiatkowska, A., Figlerowicz, M., & Ciesiołka, J. (2008). Structural domains of the 3'-terminal sequence of the hepatitis C virus replicative strand. *Biochemistry*, *47*(46), 12197–12207. https://doi.org/10.1021/bi800348g

Egger, D., Wölk, B., Gosert, R., Bianchi, L., Blum, H. E., Moradpour, D., & Bienz, K. (2002). Expression of hepatitis C virus proteins induces distinct membrane alterations including a candidate viral replication complex. *Journal of Virology*, *76*(12), 5974–5984. https://doi.org/10.1128/jvi.76.12.5974-5984.2002

Fajardo, T., Sanford, T. J., Mears, H. V., Jasper, A., Storrie, S., Mansur, D. S., & Sweeney, T. R. (2020). The flavivirus polymerase NS5 regulates translation of viral genomic RNA. *Nucleic Acids Research*, *48*(9), 5081–5093. https://doi.org/10.1093/nar/gkaa242

Fehr, C., Conrad, K. D., & **Niepmann**, M. (2012). Differential stimulation of hepatitis C virus RNA translation by microRNA-122 in different cell cycle phases. *Cell Cycle (Georgetown, Tex.)*, *11*(2), 277–285. https://doi.org/10.4161/cc.11.2.18699

Fricke, M., Dünnes, N., Zayas, M., Bartenschlager, R [Ralf], **Niepmann, M.**, & Marz, M. (2015). Conserved RNA secondary structures and long-range interactions in hepatitis C viruses. *RNA (New York, N.Y.)*, *21*(7), 1219–1232. https://doi.org/10.1261/rna.049338.114

Friebe, P., & Bartenschlager, R [Ralf] (2009). Role of RNA structures in genome terminal sequences of the hepatitis C virus for replication and assembly. *Journal of Virology*, *83*(22), 11989–11995. https://doi.org/10.1128/JVI.01508-09

Gerresheim, G. K., Dünnes, N., Nieder-Röhrmann, A., Shalamova, L. A., Fricke, M., Hofacker, I., Höner Zu Siederdissen, C., Marz, M., & **Niepmann, M**. (2017). Microrna-122 target sites in the hepatitis C virus RNA NS5B coding region and 3‘ untranslated region: Function in replication and influence of RNA secondary structure. *Cellular and Molecular Life Sciences : CMLS*, *74*(4), 747–760. https://doi.org/10.1007/s00018-016-2377-9

Gerresheim, G. K., Hess, C. S., Shalamova, L. A., Fricke, M., Marz, M., Andreev, D. E., Shatsky, I. N., & **Niepmann, M**. (2020). Ribosome Pausing at Inefficient Codons at the End of the Replicase Coding Region Is Important for Hepatitis C Virus Genome Replication. *International Journal of Molecular Sciences*, *21*(18). https://doi.org/10.3390/ijms21186955

Gholamalipour, Y., Karunanayake Mudiyanselage, A., & Martin, C. T. (2018). 3‘ end additions by T7 RNA polymerase are RNA self-templated, distributive and diverse in character-RNA-Seq analyses. *Nucleic Acids Research*, *46*(18), 9253–9263. https://doi.org/10.1093/nar/gky796

Gouttenoire, J., Castet, V., Montserret, R., Arora, N., Raussens, V., Ruysschaert, J.-M., Diesis, E., Blum, H. E., Penin, F., & Moradpour, D. (2009). Identification of a novel determinant for membrane association in hepatitis C virus nonstructural protein 4B. *Journal of Virology*, *83*(12), 6257–6268. https://doi.org/10.1128/JVI.02663-08

Hellen, C. U., & Sarnow, P. (2001). Internal ribosome entry sites in eukaryotic mRNA molecules. *Genes & development*, *15*(13), 1593–1612. https://doi.org/10.1101/gad.891101

Henke, J. I., Goergen, D., Zheng, J., Song, Y., Schüttler, C. G., Fehr, C., Jünemann, C., & **Niepmann**, M. (2008). microRNA-122 stimulates translation of hepatitis C virus RNA. *The EMBO journal*, *27*(24), 3300–3310. https://doi.org/10.1038/emboj.2008.244

Ito, T., & Lai, M. M. (1999). An internal polypyrimidine-tract-binding protein-binding site in the hepatitis C virus RNA attenuates translation, which is relieved by the 3'-untranslated sequence. *Virology*, *254*(2), 288–296. https://doi.org/10.1006/viro.1998.9541

Jang, S. K., Kräusslich, H. G., Nicklin, M. J., Duke, G. M., Palmenberg, A. C., & Wimmer, E [E.] (1988). A segment of the 5‘ nontranslated region of encephalomyocarditis virus RNA directs internal entry of ribosomes during in vitro translation. *Journal of Virology*, *62*(8), 2636–2643. https://doi.org/10.1128/JVI.62.8.2636-2643.1988

Johnson, A. G., Grosely, R., Petrov, A. N., & Puglisi, J. D. (2017). Dynamics of IRES-mediated translation. *Philosophical Transactions of the Royal Society of London. Series B, Biological Sciences*, *372*(1716). https://doi.org/10.1098/rstb.2016.0177

John Hopkins Medicine. Hepatitis 2025 https://www.hopkinsmedicine.org/infectious-diseases/about-us/our-focus/viral-hepatitis

Jopling, C. L., Yi, M., Lancaster, A. M., Lemon, S. M., & Sarnow, P. (2005). Modulation of hepatitis C virus RNA abundance by a liver-specific MicroRNA. *Science (New York, N.Y.)*, *309*(5740), 1577–1581. https://doi.org/10.1126/science.1113329

Jünemann, C., Song, Y., Bassili, G., Goergen, D., Henke, J., & **Niepmann**, M. (2007). Picornavirus internal ribosome entry site elements can stimulate translation of upstream genes. *The Journal of Biological Chemistry*, *282*(1), 132–141. https://doi.org/10.1074/jbc.M608750200

Kato, T., Furusaka, A., Miyamoto, M., Date, T., Yasui, K., Hiramoto, J., Nagayama, K., Tanaka, T., & Wakita, T. (2001). Sequence analysis of hepatitis C virus isolated from a fulminant hepatitis patient. *Journal of medical virology*, *64*(3), 334–339. https://doi.org/10.1002/jmv.1055

Khan, S., Soni, S., & Veerapu, N. S. (2020). Hcv Replicon Systems: Workhorses of Drug Discovery and Resistance. *Frontiers in Cellular and Infection Microbiology*, *10*, 325. https://doi.org/10.3389/fcimb.2020.00325

Kieft, J. S., Zhou, K., Jubin, R., & Doudna, J. A. (2001). Mechanism of ribosome recruitment by hepatitis C IRES RNA. *RNA (New York, N.Y.)*, *7*(2), 194–206. https://doi.org/10.1017/s1355838201001790

Krieger, N., Lohmann, V [V.], & Bartenschlager, R [R.] (2001). Enhancement of hepatitis C virus RNA replication by cell culture-adaptive mutations. *Journal of Virology*, *75*(10), 4614–4624. https://doi.org/10.1128/JVI.75.10.4614-4624.2001

Kurzban, G. P., Bayer, E. A., Wilchek, M., & Horowitz, P. M. (1991). The quaternary structure of streptavidin in urea. *Journal of Biological Chemistry*, *266*(22), 14470–14477. https://doi.org/10.1016/S0021-9258(18)98710-7

Lagos-Quintana, M., Rauhut, R., Yalcin, A., Meyer, J., Lendeckel, W., & Tuschl, T. (2002). Identification of tissue-specific microRNAs from mouse. *Current biology : CB*, *12*(9), 735–739. https://doi.org/10.1016/s0960-9822(02)00809-6

Laugi, H. (2020). Discovery of Hepatitis C Virus: 2020 Nobel Prize in Medicine. *Euroasian Journal of Hepato-Gastroenterology*, *10*(2), 105–108. https://doi.org/10.5005/jp-journals-10018-1326

Lee, H., Shin, H., Wimmer, E [Eckard], & Paul, A. V. (2004). Cis-acting RNA signals in the NS5B C-terminal coding sequence of the hepatitis C virus genome. *Journal of Virology*, *78*(20), 10865–10877. https://doi.org/10.1128/JVI.78.20.10865-10877.2004

Li, H.-C., Yang, C.-H., & Lo, S.-Y. (2021). Hepatitis C Viral Replication Complex. *Viruses*, *13*(3). https://doi.org/10.3390/v13030520

Li, Y., Masaki, T., Yamane, D., McGivern, D. R., & Lemon, S. M. (2013). Competing and noncompeting activities of miR-122 and the 5‘ exonuclease Xrn1 in regulation of hepatitis C virus replication. *Proceedings of the National Academy of Sciences of the United States of America*, *110*(5), 1881–1886. https://doi.org/10.1073/pnas.1213515110

Li, Y., Yamane, D., Masaki, T., & Lemon, S. M. (2015). The yin and yang of hepatitis C: Synthesis and decay of hepatitis C virus RNA. *Nature Reviews. Microbiology*, *13*(9), 544–558. https://doi.org/10.1038/nrmicro3506

Lim, S. M., Koraka, P., Osterhaus, A. D. M. E., & Martina, B. E. E. (2013). Development of a strand-specific real-time qRT-PCR for the accurate detection and quantitation of West Nile virus RNA. *Journal of Virological Methods*, *194*(1-2), 146–153. https://doi.org/10.1016/j.jviromet.2013.07.050

Lindenbach, B. D., Prágai, B. M., Montserret, R., Beran, R. K. F., Pyle, A. M., Penin, F., & Rice, C. M. (2007). The C terminus of hepatitis C virus NS4A encodes an electrostatic switch that regulates NS5A hyperphosphorylation and viral replication. *Journal of Virology*, *81*(17), 8905–8918. https://doi.org/10.1128/JVI.00937-07

Lindenbach, B. D., & Rice, C. M. (2013). The ins and outs of hepatitis C virus entry and assembly. *Nature Reviews. Microbiology*, *11*(10), 688–700. https://doi.org/10.1038/nrmicro3098

Lohmann, V., Körner, F., Herian, U., & Bartenschlager, R. (1997). Biochemical properties of hepatitis C virus NS5B RNA-dependent RNA polymerase and identification of amino acid sequence motifs essential for enzymatic activity. *Journal of virology*, *71*(11), 8416–8428. https://doi.org/10.1128/JVI.71.11.8416-8428.1997

Lohmann, V., Körner, F., Koch, J., Herian, U., Theilmann, L., & Bartenschlager, R. (1999). Replication of subgenomic hepatitis C virus RNAs in a hepatoma cell line. *Science (New York, N.Y.)*, *285*(5424), 110–113. https://doi.org/10.1126/science.285.5424.110

Lohmann, V [V.], Körner, F., Dobierzewska, A., & Bartenschlager, R [R.] (2001). Mutations in hepatitis C virus RNAs conferring cell culture adaptation. *Journal of Virology*, *75*(3), 1437–1449. https://doi.org/10.1128/JVI.75.3.1437-1449.2001

Lohmann, V [Volker] (2013). Hepatitis C virus RNA replication. *Current Topics in Microbiology and Immunology*, *369*, 167–198. https://doi.org/10.1007/978-3-642-27340-7_7

Long, C., Romero, M. E., La Rocco, D., & Yu, J. (2021). Dissecting nucleotide selectivity in viral RNA polymerases. *Computational and Structural Biotechnology Journal*, *19*, 3339–3348. https://doi.org/10.1016/j.csbj.2021.06.005

Mahias, K., Ahmed-El-Sayed, N., Masante, C., Bitard, J., Staedel, C., Darfeuille, F., Ventura, M., & Astier-Gin, T. (2010). Identification of a structural element of the hepatitis C virus minus strand RNA involved in the initiation of RNA synthesis. *Nucleic Acids Research*, *38*(12), 4079–4091. https://doi.org/10.1093/nar/gkq109

Malygin, A. A., Kossinova, O. A., Shatsky, I. N., & Karpova, G. G. (2013). Hcv IRES interacts with the 18S rRNA to activate the 40S ribosome for subsequent steps of translation initiation. *Nucleic Acids Research*, *41*(18), 8706–8714. https://doi.org/10.1093/nar/gkt632

Masaki, T., Arend, K. C., Li, Y., Yamane, D., McGivern, D. R., Kato, T., Wakita, T., Moorman, N. J., & Lemon, S. M. (2015). Mir-122 stimulates hepatitis C virus RNA synthesis by altering the balance of viral RNAs engaged in replication versus translation. *Cell Host & Microbe*, *17*(2), 217–228. https://doi.org/10.1016/j.chom.2014.12.014

Masante, C., Mahias, K., Lourenço, S., Dumas, E., Cahour, A., Trimoulet, P., Fleury, H., Astier-Gin, T., & Ventura, M. (2008). Seven nucleotide changes characteristic of the hepatitis C virus genotype 3 5‘ untranslated region: Correlation with reduced in vitro replication. *The Journal of General Virology*, *89*(Pt 1), 212–221. https://doi.org/10.1099/vir.0.83067-0

Matsuda, D., & Mauro, V. P. (2014). Base pairing between hepatitis C virus RNA and 18S rRNA is required for IRES-dependent translation initiation in vivo. *Proceedings of the National Academy of Sciences of the United States of America*, *111*(43), 15385–15389. https://doi.org/10.1073/pnas.1413472111

Matthaei, A., Joecks, S., Frauenstein, A., Bruening, J., Bankwitz, D., Friesland, M., Gerold, G., Vieyres, G., Kaderali, L., Meissner, F., & Pietschmann, T. (2024). Landscape of protein-protein interactions during hepatitis C virus assembly and release. *Microbiology Spectrum*, *12*(2), e0256222. https://doi.org/10.1128/spectrum.02562-22

Moradpour, D., & Penin, F. (2013). Hepatitis C virus proteins: From structure to function. *Current Topics in Microbiology and Immunology*, *369*, 113–142. https://doi.org/10.1007/978-3-642-27340-7_5

Murray, C. L., Jones, C. T., & Rice, C. M. (2008). Architects of assembly: Roles of Flaviviridae non-structural proteins in virion morphogenesis. *Nature Reviews. Microbiology*, *6*(9), 699–708. https://doi.org/10.1038/nrmicro1928

Nacheva, G. A., & Berzal-Herranz, A. (2003). Preventing nondesired RNA-primed RNA extension catalyzed by T7 RNA polymerase. *European Journal of Biochemistry*, *270*(7), 1458–1465. https://doi.org/10.1046/j.1432-1033.2003.03510.x

Nakabayashi, H., Taketa, K., Miyano, K., Yamane, T., & Sato, J. (1982). Growth of human hepatoma cells lines with differentiated functions in chemically defined medium. *Cancer research*, *42*(9), 3858–3863.

Nieder-Röhrmann, A., Dünnes, N., Gerresheim, G. K., Shalamova, L. A., Herchenröther, A., & **Niepmann**, M. (2017). Cooperative enhancement of translation by two adjacent microRNA-122/Argonaute 2 complexes binding to the 5' untranslated region of hepatitis C virus RNA. *The Journal of general virology*, *98*(2), 212–224. https://doi.org/10.1099/jgv.0.000697

Niepmann, M. (2013). Hepatitis C virus RNA translation. *Current Topics in Microbiology and Immunology*, *369*, 143–166. https://doi.org/10.1007/978-3-642-27340-7_6

Niepmann, M., & Gerresheim, G. K. (2020). Hepatitis C Virus Translation Regulation. *International Journal of Molecular Sciences*, *21*(7). https://doi.org/10.3390/ijms21072328

Niepmann, M., Shalamova, L. A., Gerresheim, G. K., & Rossbach, O. (2018). Signals Involved in Regulation of Hepatitis C Virus RNA Genome Translation and Replication. *Frontiers in Microbiology*, *9*, 395. https://doi.org/10.3389/fmicb.2018.00395

Ouldali, M., Moncoq, K., La Valette, A. C. de, Arteni, A. A., Betton, J.-M., & Lepault, J. (2021). Study of membrane deformations induced by Hepatitis C protein NS4B and its terminal amphipathic peptides. *Biochimica Et Biophysica Acta. Biomembranes*, *1863*(3), 183537. https://doi.org/10.1016/j.bbamem.2020.183537

Panigrahi, M., Palmer, M. A., & Wilson, J. A. (2022). Microrna-122 Regulation of HCV Infections: Insights from Studies of miR-122-Independent Replication. *Pathogens (Basel, Switzerland)*, *11*(9). https://doi.org/10.3390/pathogens11091005

Pelletier, J., & Sonenberg, N. (1988). Internal initiation of translation of eukaryotic mRNA directed by a sequence derived from poliovirus RNA. *Nature*, *334*(6180), 320–325. https://doi.org/10.1038/334320a0

Pietschmann, T., Kaul, A., Koutsoudakis, G., Shavinskaya, A., Kallis, S., Steinmann, E., Abid, K., Negro, F., Dreux, M., Cosset, F. L., & Bartenschlager, R. (2006). Construction and characterization of infectious intragenotypic and intergenotypic hepatitis C virus chimeras. *Proceedings of the National Academy of Sciences of the United States of America*, *103*(19), 7408–7413. https://doi.org/10.1073/pnas.0504877103

Quinkert, D., Bartenschlager, R [Ralf], & Lohmann, V [Volker] (2005). Quantitative analysis of the hepatitis C virus replication complex. *Journal of Virology*, *79*(21), 13594–13605. https://doi.org/10.1128/JVI.79.21.13594-13605.2005

Rai, R., & Deval, J. (2011). New opportunities in anti-hepatitis C virus drug discovery: Targeting NS4B. *Antiviral Research*, *90*(2), 93–101. https://doi.org/10.1016/j.antiviral.2011.01.009

Ray, P. S., & Das, S. (2004). Inhibition of hepatitis C virus IRES-mediated translation by small RNAs analogous to stem-loop structures of the 5‘-untranslated region. *Nucleic Acids Research*, *32*(5), 1678–1687. https://doi.org/10.1093/nar/gkh328

Rheault, M., Cousineau, S. E., Fox, D. R., Abram, Q. H., & Sagan, S. M. (2023). Elucidating the distinct contributions of miR-122 in the HCV life cycle reveals insights into virion assembly. *Nucleic Acids Research*, *51*(5), 2447–2463. https://doi.org/10.1093/nar/gkad094

Romero-Brey, I., Berger, C., Kallis, S., Kolovou, A., Paul, D., Lohmann, V [Volker], & Bartenschlager, R [Ralf] (2015). Ns5a Domain 1 and Polyprotein Cleavage Kinetics Are Critical for Induction of Double-Membrane Vesicles Associated with Hepatitis C Virus Replication. *MBio*, *6*(4), e00759. https://doi.org/10.1128/mBio.00759-15

Romero-Brey, I., Merz, A., Chiramel, A., Lee, J.-Y., Chlanda, P., Haselman, U., Santarella-Mellwig, R., Habermann, A., Hoppe, S., Kallis, S., Walther, P., Antony, C., Krijnse-Locker, J., & Bartenschlager, R [Ralf] (2012). Three-dimensional architecture and biogenesis of membrane structures associated with hepatitis C virus replication. *PLoS Pathogens*, *8*(12), e1003056. https://doi.org/10.1371/journal.ppat.1003056

Romero-López, C., & Berzal-Herranz, A. (2017). The 5BSL3.2 Functional RNA Domain Connects Distant Regions in the Hepatitis C Virus Genome. *Frontiers in Microbiology*, *8*, 2093. https://doi.org/10.3389/fmicb.2017.02093

Schenborn, E. T., & Mierendorf, R. C., Jr (1985). A novel transcription property of SP6 and T7 RNA polymerases: dependence on template structure. *Nucleic acids research*, *13*(17), 6223–6236. https://doi.org/10.1093/nar/13.17.6223

Schoch, C. L., Ciufo, S., Domrachev, M., Hotton, C. L., Kannan, S., Khovanskaya, R., Leipe, D., Mcveigh, R., O‘Neill, K., Robbertse, B., Sharma, S., Soussov, V., Sullivan, J. P., Sun, L., Turner, S., & Karsch-Mizrachi, I. (2020). Ncbi Taxonomy: A comprehensive update on curation, resources and tools. *Database : The Journal of Biological Databases and Curation*, *2020.* https://doi.org/10.1093/database/baaa062

Schult, P., Roth, H., Adams, R. L., Mas, C., Imbert, L., Orlik, C., Ruggieri, A., Pyle, A. M., & Lohmann, V [Volker] (2018). Microrna-122 amplifies hepatitis C virus translation by shaping the structure of the internal ribosomal entry site. *Nature Communications*, *9*(1), 2613. https://doi.org/10.1038/s41467-018-05053-3

Scott, S., Li, Y., Bermek, O., Griffith, J. D., Lemon, S. M., & Choi, K. H. (2023). Binding of microRNA-122 to the hepatitis C virus 5‘ untranslated region modifies interactions with poly© binding protein 2 and the NS5B viral polymerase. *Nucleic Acids Research*, *51*(22), 12397–12413. https://doi.org/10.1093/nar/gkad1000

Shimakami, T., Yamane, D., Jangra, R. K., Kempf, B. J., Spaniel, C., Barton, D. J., & Lemon, S. M. (2012). Stabilization of hepatitis C virus RNA by an Ago2-miR-122 complex. *Proceedings of the National Academy of Sciences of the United States of America*, *109*(3), 941–946. https://doi.org/10.1073/pnas.1112263109

Song, Y., Friebe, P., Tzima, E., Jünemann, C., Bartenschlager, R [Ralf], & **Niepmann**, M. (2006). The hepatitis C virus RNA 3‘-untranslated region strongly enhances translation directed by the internal ribosome entry site. *Journal of Virology*, *80*(23), 11579–11588. https://doi.org/10.1128/JVI.00675-06

Steinmann, E., & Pietschmann, T. (2010). Hepatitis C virus p7-a viroporin crucial for virus assembly and an emerging target for antiviral therapy. *Viruses*, *2*(9), 2078–2095. https://doi.org/10.3390/v2092078

Sumpter, R., Loo, Y.-M., Foy, E., Li, K., Yoneyama, M., Fujita, T., Lemon, S. M., & Gale, M. (2005). Regulating intracellular antiviral defense and permissiveness to hepatitis C virus RNA replication through a cellular RNA helicase, RIG-I. *Journal of Virology*, *79*(5), 2689–2699. https://doi.org/10.1128/JVI.79.5.2689-2699.2005

Tabata, K., Neufeldt, C. J., & Bartenschlager, R [Ralf] (2020). Hepatitis C Virus Replication. *Cold Spring Harbor Perspectives in Medicine*, *10*(3). https://doi.org/10.1101/cshperspect.a037093

Tagwerker, C., Flick, K., Cui, M., Guerrero, C., Dou, Y., Auer, B., Baldi, P., Huang, L., & Kaiser, P. (2006). A tandem affinity tag for two-step purification under fully denaturing conditions: Application in ubiquitin profiling and protein complex identification combined with in vivocross-linking. *Molecular & Cellular Proteomics: MCP*, *5*(4), 737–748. https://doi.org/10.1074/mcp.M500368-MCP200

Topi, S., Gaxhja, E., Charitos, I. A., Colella, M., & Santacroce, L. (2024). Hepatitis C Virus: History and Current Knowledge. *Gastroenterology Insights*, *15*(3), 676–707. https://doi.org/10.3390/gastroent15030049

Triana-Alonso, F. J., Dabrowski, M., Wadzack, J., & Nierhaus, K. H. (1995). Self-coded 3‘-extension of run-off transcripts produces aberrant products during in vitro transcription with T7 RNA polymerase. *The Journal of Biological Chemistry*, *270*(11), 6298–6307. https://doi.org/10.1074/jbc.270.11.6298

Vieyres, G., Thomas, X., Descamps, V., Duverlie, G., Patel, A. H., & Dubuisson, J. (2010). Characterization of the envelope glycoproteins associated with infectious hepatitis C virus. *Journal of Virology*, *84*(19), 10159–10168. https://doi.org/10.1128/JVI.01180-10

Wang, L., Jeng, K.-S., & Lai, M. M. C. (2011). Poly©-binding protein 2 interacts with sequences required for viral replication in the hepatitis C virus (HCV) 5‘ untranslated region and directs HCV RNA replication through circularizing the viral genome. *Journal of Virology*, *85*(16), 7954–7964. https://doi.org/10.1128/JVI.00339-11

Wang, Q. M., Hockman, M. A., Staschke, K., Johnson, R. B., Case, K. A., Lu, J., Parsons, S., Zhang, F., Rathnachalam, R., Kirkegaard, K., & Colacino, J. M. (2002). Oligomerization and cooperative RNA synthesis activity of hepatitis C virus RNA-dependent RNA polymerase. *Journal of Virology*, *76*(8), 3865–3872. https://doi.org/10.1128/jvi.76.8.3865-3872.2002

Weinlich, S., Hüttelmaier, S., Schierhorn, A., Behrens, S.-E., Ostareck-Lederer, A., & Ostareck, D. H. (2009). Igf2bp1 enhances HCV IRES-mediated translation initiation via the 3‘UTR. *RNA (New York, N.Y.)*, *15*(8), 1528–1542. https://doi.org/10.1261/rna.1578409

Wolff, G., Melia, C. E., Snijder, E. J., & Bárcena, M. (2020). Double-Membrane Vesicles as Platforms for Viral Replication. *Trends in Microbiology*, *28*(12), 1022–1033. https://doi.org/10.1016/j.tim.2020.05.009

WHO, Global Hepatitis report, 2024. https://www.who.int/publications/i/item/9789240091672

Yuasa, T., Ishikawa, G., Manabe, S., Sekiguchi, S., Takeuchi, K., & Miyamura, T. (1991). The particle size of hepatitis C virus estimated by filtration through microporous regenerated cellulose fibre. *The Journal of general virology*, *72 (Pt 8)*, 2021–2024. https://doi.org/10.1099/0022-1317-72-8-2021

8. Supplementary Figures

Supplementary Figure 2.1. Map of Plasmid **T7_hp_Fluc**, generated using SnapGene software.

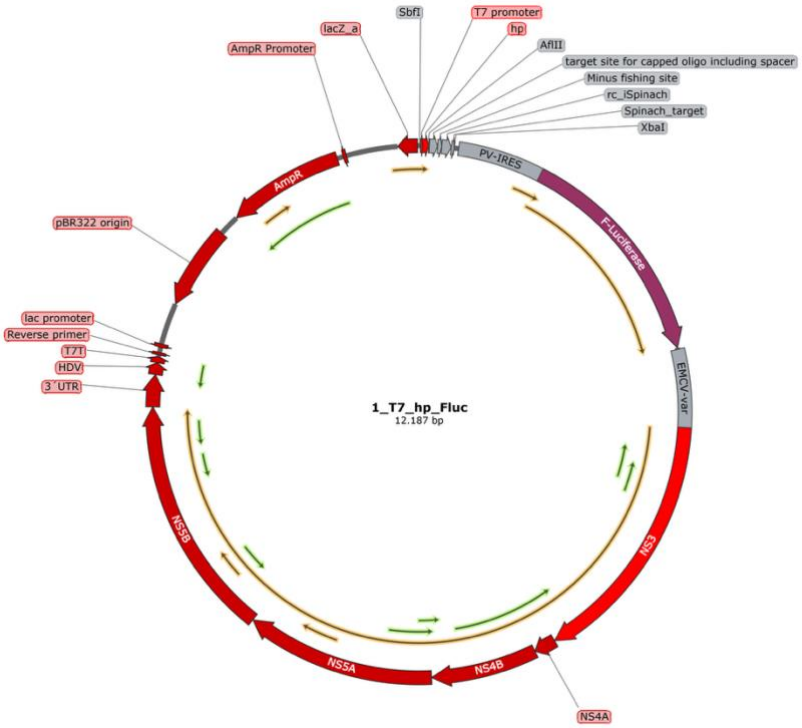

Features with Description	Start - Stop
T7 Promoter	14 -30 (17 bp)
hp (hairpin)	31 -71 (41 bp)
AflII-target site for capped oligo including spacer	72 – 137 (66 bp)
Minus fishing site (planed for primer binding specifically for minus-strand RNA detection)	138 – 167 (30 bp)
Rc_iSpinach (Reverse complement of Spinach RNA aptamer)	168 – 236 (69 bp)
Spinach_target (for minus-strand primer binding)	237 – 259 (23 bp)
PV-IRES (picorna virus internal ribosomal entry site)	292 – 917 (626 bp)
F-Luciferase (*Firefly* luciferase)	918 – 2576 (1659 bp)
EMCV-var (Encephalomyocarditis virus IRES)	2590 – 3161 (572 bp)
NS3 (wild-type NS3 coding region)	3162 – 5057 (1896 bp)
NS4A (wild-type NS4A coding region)	5058 – 5219 (162 bp)
NS4B (wild-type NS4B coding region)	5220 – 6002 (783 bp)
NS5A (wild-type NS5A coding region)	6003 – 7400 (1398 bp)
NS5B (wild-type NS5B coding region)	7401 – 9176 (1776 bp)
3´UTR (HCV 3´ untranslated region)	9177 – 9412 (236 bp)
HDV (Hepatitis D virus ribozyme)	9413 – 9499 (87 bp)
T7T (T7 RNA Polymerase Terminator)	9500 – 9546 (47 bp)
PBR322 origin	9949 – 10,568 (620 bp)
AmpR (Ampicillin resistance gene)	10,723 – 11,583 (861 bp)

Features in grey letters represent similar sequence that are similar in all plasmids, with only the start and stop positions shifted forward according to the changing 5-sequence (shown in black letters).

Supplementary Figure 2.2. Map of Plasmid **T7_SLI-II_Fluc**, generated using SnapGene software.

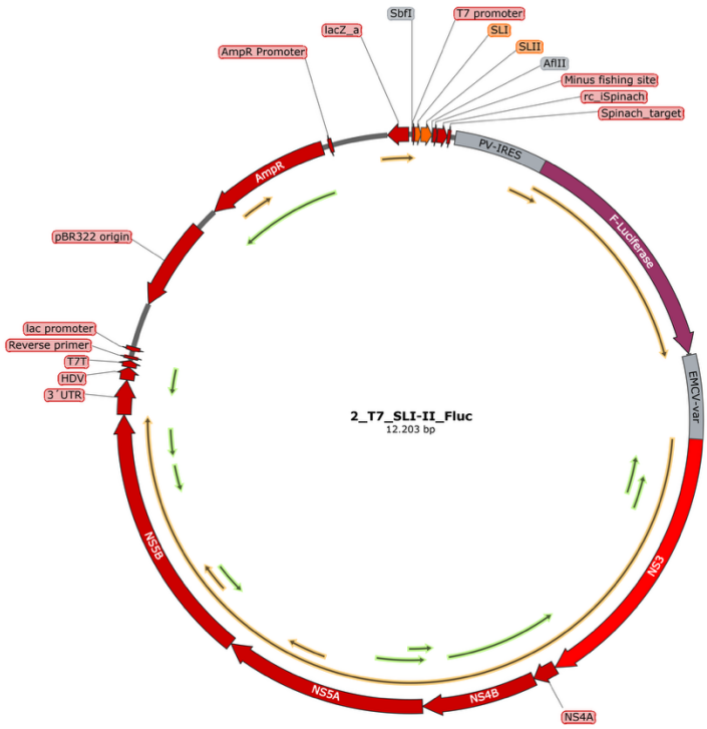

Features with Description	Start - Stop
T7 Promoter	14 -30 (17 bp)
SL-I (Stem loop I)	31 -72 (42 bp)
SL-II (Stem loop II)	73 – 147 (75 bp)

Other features that are similar in all plasmids are shown in grey in Plasmid 2.1

Supplementary Figure 2.3. Map of Plasmid **T7_SLI-III_Fluc**, generated using SnapGene software.

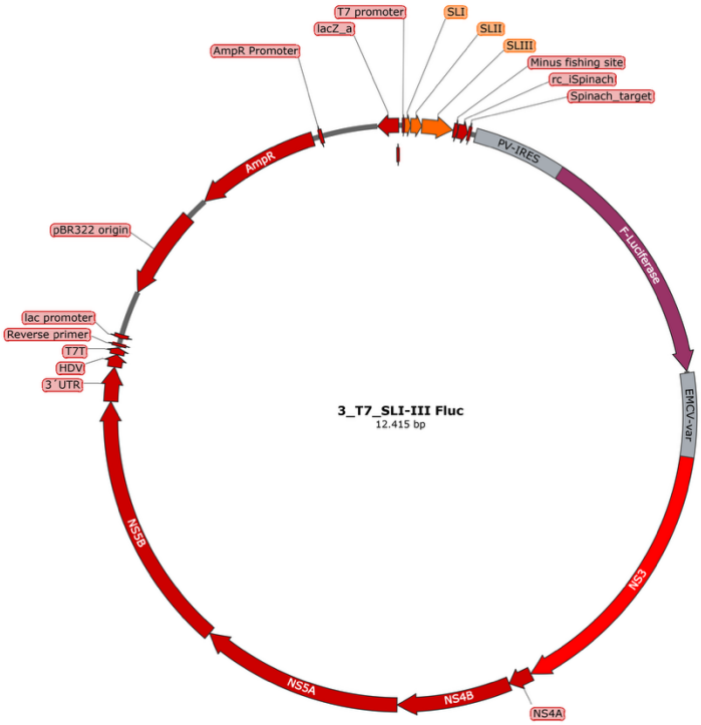

Features with Description	Start - Stop
T7 Promoter	14 -30 (17 bp)
SL-I (Stem loop I)	31 -72 (42 bp)
SL-II (Stem loop II)	73 – 147 (75 bp)
SL-III (Stem loop III)	148 – 359 (212 bp)

Other features that are similar in all plasmids are shown in grey in Plasmid 2.1.

Supplementary Figure 2.4. Map of Plasmid **T7_SLI-III_ΔIIIb_Fluc**, generated using SnapGene software.

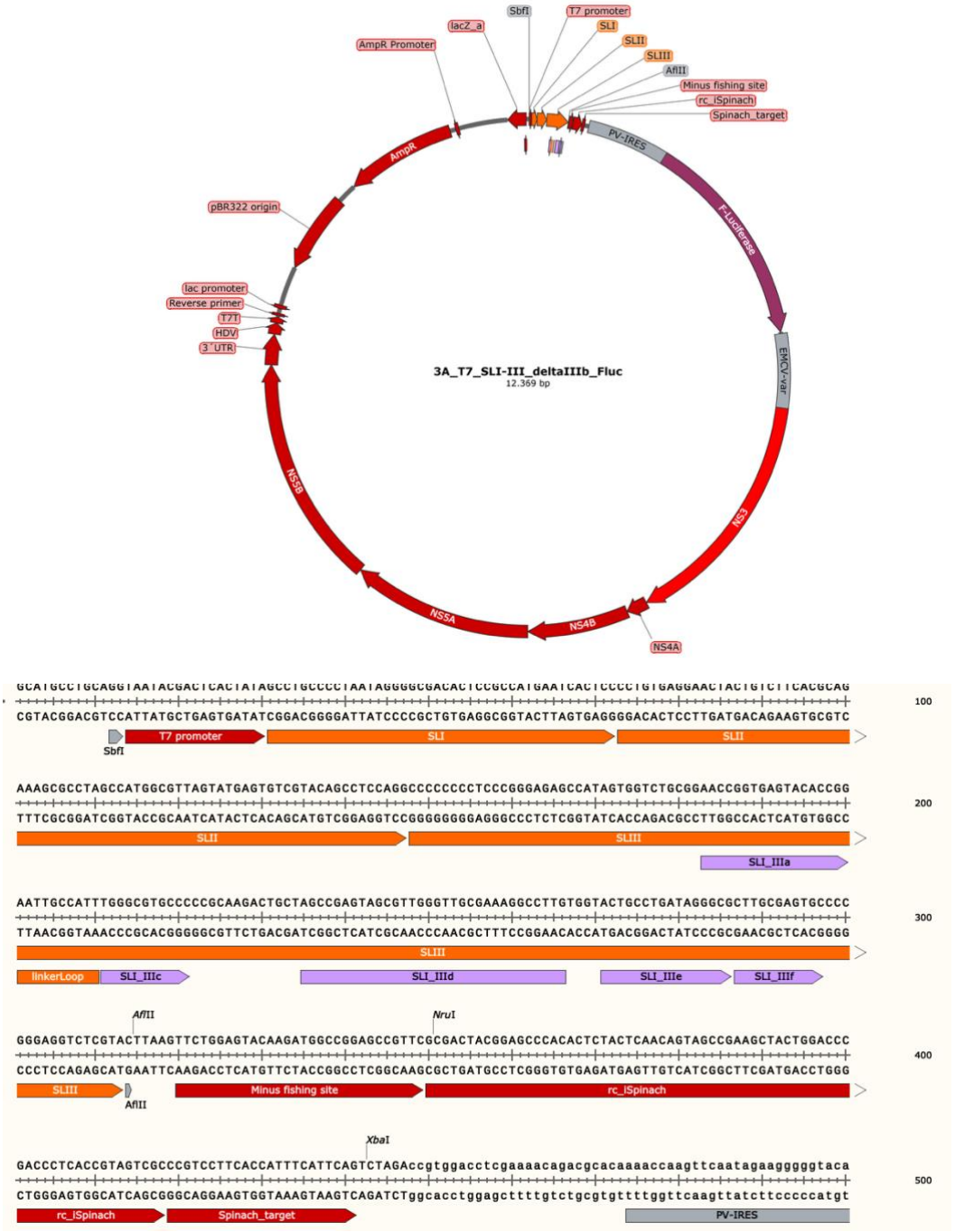

Features with Description	Start - Stop
T7 Promoter	14 -30 (17 bp)
SL-I (Stem loop I)	31 -72 (42 bp)
SL-II (Stem loop II)	73 – 147 (75 bp)
SL-III ΔIIIb (Stem loop III with a linker loop instead of IIIb sequence)	148 – 313 (166 bp)

Other features that are similar in all plasmids are shown in grey in Plasmid 2.1.

Supplementary Figure 2.5. Map of Plasmid **T7_SLI-III_mutIIId/ IIIe_Fluc**, generated using SnapGene software.

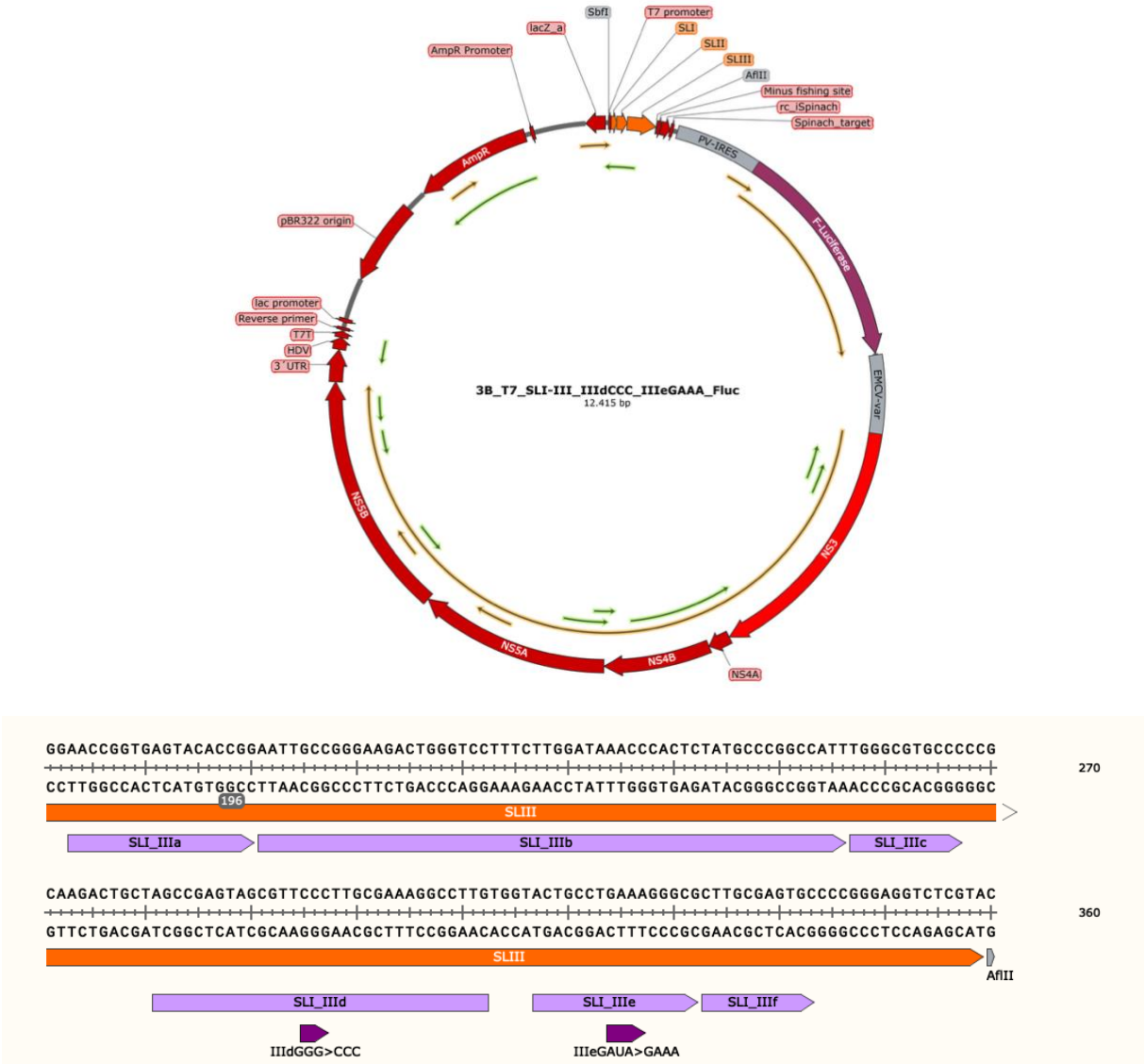

Features with Description	Start - Stop
T7 Promoter	14 -30 (17 bp)
SL-I (Stem loop I)	31 -72 (42 bp)
SL-II (Stem loop II)	73 – 147 (75 bp)
SL-III mutIIId/ IIIe (Stem loop III with mutated IIId and IIIe sequence)	148 – 359 (212 bp)

Other features that are similar in all plasmids are shown in grey in Plasmid 2.1.

Supplementary Figure 2.6. Map of Plasmid **T7_5UTR_core_3xHiBiT_Fluc**, generated using SnapGene software.

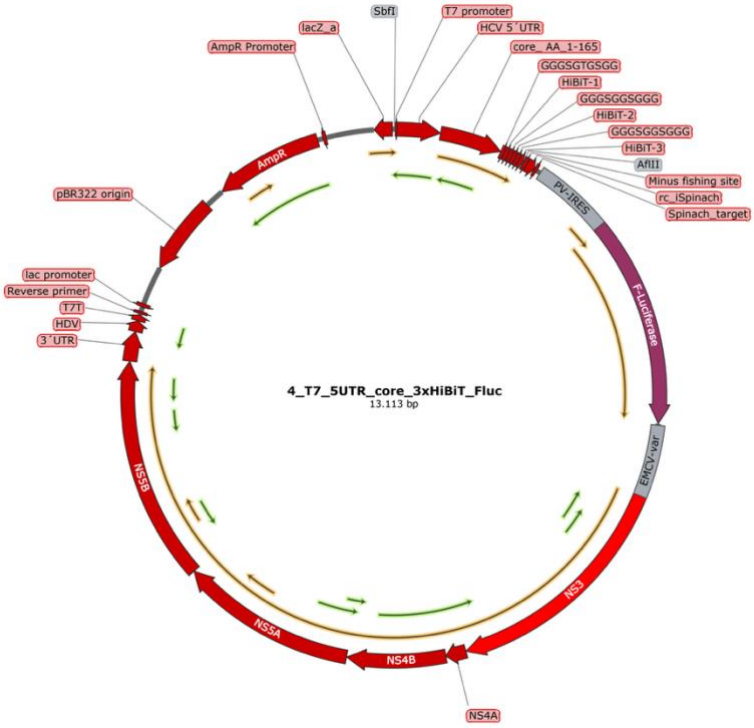

Features with Description	Start - Stop
T7 Promoter	14 -30 (17 bp)
5´UTR (HCV complete 5´ untranslated region)	31 -370 (340 bp)
Core (HCV core sequence 1 – 165 AA)	371 – 865 (495 bp)
3x HiBiT with GGGSGTGSGG linkers	866 – 1054 (189 bp)

Other features that are similar in all plasmids are shown in grey in Plasmid 2.1

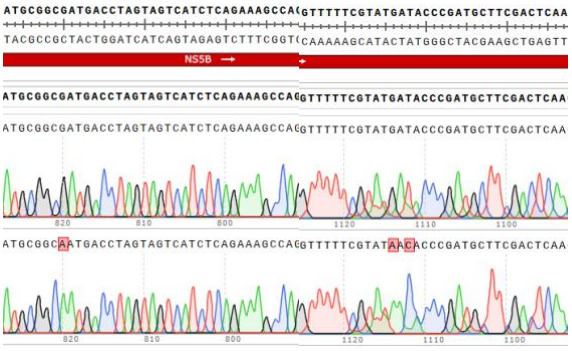

Substitution of G < A and GAT to AAC, indicating D318N and D220N, respectively, in the negative control NGND.

Supplementary Figure 2.7. Map of Plasmid **T7_5´UTR_ΔIIIb_Fluc**, generated using SnapGene software.

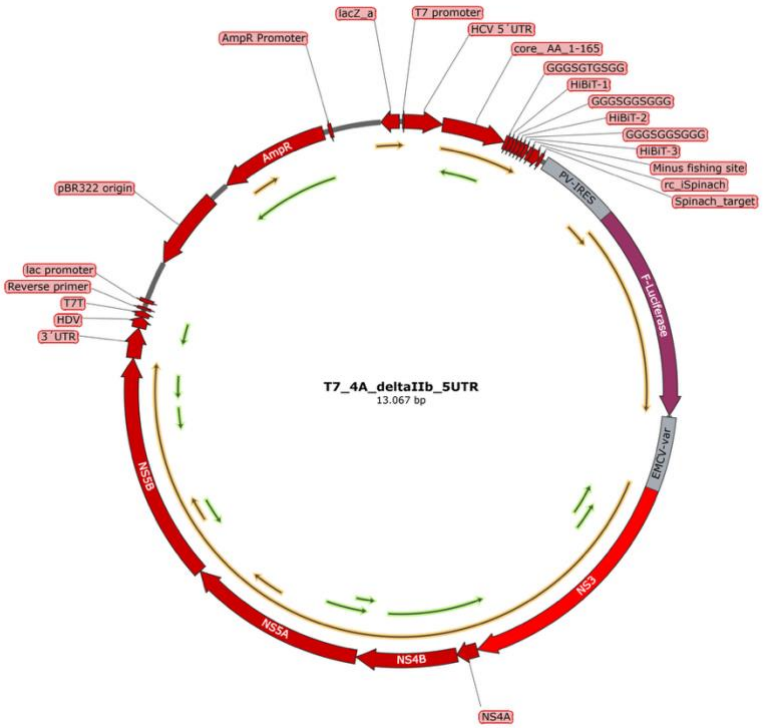

Features with Description	Start - Stop
T7 Promoter	14 -30 (17 bp)
5´UTR ΔIIIb (HCV 5´ untranslated region with linker instead of IIIb), similar as shown in SLI-III ΔIIIb	31 -325 (294 bp)
Core (HCV core sequence 1 – 165 AA)	326 – 821 (495 bp)
3x HiBiT with GGGSGTGSGG linkers	822 – 1011 (189 bp)

Other features that are similar in all plasmids are shown in grey in Plasmid 2.1.

Supplementary Figure 2.8. Map of Plasmid **T7_5´UTR_mutIIId/e_Fluc**, generated using SnapGene software.

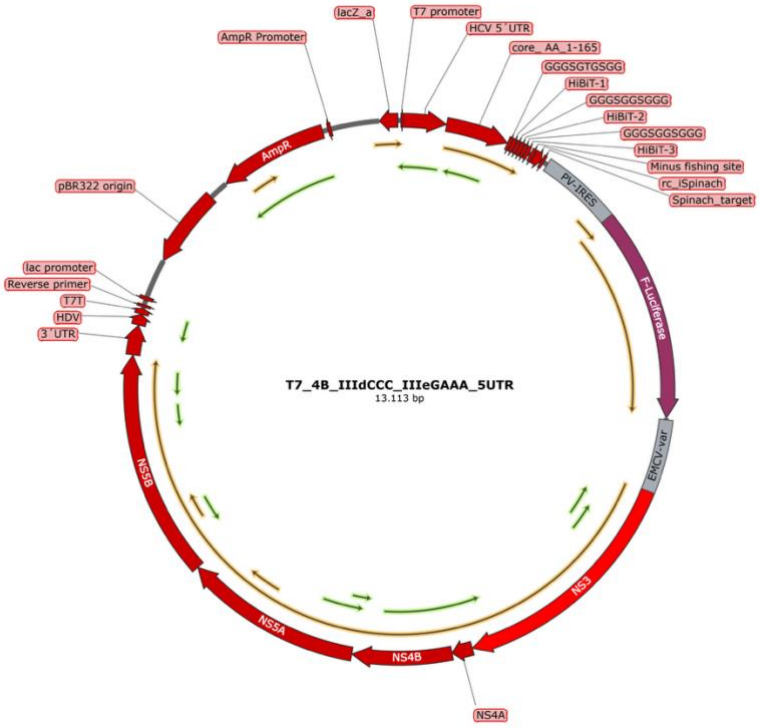

Features with Description	Start - Stop
T7 Promoter	14 -30 (17 bp)
5´UTR mutIIId/e (HCV 5´ untranslated region with mutated IIId and IIIe) similar as shown in SLI-III mutIIId/e	31 -370 (340 bp)
Core (HCV core sequence 1 – 165 AA)	371 – 865 (495 bp)
3x HiBiT with GGGSGTGSGG linkers	866 – 1054 (189 bp)

Other features that are similar in all plasmids are shown in grey in Plasmid 2.1.

Supplementary Figure 2.9. Map of Plasmid **3rd_gen-ins-2nd_gen_BB-SbfI_BbvCI (core-HiBiT)**, generated using SnapGene software.

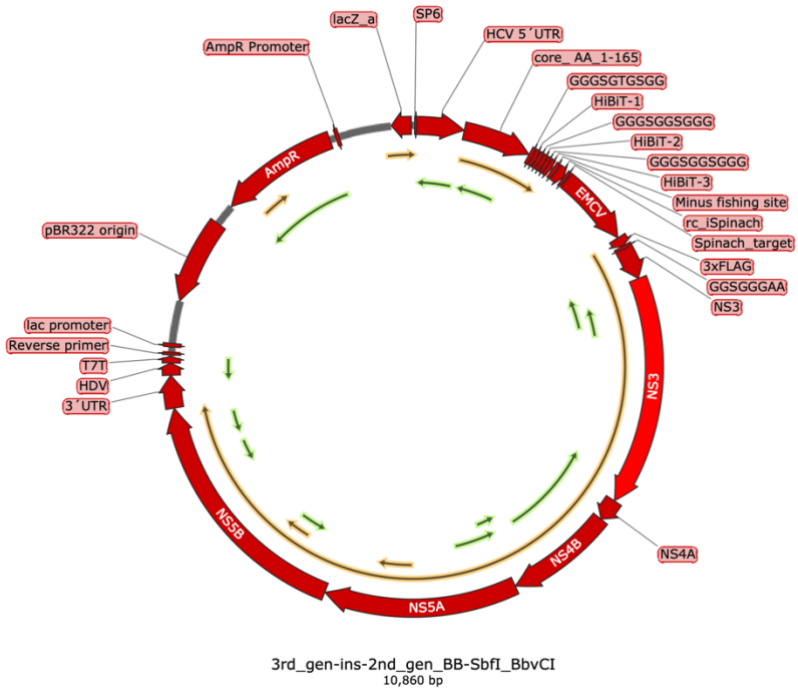

Features with Description	Start - Stop
SP6 Promoter	14 -30 (17 bp)
5'UTR mutIIId/e (HCV 5 untranslated region with mutated IIId and IIIe) similar as shown in SLI-III mutIIId/e	31 -370 (340 bp)
Core (HCV core sequence 1 – 165 AA)	371 – 865 (495 bp)
3x HiBiT with GGGSGTGSGG linkers	866 – 1054 (189 bp)
Minus fishing site (planed for primer binding specifically for minus-strand RNA detection)	1064 – 1093 (30 bp)
Rc_iSpinach (Reverse complement of Spinach RNA aptamer)	1094 – 1162 (69 bp)
EMCV-IRES (Encephalomyocarditis virus IRES)	1192– 1744 (572 bp)
3x Flag and GGSGGGAA linker	1745 – 1837 (93 bp)
NS3 (wild-type NS3 coding region)	1838 – 3730 (1893 bp)
NS4A (wild-type NS4A coding region)	3731 – 3892 (162 bp)
NS4B (wild-type NS4B coding region)	3893 – 4675 (783 bp)
NS5A (wild-type NS5A coding region)	4676 – 6073 (1398 bp)
NS5B (wild-type NS5B coding region)	6078 – 7849 (1776 bp)
3'UTR (HCV 3' untranslated region)	7850 – 8085 (236 bp)
HDV (Hepatitis D virus ribozyme)	8086 – 8172 (87 bp)
T7T (T7 RNA Polymerase Terminator)	8173 - 8219 (47 bp)
PBR322 origin	8622 – 9241 (620 bp)
AmpR (Ampicillin resistance gene)	9396 – 10,256 (861 bp)

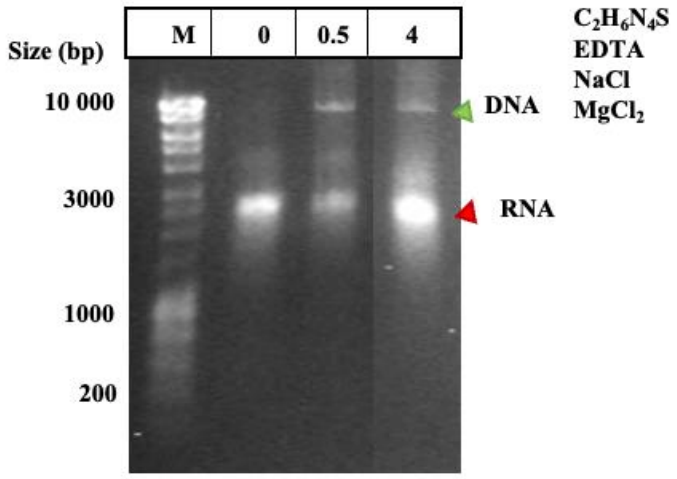

Supplementary Figure 3.1.1. Detection of plasmid DNA contamination in RNA samples generated by *in vitro*-transcription. RNA Purification was performed using acid phenol-chloroform extraction (pH ~ 4.5) in the presence of sodium isothiocyanate (0.5 and 4 M), followed by ethanol precipitation. Approximately 500 ng of RNA was visualized on 0.8 % agarose gel. The presence of salts in the sample caused the plasmid DNA to transfer into the aqueous phase, reducing RNA purity and potentially affecting the quality of RNA prepared for the following transfection.

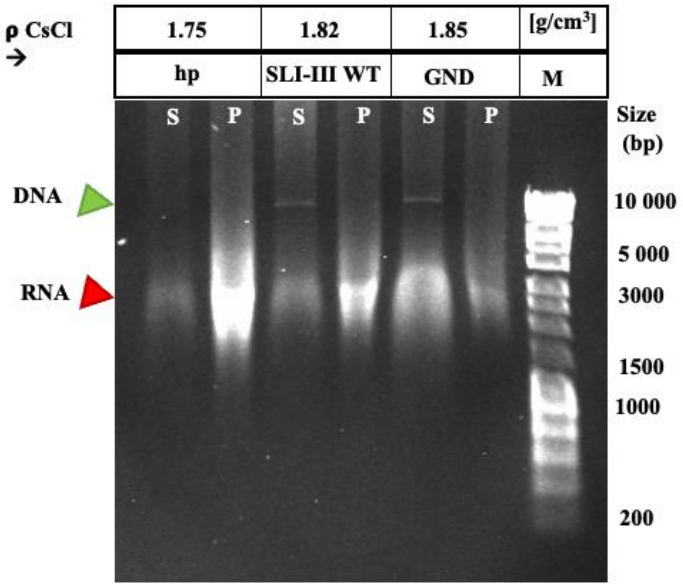

Supplementary Figure 3.1.2. Representation of the RNA purification quality isolated using CsCl purification method. RNA synthesized by *in vitro*-transcription was purified using CsCl cushions with densities of 1.75, 1.82 and 1.85 g/cm^3 via ultracentrifugation for 18 – 20 hrs. The resulting RNA pellet was dissolved in DNase-/RNase-free H_2O. To remove residual high salt content, the RNA solution was subjected to repeated ethanol-precipitation including 3x washes with 70% ethanol. Approximately 700 ng of RNA was visualized on 0.8 % agarose gel. "P" denotes the pellet obtained after ultracentrifugation, while "S" represents the supernatant collected after removing the CsCl layer. This purification method resulted in significant RNA degradation, as evident from the gel image.

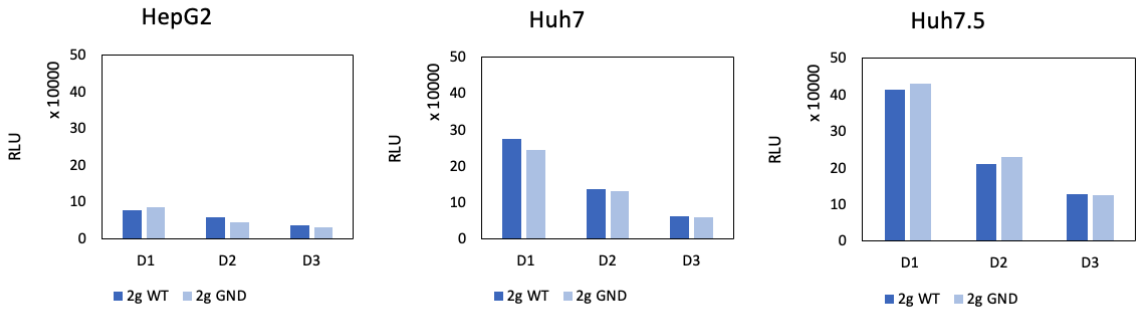

Supplementary Figure 3.1.3. Representation of HiBiT-expression in different hepatocyte cell lines over time. Equal amounts of 2nd generation replicon RNA were transfected to HepG2, Huh-7 and Huh-7.5 cells. Expression of HiBiT-tagged NS3 was monitored form Day 1 to Day 3 (D1, D2 and D3). Among the tested cell lines, Huh-7.5 exhibited the highest levels of protein expression and was therefore selected for all assays during this study.

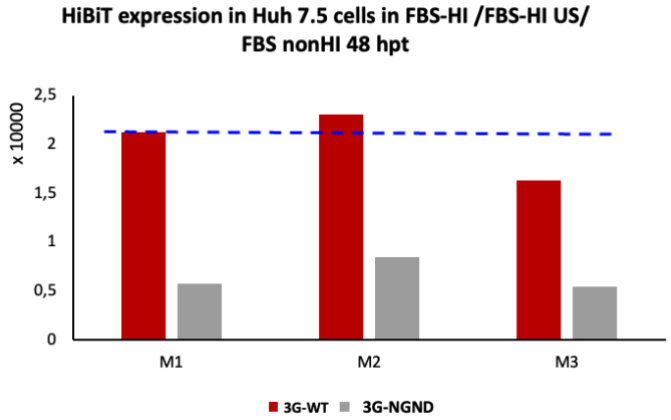

Supplementary Figure 3.1.4. HiBiT-expression in Huh-7.5 cells cultured with different fetal-bovine-sera (FBS). Huh-7.5 cells were cultured in three media conditions: M1 – DMEM + heat-inactivated FBS (Brazil origin); M2 – DMEM + heat-inactivated FBS (US origin); M3 – DMEM + non-heat-inactivated FBS (Brazil origin). Equal amounts of 3rd generation replicon RNA were transfected into cells in each condition. HiBiT-tagged NS3 was quantified at 48 hpt. Red bars represent 3rd generation replicon RNA wild-type (WT) and grey bars represent negative control (GND). Cells cultured in M2 exhibited the highest expression, leading to the selection of US-origin heat-inactivated FBS for general cell culture throughout this study.

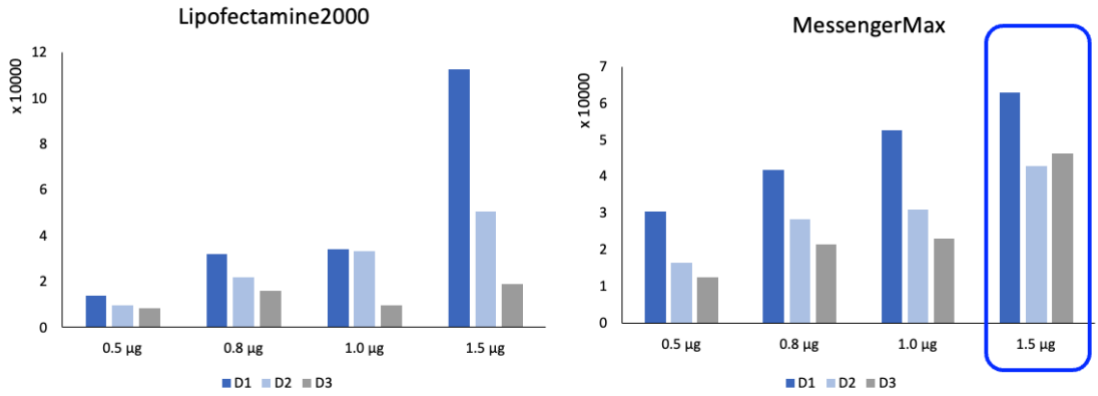

Supplementary Figure 3.1.5. Minimum amount of replicon RNA with appropriate transfection reagent required to exhibit an increase in HiBiT-expression level over time. Huh-7.5 cells were transfected with 0.5, 0.8, 1.0 and 1.5 µg of replicon RNA using two different transfection reagents: Lipofectamine 2000 and MessengerMax. HiBiT expression was measured at Day 1, Day 2 and Day 3 (D1, D2 and D3). A dose of 1.5 µg was identified as the minimum amount required to show a detectable increase in HiBiT expression on Day 3, when transfected with MessengerMax.

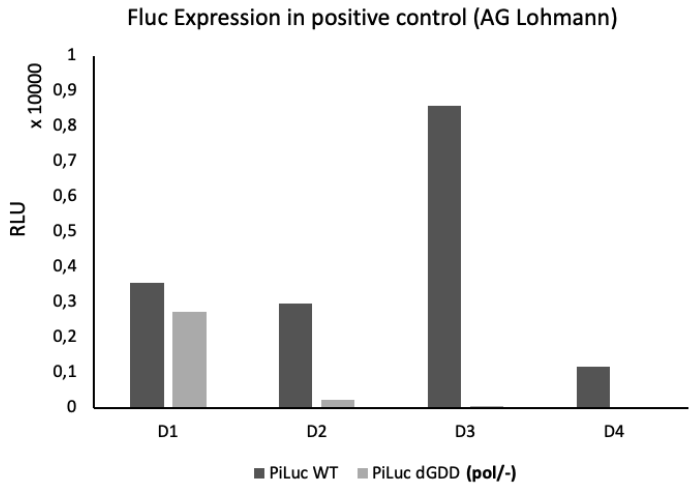

Supplementary Figure 3.1.6. *Firefly*-luciferase expression in positive control (AG Lohmann) over time. Huh-7.5 were cultured with heat-inactivated FBS (origin: US), transfected with 2.5 µg of replicon RNA (positive control kindly provided by AG Lohmann) using MessengerMax. Fluc-expression peaked on Day 3 (72 hpt), confirming the validity of all experimental conditions.

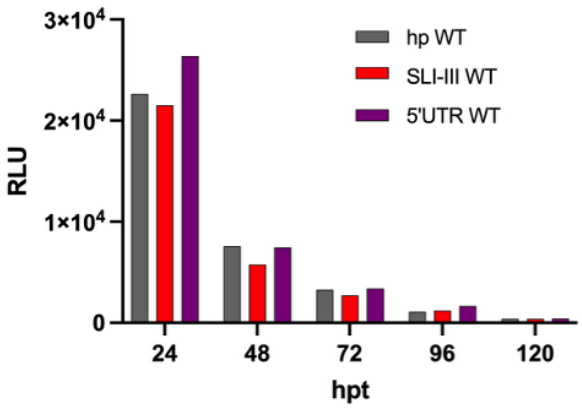

Supplementary Figure 3.1.7. *Firefly* luciferase expression in Huh-7.5 cells over time using a smaller version of 4th generation replicon RNA. Approximately 4700 nt form 5´end of 4th generation replicon RNA was generated by in-vitro transcription and transfected into Huh-7.5 cells. FLuc-expression was detectable up to 120 hpt, indicating that input RNA remains stable inside the cells for an extended period. The presence of input RNA may correlate with nascent RNA, overestimating the RT-qPCR signals and thereby distorting actual results.

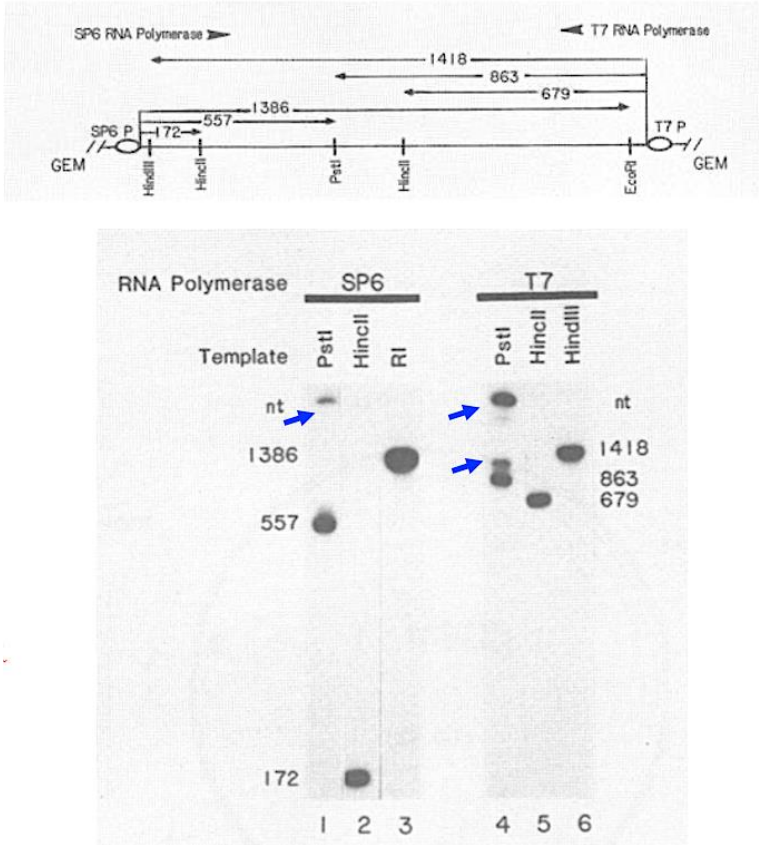

Supplementary Figure 3.2.1. SP6 polymerase generates significantly fewer RNA byproducts during *in vitro*-transcription compared to T7 polymerase. Template DNA used for RNA synthesis was restricted using the restriction enzyme Pst1, which leaves 3´-overhang. This overhang may lead to copy-back transcription and subsequent RNA byproduct formation (indicated with blue arrows on the gel image). However, the extent of byproduct-synthesis is significantly lower when *in vitro*-transcription is performed using SP6 polymerase as compared to T7 polymerase (Schenborn et al., 1985)

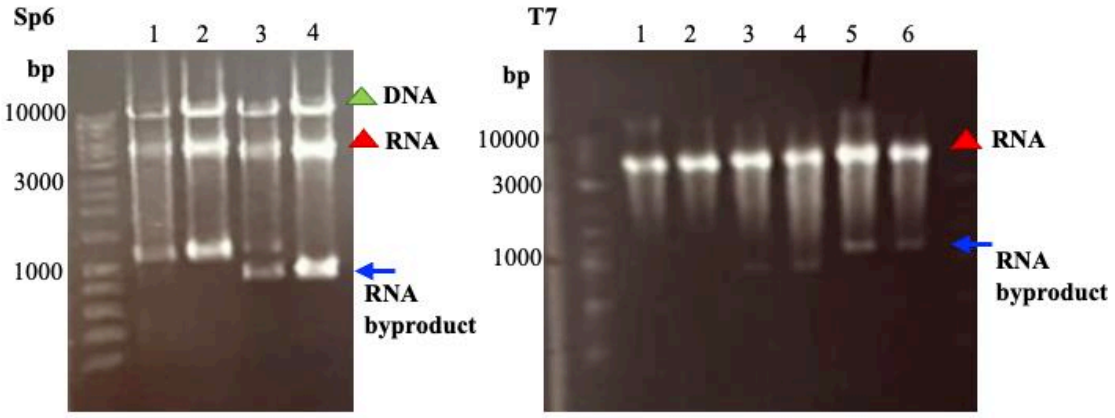

Supplementary Figure 3.2.2. SP6 polymerase produces significantly lower RNA yield and similar levels of RNA byproducts during *in vitro*-transcription of ~ 12,000 nt RNA. *In vitro*-transcription was performed using SP6 polymerase to synthesize RNA of ~ 12,000 nt in length. Approximately 500 ng RNA was visualized on 0.8 % agarose gel. The gel image (left) shows equal amounts of desired RNA and RNA byproducts. When SP6-promoter was replaced by T7 and *in vitro*-transcription was performed using the same protocol, a significant increase in the yield of desired RNA was observed (right).

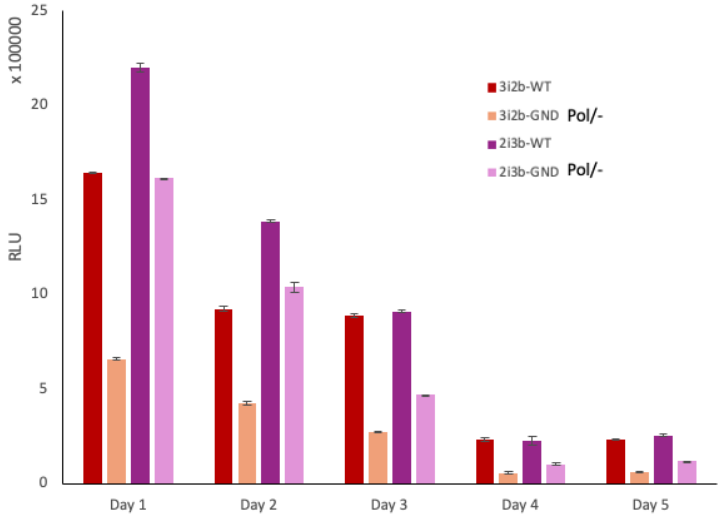

Supplementary Figure 3.2.3. HiBiT expression over time in 3rd generation and 2nd generation replicon system. Huh-7.5 cells were transfected with 0.8 to 1.0 µg of replicon RNA, either 3rd generation or 2nd generation, along with the corresponding negative controls. Expression of HiBiT-tagged core (3rd generation) and HiBiT-tagged NS3 were monitored over time, as an indirect indicator for replication. No increase in protein-expression was detected up to 120 hpt.

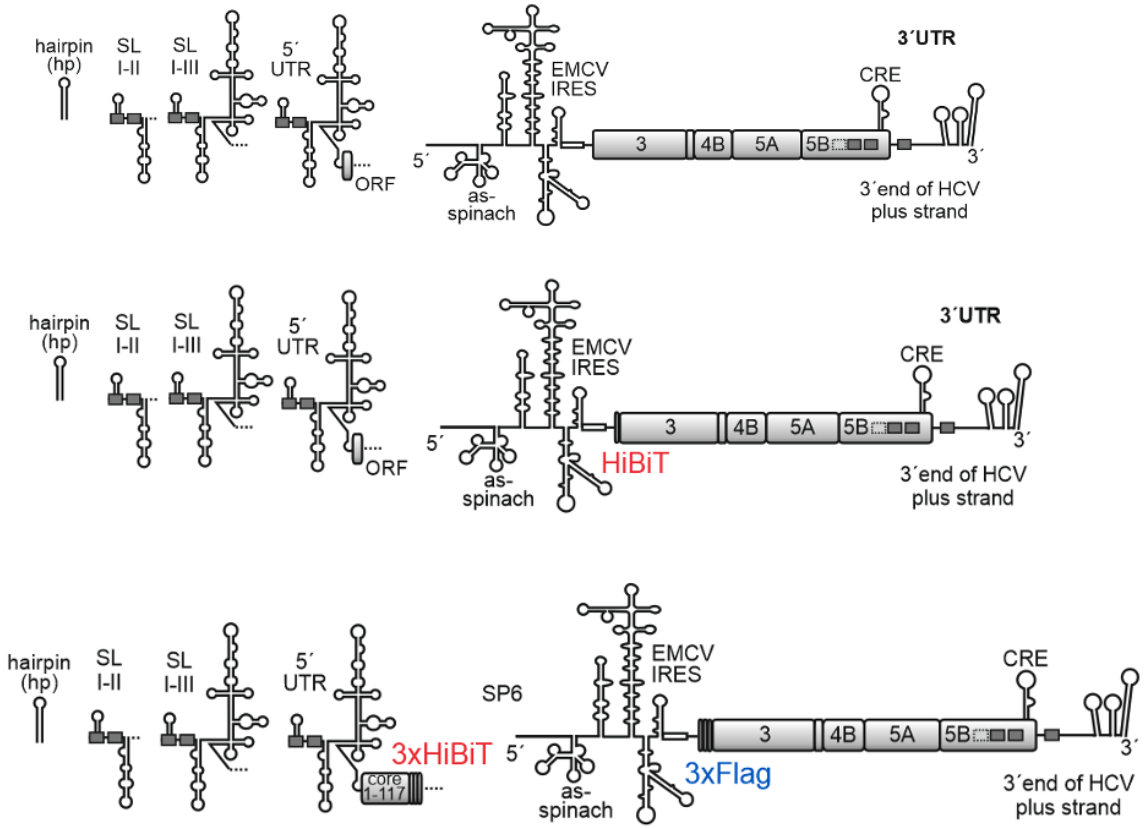

Supplementary Figure 3.2.4. Schematic representation of replicon systems along with the 5´UTR variants used in previous studies (1st and 2nd generation: upper and middle panels, respectively) and in the current study (3rd generation: lower panel). The HiBiT-tagged NS3 in 2nd generation replicon and the 3x HiBiT-tagged core in 3rd generation replicon system enable quantitative measurement of translation in both systems. A 3x Flag was included for detection by western blot analysis.

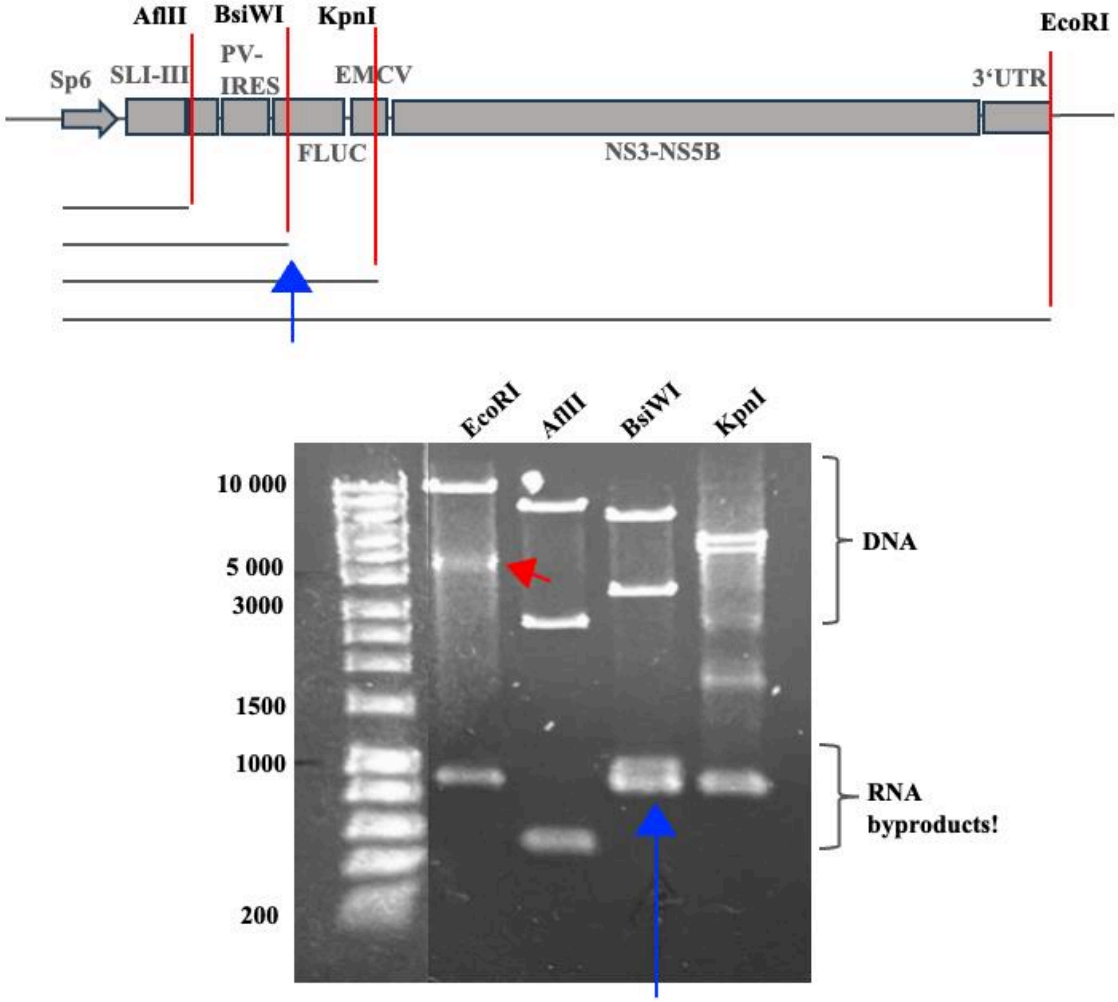

Supplementary Figure 3.2.5. Evidence of cryptic termination of SP6 polymerase at 3´-end of the PV-IRES resulting in RNA byproduct formation during *in vitro*-transcription. Template DNA corresponding to 4th generation replicon RNA with SP6 promoter was linearized with EcoRI. The linearized template DNA was further restricted using three different restriction enzymes: AflII, BsiWI and KpnI, as depicted in the schematic representation (top). *In vitro*-transcription was performed using SP6 RNA polymerase with the restricted DNA templates. The resulting RNA products were visualized on 0.8 % agarose gel. Linearization with EcoRI produced two RNA species: the upper band (indicated by the red arrow) corresponds to the expected full-length transcript, while the lower band represents a smaller RNA byproduct. In contrast, AflII-restricted template DNA yielded a single RNA product, which did not match the size of the byproduct observed with the EcoRI-linearized template. Notably, transcription from the BsiWI-restricted template generated two RNA species of slightly different sizes, the upper band represents the corresponding RNA product, whereas the lower band (indicated by the blue arrow) represents the RNA byproduct similar in size to that seen with EcoRI. These results suggest a potential cryptic termination site for SP6 polymerase located near the 3´-end of PV-IRES.

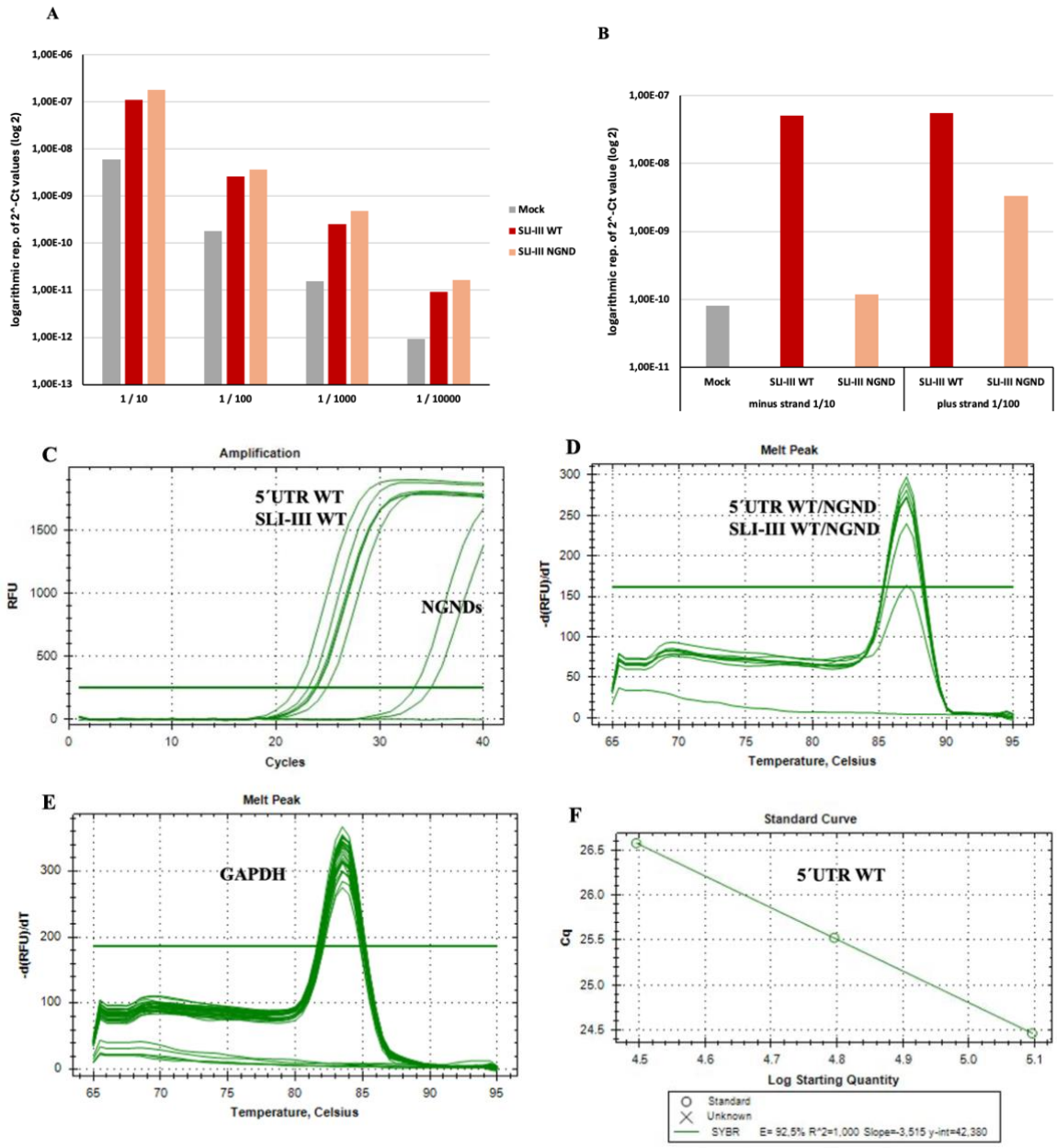

Supplementary Figure 3.2.6. Representation of RT-qPCR Results obtained from optimization experiments assessing sample dilution, primer dilution as well as primer specificity, using the complete 5´UTR and SLI-III wild-type constructs as positive controls and the corresponding NGNDs as negative controls. **(A)** Sample dilution series using 1/10, 1/100, 1/1000 and 1/10.000 dilutions of cDNA for positive-strand analysis. **(B)** Results showing comparable cDNA dilutions of 5EU-labelled negative-strand RNA abundance and non-5EU-labelled positive-strand RNA abundance during strand-specific detection, indicating that a 1/10 dilution of 5EU-labelled negative-stand RNA was comparable to a 1/100 dilution of non-5EU-labelled positive-strand RNA. **(C)** RT-qPCR curves exhibiting negative-strand abundance in biological replicates of 5´UTR and SLI-III wild-type samples, together with their corresponding negative controls (NGNDs). **(D)** Melting curves corresponding to the samples shown in (C). **(E)** Melting curves corresponding to GAPDH for all samples used in this study. **(F)** Standard curve analysis of the 5´UTR WT using tagged RT-qPCR primers for negative-strand RNA detection, measured and calculated by Mozhdeh Khajouei.

VIII. Publications, Poster presentations, Conferences and supported Thesis Projects

Publication 02.04.2026 (International Journal of Molecular Sciences)

Attiya Qadoos Malik, Lyudmila Shalamova, Mozhdeh Khajouei, Jonas Budnik, Anna-Lena Hell, Elena Jost, Gesche K. Gerresheim, Oliver Rossbach, **Michael Niepmann**. **Hepatitis C Virus 5´UTR sequences that bind eIF3 and ribosomal 40S subunits confer stimulation of negative strand RNA synthesis.**

Malik, A.Q.; Shalamova, L.; Khajouei, M.; Budnik, J.; Hell, A.-L.; Jost, E.; Gerresheim, G.K.; Rossbach, O.; Niepmann, M. Hepatitis C Virus 5'UTR Sequences That Bind eIF3 and Ribosomal 40S Subunits Confer Stimulation of Minus-Strand RNA Synthesis. *Int. J. Mol. Sci.* **2026**, *27*, 3234. https://doi.org/10.3390/ijms27073234

Poster Presentation

25 – 28.03.2024	33rd Annual Meeting of the Society of Virology, Gesellschaft für Virologie, Vienna, Austria (Together with Mozhdeh Khajouei) "Investigation of the molecular mechanisms of the lnc-ITM2C-GPR55_ISG regulation axis"
01 - 04.10.2023	29th International Symposium on Hepatitis C Virus, Flaviviruses, and Related Viruses, Atlanta, USA (Together with Mozhdeh Khajouei) "Investigation of the molecular mechanisms of the lnc-ITM2C-GPR55_ISG regulation axis"

Conferences

25 – 28.09.2024	30th International Symposium on Hepatitis C Virus, Flaviviruses and related Viruses, Oxford, UK
25 – 28.03.2024	33rd Annual Meeting of the Society of Virology, Gesellschaft für Virologie, Vienna, Austria
01 - 04.10.2023	29th International Symposium on Hepatitis C Virus, Flaviviruses, and Related Viruses, Atlanta, USA
28 - 31.03.2023	32nd Annual Meeting of the Society of Virology, Gesellschaft für Virologie, Ulm
06 - 09.07.2022	28th International Symposium on Hepatitis C Virus, Flaviviruses and related viruses, Ghent, Belgien
30 - 31. 05.2022	TRR 179 International Symposium "Viral hepatitis and beyond: from basic science to cure", Freiburg

Supported Thesis Projects

MD Thesis Johanna Schneekloth
MD Thesis Ragna Weitz
MD Thesis Elena Jost
MD Thesis Michelle Tschassem Tagny

IX. Acknowledgments

I would like to sincerely thank **Prof. Dr. Michael Niepmann** for his kind and supportive supervision throughout this work. He was always willing to help by sharing his extensive experience, patiently explaining complex theoretical concepts, providing valuable advice to overcome experimental challenges, writing manuscript, arranging opportunities to attend SFB meetings as well as national and international conferences, and enabling communications with other research groups to support this project over the entire period. I would also like to express my sincere gratitude to **Prof. Lohmann** for his valuable advice and generous support, in particular for kindly providing the positive control, useful transfection protocols and the various cell lines used in this study.

I am also very grateful to all my wonderful lab colleagues for their help and support, and for sharing all the good and challenging experiences we went through together. Special thanks go to my colleague and friend **Mozhdeh Khajouei** for always being there and providing support in every possible way. I would also like to thank the colleagues from AG Borggrefe for generously allowing to use their apparatus and providing help whenever needed.

Furthermore, I would like to express my heartfelt thanks to my better half, **Suhail Malik**, and my daughter, **Dua Malik**, for their constant support and for making extra efforts to ease this challenging period. Very special thanks go to my dear friend **Shama Malik** for her moral support, motivation during difficult times, and for sharing all the ups and downs with genuine care. I am also deeply grateful to my parents and parents-in-law for their love, care, help and prayers.

Finally, I would like to thank **Justus Liebig University**, the **Deutsche Forschungsgemeinschaft (DFG)**, as well as **SFB 1021** for funding this project and for providing me with the opportunity to satisfy my curiosity and deepen my knowledge of virology. I am also grateful for the seminars organized and the opportunities provided to expand scientific research knowledge through interactions among different research groups. A big thank you to the entire staff of the Institute of Biochemistry for providing a friendly and supportive environment throughout the entire period of my work.

X. Versicherung der Eigenständigkeit

„Ich erkläre: Ich habe die vorgelegte Dissertation selbstständig und ohne unerlaubte fremde Hilfe und nur mit den Hilfen angefertigt, die ich in der Dissertation angegeben habe. Alle Textstellen, die wörtlich oder sinngemäß aus veröffentlichten Schriften entnommen sind, und alle Angaben, die auf mündlichen Auskünften beruhen, sind als solche kenntlich gemacht. Ich stimme einer evtl. Überprüfung meiner Dissertation durch eine Antiplagiat-Software zu. Bei den von mir durchgeführten und in der Dissertation erwähnten Untersuchungen habe ich die Grundsätze guter wissenschaftlicher Praxis, wie sie in der „Satzung der Justus-Liebig-Universität Gießen zur Sicherung guter wissenschaftlicher Praxis“ niedergelegt sind, eingehalten.“

Angaben zu auf künstlicher Intelligenz (KI) basierender Hilfen wie ChatGPT oder SchulKI von OpenAI oder Gemini von Google zur Erstellung meiner Dissertation (Zutreffendes angekreuzt):

☐ Ich habe bei der Erstellung dieses Textes kein KI-Tool verwendet.

☐ Ich habe ein KI-Tool in den folgenden Bereichen eingesetzt (Mehrfachnennungen möglich):

- ☐ Ideen finden, meine Kreativität anregen
- ☐ Verstehen von Konzepten, Recherche von Fakten und Definitionen
- ☐ Optimierung eines von mir verfassten Textes
- ☐ Erstellen ganzer Textpassagen nach meinen Vorgaben

Folgende KI-Tools habe ich verwendet, damit aufgeführte Teile meines Textes von dem Tool wie folgt profitiert haben:

Nachdem ich meine Texte selbst erstellt habe, habe ich zur vollständigen grammatikalischen Überprüfung den Rat von ChatGPT (auf Basis von GPT-5) eingeholt und diesen sehr selektiv angewendet.

Datum: _____ Unterschrift: _____

International Journal of
Molecular Sciences

MDPI

Article

Hepatitis C Virus 5′UTR Sequences That Bind eIF3 and Ribosomal 40S Subunits Confer Stimulation of Minus-Strand RNA Synthesis

Attiya Qadoos Malik [1], Lyudmila Shalamova [1,2], Mozhdeh Khajouei [1], Jonas Budnik [1,3], Anna-Lena Hell [1,4], Elena Jost [1,5], Gesche K. Gerresheim [1,6], Oliver Rossbach [7] and Michael Niepmann [1,*]

1 Institute of Biochemistry, Faculty of Medicine, Justus-Liebig-University, 35392 Giessen, Germany; qadoos@gmx.de (A.Q.M.); lyudmila.shalamova@vetmed.uni-giessen.de (L.S.); khajoueimozhdeh@gmail.com (M.K.); jonas.budnik@gmail.com (J.B.); anna-lenahell@gmx.de (A.-L.H.); jost.elena@web.de (E.J.); gesche.gerresheim@gmx.de (G.K.G.)
2 Institute for Virology, Faculty of Veterinary Medicine, Justus-Liebig-University, 35392 Giessen, Germany
3 Department of Anesthesiology, Intensive Care Medicine and Pain Therapy, University Hospital Giessen, Justus-Liebig-University, 35392 Giessen, Germany
4 Medical Faculty, RWTH Aachen University, 52074 Aachen, Germany
5 University Children's Hospital, University Medical Center Hamburg-Eppendorf, 20246 Hamburg, Germany
6 Institute for Virology, Philipps-University Marburg, 35043 Marburg, Germany
7 Institute of Biochemistry, Faculty of Biology and Chemistry, Justus-Liebig-University, Heinrich-Buff-Ring 17, 35392 Giessen, Germany; oliver.rossbach@chemie.bio.uni-giessen.de
* Correspondence: michael.niepmann@biochemie.med.uni-giessen.de

Abstract

Hepatitis C Virus (HCV) is a plus-strand RNA virus that replicates its genome via a minus-strand intermediate, which in turn is the template for the synthesis of progeny plus-strand genomes. In order to characterize sequence elements in the HCV 5′-untranslated region (5′UTR) that are possibly involved in the regulation of minus-strand RNA synthesis starting at the genome's 3′end, we used a replicon system in which a possible function of these sequences is uncoupled from other functions like translation regulation. For the specific detection by RT-qPCR of minus strands newly synthesized in the cells from the transfected replicon RNAs, we carefully eliminated the contaminating DNA and transfected RNA and avoided self-priming caused by hairpin formation. We found that the absence of any HCV sequences at the 5′end does not allow genome replication. Stem-loop I-II sequences only allow extremely low-level replication, whereas the presence of stem-loops I-III or the complete 5′UTR allows efficient replication. The mutation of sequences required for the binding of translation initiation factor 3 (eIF3) and the ribosomal 40S subunit in the 5′UTR of the plus strand severely impairs minus-strand synthesis. This suggests that eIF3 and the 40S subunit are involved in plus-strand 5′-3′-end communication and the regulation of minus-strand synthesis.

Keywords: plus-strand; positive-strand; negative-strand; replication; encapsidation; packaging

Academic Editor: Hirayuki Enomoto

Received: 26 February 2026
Revised: 26 March 2026
Accepted: 30 March 2026
Published: 2 April 2026

1. Introduction

HCV mainly infects liver cells and can cause liver cirrhosis and liver cancer. The genome of HCV is a plus-strand RNA of about 9600 bases [1,2] that replicates via a minus-strand antigenome [3–7]. The 5′end of the plus strand has no standard m^7G Cap but often contains an FAD Cap [8] as protection against exonucleases, and translation of the viral polyprotein is started by an Internal Ribosome Entry Site (IRES) element [9,10]. This

arrangement has the advantage that both extreme ends of the RNA genome (on the plus and on the minus strand) are available for replication-active RNA *cis*-signals. Several RNA secondary structures in the plus strand are involved in the regulation of viral RNA replication; these structures are located largely at the ends but also in the internal regions of the RNA genome [2,5,7,11–18]. To a minor extent, functional RNA secondary structures are also present at the end of the minus strand [2,16,19–24].

Replication of the HCV plus-strand RNA starts at the 3′end of the 3′UTR (Figure 1A), which has a very characteristic organization. The polyprotein stop codon is followed by a binding site for the liver-specific microRNA-122 (miR-122), a polyU/C tract and the highly conserved so-called 3′X region [25,26]. The 3′X region comes in two possible conformations, one containing three stem-loops (counted from the 3′end SL1, SL2 and SL3), or SL2 and SL3 can refold to form one longer stem-loop that is suspected to act as a dimer linkage sequence (DLS) for genome dimerization [5,27].

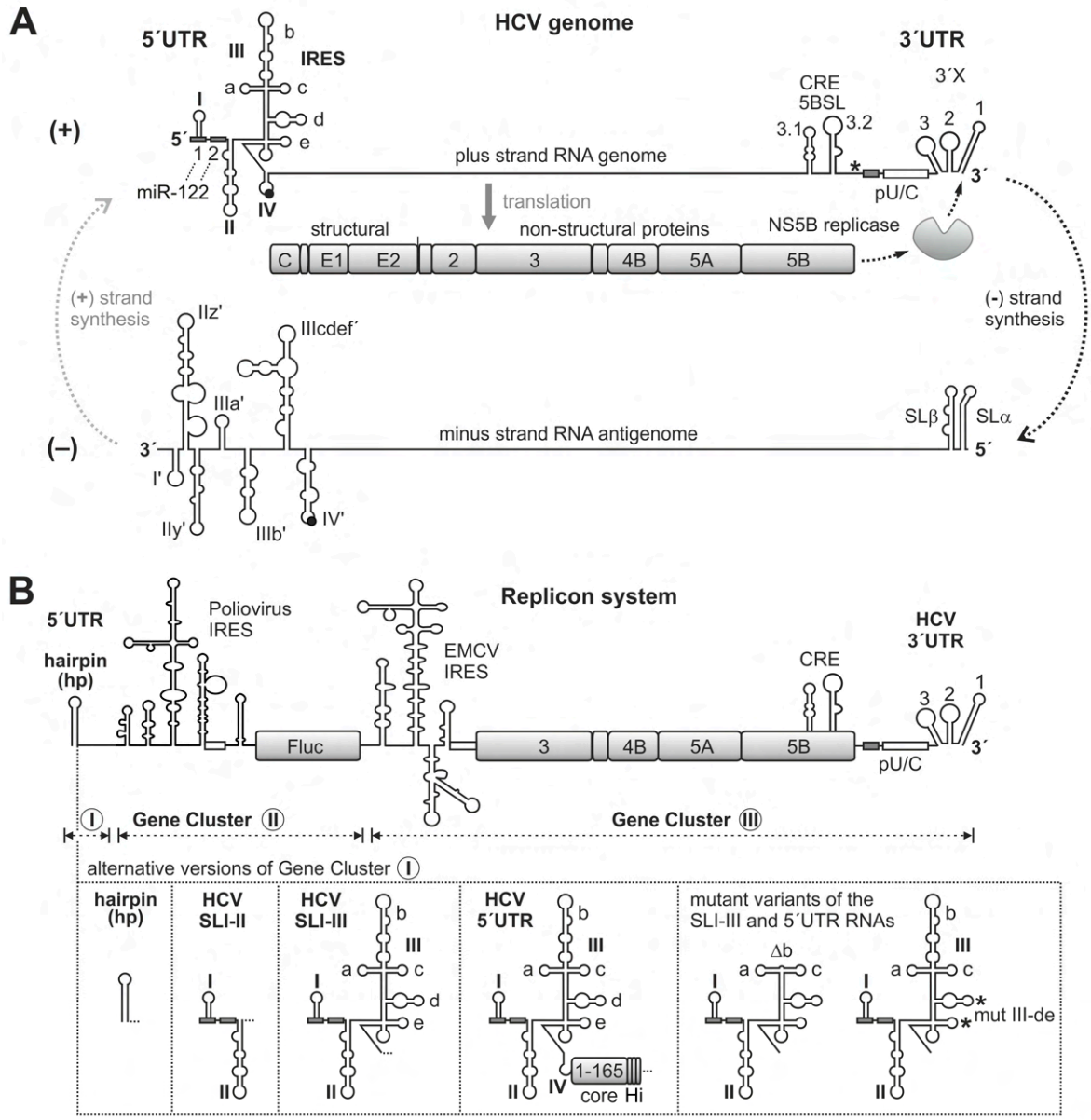

Figure 1. HCV genome replication and the replicon system. (**A**) The HCV plus (or "positive")-strand RNA genome with the 5′ untranslated region (5′UTR), the polyprotein coding sequence (CDS) and

the 3′UTR. In the 5′UTR, the RNA secondary structure stem-loops (SLs) II–IV constitute the internal ribosome entry site (IRES) element that starts the translation of the polyprotein at the AUG (black dot) in SLIV. The 3′UTR downstream of the CDS stop codon (*) contains a polyU/C-tract (pU/C) and conserved stem-loops at the end. Binding sites for microRNA-122 (miR-122) are indicated by gray boxes. The non-structural (NS) protein NS5B is the RNA-dependent RNA polymerase (RdRP or "replicase") that starts the synthesis of the minus (or "negative")-strand RNA at the 3′end of the plus strand. In the NS5B coding sequence, a *cis*-replication element (CRE) is required for replication. The minus strand has RNA secondary structures in its 5′- and 3′-regions that do not exactly mirror those in the plus strand due to different G-U base pairs. Progeny plus-strand RNA genomes are then replicated from the minus strand starting at its 3′end. (**B**) The HCV RNA replicon system contains three independent gene clusters (I, II and III). In Gene Cluster III, an Encephalomyocarditis Virus (EMCV) IRES drives expression of the NS3–NS5B proteins that are required for RNA genome replication, and the CRE and the HCV 3′UTR provide *cis* signals involved in the start of minus-strand RNA synthesis. In Gene Cluster II, the Poliovirus IRES drives the translation of an independent reporter, firefly luciferase (Fluc). At the 5′end of the replicon RNA, Gene Cluster I contains either a strong stem-loop ("hairpin") that protects the RNA against degradation, or various lengths of the HCV 5′UTR. In the complete 5′UTR version, the HCV IRES initiates the translation of the C-terminally truncated HCV Core protein with a triple HiBiT tag (Hi). In the SLI-III or complete 5′UTR versions of this Gene Cluster I, a deletion of SLIIIb (ΔIIIb) impairs the binding of eIF3, or mutation of SLs IIId and IIIe (*, mutIIId/e) impair the binding of the small ribosomal 40S subunit.

In addition to *cis*-elements in the 3′UTR, two RNA secondary structures upstream of the NS5B stop codon [2,7] are also required for replication. These comprise the so-called *cis*-replication element (CRE) with the 5BSL3.2 (also called SLV) and the upstream 5BSL3.1 (SLVI) [28,29]. The CRE is also involved in long-range RNA-RNA interactions (LRIs) with the 3′UTR and the 5′UTR [2,7,30,31]. The most prominent of these LRIs is the interaction of the apical loop of the CRE/5BSL3.2 with the SL2 of the 3′UTR, also called a "kissing-loop" interaction [32,33].

To start minus-strand synthesis, the NS5B replicase needs to bind to the HCV 3′UTR and start the synthesis of the minus strand [34]. In biochemical activity assays that come in a setting with reduced complexity, the start of RNA synthesis by NS5B can occur on the 3′end of a single-stranded RNA template. In this context, NS5B has a preference for GTP as a starter nucleotide [35,36]. After a slow initiation process with the incorporation of the first two or three nucleotides, beginning with the next nucleotide, the K_M for nucleotide incorporation drops sharply, indicating a transition from an inefficient initiation mode to an efficient elongation mode [35,37,38]. Thereby, the polymerase can also use the 3′-terminal U of the template to incorporate FAD as a starter nucleotide [8,39].

However, the interaction of the NS5B replicase with its genuine RNA template comes with several different aspects and appears rather complicated. The formation of the strong stem of SL1 at the very 3′end of the RNA genome (see Figure 1A) is highly conserved [2] and required for efficient replication. Mutations affecting this stem, including the mutation of the terminal U residue that can be involved in a G-U base pair, impair replication [13,40]. In in vitro assays in the absence other HCV replication protein functions, the 3′end of the plus strand is a much worse template for the NS5B polymerase than the 3′end of the minus strand [41]. Nevertheless, the replicase obviously needs to bind to the 3′-terminal SL1, and this stem must be unwound to allow NS5B to access the 3′end of the plus strand. In HCV replication complexes, the unwinding of SL1 likely takes place due to the helicase activity of NS3 [42]. Likely compensating for this inefficient template situation, the NS5B protein also binds to sequences in the upstream NS5B coding region. There, the CRE 5BSL3.2 and the 5BSL3.1 both bind NS5B [29,43], with a stronger contribution of 5BSL3.2 [29]. Also downstream of the stop codon, NS5B can bind to polyU and to the SL2 of the 3′X region [29,34,43,44]. Thereby, the affinity of the replicase to the RNA regions like the

5BSL3.2 or the polyU is higher than its affinity to the 3′X region [44,45], although the latter contains its genuine RNA synthesis start position.

Thus, the 3′end of the HCV plus-strand RNA genome is—on first glance—evolved to be a "difficult" template for its polymerase, since obviously melting the strong stem of SL1 is required in order to bind the very 3′terminal nucleotide of the template strand. Therefore, besides the contribution of the NS3 helicase function in melting the SL1 [42], the formation of dimers or oligomers by the NS5B protein [46–52] might support a multi-point interaction of NS5B with upstream RNA elements that stabilize NS5B binding to its genuine template. In this context, the pausing of two ribosomes with nearly completely folded NS5B proteins at the NS5B stop codon and on conserved slow codons directly upstream may support both NS5B dimerization and its search for the multiple binding sites on its own template RNA in *cis* [52,53]. This multi-point tethering of some NS5B molecules in the oligomer to higher-affinity binding sites may then allow another monomer of the NS5B oligomer to interact more transiently with the actual start site in *cis*. These more transient interactions with the actual start site may be required for an escape of the polymerase from the transcription start site and the transition from initiation to elongation ("promoter escape"). Finally, this whole complicated setting may serve to make the HCV 3′end available as a substrate only to the HCV replication machinery in *cis* and not to other (cellular) polymerases. In turn, this may ensure the specificity of the HCV replication machinery only for its genuine viral template.

Considering the polymerase starting RNA synthesis at the RNA genome's 3′end, two major aspects appear evident. On the one hand, a collision between ribosomes translating the plus-strand RNA in the 5′- to 3′-direction with the polymerase synthesizing the minus strand in the opposite direction should be avoided. This scenario would require a mutual negative regulation of translation versus replication. On the other hand, in analogy to the Cap-polyA interaction in cellular mRNAs, a 5′-3′-interaction in viral genomes should ensure that only intact, undegraded viral RNA genomes are both efficiently translated and efficiently replicated. Therefore, it makes sense that the HCV 3′UTR stimulates translation directed by the 5′UTR IRES (ref. [54] and references therein). Vice versa, it also makes sense that only intact, undegraded viral RNA genomes are worth being replicated efficiently. Thus, it can be suspected that in this scenario, sequences at the 5′end might stimulate the initiation of minus-strand RNA synthesis at the genome's 3′end in *cis*.

In this study, we therefore aimed to identify sequences in the 5′UTR of the HCV plus strand that regulate minus-strand synthesis via communication between the 5′- and 3′ends of the plus strand. In principle, in experiments addressing such a question, the molecular process under investigation (here: minus-strand RNA synthesis) needs to be uncoupled from all other processes like translation, plus-strand synthesis, genome packaging, virion assembly and so on. In comparison, the few studies that fulfill the above uncoupling requirements for the investigation of the start of plus-strand RNA synthesis at the 3′end of the minus strand have used a two-component in vitro system with (1) a purified RNA template representing only the 3′end of the minus strand and (2) a recombinantly expressed and purified NS5B polymerase, with the readout being newly synthesized short pieces of plus-strand RNA [21,23,24]. These studies showed that certain sequences and RNA secondary structures at the 3′end of the minus strand facilitate the plus-strand RNA synthesis initiation by NS5B. In contrast, other studies that investigated determinants at the 5′end of the annotated genome that are involved in the regulation of RNA synthesis [12,14–16] used subgenomic HCV replicon systems that contain both genome ends, usually measuring plus-strand genome abundance as a readout for replication capability. However, this readout is generated by the intracellular replication of the replicon RNA, which involves repeated rounds of minus- and plus-strand synthesis (referred to as "roundabout" amplification of replicon RNA).

However, such replicon systems capable of "roundabout" amplification come with two intrinsic properties that—strictly speaking—preclude an easy and unambiguous assignment of cause–effect relationships. These two challenges may sound similar on first glance but they are different: (1) these replicon systems contain *cis* elements at both genome ends, and it appears difficult to clarify if a sequence under investigation acts on the genome's 5′end function, or if it acts (possibly by long-range interactions) on the functionality of the genome's 3′end in replication. (2) It is even more difficult to find out by genetic experiments if a *cis*-element under investigation actually exerts its function on the physical level of the plus strand or on the physical level of the minus strand. For example, mutations that are inserted in a double-stranded DNA plasmid that serves as a transcription template for a plus-strand replicon RNA may have been planned to affect the function of the stem-loop I close to the 5′end of the plus strand (Figure 1A). However, we must ask the question of whether the mutation actually affects the function of the SLI in the plus strand, or if the mutation actually affects the function of the reverse complement SLI′ element at the 3′end of the minus strand, or both. This intrinsic logical dilemma with overlapping *cis* elements on both opposite strands is the reason why some studies investigated the function of RNA secondary structure elements at the 3′end of the minus strand in in vitro systems of reduced complexity [21,23,24].

In the absence of a fully functional in vitro system for the investigation of minus-strand synthesis initiation at the 3′end of the plus strand, the above problems regarding the unambiguous assignment of cause–effect relationships can be avoided at least partially by (1) using a replicon system in which the possible function of 5′UTR sequences in regulating the efficiency of minus-strand RNA synthesis at the genome's 3′end is uncoupled from other functions, and by (2) measuring the abundance of the direct product of the function under investigation, i.e., minus-strand abundance.

Therefore, regarding point (1), we developed a replicon system that comes with the HCV 5′UTR sequences completely uncoupled from all other functions, and in its basic form it actually has no HCV 5′UTR sequences (Figure 1B). Regarding point (2), we used RNA purification and RT-qPCR for the specific detection of only HCV minus-strand RNAs. In fact, the latter point proved by far to be more difficult than expected; in particular, the removal of contaminating DNA and unwanted RNA degradation products required a largely improved protocol for RNA purification.

Our results show that (1) replicons lacking any HCV sequences at the 5′end are incapable of replication, (2) in contrast to previous reports [12,14,16], replicons only containing the HCV 5′UTR stem-loops I and II replicate only on an extremely low level, (3) the presence of 5′UTR sequences including SLs I-III or the complete 5′UTR allows efficient minus-strand synthesis, and (4) sequences in the 5′UTR that are required for the binding of the translation initiation factor eIF3 and the ribosomal 40S subunit stimulate RNA synthesis. These results indicate that eIF3 and the 40S ribosome play an important role not only in translation directed by the HCV IRES, but also in 5′-3′end communication and the regulation of minus-strand synthesis.

2. Results

2.1. A Replicon System for the Detection of Uncoupled HCV Minus-Strand Synthesis

In order to investigate a possible contribution of HCV 5′UTR sequences to the regulation of minus-strand synthesis, we developed a replicon system that contains three Gene Clusters (Figure 1B, for details please see Section 4). Gene Cluster I contains the HCV 5′UTR sequences under investigation or only a hairpin (hp) as a negative control. Gene Cluster II provides an independent expression cassette for the indirect quantification of replicon RNA abundance by virtue of *Firefly* luciferase (Fluc) expression under Poliovirus

IRES control. Gene Cluster III contains the EMCV IRES driving expression of the HCV NS3 to NS5B replication proteins, followed by the HCV 3′UTR as the platform for launching minus-strand RNA synthesis. By this arrangement, a potential role of HCV sequences at the genome's 5′end in regulating RNA synthesis at the genome's 3′end is completely uncoupled from the expression of the HCV replication proteins and other functions.

2.2. Improvement of Specific Detection of HCV Minus Strands

The reliable quantification of minus strands as the direct product of the function under investigation required a considerable improvement of RNA purification and detection methods. Starting from the in vitro synthesis of the plus-strand replicon RNA to be transfected through to the final RT and qPCR reactions for detection of newly synthesized minus strands, the entire procedure comprises a series of optimized methods that were carefully adapted to ensure highly accurate measurement of minus-strand abundance.

In comparison to standard procedures, five parts of the procedure were largely improved (Figure 2): (I) the refined removal of residual plasmid template DNA after in vitro transcription, (II) the addition of 5-Ethynyl-Uridine (5EU) to the cells to only label RNA newly synthesized after replicon transfection, (III) the extremely careful DNA removal after RNA isolation from cells, (IV) the specific enrichment of only 5EU-labeled RNA that was newly synthesized after transfection, and (V) primer annealing RT and qPCR reactions were performed under conditions of uninterrupted high temperature, as well as the use of tagged primers to improve the specificity of target detection [55].

Before we applied these improvements, the background of the RT-qPCR reactions with replication-defective constructs (Pol −) was up to 25% of the 5′UTR WT construct. This was likely due to a variety of problems that generate false–positive signals with any of the replicon RNA constructs, including the polymerase-deficient negative controls. These problems are: (1) partially degraded residual template plasmid DNA oligonucleotides could hybridize to the in vitro transcribed RNA and later act as unwanted RT primers. (2) Minute amounts of longer plasmid DNA pieces could even serve as qPCR templates on their own. (3) The SL1 hairpin of the HCV 3′UTR can give rise to self-primed copy-back synthesis of minus-strand RNAs by the T7 RNA polymerase, already using the freshly made RNA product as a template during the in vitro transcription (ref. [56] and references therein). (4) In the transfected cells, partially degraded RNA oligonucleotides from regions of RNA secondary structures, derived from the large amounts of transfected replicon plus-strand RNAs, can hybridize to residual plus-strand pieces and act as unwanted primer/template combinations in the RT reaction. (5) In the RT reaction, the SL1 hairpin at the HCV 3′UTR 3′end can give rise to reverse transcription synthesis of minus-strand sequences in any replicon construct.

After applying the above improvements, the background in the negative controls dropped to about 2.5% at early time points (4 and 24 hpt, hours post-transfection) and to about 0.025–0.03% at later time points (72 hpt, also see Figures below). The higher background signals at early times after transfection are likely due to residual partially degraded RNA primer/template combinations generated from the transfected plus strands (the above point 4). These RNAs are subject to ongoing degradation in the cells after transfection, and therefore the background drops with increasing time after transfection. Perhaps such background could be further reduced by washes of the biotinylated minus-strand RNAs on the streptavidin beads with wash buffers that contain reagents stripping off RNA from RNA, like urea or guanidinium, plus EDTA.

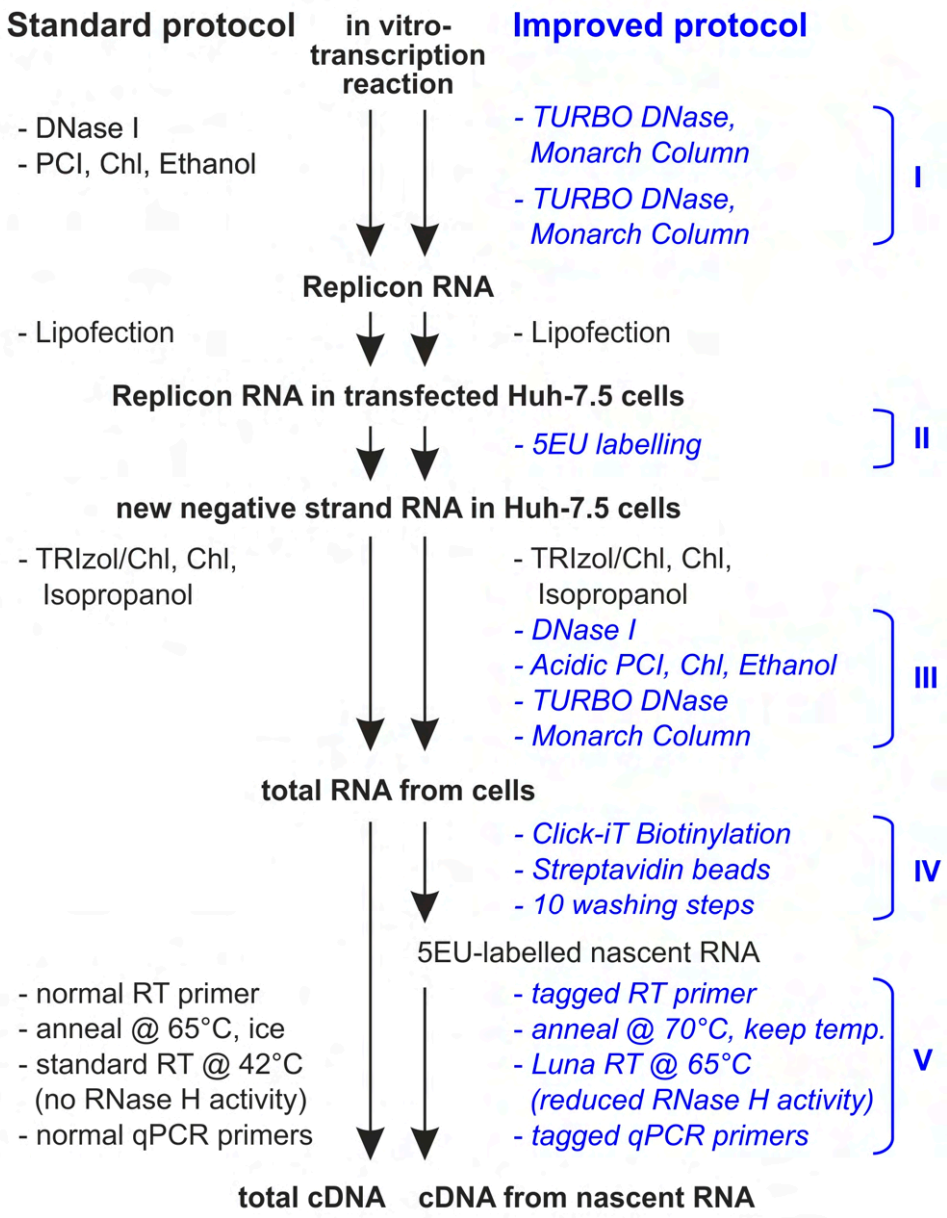

Figure 2. Improved RNA purification before and after transfection of HCV replicon RNA. On the left, standard procedures (black) are shown for RNA purification after in vitro transcription and during isolation of RNA from transfected cells. On the right, five phases of improved procedures (blue) are shown. In general, after RNA isolation from cells using standard TRIzol purification, five additional purification steps with four different physico-chemical mechanisms of separation were applied, namely enzymatic degradation (DNase and TURBO DNase), aqueous/organic partitioning (with acidic phenol), salt-mediated polar interactions (with Monarch silica matrix columns) and affinity purification of the biotinylated RNA. In particular, labeling of RNA newly synthesized in the cells with 5-Ethynyl-Uridine (5EU) after transfection of the replicon RNA (phase II) allows biotinylation of that RNA, followed by purification on streptavidin beads (phase IV). Replicon RNAs isolated in this way were used for detection on minus strands, whereas plus strands were detected after improved RNA isolation but without purification using streptavidin beads. During annealing of a tagged primer for reverse transcriptase (RT) and qPCR reactions, high temperature (70 °C/65 °C) was applied without interruption. This helps to reduce self-priming of the hairpin at the HCV 3′UTR 3′end, as well as unwanted priming by copurified residual RNA and DNA oligonucleotides that were generated by degradation. PCl: phenol/chloroform/isoamylalcohol (125:25:1) treatment; Chl: chloroform treatment; Ethanol: ethanol precipitation and washing.

2.3. Contribution of HCV 5′UTR Sequences to HCV RNA Genome Replication

First, the replicon with the complete HCV 5′UTR in Gene Cluster I was used, in the form with replication-competent NS5B polymerase (Pol +) or with the NGND mutationdisabling polymerase activity (Pol −). For comparison, the basic "hp" construct was used in which the 5′-terminal HCV sequences were replaced by a protective strong stem-loop (see Figure 1B). The transfected plus strands of different constructs were degraded over time equally well (Figure 3A). Thus, differential degradation of the transfected plus-strand RNAs is not supposed to give rise to differences in minus-strand synthesis between constructs. Moreover, this also indicates that the hairpin at the 5′end of the "hp" replicon protects that RNA as well as the others are protected by the genuine HCV 5′UTR RNA secondary structures. *Firefly* luciferase activity was used as an indirect measure for plus-strand abundance of the 5′UTR replicons (Figure 3B). Also here, at earlier time points (4 and 24 hpt), both NS5B polymerase-competent and -defective constructs expressed Fluc equally well, consistent with the presence and translation of the transfected plus-strand RNA detected in Figure 3A. While Fluc activity is fully maintained in polymerase WT constructs at later time points, it declines in Pol-deficient constructs. This suggests that the transfected RNA is further degraded, and Fluc is expressed further only from those constructs with an active NS5B polymerase that replicate and produce progeny plus strands.

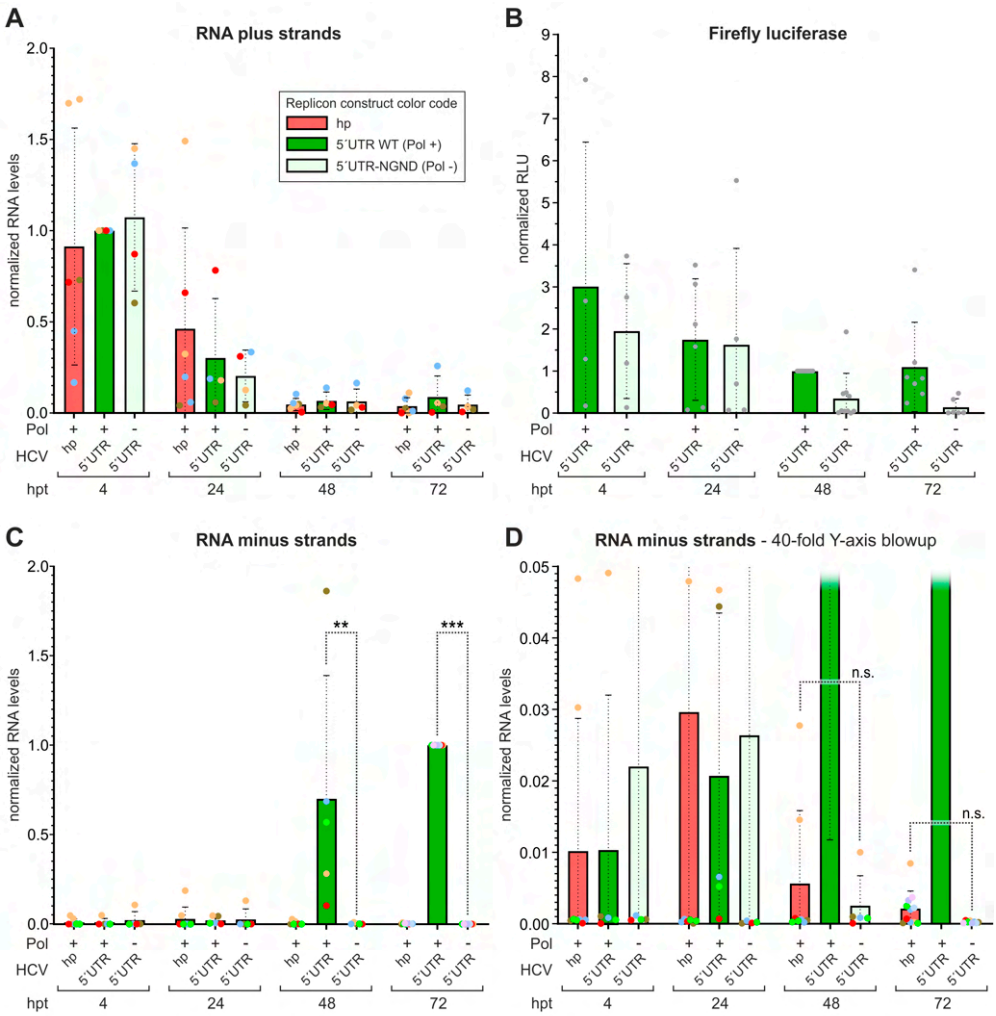

Figure 3. Detection of HCV replicon minus-strand RNA synthesis. In vitro transcribed RNAs of three replicon constructs were transfected into Huh-7.5 cells. The "hp" construct has only a protective stem-loop at its 5′end ("Gene Cluster I", see Figure 1B), while the "5′UTR" constructs

have the complete HCV 5′UTR. The latter come with either wild-type NS5B polymerase activity (WT; Pol +), or with the NGND mutation in the NS5B active center (Pol −). At 4, 24, 48 and 72 h after transfection (hpt), cells were either lysed and the cell extracts were used for RNA isolation and detection (**A**,**C**,**D**), or separate cell lysates were prepared for firefly luciferase (Fluc) measurement (**B**). The same construct color code is used through all panels. (**A**) Detection of HCV replicon RNA plus strands by specific strand-specific RT-qPCR. Values show means and standard deviations (SDs), dots show values of individual experiments. (**B**) Firefly luciferase (Fluc) activity expressed from Gene Cluster II as an indirect measure for replicon RNA plus-strand abundance. (**C**) Detection of HCV replicon minus strands by strand-specific RT-qPCR after 5EU labeling, biotin linkage and streptavidin bead purification of RNA newly synthesized in the Huh-7.5 cells after replicon RNA transfection (see improved protocol in Figure 2). (**D**) 40-fold magnification ("blowup") of Y-axis from (**C**) to show low-value details. At 72 hpt, the 5′UTR-NGND (Pol-) replicon showed 0.025% of the 5′UTR WT (Pol +), with an SD of 0.014%. Statistical significance for pair-wise comparisons is shown with ** $p < 0.01$; *** $p < 0.001$; and $p > 0.05$ not significant (n.s.).

Minus-strand-specific RT-qPCR (Figure 3C) shows the detectable production of minus strands after 48 hpt and later. In the magnification in Figure 3D, we see that the background caused by primer/template combinations derived from degraded plus strands declines with time, reaching about 0.025% at 72 hpt (see technical discussion in Section 4). Importantly, the hp construct is negative in this minus-strand assay. This means that HCV RNA replication is not possible without a genuine HCV sequence at the 5′end of the annotated genome. However, at these late time points, it is not possible to decide at which stage of RNA replication the missing sequences would be required, and it is likely that they can also act at the 3′end of the minus strand [21,23,24].

In a more detailed analysis, we looked at the role of the different RNA secondary structure domains of the HCV 5′UTR (Figure 4). Here, either the HCV 5′UTR stem-loops I and II including the sequence in between were present in the SLI-II construct (compare Figure 1B), or SLI-III, or the complete 5′UTR with the core protein. The transfected RNAs of all constructs were degraded equally well over time after transfection (Figure 4A). Minus strands again could be detected well with both the SLI-III and the 5′UTR replicons at 48 and 72 hpt (Figure 4B). Thereby, the 5′UTR replicon performed slightly better than the SLI-III construct (significant at 72 hpt). The SLI-II construct performed much worse; however, in the magnification (Figure 4C) we see at 72 hpt that the SLI-II construct actually shows residual replication (about 2% of the WT), which is significantly different from the polymerase-deficient 5′UTR construct. Nevertheless, the SLI-II construct replicates far worse than the SLI-III and 5′UTR constructs (Figure 4B). This indicates that the stem-loop regions I and II of the HCV 5′UTR allow only a very basic replication with extremely low efficiency, and the regions of the SLs III and IV contain important determinants required for replication.

2.4. Mutations That Affect Binding of eIF3 and the 40S Subunit to the HCV 5′UTR Impair Replication

According to the results described above, the replicon constructs containing SLI-III or the complete 5′UTR in Gene Cluster I allowed efficient minus-strand production and thereby supported replication, in contrast to the SLI-II construct that shows extremely inefficient replication. Thus, the large stem-loop "domain" SLIII contains determinants that strongly stimulate minus-strand synthesis. In the large SLIII domain, the small sub-domain stem-loops IIIa and IIIb contribute to the binding of eIF3, and the deletion of stem-loop IIIb abolishes the binding of eIF3 without affecting the binding of the 40S subunit [57]. The small stem-loops IIIc, IIId and IIIe are required for the binding of the 40S subunit, and the mutation of either SLIIId or SLIIIe abolishes the binding of the 40S subunit without affecting the eIF3 binding [57].

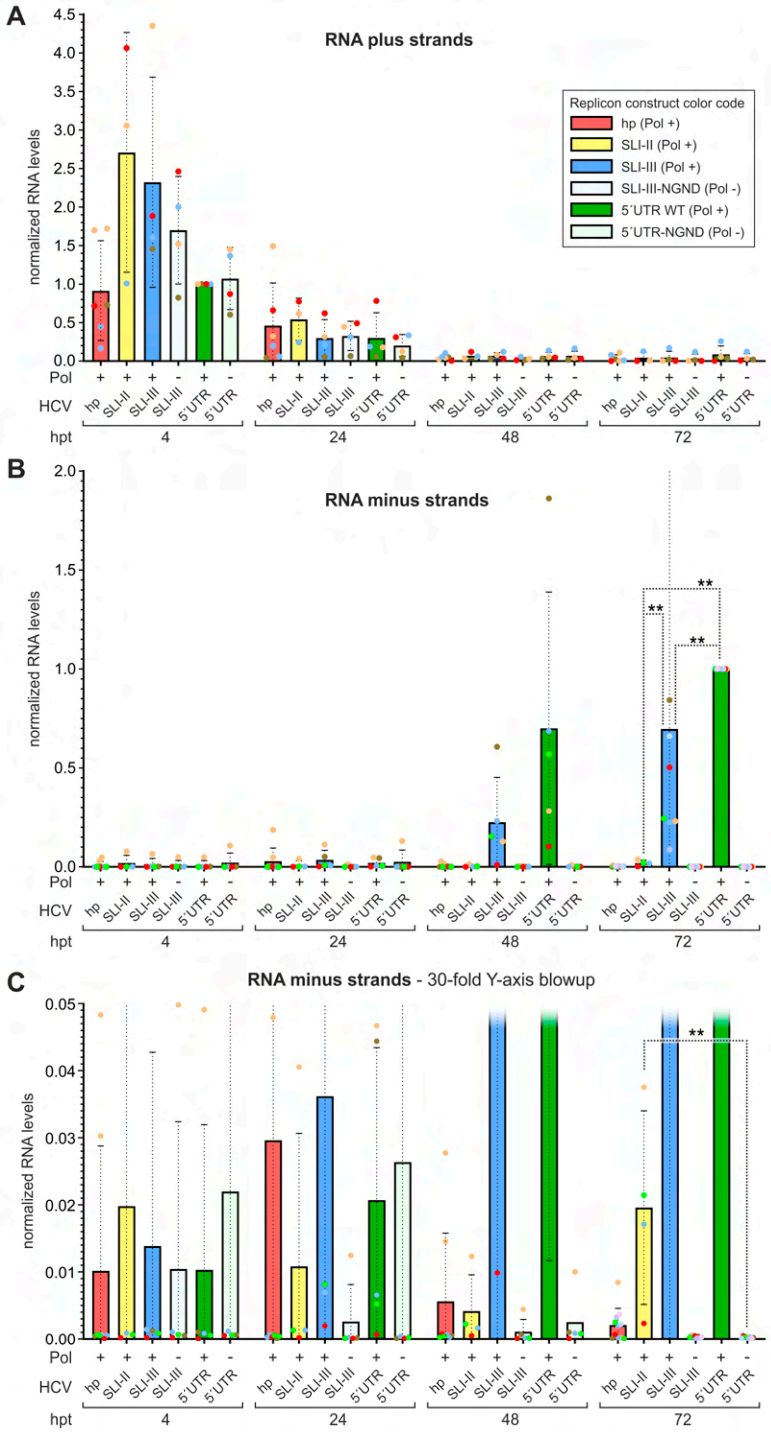

Figure 4. Minus-strand synthesis proficiency of HCV replicon RNAs with different lengths of 5′UTR sequences. Replicon constructs contain either the hairpin (hp) or HCV 5′UTR sequences as shown in Figure 1B, lower panel, with the NS5B replicase active (Pol +) or inactive (Pol −). The experiment was performed as shown in Figure 3, and the same construct color code is used through all panels. (**A**) Strand-specific RT-qPCR detection of plus strands. (**B**) Strand-specific RT-qPCR detection of 5EU labeled minus strands. (**C**) 30-fold magnification of Y-axis from (**B**) to show low-value details. At 72 hpt, the SLI-III-NGND (Pol −) replicon showed 0.032% of the SLI-III WT (Pol +), with an SD of 0.016%. Statistical significance for pair-wise comparisons is shown with ** $p < 0.01$.

Therefore, in the SLI-III as well as in the 5′UTR constructs, we applied mutations affecting the eIF3 or 40S binding. We deleted the small sub-domain SLIIIb (construct name appendix "-Δb") to abolish the eIF3 binding without affecting the 40S subunit binding.

Likewise, we mutated both small sub-domains SLIIId and SLIIIe (name appendix "-de") to abolish the 40S subunit binding without affecting the eIF3 binding (compare Figure 1B, right part of lower panel). Our results in Figure 5A show that deletion of SLIIIb (SLI-III-Δb) reduces minus-strand synthesis to a similar level as the SLI-III-de mutation in both constructs, i.e., to about 50% of WT in the SLI-III context and to about 30% in the 5′UTR context.

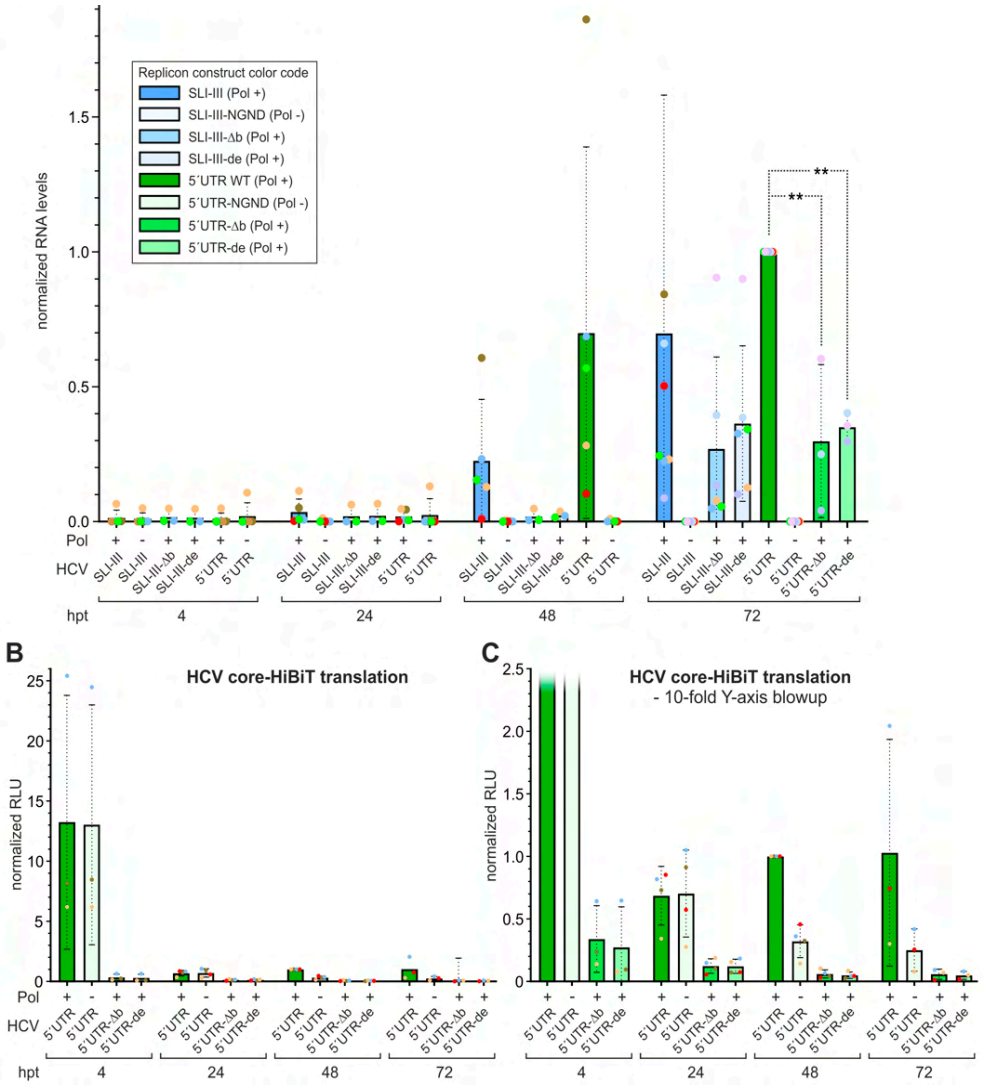

Figure 5. Effect of mutations affecting binding of eIF3 and the ribosomal 40S subunit on minus-strand synthesis. (**A**) Strand-specific RT-qPCR detection of 5EU labeled minus strands. In constructs "Δb" the SLIIIb was deleted (compare Figure 1B, lower panel), which severely affects eIF3 binding. In mutant constructs "de" the SLIIId and SLIIIe were mutated, which severely affects 40S subunit binding. (**B**) Expression of HCV core protein with C-terminal triple HiBiT tags from of the above constructs. This expression is a direct measure for the ability of the respective HCV IRES in Gene Cluster I to mediate IRES-dependent translation. (**C**) 10-fold magnification of Y-axis from (**B**) to show low-value details. Statistical significance for pair-wise comparisons is shown with ** $p < 0.01$.

As a control, we measured Core-HiBiT expression in the 5′UTR context. As expected, both mutations disable translation directed by the mutated HCV IRES in Gene Cluster I (Figure 5B,C). The magnification of the Core-HiBiT data (Figure 5C) shows that up to 24 hpt the Core-HiBiT expression from Gene Cluster I remains the same when polymerase-proficient (Pol +) and polymerase-deficient (Pol −) 5′UTR constructs are compared. This indicates that up to 24 h after transfection, HCV IRES-directed translation in Gene Cluster

I largely reflects the translation of the transfected replicon RNAs and remains largely unaffected by a NS5B polymerase defect. In contrast, after 24 hpt (i.e., at 48 and 72 hpt), the (Pol −) construct's HiBiT expression strongly declines in comparison to the (Pol +) construct. This indicates that from this time, mainly replicon RNA genomes are detected that are protected in HCV replication complexes and/or produced by "roundabout" amplification.

3. Discussion

In this study, we investigated the role of sequences in the HCV 5′UTR in the regulation of minus-strand synthesis that starts at the 3′end of the plus-strand. We found that the complete absence of HCV sequences at the genome 5′end abolishes RNA replication. The mere presence of SLI and SLII (including the two miR-122 binding sites in between) allows only very low-level minus-strand synthesis (about 2% of WT 5′UTR), whereas the constructs SLI-III and the complete 5′UTR allow efficient minus-strand synthesis.

The replicon construct with only an artificial hairpin but no HCV sequences at the 5′end of the plus strand could in principle exhibit minus-strand synthesis completely uncoupled from other processes. This construct shows no replication, and by that it demonstrates that HCV sequences at the plus-strand 5′end or at the minus-strand 3′end are absolutely required for minus-strand synthesis or replication, respectively. However, a limitation of our study (and others) is that whenever we add any genuine HCV sequences at the 5′end of the replicon, "roundabout" amplification is—strictly speaking—no longer excluded. While our replicon system does uncouple minus-strand synthesis from translation, assembly and packaging, it cannot specifically rule out possible effects on positive-strand RNA synthesis. Thus, we face the dilemma that mutations in the annotated plus-strand sequence may either affect the function of the physical plus strand, or they may affect the function of the opposite minus strand (or both). In the above-mentioned case of the SLI-II construct, comparison of RNA synthesis efficiencies from different studies may help; however, we must face the objection that the use of different experimental systems may also contribute to such differences.

Importantly, our mutations in the SLIII domain of the plus strand come with some features that make it rather unlikely that only the function of the opposing minus strand is affected. Those sequences or RNA secondary structure elements in the SLIII domain that bind the translation initiation factor eIF3 (namely, the subdomain SLIIIa and, more important, SLIIIb) are important in this context. The deletion of SLIIIb solely knocks out the binding of eIF3, without affecting the binding of the small ribosomal 40S subunit [57]. Hereby, our precise deletion of the plus strand SLIIIb differs from mutations placed by other groups in the opposing minus-strand 3′region. Mutations affecting the stem base of minus-strand SL-E1 (the approximate mirror of the plus strand SLIIIb) [24] precisely affect or compensate secondary structure features that are unique to the minus strand SL-E1 but not to the plus strand SLIIIb and this proves the presence and importance of these secondary structures in the minus strand. Though approximately a mirror image, the minus-strand SL-E1 still does not represent the entire SLIIIb of the plus strand. The apical loop in the minus-strand SL-E1 is larger, and the upstream sequence of the stem is moved in comparison to its plus-strand SLIIIb counterpart [24], resulting in a different base pairing in the stem. In contrast, our precise deletion of the SLIIIb accurately deletes only the plus-strand SLIIIb (please compare [57]) and leaves the remainder of the SLIII's apical four-way junction intact; this is the mutation that precisely knocks out the eIF3 binding [57].

Similarly, the mutation of sub-domain stem-loops SLIIId and SLIIIe solely impairs the binding of the 40S subunit, without affecting the eIF3 binding [57]. Here, we have precisely mutated each of the three nucleotides in the apical loops of the stable small stem-loops SLIIId and SLIIIe that are embedded in a well documented overall RNA secondary and

tertiary structure setting of the plus-strand SLIII domain and were shown in many studies to precisely knock out the 40S subunit binding and other functions that depend on precise RNA structure [30,31,57–61].

Importantly, the functional effect of these mutations on minus-strand synthesis is the same as that of the SLIIIb deletion in both the SLI-III and the 5′UTR construct, although the structural features of these two types of mutations as well as their effects on the binding of eIF3 or the 40S subunit, respectively, are completely different. This strongly argues for their function in the plus strand but not in the minus strand. Moreover, the opposing minus-strand sequences (i.e., upstream of the minus-strand SL-E1) appear rather volatile in their predicted structures [2,19–24]. Therefore, we conclude that the sequences in the plus-strand SLIII domain that bind eIF3 and the 40S subunit are essential for efficient minus-strand synthesis.

In other studies using replicon systems, the SLI-II region and the SLIII region were shown to be important for replication [12,14,16], with a tendency for a greater importance of the SLI-II region, and some differences between the studies that likely depend on replicon design as well as methods and times of output measurements. Thus, we are in agreement with the above studies that SLIII region sequences are also very important for replication, while our study places greater emphasis on the importance of the SLIII sequences. Importantly, going beyond the above studies, we show here that two different types of small mutations that each specifically recruit one particular translation machinery component (either eIF3 or the 40S subunit) reduce replication efficiency to about 40–50%. Thus, it appears as if we have hit—with both different types of mutations—a kind of "master regulator" function in the plus-strand's SLIII domain that is involved in HCV RNA 5′-3′end communication via eIF3 and the 40S subunit.

Our results are consistent with the findings from the laboratory of Jennifer Doudna that the 40S subunit and eIF3 each bind with quite similar affinities to the HCV IRES or the 3′UTR. The isolated 40S subunit binds to the 3′UTR [62] with a K_D of about 3.5 to 6.7 nM [63], which is only slightly higher than the K_D of 2.0 nM for the binding to the IRES [57]. The K_D of the binding of eIF3 to the HCV 3′UTR was found to be about 8.9 nM [63], which is lower than the K_D of 35 nM for the binding of eIF3 to the IRES [57]. Accordingly, the combined 40S-eIF3 complex has a K_D of 1 nM for its binding to the 3′UTR [63], which is the same as for its binding to the IRES [57]. Also, for other plus-strand RNA viruses, the interaction of eIF3 and the 40S subunits with the 3′- and 5′-UTR was shown. In Barley Yellow Dwarf Virus (BYDV) RNA, both the 5′UTR and a cap-independent translation enhancer element (CITE) in the 3′UTR bind eIF3 and the 40S subunit with similar affinities [64]. The 3′UTR of West Nile Virus (WNV) directly recruits ribosomal 40S subunits to stimulate translation [65]. However, these above studies focused on the regulation of translation, not replication. Nevertheless, it is tempting to speculate if the binding of translation initiation components to the 3′UTR may not only regulate translation but also the replication of these viruses and perhaps also of other plus-strand RNA viruses.

Some hypotheses about the events taking place at the ends of the HCV genome as well as their implications for the HCV life cycle have been proposed, but the situation still appears to not be completely understood. Here, we suggest a hypothesis that combines as many of the facts as possible. As detailed above, both the 40S subunit and eIF3 bind both the IRES and the 3′UTR with the same high affinity [57,63], making 40S and eIF3 the most prominent candidates for triggering a 5′-3′-end interaction. Partial hybridization of the genome ends may support this circularization [2].

In vitro assays for the binding of miR-122 to both target sites in the 5′UTR in the absence of Ago proteins revealed a K_Ds between 11 and 900 nM for both sites, or even much higher for site 2, depending on the flanking sequences and the conditions in the

study [66,67]. In cells, the binding of both miR-122/Ago2 complexes occurs cooperatively [68,69], and Ago2 protein (initially described as "eIF2C" from ribosomal salt wash) can routinely interact with ribosomes [70]. The 3′UTR also contains a conserved miR-122 binding site [2]. The binding of miR-122 to the 5′UTR shapes the IRES towards the formation of SLII and thus to the translation-active conformation [71,72], thereby supporting the 40S binding. The NS5B polymerase likely acts as a dimer or oligomer, and NS5B appears to make multi-point interactions with the CRE, the polyU, its actual start site at the 3′end [29,34,43–45], and NS5B can also bind ribosomes [73]. Moreover, the binding of NS5B to the HCV 5′end is stimulated by miR-122 [67], and the K_D of the NS5B-5′UTR interaction is by far lower than the K_D of the interaction of Poly(rC) Binding Protein 2 (PCBP2) with the 5′UTR [67].

PCBP2 has three RNA-binding domains and multimerizes [74,75]; it can bind to the SLI of the 5′UTR [76,77], to the C-rich seed sequence of the second miR-122 binding site upstream of SLII [78], and more weakly to the 3′UTR [76,77,79], and it can induce HCV RNA genome circularization in vitro [67,77]. The binding of miR-122 and PCBP2 at the 5′end appears mutually exclusive [67,78], but nevertheless miR-122 stimulation of viral RNA synthesis was reported to be PCBP2 dependent [78]. In in vitro assays, PCBP2 competes with the NS5B binding to the HCV 5′UTR 5′-terminus [67], and PCBP2 limits HCV genome packaging [80].

Thus, there appear to exist at least four different states of the HCV RNA in complex with factors (Figure 6). In state 1 (Figure 6B), miR-122/Ago complexes bind to the 5′UTR (without PCBP2) and perhaps to the 3′UTR, and the IRES folds into the translation-competent state with SLII and binds the ribosomal 40S subunit and eIF3. In this state, the pilot rounds of polyprotein translation are started. In state 2 (Figure 6C)—after the first ribosomes have completed polyprotein translation—NS5B binds in a multi-point interaction with the CRE, the polyU, the 3′end and the 5′UTR, with the latter being stimulated by miR-122.

It is not clear if the binding of Ago2/miR-122 complexes to the 3′UTR still occurs simultaneously or if they are released upon the NS5B binding in this state, but a transient interaction of miR-122/Ago complexes, NS5B, eIF3 and the 40S subunit on the RNA might explain how miR-122 actually stimulates HCV RNA replication [81].

This multi-point interaction appears to be required to support the initial start of minus-strand synthesis, since the 3′end of the plus strand is a much worse template for the NS5B polymerase than the 3′end of the minus strand [41]. This, in turn, may contribute to the selectivity of NS5B for its genuine template (as outlined above).

In state 3 (Figure 6D), NS5B uses the plus strand as a template to synthesize the minus strand, and ribosomes, eIF3, miR-122/Ago complexes and other factors are displaced from the RNA. From this state, the minus strand is used as a template for the synthesis of progeny plus strands, resulting in the double-strand (ds) RNA intermediate. It is likely that the genome then undergoes repeated rounds of "roundabout" amplification. From that, progeny plus strands can be used for the assembly of new virus particles. Alternatively, the progeny plus strands can be used for the bulk translation of viral proteins (Figure 6B) to yield sufficient structural proteins for assembly. State 4 in between (Figure 6E) has a dimer of PCBP2 bound to the SLI in the 5′UTR, connecting it with the 3′UTR and circularizing the genome. The functional logic of states 1, 2 and 3 appears clear, but what is the function of state 4? Does the binding of PCBP2 just serve to limit the exit of genomes towards the assembly [80] before enough structural proteins have accumulated, and is there a competition between the binding of PCBP2 (Figure 6E) and the binding of miR-122/Ago and translation components (Figure 6B) and thus between the fate of the RNA genome to undergo either further bulk translation or assembly?

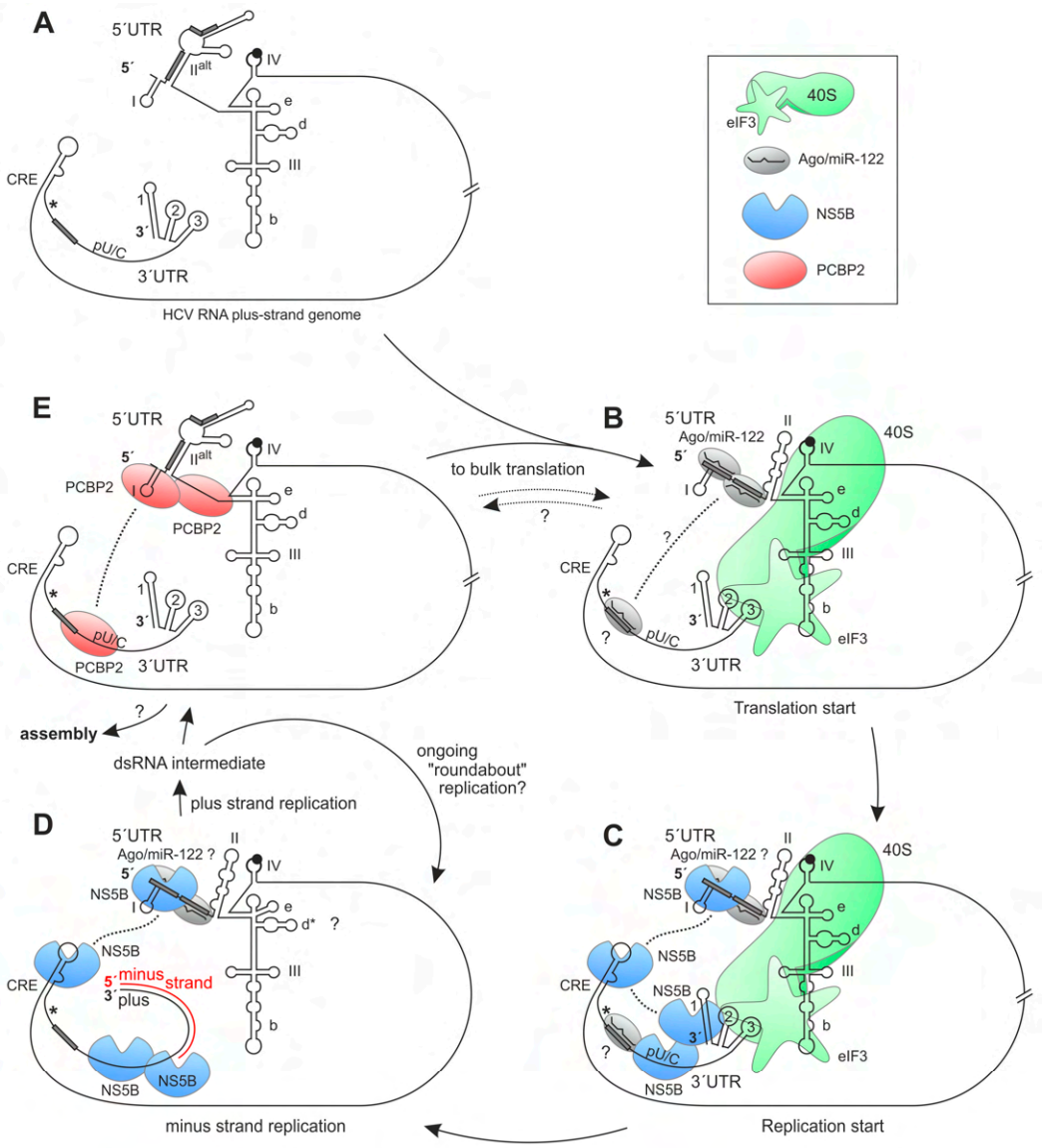

Figure 6. Model of the possible interactions of 40S ribosomes, eIF3, miR-122/Ago complexes, NS5B and PCBP2 with the HCV 5′- and 3′-UTRs. (**A**) The HCV plus-strand RNA with the 5′- and 3′UTRs. In the 5′UTR, the SLII and the region between SLI and SLII are refolded to an alternative version of SLII, SLII^{alt}, in which both miR-122 binding sites are covered. The black dot indicates the polyprotein start codon. (**B**) Binding of two miR-122/Ago complexes to the 5′UTR, refolding of SLII, and binding of 40S subunit and eIF3 to both UTRs starts the pilot round of translation. (**C**) After the first ribosomes have translated the polyprotein, NS5B dimers or oligomers (in replication complexes with other replication proteins, including the protease/helicase NS3, not shown here) bind in multi-point interactions to the CRE, polyU, 3′end and the 5′end with miR-122/Ago complexes, and NS5B starts minus-strand synthesis at the 3′end of the plus strand. (**D**) NS5B synthesizes the minus strand on the plus-strand template; other factors are likely displaced from the RNA. The small stem-loop d* may form as an alternative secondary structure in the large stem-loop domain III upon ribosome release. (**E**) PCBP2 binds to the 5′UTR and 3′UTR and maintains genome circularization. For details, please see main text and also compare Figure 1A.

The above scenario could also be compatible with a contribution of NS5B to the selection of the HCV RNA genome for encapsidation (packaging) into assembling virus particles. Until now, not a single "encapsidation signal" was identified; however, the specificity of HCV RNA genome encapsidation may be accomplished by a combination of determinants or events, respectively. In comparison, in Hepatitis B Virus (HBV), a single clearly defined

RNA signal is necessary and sufficient for specific RNA pregenome encapsidation [82], and it interacts specifically with one molecule of the viral polymerase [83]. In contrast, in Human Immunodeficiency Virus (HIV), encapsidation of the viral RNA genome is accomplished by its interaction with the more abundant gag capsid protein, but it is likely that a kinetic component is involved in rendering packaging selectivity [84]. In contrast, in the HCV genome, several *cis*-acting signals were described to contribute to encapsidation, like the 3′UTR [85] and some small stems with G-rich loops that are scattered over the RNA genome and interact with the core protein [86]. Perhaps both specific RNA *cis*-determinants and spatial and kinetic aspects act together. The HCV RNA plus strand is specifically recognized by the above-described multi-point interaction of NS5B with the CRE, polyU and 3′X. During replication, the progeny plus strands may slide like they are on a railway formed of NS5A and NS5B in order to reach the core proteins in the protected environment of the replication organelles [87], where finally the small stems with G-rich loops scattered over the RNA genome tether the RNA to the core proteins inside the growing particle. In total, this perhaps provides enough specificity for a selective incorporation of HCV RNA genomes into the assembling virus particles, without a further need for "the one" single, required and sufficient RNA–protein recognition event as occurs in HBV.

4. Materials and Methods

Replicon plasmids: The so-called 4th generation replicon RNA sequence contains three functionally independent Gene Clusters (Figure 1B). Gene Cluster I contains the HCV 5′UTR sequences which are under investigation for their possible function in the stimulation of minus-strand RNA synthesis. Alternatively, only a hairpin is used as the negative control. Gene Cluster I is described with its variations in detail below. Gene Cluster II contains an independent protein expression cassette with the *Firefly* luciferase (Fluc) gene [88] under translational control of the Poliovirus IRES (GenBank: V01149.1, position 117–742). Gene Cluster III contains two principal regions: (i) the IRES of Encephalomyocarditis virus, EMCV (GenBank: NC_001479.1, pos. 263–830) fused by the sequence ACCATG to the downstream HCV NS3 to the NS5B replication protein coding sequence (GeneBank: AB047639, pos. 3431–9442), and (ii) the HCV 3′UTR, which serves as the start point for minus-strand RNA synthesis (pos. 9443–9678) [89].

Downstream of this replicon RNA sequence follows a Hepatitis Delta Virus (HDV) genomic ribozyme sequence (GeneBank: M21012.1, pos. 686–772) that serves to generate an authentic 3′end of the HCV 3′UTR. The HDV ribozyme is followed by a phage T7 terminator sequence (GeneBank NC_001604.1, pos. 24164–24210) to avoid run-through transcripts from plasmid templates that might have escaped HDV ribozyme cleavage or linearization at the downstream EcoRI cleavage site. In selected constructs, a wild-type (WT) construct with functional NS5B RNA-dependent RNA polymerase (RdRP or "replicase") and a polymerase-defective variant were each made. The defective construct had not only the GDD motif in the active center mutated to GND [90] (with D318 mutated to N) but also the upstream D220 mutated to N [90]; these substitutions inhibit polymerase function by preventing the essential binding of Mg^{2+} ions. This type of polymerase-defective construct was named "NGND" or "Pol −" for short.

Gene Cluster I comes in different variations (see Figure 1B, lower panel). Replicon RNA in vitro transcription is started from a T7 promoter upstream of Gene Cluster I. In this T7 promoter sequence (TAATACGACTCACTATAG), the last G is the first transcribed nucleotide. In Gene Cluster I, the basic negative control "hp" construct contains a 5′-terminal "hairpin" stem-loop structure with a stem of 19 uninterrupted base pairs (bp) (74% GC content; including the first transcribed G) and a tetraloop for providing stability against exonucleases. This hairpin is followed by a 220 nucleotide (nt) spacer. In all constructs

containing HCV 5′UTR sequences, the last G of the promoter sequence replaces the first authentic HCV nucleotide (A → G) of the Jc1 chimeric isolate [89] for higher transcription efficiency; in natural HCV isolates this first nucleotide can be G > A > U [2]. Moreover, the spacer was reduced to about 160 nts. In the construct SLI-II, HCV sequences from pos. 2 to 117 replace the hairpin of the basic "hp" construct. Together with the A → G exchange of the promoter sequence, these nucleotides represent pos. 1 to 117 of the HCV 5′UTR, ending at the last nucleotide of stem-loop II [10]. In the SLI-III construct, the HCV sequences extend to pos. 329; thus, this construct contains all SL I, II and III sequences, ending just upstream of the SLIV. In the HCV 5′UTR construct, the entire HCV 5′UTR is present along with the sequence coding for amino acids (AA) 1 to 165 of the HCV core protein. This avoids the C-terminal core protein cleavage sites and the hydrophobic membrane anchor [91,92]. Three copies of the HiBiT tag [93], each preceded by 10 AA Gly/Ser-linkers, are fused to the core C-terminus.

In both the SLI-III and the 5′UTR constructs, each two types of mutations were applied that impair the binding of eIF3 or the small ribosomal 40S subunit to the HCV IRES [57]. In the SLI-III ΔIIIb construct (in short "Δb") the apical stem-loop IIIb of the SLIII domain which binds eIF3 [57,94] is replaced by a small unrelated stem-loop sequence (AATTGCCATT), while the mutIIId/e construct (in short "de") contains two mutations both in stem-loop regions IIId (GGG > CCC) and IIIe (GAUA > GAAA) which impair the 40S subunit binding [57].

Reagents: Enzymes: T7 RNA polymerase (New England Biolabs (NEB), Frankfurt am Main, Germany; M0251L); DNase I (RNase free) (NEB M0303S); TURBO DNase (Thermo Fisher Scientific, Waltham, MA, USA; AM2238); Maxima Reverse Transcriptase (Thermo Fisher EP0743). Kits: Click iT Nascent RNA Capture Kit (Invitrogen, Life Technologies GmbH, Darmstadt, Germany; C10365); Monarch RNA isolation kit (NEB T2040L); LunaScript RT Master Mix Kit (Primer-free) (NEB E3025L); Luna Universal qPCR Master Mix (NEB M3003); Steady-Glo Luciferase Assay System (Promega, Walldorf, Germany; E2510); Nano-Glo HiBiT Lytic Detection System (Promega; N3030).

Non-standard chemicals: Lipofectamine MessengerMax Transfection reagent (Invitrogen; LMRNA008); Acidic phenol/chloroform/isoamylalcohol (PCI) (125/24/1, pH 4.5, Thermo Fisher; AM9722); Biotin-X-azide (carboxamide-6-azidohexanyl biotin) (Lumiprobe Life science solutions, Hannover, Germany; 2730-100 mg).

Biological Resources: Huh-7.5 cells [95]; Hepatitis C Virus clone Jc1 [89]; Poliovirus IRES [96]; Firefly luciferase [88]; EMCV IRES [97].

In vitro transcription and RNA purification: The 11955 nt RNA corresponding to the 4th generation replicon system was always freshly synthesized before transfection into Huh-7.5 cells. The plasmid template DNA was linearized prior to in vitro transcription with EcoRI. The in vitro transcription reactions included the buffer provided by the supplier, plus 5 mM of additional $MgCl_2$, 4 mM rNTPs, 10 mM DTT, 0.5 µL Murine RNase Inhibitor, 2 µL of T7 polymerase and 1 µg of template DNA in a total volume of 50 µL and were incubated at 37 °C for 4 hrs. After in vitro transcription, the template DNA was digested by adding 2 µL of TURBO DNase I (NEB) and incubating for 30 min at 37 °C. The RNA was purified using a Monarch column (NEB) and eluted in water. TURBO-DNase digest and column purification were then repeated.

Transfection of RNA by Lipofection: RNA was transfected into Huh-7.5 cells at ~90% confluency in 6-well or 12-well plates. The lipofection reagent, Lipofectamine MessengerMax (ThermoFisher, LMRNA008), was used at a 3:1 ratio (3 µL for 1 µg of RNA). RNA and Lipofectamine were first mixed separately with Opti-MEM and then combined to make one transfection solution. To this end, for each well, 3.5 µg RNA (6-well) or 1.9 µg (12-well) was thoroughly mixed with 100 µL of Opti-MEM by gentle vortexing. In another vial, the

appropriate amount of Lipofectamine was mixed with 100 µL of Opti-MEM for each well and mixed by vortexing. Both solutions were combined after 5 min of incubation at room temperature and incubated for a further 15 min. Meanwhile, the Huh-7.5 cells were washed with 1× PBS, and 800 µL Opti-MEM (6-well) or 300 µL (12-well) was gently added to the cells. At this point, 0.1 mM of 5-Ethynyl Uridine (5EU) was pre-mixed with the Opti-MEM if a nascent RNA capture assay was planned. The transfection solution was added dropwise to the cells, and the plates were gently rocked back and forth to ensure complete mixing of all reagents. The cells were incubated at 37 °C. The medium was replaced by complete medium after 4 h.

Total RNA Extraction using TRIzol: Total RNA was extracted from the Huh-7.5 cells at certain time points (4, 24, 48 and 72 hpt). After the medium was removed from the cells, 1 mL of TRIzol was added directly to the cells and incubated for 5 min at room temperature. The lysed cells were mixed thoroughly in TRIzol by pipetting up and down several times and transferred to 1.5 mL sterile tubes. A total of 200 µL chloroform was added to the lysate and mixed properly by inverting the tubes 20 times. The solution was incubated for a further 3 min at room temperature and then centrifuged at 14,000 rpm for 15 min at 4 °C. The upper aqueous phase contained RNA as well as traces of residual genomic DNA. Approximately 400–500 µL of the upper phase was transferred to new tubes, carefully avoiding the interphase.

Extending the standard RNA purification procedure using TRIzol, again 200 µL chloroform was added and mixed thoroughly by inverting the tubes 20 times to remove residual traces of phenol. The solution was centrifuged at 14,000 rpm for 5 min at 4 °C and the upper aqueous phase was transferred to new tubes. An equal volume of ice-cold isopropanol was added along with 1.5 µL of GlycoBlue (15 mg/mL), mixed well and incubated at −20 °C overnight. RNA was pelleted by centrifugation at 14,000 rpm for 30 min at 4 °C. The pellet was washed twice with 70% ethanol, air-dried for 10 min, and gently dissolved in 30 µL of deionized water.

At this stage, commonly used standard RNA purification procedures end. However, such RNA preparations still contain traces of genomic DNA and also residual transfected plasmid DNA as contamination. Therefore, 2 µL DNase I (NEB) was added to the RNA along with 10× DNase I buffer, 0.5 µL murine RNase Inhibitor and water up to 100 µL. Reactions were incubated at 37 °C for 30 min. The mixture was then diluted to 200 µL, and RNA was extracted using acidic phenol (Phenol/Chloroform/Isoamyl alcohol; 125:24:1; pH ~ 4.5; ThermoFisher). Separation of DNA from RNA is then based on their differential solubility in the aqueous and phenol phases at specific pH levels [98]. Both DNA and RNA are soluble in the aqueous phase when the pH is around 6 to 7. At lower pH, phosphate backbones are more protonated, and DNA can partition into the more hydrophobic phenol phase. In contrast, RNA remains largely in the aqueous phase due to the additional hydrophilic 2′-hydroxyl group. This separation works best with high (5/1) phenol/chloroform ratios, where the presence of residual water in the phenol phase [99], in combination with the low concentration of hydrophobic chloroform, provides a largely hydrophobic but still slightly hydrophilic environment for the DNA. The RNA was then collected from the upper aqueous phase by standard ethanol precipitation and dissolved in water.

To ensure complete elimination of contaminating DNA, the DNase treatment was then repeated, this time using 2 µL of TURBO DNase along with the appropriate buffer and 0.5 µL of murine RNase Inhibitor in a final volume of 50 µL. Finally, the RNA was additionally purified using silica-based Monarch kit (NEB) columns according to the manufacturer's instructions. The purified RNA (virtually free of contaminating DNA) was eluted in 20 µL of water. The amount of RNA was determined using a Qubit reader, and integrity was checked by agarose gel electrophoresis.

Reverse transcription and quantitative PCR reactions: RT-qPCR was applied for the strand-specific quantification of the RNA synthesized by the HCV replicon system inside the Huh-7.5 cells. All primers for plus- and minus-strand detection target different parts of the EMCV IRES region which is artificial for eukaryotic cells and thus unique for the replicon system. For HCV plus-strand RNA as well as GAPDH mRNA detection, 1 µg of RNA in 7 µL water was heated to 70 °C for 5 min. Meanwhile, 10 µM RT primer "D_TAG_RT_plus_1" (gcaggagctaagcgctggTcaggagctaagAAGACCCCTAGGAATGCTC-GTCAAGAAGACAGGGCC) was also preheated at 70 °C. After 5 min, 1 µL of primer was added to the RNA, keeping reactions constantly at 70 °C on a heating incubator. The temperature was then decreased to 65 °C without removing the tubes from the incubator. During the temperature drop, 2 µL of LunaScript RT Master Mix Kit (Primer-free) (which includes LunaScript Reverse Transcriptase with reduced RNase H activity) was added to the tubes to reach a total volume of 10 µL and mixed by pipetting up and down. The RT reaction for plus-strand detection was then performed at 65 °C for 20 min, followed by inactivation of the reverse transcriptase at 95 °C for 1 min. RT for GAPDH was performed at 55 °C for 20 min, followed by RT inactivation.

For the plus-strand qPCR reaction, 2 µL of 1:10 or 1:100 cDNA dilution was mixed with 10 µL of Luna Universal qPCR Master Mix (which includes Hot Start Taq DNA Polymerase), 0.1 µM forward primer "Amp_1_plus_F" (CGAAGCCGCTTGGAATAAGGCC-GGTGTG) and 0.2 µM reverse primer "D_TAG " (gcaggagctaagcgctggTcaggagctaag) in a final reaction volume of 20 µL; alternatively, all volumes were scaled down to reach a final reaction volume of 10 µL. The reaction mix was transferred to 96-well plates which were sealed immediately to prevent any contamination. The qPCR program for plus-strand detection was as follows: initial denaturation at 94 °C for 60 s; then 40 cycles of denaturation at 94 °C for 30 s and annealing/elongation at 62 °C for 30 s, followed by a final melting curve analysis at 85 °C. For GAPDH detection, primer "GAPDH 2_rev" (ACCACCCT-GTTGCTGTAGCCAA) was used as RT primer and qPCR reverse primer, "GAPDH 2_for" (GTCTCCTCTGACTTCAACAGCG) as qPCR forward primer; the qPCR parameters were the same as before except that annealing was performed at 55 °C. RT-qPCR for minus-strand detection was performed as described in the following nascent RNA capture assay.

Nascent RNA Capture Assay: The nascent RNA capture assay allows the screening of newly synthesized RNA from the whole content of the total RNA present inside the Huh-7.5 cells. In conventional transfection and RNA extraction protocols, the RNA extracted from the cells contains both the newly synthesized minus-strand RNA produced after transfection of the in vitro transcribed HCV replicon RNAs, as well as all pre-existing plus strands and other RNA (including residual undegraded template DNA) that were transfected to the cells. However, some of the transfected HCV plus-strand RNA itself remains functional inside the cells even after 120 hpt and increases the RT-qPCR signals drastically, even in the negative controls with replication-deficient constructs. A large part of these false positive signals may be due to partially degraded RNA oligonucleotides that act as unwanted primers in the RT reaction.

To overcome this problem, the nascent RNA is labeled using modified uridine molecules (5-Ethynyl-Uridine, 5EU) which are added to the cell culture medium only at the time of transfection. In this way, only RNA newly synthesized after transfection is labeled with 5EU, while the bulk of pre-existing RNA in the cell remains unlabeled, as well as the transfected RNA and all DNA in the cell. Total RNA is extracted from the cells by TRIzol extraction and further purification. In the total RNA preparation, an azide-modified biotin molecule is then covalently bound to the incorporated 5EU through a copper-catalyzed click reaction. The biotin-labeled RNA can then be specifically captured using streptavidin magnetic beads, extensively washed, and immediately used for strand-specific detection

via RT-qPCR, while all non-5EU-labeled RNAs and DNA are efficiently removed during the washing steps. All necessary reagents for the assay were provided in the "Click iT Nascent RNA Capture Kit".

Nascent RNA labeling with 5EU: 0.1 mM of 5EU was added to the Opti-MEM at the time of lipofection. After 4 h, the Opti-MEM was replaced with complete medium supplemented with 0.2 mM 5EU. The same amount of 5EU was additionally supplemented every 24 h.

EU-Total RNA extraction: After the Total RNA Extraction using TRIzol (see above) at specific time points (4, 24, 48 and 72 hpt) and all further DNase digestion and purification steps, the total EU-RNA was eluted from the Monarch columns in 20 µL of water. The concentration was determined using a Qubit Fluorometer, and the integrity was checked by gel electrophoresis. RNA was stored at −20 °C until further use.

Biotinylation: Purified total RNA including the 5EU-labeled RNA (8–10 µg) was mixed with 0.5 mM Biotin-X-azide, 2 mM $CuSO_4$ and 25 µL Click-iT EU buffer (Component B) to prepare a final 50 µL reaction cocktail. To this cocktail, 1.25 µL of Click-iT reaction buffer additive 1 (Component E) was added and mixed immediately by pipetting up and down. This marked the initiating point of the click reaction between 5EU and biotin-azide. After 3 min, 1.5 µL Click-iT reaction buffer additive 2 (Component F) was added, which caused the solution to turn dark brown. The click reaction was incubated at room temperature with agitation at 300 rpm for 30 min.

The procedure was followed by extraction. To the click reaction, 700 µL chilled ethanol (100%) and 75 µL of 5 M ammonium acetate were added to precipitate all the RNA (including the biotinylated EU-RNA) at −40 °C overnight. The RNA was pelleted by centrifugation at 14,000 rpm for 20 min at 4 °C. The supernatant was removed, and the pellet was washed twice with 70% ethanol. The RNA was air-dried for 10 min and finally dissolved in 20 µL of deionized water. The concentration was determined by Qubit Fluorometer. Biotinylation did not significantly affect total RNA yield; approximately 90% of the starting material was recovered. The RNA was stored at −20 °C.

Purification of 5EU-labeled RNA with Streptavidin Magnetic Beads: Before binding, 48 µL aliquots of streptavidin magnetic beads per vial were immobilized on a magnetic rack, the supernatant was removed, and the beads were resuspended in 480 µL of Component J. The beads were immobilized again on the magnetic rack for 1 min, and the supernatant was discarded. The washing step was repeated another two times. Finally, the beads were resuspended in 48 µL of Component J. The RNA binding reaction was prepared by adding 31 µL of Click-iT RNA Binding Buffer (Component G) to 1 µg of the RNA preparation including the biotinylated EU-RNA, along with 0.5 µL of murine RNase inhibitor (NEB), and deionized water added to a final volume of 62 µL. The reactions were heated to 70 °C for 5 min. Next, each 12 µL of the streptavidin magnetic beads, previously washed and resuspended in Component J, were immediately added to each RNA binding reaction, mixed thoroughly by pipetting up and down, and the tubes returned to room temperature. To facilitate the binding of biotinylated EU-RNA to the beads, the reaction tubes were agitated at 300 rpm at room temperature for 30 min.

The streptavidin magnetic beads with the bound 5EU-labeled RNA were then washed ten times to remove contaminating non-biotinylated RNA. The beads were immobilized on a magnetic rack for 1 min, the supernatant was discarded, and the beads were thoroughly resuspended in 120 µL of Click-iT Reaction Wash Buffer 1 (Component I). The beads were immobilized again for 1 min, and the supernatant was removed and replaced by fresh 120 µL of Component I. The wash step was repeated for a total of 5 times using Component I. The washing procedure was then repeated an additional five times using 120 µL of

Click-iT Reaction Wash Buffer 2 (Component J). Finally, the beads were resuspended in 12 µL of Component J and immediately used for the reverse transcription reaction.

Reverse Transcription and qPCR reactions for minus-strand detection: 12 µL of RNA bound streptavidin beads, resuspended in sterile Click-iT reaction Wash Buffer 2 (Component J), were diluted to a final volume of 15 µL in 0.2 mL DNase-/RNase-free PCR tubes and heated up to 70 °C for 5 min. Meanwhile, the RT primer "D_TAG_RT_minus_2" (gcaggagctaagcgctggTcaggagctaagGTAGCGACCCTTTGCAGGCAGCGGAACC) was also preheated at 70 °C. After 5 min, 1 µL (10 µM) of the preheated primer was added to the bead suspension while maintaining the temperature at 70 °C. Subsequently, the temperature was reduced to 65 °C, without removing the tubes from the incubator. During the temperature drop, 4 µL of LunaScript RT Master Mix (Primer-free) (including LunaScript Reverse Transcriptase) was added to the reaction and mixed by pipetting up and down. The reverse transcription reaction was performed at 65 °C for 30 min with gentle agitation at 300 rpm. Following the reaction, the PCR tubes were transferred to a thermal cycler for enzyme inactivation at 95 °C for 1 min, followed by a hold at 4 °C. The beads were then centrifuged briefly, and 10 µL of the cDNA in the supernatant was carefully transferred to fresh, sterile 0.2 mL tubes for downstream applications.

For the minus-strand qPCR reaction, the cDNA synthesized in the previous step was immediately used by dilution at a ratio of 1:10 with water, and mixed thoroughly with 10 µL of Luna Universal qPCR Master Mix (which includes Hot Start *Taq* Pol), 0.1 µM of forward primer "D_TAG" (gcaggagctaagcgctggTcaggagctaag) and 0.2 µM of reverse primer "Amp_2_minus_R" (ACGTGGCACTGGGGTTGTGCCG) in a final reaction volume of 20 µL. The reaction mix was transferred to 96-well plates which were sealed instantly to prevent contamination. The qPCR program is as follows: initial denaturation at 94 °C for 60 s, then 39 cycles of denaturation at 94 °C for 30 s and annealing/elongation at 62 °C for 30 s, followed by a final melting curve analysis at 85 °C.

Firefly Luciferase Assay: The reagent (Steady-Glo Luciferase Assay System) was prepared by adding lysis buffer to the lyophilized luciferin substrate and mixed thoroughly. Protein expression was measured usually at 4, 24, 48 and 72 hpt. The cells in 6-well plates were washed with 1× PBS, and 120 µL *firefly* luciferase assay reagent was added dropwise directly onto the cells. The cells were incubated in the dark at room temperature for 10 min. After that, the cells were detached from the bottom using an appropriate cell scraper, and the whole lysate was transferred to a transparent tube for measurement in a Bethold Lumat LB 9501 luminometer.

HiBiT Assay: Expression of viral proteins inside Huh-7.5 cells was measured by bioluminescence using the Nano-Glo HiBiT Lytic Detection System (Promega), which is based on a genetically engineered split Nanoluciferase system [93]. The system requires an 11-amino acid sequence tag ("HiBiT"-tag) fused to the protein of interest. This HiBiT-tag binds with a high affinity to "LgBit", the large part of Nanoluciferase, constituting a bright luminescent "NanoBit" enzyme. The bioluminescence emitted by the reaction is measured by a luminometer. In some versions of the HCV replicon system used here, a triple HiBiT was fused at the C-terminus of the truncated core protein. The HiBiT lytic buffer was prepared by adding 1:50 volume of HiBiT substrate and 1:100 volume of LgBiT protein at room temperature. The medium was removed, and the cells were washed with 1× PBS. The HiBiT lytic buffer mixture was added dropwise directly onto the cells (120 µL for 6-well and 60 µL for 12-well plates) and incubated in the dark at room temperature for 10 min. The cells were detached from the bottom using a scraper, and the whole lysate was transferred to transparent tubes for bioluminescence measurement.

Data processing: The Ct values obtained from RT-qPCR curves (using the Bio-Rad CFX Maestro Software (www.bio-rad.com/de-de/product/cfx-maestro-software-for-cfx-

real-time-pcr-instruments; Version 1.0, accessed on 26 February 2018) for Real-Time PCR) were first normalized to the corresponding expression value obtained with GAPDH mRNA (ΔCt = Ct [sample] − Ct [GAPDH]). Then, all these $\log_2$-scale ΔCt values were transformed to linear scale $2^{-\Delta Ct}$ values. Then, we applied "day-to-day" normalization, i.e., all experimental values of all constructs of one day's experiment were divided by the value obtained with the WT in that experiment (usually 5′UTR WT at 72 hpt). As a result, all values in a day's experiment were normalized to its WT, with the WT = 1.0. After this day-to-day normalization, mean and standard deviation (SD) values were calculated for the various constructs from all similar experiments performed on different days. Raw data processing and calculations were usually performed in Microsoft Excel. Statistical significance for pairwise comparisons was assessed using a Mann–Whitney U-Test in GraphPad Prism software version 8.0.0 for Windows, GraphPad Software, San Diego, CA, USA, www.graphpad.com (* $p < 0.05$; ** $p < 0.01$; *** $p < 0.001$; **** $p < 0.0001$), with p-values > 0.05 considered not significant (n.s.). The relative light units (RLUs) obtained from the *firefly* luciferase and HiBiT assay measurements were first corrected by subtraction of the corresponding mock values. Then, RLUs were day-to-day-normalized to the expression level of the 5′UTR at 72 hpt unless stated otherwise, including statistical analyses as described above.

Novel Programs, Software, Algorithms: none.

Web Sites/Data Base Referencing: Vienna RNAalifold WebServer (http://rna.tbi.univie.ac.at/cgi-bin/RNAWebSuite/RNAalifold.cgi, accessed on 29 March 2026) with the new RNAalifold with RIBOSUM scoring [100]. For visualization of predicted RNA structures, RNA sequences and Vienna dot-bracket outputs from RNAalifold [100] were loaded into VARNA v3-93 (https://varna.lisn.upsaclay.fr/, accessed on 29 March 2026) [101].

Author Contributions: Conceptualization: A.Q.M., L.S. and M.N.; Methodology: A.Q.M., M.K., L.S., J.B., A.-L.H., E.J., G.K.G., O.R. and M.N.; Investigation: A.Q.M., M.K., L.S., J.B., A.-L.H., E.J., G.K.G., O.R. and M.N.; Writing—Original Draft: A.Q.M. and M.N.; Writing—Review and Editing: A.Q.M. and M.N.; Funding Acquisition: O.R. and M.N.; Supervision: M.N. All authors have read and agreed to the published version of the manuscript.

Funding: This work was supported by the Deutsche Forschungsgemeinschaft (DFG, German Research Foundation)—[grant number 197785619]—SFB 1021 (Project A03 to A.Q.M., M.K. and M.N.), DFG Research Training Group RTG 2355 (to O.R. and M.N.), and a "Promotionsabschlussförderung" of Justus-Liebig-University Giessen to A.Q.M. and M.K.

Institutional Review Board Statement: Not applicable.

Informed Consent Statement: Not applicable.

Data Availability Statement: The original contributions presented in this study are included in the article. Further inquiries can be directed to the corresponding author.

Acknowledgments: We thank Charles M. Rice (Rockefeller University, NY) for the Huh-7.5 cells, Ralf Bartenschlager (Heidelberg) and Thomas Pietschmann (Hannover) for the Jc1 clone, and Volker Lohmann (Heidelberg) for advice.

Conflicts of Interest: The authors declare no conflicts of interest.

Abbreviations

The following abbreviations are used in this manuscript:

3′UTR	3′Untranslated Region
3′X	highly conserved terminal part of the HCV 3′UTR
5′UTR	5′Untranslated Region
40S	small ribosomal 40S subunit

5BSL3.*	Stem-Loop in the NS5B coding region
Ago	Argonaute protein
CRE	*Cis* Replication Element
eIF3	eukaryotic (Translation) Initiation Factor 3
EMCV	Encephalomyocarditis Virus
Fluc	*Firefly* luciferase
HBV	Hepatitis B Virus
HCV	Hepatitis C Virus
HDV	Hepatitis Delta Virus
HiBiT	An 11 amino acid peptide complementing a defective Nanoluciferase
IRES	Internal Ribosome Entry Site
K_D	Dissociation constant
NS3	Non-Structural Protein 3
NS5B	Non-Structural Protein 5B
PCBP2	poly(rC) Binding Protein 2
polyU	poly uridine tract
polyA	poly adenylate tract
qPCR	quantitative (Real-Time) Polymerase Chain Reaction
RT	Reverse Transcriptase or Reverse Transcription
SL	stem-loop

References

1. Choo, Q.L.; Kuo, G.; Weiner, A.J.; Overby, L.R.; Bradley, D.W.; Houghton, M. Isolation of a cDNA clone derived from a blood-borne non-A, non-B viral hepatitis genome. *Science* **1989**, *244*, 359–362. [CrossRef] [PubMed]
2. Fricke, M.; Dünnes, N.; Zayas, M.; Bartenschlager, R.; Niepmann, M.; Marz, M. Conserved RNA secondary structures and long-range interactions in hepatitis C viruses. *RNA* **2015**, *21*, 1219–1232. Erratum in *RNA* **2016**, *22*, 1640.1. [CrossRef] [PubMed]
3. Lohmann, V.; Körner, F.; Koch, J.; Herian, U.; Theilmann, L.; Bartenschlager, R. Replication of subgenomic hepatitis C virus RNAs in a hepatoma cell line. *Science* **1999**, *285*, 110–113. [CrossRef]
4. Lohmann, V. Hepatitis C Virus RNA Replication. In *Hepatitis C Virus: From Molecular Virology to Antiviral Therapy; Current Topics in Microbiology and Immunology*; Springer: Berlin/Heidelberg, Germany, 2013; Volume 369, pp. 167–198. [CrossRef]
5. Niepmann, M.; Shalamova, L.A.; Gerresheim, G.K.; Rossbach, O. Signals Involved in Regulation of Hepatitis C Virus RNA Genome Translation and Replication. *Front. Microbiol.* **2018**, *9*, 395. [CrossRef]
6. Tabata, K.; Neufeldt, C.J.; Bartenschlager, R. Hepatitis C Virus Replication. *Cold Spring Harb. Perspect. Med.* **2020**, *10*, a037093. [CrossRef]
7. Romero-López, C.; Berzal-Herranz, A. The Role of the RNA-RNA Interactome in the Hepatitis C Virus Life Cycle. *Int. J. Mol. Sci.* **2020**, *21*, 1479. [CrossRef]
8. Sherwood, A.V.; Rivera-Rangel, L.R.; Ryberg, L.A.; Larsen, H.S.; Anker, K.M.; Costa, R.; Vagbo, C.B.; Jakljevic, E.; Pham, L.V.; Fernandez-Antunez, C.; et al. Hepatitis C virus RNA is 5′-capped with flavin adenine dinucleotide. *Nature* **2023**, *619*, 811–818. [CrossRef]
9. Tsukiyama-Kohara, K.; Iizuka, N.; Kohara, M.; Nomoto, A. Internal ribosome entry site within hepatitis C virus RNA. *J. Virol.* **1992**, *66*, 1476–1483. [CrossRef]
10. Niepmann, M.; Gerresheim, G.K. Hepatitis C Virus Translation Regulation. *Int. J. Mol. Sci.* **2020**, *21*, 2328. [CrossRef]
11. Yanagi, M.; St Claire, M.; Emerson, S.U.; Purcell, R.H.; Bukh, J. In vivo analysis of the 3′ untranslated region of the hepatitis C virus after in vitro mutagenesis of an infectious cDNA clone. *Proc. Natl. Acad. Sci. USA* **1999**, *96*, 2291–2295. [CrossRef] [PubMed]
12. Friebe, P.; Lohmann, V.; Krieger, N.; Bartenschlager, R. Sequences in the 5′ nontranslated region of hepatitis C virus required for RNA replication. *J. Virol.* **2001**, *75*, 12047–12057. [CrossRef] [PubMed]
13. Friebe, P.; Bartenschlager, R. Genetic analysis of sequences in the 3′ nontranslated region of hepatitis C virus that are important for RNA replication. *J. Virol.* **2002**, *76*, 5326–5338. [CrossRef]
14. Kim, Y.K.; Kim, C.S.; Lee, S.H.; Jang, S.K. Domains I and II in the 5′ nontranslated region of the HCV genome are required for RNA replication. *Biochem. Biophys. Res. Commun.* **2002**, *290*, 105–112. [CrossRef]
15. Diviney, S.; Tuplin, A.; Struthers, M.; Armstrong, V.; Elliott, R.M.; Simmonds, P.; Evans, D.J. A hepatitis C virus cis-acting replication element forms a long-range RNA-RNA interaction with upstream RNA sequences in NS5B. *J. Virol.* **2008**, *82*, 9008–9022. [CrossRef]

16. Friebe, P.; Bartenschlager, R. Role of RNA structures in genome terminal sequences of the hepatitis C virus for replication and assembly. *J. Virol.* **2009**, *83*, 11989–11995. [CrossRef]
17. Mauger, D.M.; Golden, M.; Yamane, D.; Williford, S.; Lemon, S.M.; Martin, D.P.; Weeks, K.M. Functionally conserved architecture of hepatitis C virus RNA genomes. *Proc. Natl. Acad. Sci. USA* **2015**, *112*, 3692–3697. [CrossRef]
18. Pirakitikulr, N.; Kohlway, A.; Lindenbach, B.D.; Pyle, A.M. The Coding Region of the HCV Genome Contains a Network of Regulatory RNA Structures. *Mol. Cell* **2016**, *62*, 111–120. [CrossRef]
19. Schuster, C.; Isel, C.; Imbert, I.; Ehresmann, C.; Marquet, R.; Kieny, M.P. Secondary structure of the 3′ terminus of hepatitis C virus minus-strand RNA. *J. Virol.* **2002**, *76*, 8058–8068. [CrossRef] [PubMed]
20. Smith, R.M.; Walton, C.M.; Wu, C.H.; Wu, G.Y. Secondary structure and hybridization accessibility of hepatitis C virus 3′-terminal sequences. *J. Virol.* **2002**, *76*, 9563–9574. [CrossRef] [PubMed]
21. Astier-Gin, T.; Bellecave, P.; Litvak, S.; Ventura, M. Template requirements and binding of hepatitis C virus NS5B polymerase during in vitro RNA synthesis from the 3′-end of virus minus-strand RNA. *FEBS J.* **2005**, *272*, 3872–3886. [CrossRef]
22. Dutkiewicz, M.; Swiatkowska, A.; Figlerowicz, M.; Ciesiolka, J. Structural domains of the 3′-terminal sequence of the hepatitis C virus replicative strand. *Biochemistry* **2008**, *47*, 12197–12207. [CrossRef]
23. Masante, C.; Mahias, K.; Lourenco, S.; Dumas, E.; Cahour, A.; Trimoulet, P.; Fleury, H.; Astier-Gin, T.; Ventura, M. Seven nucleotide changes characteristic of the hepatitis C virus genotype 3 5′ untranslated region: Correlation with reduced in vitro replication. *J. Gen. Virol.* **2008**, *89*, 212–221. [CrossRef]
24. Mahias, K.; Ahmed-El-Sayed, N.; Masante, C.; Bitard, J.; Staedel, C.; Darfeuille, F.; Ventura, M.; Astier-Gin, T. Identification of a structural element of the hepatitis C virus minus strand RNA involved in the initiation of RNA synthesis. *Nucleic Acids Res.* **2010**, *38*, 4079–4091. [CrossRef] [PubMed]
25. Tanaka, T.; Kato, N.; Cho, M.J.; Shimotohno, K. A novel sequence found at the 3′ terminus of hepatitis C virus genome. *Biochem. Biophys. Res. Commun.* **1995**, *215*, 744–749. [CrossRef]
26. Kolykhalov, A.A.; Feinstone, S.M.; Rice, C.M. Identification of a highly conserved sequence element at the 3′ terminus of hepatitis C virus genome RNA. *J. Virol.* **1996**, *70*, 3363–3371. [CrossRef] [PubMed]
27. Cristofari, G.; Ivanyi-Nagy, R.; Gabus, C.; Boulant, S.; Lavergne, J.P.; Penin, F.; Darlix, J.L. The hepatitis C virus Core protein is a potent nucleic acid chaperone that directs dimerization of the viral (+) strand RNA in vitro. *Nucleic Acids Res.* **2004**, *32*, 2623–2631. [CrossRef] [PubMed]
28. You, S.; Stump, D.D.; Branch, A.D.; Rice, C.M. A cis-acting replication element in the sequence encoding the NS5B RNA-dependent RNA polymerase is required for hepatitis C virus RNA replication. *J. Virol.* **2004**, *78*, 1352–1366. [CrossRef]
29. Lee, H.; Shin, H.; Wimmer, E.; Paul, A.V. cis-acting RNA signals in the NS5B C-terminal coding sequence of the hepatitis C virus genome. *J. Virol.* **2004**, *78*, 10865–10877. [CrossRef]
30. Romero-Lopez, C.; Berzal-Herranz, A. A long-range RNA-RNA interaction between the 5′ and 3′ ends of the HCV genome. *RNA* **2009**, *15*, 1740–1752. [CrossRef]
31. Romero-Lopez, C.; Barroso-Deljesus, A.; Garcia-Sacristan, A.; Briones, C.; Berzal-Herranz, A. End-to-end crosstalk within the hepatitis C virus genome mediates the conformational switch of the 3′X-tail region. *Nucleic Acids Res.* **2014**, *42*, 567–582. [CrossRef]
32. Friebe, P.; Boudet, J.; Simorre, J.P.; Bartenschlager, R. Kissing-loop interaction in the 3′ end of the hepatitis C virus genome essential for RNA replication. *J. Virol.* **2005**, *79*, 380–392. [CrossRef]
33. You, S.; Rice, C.M. 3′ RNA elements in hepatitis C virus replication: Kissing partners and long poly(U). *J. Virol.* **2008**, *82*, 184–195. [CrossRef] [PubMed]
34. Cheng, J.C.; Chang, M.F.; Chang, S.C. Specific interaction between the hepatitis C virus NS5B RNA polymerase and the 3′ end of the viral RNA. *J. Virol.* **1999**, *73*, 7044–7049. [CrossRef] [PubMed]
35. Zhong, W.; Ferrari, E.; Lesburg, C.A.; Maag, D.; Ghosh, S.K.; Cameron, C.E.; Lau, J.Y.; Hong, Z. Template/primer requirements and single nucleotide incorporation by hepatitis C virus nonstructural protein 5B polymerase. *J. Virol.* **2000**, *74*, 9134–9143. [CrossRef]
36. Zhong, W.; Uss, A.S.; Ferrari, E.; Lau, J.Y.; Hong, Z. De novo initiation of RNA synthesis by hepatitis C virus nonstructural protein 5B polymerase. *J. Virol.* **2000**, *74*, 2017–2022. [CrossRef] [PubMed]
37. Ferrari, E.; He, Z.; Palermo, R.E.; Huang, H.C. Hepatitis C virus NS5B polymerase exhibits distinct nucleotide requirements for initiation and elongation. *J. Biol. Chem.* **2008**, *283*, 33893–33901. [CrossRef]
38. Harrus, D.; Ahmed-El-Sayed, N.; Simister, P.C.; Miller, S.; Triconnet, M.; Hagedorn, C.H.; Mahias, K.; Rey, F.A.; Astier-Gin, T.; Bressanelli, S. Further insights into the roles of GTP and the C terminus of the hepatitis C virus polymerase in the initiation of RNA synthesis. *J. Biol. Chem.* **2010**, *285*, 32906–32918. [CrossRef]
39. Wang, D.P.; Zhao, R.; Hu, W.S.; Li, H.N.; Cao, J.M.; Zhou, X.; Xiang, Y. Structural insights into polymerase-catalyzed FAD capping of hepatitis C virus RNA. *Nat. Commun.* **2025**, *16*, 7298. [CrossRef]
40. Yi, M.; Lemon, S.M. Structure-function analysis of the 3′ stem-loop of hepatitis C virus genomic RNA and its role in viral RNA replication. *RNA* **2003**, *9*, 331–345. [CrossRef]

41. Reigadas, S.; Ventura, M.; Sarih-Cottin, L.; Castroviejo, M.; Litvak, S.; Astier-Gin, T. HCV RNA-dependent RNA polymerase replicates in vitro the 3′ terminal region of the minus-strand viral RNA more efficiently than the 3′ terminal region of the plus RNA. *Eur. J. Biochem.* **2001**, *268*, 5857–5867. [CrossRef]
42. Ralfs, P.; Bressanelli, S.; Gunter, L.M.; Gabel, A.; Rothhaar, P.; Price, K.J.; Tubiana, T.; Munschauer, M.; Frick, D.N.; Lohmann, V. Hepatitis C virus NS3 helicase contributes to (−) strand RNA synthesis. *Nat. Commun.* **2025**, *16*, 8006. [CrossRef]
43. Zhang, J.; Yamada, O.; Sakamoto, T.; Yoshida, H.; Araki, H.; Murata, T.; Shimotohno, K. Inhibition of hepatitis C virus replication by pol III-directed overexpression of RNA decoys corresponding to stem-loop structures in the NS5B coding region. *Virology* **2005**, *342*, 276–285. [CrossRef]
44. Oh, J.W.; Sheu, G.T.; Lai, M.M. Template requirement and initiation site selection by hepatitis C virus polymerase on a minimal viral RNA template. *J. Biol. Chem.* **2000**, *275*, 17710–17717. [CrossRef] [PubMed]
45. Kim, M.; Kim, H.; Cho, S.P.; Min, M.K. Template requirements for de novo RNA synthesis by hepatitis C virus nonstructural protein 5B polymerase on the viral X RNA. *J. Virol.* **2002**, *76*, 6944–6956. [CrossRef] [PubMed]
46. Wang, Q.M.; Hockman, M.A.; Staschke, K.; Johnson, R.B.; Case, K.A.; Lu, J.; Parsons, S.; Zhang, F.; Rathnachalam, R.; Kirkegaard, K.; et al. Oligomerization and cooperative RNA synthesis activity of hepatitis C virus RNA-dependent RNA polymerase. *J. Virol.* **2002**, *76*, 3865–3872. [CrossRef]
47. Labonte, P.; Axelrod, V.; Agarwal, A.; Aulabaugh, A.; Amin, A.; Mak, P. Modulation of hepatitis C virus RNA-dependent RNA polymerase activity by structure-based site-directed mutagenesis. *J. Biol. Chem.* **2002**, *277*, 38838–38846. [CrossRef] [PubMed]
48. Bellon-Echeverria, I.; Lopez-Jimenez, A.J.; Clemente-Casares, P.; Mas, A. Monitoring hepatitis C virus (HCV) RNA-dependent RNA polymerase oligomerization by a FRET-based in vitro system. *Antivir. Res.* **2010**, *87*, 57–66. [CrossRef]
49. Clemente-Casares, P.; Lopez-Jimenez, A.J.; Bellon-Echeverria, I.; Encinar, J.A.; Martinez-Alfaro, E.; Perez-Flores, R.; Mas, A. De novo polymerase activity and oligomerization of hepatitis C virus RNA-dependent RNA-polymerases from genotypes 1 to 5. *PLoS ONE* **2011**, *6*, e18515. [CrossRef]
50. Lopez-Jimenez, A.J.; Clemente-Casares, P.; Sabariegos, R.; Llanos-Valero, M.; Bellon-Echeverria, I.; Encinar, J.A.; Kaushik-Basu, N.; Froeyen, M.; Mas, A. Hepatitis C virus polymerase-polymerase contact interface: Significance for virus replication and antiviral design. *Antivir. Res.* **2014**, *108*, 14–24. [CrossRef]
51. Chinnaswamy, S.; Murali, A.; Li, P.; Fujisaki, K.; Kao, C.C. Regulation of de novo-initiated RNA synthesis in hepatitis C virus RNA-dependent RNA polymerase by intermolecular interactions. *J. Virol.* **2010**, *84*, 5923–5935. [CrossRef]
52. Gerresheim, G.K.; Hess, C.S.; Shalamova, L.A.; Fricke, M.; Marz, M.; Andreev, D.E.; Shatsky, I.N.; Niepmann, M. Ribosome Pausing at Inefficient Codons at the End of the Replicase Coding Region Is Important for Hepatitis C Virus Genome Replication. *Int. J. Mol. Sci.* **2020**, *21*, E6955. [CrossRef]
53. Kazakov, T.; Yang, F.; Ramanathan, H.N.; Kohlway, A.; Diamond, M.S.; Lindenbach, B.D. Hepatitis C virus RNA replication depends on specific cis- and trans-acting activities of viral nonstructural proteins. *PLoS Pathog.* **2015**, *11*, e1004817. [CrossRef] [PubMed]
54. Song, Y.; Friebe, P.; Tzima, E.; Jünemann, C.; Bartenschlager, R.; Niepmann, M. The hepatitis C virus RNA 3′-untranslated region strongly enhances translation directed by the internal ribosome entry site. *J. Virol.* **2006**, *80*, 11579–11588. [CrossRef] [PubMed]
55. Dobson, S.J.; Ward, J.C.; Herod, M.R.; Rowlands, D.J.; Stonehouse, N.J. A highly discriminatory RNA strand-specific assay to facilitate analysis of the role of cis-acting elements in foot-and-mouth disease virus replication. *J. Gen. Virol.* **2023**, *104*, 001871. Erratum in *J. Gen. Virol.* **2024**, *105*, 001993.[CrossRef]
56. Gholamalipour, Y.; Johnson, W.C.; Martin, C.T. Efficient inhibition of RNA self-primed extension by addition of competing 3′-capture DNA-improved RNA synthesis by T7 RNA polymerase. *Nucleic Acids Res.* **2019**, *47*, e118. [CrossRef]
57. Kieft, J.S.; Zhou, K.; Jubin, R.; Doudna, J.A. Mechanism of ribosome recruitment by hepatitis C IRES RNA. *RNA* **2001**, *7*, 194–206. [CrossRef]
58. Spahn, C.M.; Kieft, J.S.; Grassucci, R.A.; Penczek, P.A.; Zhou, K.; Doudna, J.A.; Frank, J. Hepatitis C virus IRES RNA-induced changes in the conformation of the 40s ribosomal subunit. *Science* **2001**, *291*, 1959–1962. [CrossRef]
59. Boehringer, D.; Thermann, R.; Ostareck-Lederer, A.; Lewis, J.D.; Stark, H. Structure of the hepatitis C Virus IRES bound to the human 80S ribosome: Remodeling of the HCV IRES. *Structure* **2005**, *13*, 1695–1706. [CrossRef]
60. Babaylova, E.; Graifer, D.; Malygin, A.; Stahl, J.; Shatsky, I.; Karpova, G. Positioning of subdomain IIId and apical loop of domain II of the hepatitis C IRES on the human 40S ribosome. *Nucleic Acids Res.* **2009**, *37*, 1141–1151. [CrossRef]
61. Berry, K.E.; Waghray, S.; Mortimer, S.A.; Bai, Y.; Doudna, J.A. Crystal structure of the HCV IRES central domain reveals strategy for start-codon positioning. *Structure* **2011**, *19*, 1456–1466. [CrossRef] [PubMed]
62. Wood, J.; Frederickson, R.M.; Fields, S.; Patel, A.H. Hepatitis C virus 3′X region interacts with human ribosomal proteins. *J. Virol.* **2001**, *75*, 1348–1358. [CrossRef] [PubMed]
63. Bai, Y.; Zhou, K.; Doudna, J.A. Hepatitis C virus 3′UTR regulates viral translation through direct interactions with the host translation machinery. *Nucleic Acids Res.* **2013**, *41*, 7861–7874. [CrossRef] [PubMed]

64. Bhardwaj, U.; Powell, P.; Goss, D.J. Eukaryotic initiation factor (eIF) 3 mediates Barley Yellow Dwarf Viral mRNA 3′-5′ UTR interactions and 40S ribosomal subunit binding to facilitate cap-independent translation. *Nucleic Acids Res.* **2019**, *47*, 6225–6235. [CrossRef] [PubMed]
65. Ramos-Lorente, S.E.; Berzal-Herranz, B.; Romero-Lopez, C.; Berzal-Herranz, A. Recruitment of the 40S ribosomal subunit by the West Nile virus 3′ UTR promotes the cross-talk between the viral genomic ends for translation regulation. *Virus Res.* **2024**, *343*, 199340. [CrossRef]
66. Mortimer, S.A.; Doudna, J.A. Unconventional miR-122 binding stabilizes the HCV genome by forming a trimolecular RNA structure. *Nucleic Acids Res.* **2013**, *41*, 4230–4240. [CrossRef]
67. Scott, S.; Li, Y.; Bermek, O.; Griffith, J.D.; Lemon, S.M.; Choi, K.H. Binding of microRNA-122 to the hepatitis C virus 5′ untranslated region modifies interactions with poly(C) binding protein 2 and the NS5B viral polymerase. *Nucleic Acids Res.* **2023**, *51*, 12397–12413. [CrossRef]
68. Thibault, P.A.; Huys, A.; Amador-Canizares, Y.; Gailius, J.E.; Pinel, D.E.; Wilson, J.A. Regulation of Hepatitis C Virus Genome Replication by Xrn1 and MicroRNA-122 Binding to Individual Sites in the 5′ Untranslated Region. *J. Virol.* **2015**, *89*, 6294–6311. [CrossRef]
69. Nieder-Röhrmann, A.; Dünnes, N.; Gerresheim, G.K.; Shalamova, L.A.; Herchenröther, A.; Niepmann, M. Cooperative enhancement of translation by two adjacent microRNA-122/Argonaute 2 complexes binding to the 5 untranslated region of Hepatitis C Virus RNA. *J. Gen. Virol.* **2017**, *98*, 212–224. [CrossRef]
70. Roy, A.L.; Chakrabarti, D.; Datta, B.; Hileman, R.E.; Gupta, N.K. Natural mRNA is required for directing Met-tRNA(f) binding to 40S ribosomal subunits in animal cells: Involvement of Co-eIF-2A in natural mRNA-directed initiation complex formation. *Biochemistry* **1988**, *27*, 8203–8209. [CrossRef]
71. Schult, P.; Roth, H.; Adams, R.L.; Mas, C.; Imbert, L.; Orlik, C.; Ruggieri, A.; Pyle, A.M.; Lohmann, V. microRNA-122 amplifies hepatitis C virus translation by shaping the structure of the internal ribosomal entry site. *Nat. Commun.* **2018**, *9*, 2613. [CrossRef]
72. Rheault, M.; Cousineau, S.E.; Fox, D.R.; Abram, Q.H.; Sagan, S.M. Elucidating the distinct contributions of miR-122 in the HCV life cycle reveals insights into virion assembly. *Nucleic Acids Res.* **2023**, *51*, 2447–2463. [CrossRef] [PubMed]
73. Tanaka, T.; Sugiyama, K.; Ikeda, M.; Naganuma, A.; Nozaki, A.; Saito, M.; Shimotohno, K.; Kato, N. Hepatitis C virus NS5B RNA replicase specifically binds ribosomes. *Microbiol. Immunol.* **2000**, *44*, 543–550. [CrossRef]
74. Kim, J.H.; Hahm, B.; Kim, Y.K.; Choi, M.; Jang, S.K. Protein-protein interaction among hnRNPs shuttling between nucleus and cytoplasm. *J. Mol. Biol.* **2000**, *298*, 395–405. [CrossRef] [PubMed]
75. Bedard, K.M.; Walter, B.L.; Semler, B.L. Multimerization of poly(rC) binding protein 2 is required for translation initiation mediated by a viral IRES. *RNA* **2004**, *10*, 1266–1276. [CrossRef]
76. Fukushi, S.; Okada, M.; Kageyama, T.; Hoshino, F.B.; Nagai, K.; Katayama, K. Interaction of poly(rC)-binding protein 2 with the 5′-terminal stem loop of the hepatitis C-virus genome. *Virus Res.* **2001**, *73*, 67–79. [CrossRef]
77. Wang, L.; Jeng, K.S.; Lai, M.M. Poly(C)-binding protein 2 interacts with sequences required for viral replication in the hepatitis C virus (HCV) 5′ untranslated region and directs HCV RNA replication through circularizing the viral genome. *J. Virol.* **2011**, *85*, 7954–7964. [CrossRef]
78. Masaki, T.; Arend, K.C.; Li, Y.; Yamane, D.; McGivern, D.R.; Kato, T.; Wakita, T.; Moorman, N.J.; Lemon, S.M. miR-122 stimulates hepatitis C virus RNA synthesis by altering the balance of viral RNAs engaged in replication versus translation. *Cell Host Microbe* **2015**, *17*, 217–228. [CrossRef]
79. Pan, T.; Fang, C.; Yi, Z.; Yang, P.; Yuan, Z. Subproteomic analysis of the cellular proteins associated with the 3′ untranslated region of the hepatitis C virus genome in human liver cells. *Biochem. Biophys. Res. Commun.* **2006**, *347*, 683–691. [CrossRef]
80. Cousineau, S.E.; Camargo, C.; Sagan, S.M. Poly(rC)-Binding Protein 2 Does Not Directly Participate in HCV Translation or Replication, but Rather Modulates Genome Packaging. *Viruses* **2024**, *16*, 1220. [CrossRef]
81. Jopling, C.L.; Yi, M.; Lancaster, A.M.; Lemon, S.M.; Sarnow, P. Modulation of hepatitis C virus RNA abundance by a liver-specific microRNA. *Science* **2005**, *309*, 1577–1581. [CrossRef] [PubMed]
82. Junker-Niepmann, M.; Bartenschlager, R.; Schaller, H. A short cis-acting sequence is required for hepatitis B virus pregenome encapsidation and sufficient for packaging of foreign RNA. *EMBO J.* **1990**, *9*, 3389–3396. [CrossRef]
83. Bartenschlager, R.; Schaller, H. Hepadnaviral assembly is initiated by polymerase binding to the encapsidation signal in the viral RNA genome. *EMBO J.* **1992**, *11*, 3413–3420. [CrossRef]
84. Rein, A. RNA Packaging in HIV. *Trends Microbiol.* **2019**, *27*, 715–723. [CrossRef]
85. Shi, G.; Ando, T.; Suzuki, R.; Matsuda, M.; Nakashima, K.; Ito, M.; Omatsu, T.; Oba, M.; Ochiai, H.; Kato, T.; et al. Involvement of the 3′ Untranslated Region in Encapsidation of the Hepatitis C Virus. *PLoS Pathog.* **2016**, *12*, e1005441. [CrossRef]
86. Stewart, H.; Bingham, R.J.; White, S.J.; Dykeman, E.C.; Zothner, C.; Tuplin, A.K.; Stockley, P.G.; Twarock, R.; Harris, M. Identification of novel RNA secondary structures within the hepatitis C virus genome reveals a cooperative involvement in genome packaging. *Sci. Rep.* **2016**, *6*, 22952. [CrossRef]

87. Lindenbach, B.D.; Rice, C.M. The ins and outs of hepatitis C virus entry and assembly. *Nat. Rev. Microbiol.* **2013**, *11*, 688–700. [CrossRef] [PubMed]
88. de Wet, J.R.; Wood, K.V.; DeLuca, M.; Helinski, D.R.; Subramani, S. Firefly luciferase gene: Structure and expression in mammalian cells. *Mol. Cell. Biol.* **1987**, *7*, 725–737. [CrossRef] [PubMed]
89. Pietschmann, T.; Kaul, A.; Koutsoudakis, G.; Shavinskaya, A.; Kallis, S.; Steinmann, E.; Abid, K.; Negro, F.; Dreux, M.; Cosset, F.L.; et al. Construction and characterization of infectious intragenotypic and intergenotypic hepatitis C virus chimeras. *Proc. Natl. Acad. Sci. U S A* **2006**, *103*, 7408–7413. [CrossRef] [PubMed]
90. Lohmann, V.; Körner, F.; Herian, U.; Bartenschlager, R. Biochemical properties of hepatitis C virus NS5B RNA-dependent RNA polymerase and identification of amino acid sequence motifs essential for enzymatic activity. *J. Virol.* **1997**, *71*, 8416–8428. [CrossRef]
91. Matsumoto, M.; Hwang, S.B.; Jeng, K.S.; Zhu, N.; Lai, M.M. Homotypic interaction and multimerization of hepatitis C virus core protein. *Virology* **1996**, *218*, 43–51. [CrossRef]
92. Moradpour, D.; Penin, F. Hepatitis C virus proteins: From structure to function. In *Hepatitis C Virus: From Molecular Virology to Antiviral Therapy; Current Topics in Microbiology and Immunology*; Springer: Berlin/Heidelberg, Germany, 2013; Volume 369, pp. 113–142. [CrossRef]
93. Dixon, A.S.; Schwinn, M.K.; Hall, M.P.; Zimmerman, K.; Otto, P.; Lubben, T.H.; Butler, B.L.; Binkowski, B.F.; Machleidt, T.; Kirkland, T.A.; et al. NanoLuc Complementation Reporter Optimized for Accurate Measurement of Protein Interactions in Cells. *ACS Chem. Biol.* **2016**, *11*, 400–408. [CrossRef]
94. Iwasaki, W.; Kashiwagi, K.; Sakamoto, A.; Nishimoto, M.; Takahashi, M.; Machida, K.; Imataka, H.; Matsumoto, A.; Shichino, Y.; Iwasaki, S.; et al. Structural insights into the role of eIF3 in translation mediated by the HCV IRES. *Proc. Natl. Acad. Sci. USA* **2025**, *122*, e2505538122. [CrossRef] [PubMed]
95. Blight, K.J.; McKeating, J.A.; Rice, C.M. Highly permissive cell lines for subgenomic and genomic hepatitis C virus RNA replication. *J. Virol.* **2002**, *76*, 13001–13014. [CrossRef] [PubMed]
96. Ochs, K.; Zeller, A.; Saleh, L.; Bassili, G.; Song, Y.; Sonntag, A.; Niepmann, M. Impaired binding of standard initiation factors mediates poliovirus translation attenuation. *J. Virol.* **2003**, *77*, 115–122. [CrossRef]
97. Jang, S.K.; Kräusslich, H.G.; Nicklin, M.J.; Duke, G.M.; Palmenberg, A.C.; Wimmer, E. A segment of the 5′ nontranslated region of encephalomyocarditis virus RNA directs internal entry of ribosomes during in vitro translation. *J. Virol.* **1988**, *62*, 2636–2643. [CrossRef] [PubMed]
98. Xu, L.; Sun, L.; Guan, G.; Huang, Q.; Lv, J.; Yan, L.; Ling, L.; Zhang, Y. The effects of pH and salts on nucleic acid partitioning during phenol extraction. *Nucleosides Nucleotides Nucleic Acids* **2019**, *38*, 305–320. [CrossRef]
99. Verma, A.; Prasad, N.E.; Srivastava, J.; Saha, S. Probing the Heterogeneity of Ionic Liquids in Solution through Phenol-Water Phase Behavior. *Electro Phys. Theor. Chem.* **2019**, *4*, 49–58. [CrossRef]
100. Bernhart, S.H.; Hofacker, I.L.; Will, S.; Gruber, A.R.; Stadler, P.F. RNAalifold: Improved consensus structure prediction for RNA alignments. *BMC Bioinform.* **2008**, *9*, 474. [CrossRef]
101. Darty, K.; Denise, A.; Ponty, Y. VARNA: Interactive drawing and editing of the RNA secondary structure. *Bioinformatics* **2009**, *25*, 1974–1975. [CrossRef]